Telcordia Technologies
Performance from Experience

Approved for Public Release, Distribution Unlimited

Physical-Layer Modeling of UWB Interference Effects

Dr. Jay E. Padgett (P.I.)
Dr. John C. Koshy
Dr. Anthony A. Triolo

Wireless Systems and Networks Research,
Telcordia Technologies, Inc.

January 10, 2003

Sponsored by
Defense Advanced Research Projects Agency
Advanced Technology Office
Analysis and Simulation of UWB Interference Effects – NETEX Program
ARPA Order No. N626/00
Issued by DARPA/CMO under Contract #MDA972-02-C-0056

Distribution

DARPA/CMO Attn: Mr. Anthony E. Cicala 3701 North Fairfax Drive Arlington, VA 22203-1714 acicala@darpa.mil (one copy)	DARPA/ATO Attn: Mr. Steve Griggs 3701 North Fairfax Drive Arlington, VA 22203-1714 sgriggs@darpa.mil (two copies)
DARPA/ATO Attn: Mr. Patrick Bailey 3701 North Fairfax Drive Arlington, VA 22203-1714 (one copy)	Defense Contract Management Agency DCMA Springfield DCMAE-GXTB DCMA Springfield Bldg 1, ARDEC Picatinny Arsenal, NJ 07086-5000 (one copy)

Contact information:

Dr. Jay Padgett
Senior Research Scientist
Telcordia Technologies
Room 3Z-370
331 Newman Springs Road
Red Bank, NJ 07701

tel: 732-758-2043
fax:732-758-4372
jpadgett@telcordia.com

Report Documentation Page

Form Approved
OMB No. 0704-0188

1. REPORT DATE	2. REPORT TYPE	3. DATES COVERED
2003	**N/A**	**-**

4. TITLE AND SUBTITLE	5a. CONTRACT NUMBER
Physical-Layer Modeling of UWB Interference Effects	5b. GRANT NUMBER
	5c. PROGRAM ELEMENT NUMBER
6. AUTHOR(S)	5d. PROJECT NUMBER
	5e. TASK NUMBER
	5f. WORK UNIT NUMBER
7. PERFORMING ORGANIZATION NAME(S) AND ADDRESS(ES) **Wireless Systems and Networks Research, Telcordia Technologies, Inc.**	8. PERFORMING ORGANIZATION REPORT NUMBER
9. SPONSORING/MONITORING AGENCY NAME(S) AND ADDRESS(ES)	10. SPONSOR/MONITOR'S ACRONYM(S)
	11. SPONSOR/MONITOR'S REPORT NUMBER(S)

12. DISTRIBUTION/AVAILABILITY STATEMENT
Approved for public release, distribution unlimited

13. SUPPLEMENTARY NOTES
The original document contains color images.

14. ABSTRACT

15. SUBJECT TERMS

16. SECURITY CLASSIFICATION OF:			17. LIMITATION OF ABSTRACT	18. NUMBER OF PAGES	19a. NAME OF RESPONSIBLE PERSON
a. REPORT	b. ABSTRACT	c. THIS PAGE			
unclassified	**unclassified**	**unclassified**	**UU**	**221**	

Executive Summary

The NETEX program is focused initially on understanding the effects of interference from ultra-wideband (UWB) transmitters on legacy military radio receivers, nearly all of which are narrowband (NB) relative to the UWB signal, which can have a bandwidth on the order of 1 GHz. The purpose of this report is to document a set of mathematical models which have been developed to analyze the impact of UWB signals on NB receivers. This analysis work is being done in parallel with a UWB interference testing program being conducted by other parties.

There are two main components to the work presented here. The first is a detailed analysis of the power spectral density (PSD) of the UWB signal, which shows the distribution of the UWB transmit power over frequency. The PSD is determined by (1) the spectrum of the basic UWB pulse; and (2) pulse position modulation/dithering and pulse amplitude modulation. A clear understanding of the PSD is important, because the main factor that determines the impact on a NB receiver is the total average UWB interference power within the receiver passband. This is demonstrated by the second main component of the report, which is a set of models describing the impact of UWB interference on several different representative receiver types, both digital and analog.

The PSD gives the average power-per-Hz as a function of frequency for the UWB signal. The UWB PSD models developed here allow the PSD to be computed analytically for a wide range of different UWB signal types, and include the effects of pulse-position modulation (PPM), random or periodic pseudo-random dithering of the pulse position, modulation or random (or pseudo-random) coding of the pulse amplitude, modulation symbols that include multiple UWB frames (giving integration gain), and modulation of the actual pulse repetition frequency (PRF) by either a periodic PRF-modulating signal or by a random process such as a data signal. Given either a specific modulation data sequence and dithering code, or the relevant statistical descriptions, the PSD can be calculated using the models developed here. These models can also be used as a basis for developing UWB signals with specific desired spectral properties (e.g., so that little or no power falls into certain bands), which is a potential area for further work.

The UWB signal is filtered by the NB receiver intermediate frequency (IF) bandwidth before affecting the demodulator/detector functions. It is therefore important to understand the IF output waveform associated with the UWB interference. The IF output interference is analyzed in detail, and a procedure for simulating the IF output interference is described and example results are given and compared to the analytic results from the PSD analysis. The nature of the IF output interference depends on the relationship between the UWB pulse rate and the IF bandwidth of the NB receiver. If the pulse rate is high compared to the IF bandwidth, the IF output interference will consist of a tone (single frequency, CW), or a noise-like waveform, or some combination of the two, as determined by the pulse dithering and modulation. Conversely, if the IF bandwidth exceeds the pulse rate, then the IF resolves each pulse in time and the IF

output interference appears as a series of pulses, which have the temporal shape of the IF filter impulse response.

Accordingly, the models for NB receiver impact account for tone interference, noise-like interference, and impulsive interference. The digital modulation techniques investigated were phase-shift keying (PSK) with coherent detection, frequency-shift keying (FSK) with coherent detection, and FSK with non-coherent detection. Impact was measured in terms of the bit error rate (BER). An analog FM receiver was also investigated, with impact measured in terms of baseband signal-to-noise ratio (SNR). In all four cases, the main factor determining impact was the ratio of the received desired signal power to the average received UWB interference power within the receiver passband (IF bandwidth). The exact impact was found to vary depending on the form of the interference. With the digital receivers, tone interference was generally more benign than Gaussian noise of the same average power, and its effect was found to depend on the tone frequency. With FM, the effect of tone interference also depends on the tone frequency, and in the worst case (offset from the carrier by the baseband bandwidth), the impact was more severe than that of Gaussian noise with the same average power.

When the UWB pulse rate exceeds the IF bandwidth and the pulse position is dithered, the IF output interference appears noise-like, and the impact is similar to that of Gaussian noise, although somewhat less severe in the digital cases at low BER. This is because the peak-to-average ratio of the interference is limited, which is not the case for Gaussian noise. The higher the pulse rate, the nearer the impact is to the Gaussian case.

For the digital receivers, if the pulse rate is less than or equal to the IF bandwidth, the BER is nearly constant as the carrier to interference ratio (CIR) increases, then drops sharply to zero as the CIR becomes greater than some threshold value. That CIR threshold is inversely proportional to the pulse rate. This is because the energy per pulse is inversely proportional to the pulse rate, for constant average UWB interference power. For a range of CIR below this threshold, low pulse-rate UWB interference affects the receiver more severely than Gaussian noise, compared on the basis of average in-band noise or interference power. With FM, there is a similar effect with low pulse rates. Above a CIR threshold, the FM receiver impact is the same as Gaussian noise. The threshold varies inversely with the ratio of the pulse rate to the IF bandwidth, just as with the digital receivers. If the pulse rate is equal to the IF bandwidth, the threshold is about 6 dB. This is the same as the threshold for both coherent and non-coherent FSK when the pulse rate is equal to the IF bandwidth.

The models developed here provide the means for a preliminary assessment of the requirements for coexistence of UWB and NB radios, and for analytically reproducing the test results. Clearly, there is much more yet to be done, including application of these models to a number of specific cases of interest, as well as extending and refining the models to study situations that are impractical to test, such as aggregate interference scenarios. Other areas for further work include development of UWB signal design techniques to yield desirable spectra, and UWB receiver techniques to combat interference from narrowband transmitters.

Contents

Chapter 1: INTRODUCTION

1.1. Objectives

The overall goal of the NETEX program is to understand the limitations on the coexistence of ultra wide band (UWB) devices and other military radios, from a radio interference perspective. The primary initial concern is the potential for interference from UWB transmitters to other radios; interference from other radios to UWB receivers is a secondary concern at this point.

The NETEX program includes two components that are directed at the coexistence issue: (1) a test program, in which selected military radios are subjected to specified UWB test waveforms, and performance degradations noted; and (2) an analysis program, in which mathematical models and simulations are used to characterize UWB signals and to analyze their impact on different types of narrowband (NB) receivers. This report documents the work of the first phase of the analysis program, which is the development of the basic mathematical models that are needed to perform the interference impact analysis.

Whenever multiple radios are used in the same tactical environment (aircraft, battlefield situation, etc.), interference potential exists and must be managed by design and by deployment coordination. With narrowband radios, coordination often is straightforward because frequency separation can be used. UWB signals, however, can have bandwidths on the order of 1 GHz or more. The UWB bandwidth therefore spans the bands used by many other radios, making UWB/NB coexistence more complex than NB/NB coexistence. Nevertheless, there are a number of approaches that can be used, either individually or in combination, to allow UWB and NB radios to coexist:

- Filtering of the UWB signal: A UWB signal will be naturally high-pass filtered by its antenna, so often very little power may be transmitted within the VHF and lower UHF bands. It is also possible to apply additional filtering, although such filtering will distort the UWB pulse waveform, which may compromise reception of the UWB signal itself.
- Spatial separation: For some applications, it may be possible to guarantee that there will be some minimum distance between a UWB transmitter and potential victim narrowband receivers.
- UWB signal design: As will be seen, the power spectrum of a UWB signal depends not only on the spectrum of the pulse itself, but on the amplitude and position modulation of the pulse, as well as the average pulse rate. Pulse waveforms and/or pulse repetition algorithms can be designed to avoid transmitting significant power within a particular narrow band.
- Application-managed transmit coordination: In integrated applications, the UWB devices might be used in concert with other radios, and coexistence might be enforced by a higher-layer control process which ensures that UWB devices do not transmit when other radios are attempting to receive, and vice versa.

In sum, as with many other types of radios, successful coexistence between UWB devices and other radios is unlikely to be achieved by accident, but it appears feasible to achieve it by design. To do so, it is important to have a detailed understanding of how the UWB signal spectrum and the impact of the UWB signal on a narrowband receiver are affected by the design parameters of the UWB signal and the receiver properties. Developing such an understanding is the main focus of this report.

The approach used is to develop general mathematical models of the UWB signal and the narrowband receiver. This not only sets the stage for interference impact analysis, but also provides insights into general principles of UWB operation and interference mechanisms that often are not obvious from test results, or even from simulations.

1.2. Report Overview

Chapter 2 gives a brief technical overview of the UWB signal and the effective interference from the UWB signal to a narrowband receiver. The intent is to provide a high-level mathematical description of the situation being modeled, to familiarize the reader with the notation and general modeling approach, and to provide a quantitative perspective on the work reported here.

Chapter 3 focuses on the power spectral density (PSD) of the UWB signal. Since a clear understanding of the PSD is important, both for interference analysis and for UWB signal design, considerable work was done on the PSD analysis. A new method for calculating the UWB PSD was developed, which simplifies the calculations compared to other techniques available in the literature. This method is explained in the body of Chapter 3, with a formal proof in Annex 3A.[1] Expressions for the PSD were also developed independently using two different approaches from the literature, to ensure that the final PSD model is correct. These are documented in Annexes 3C and 3D.

Chapter 3 also develops expressions for complex "generalized" UWB signals that may include integration gain (multiple UWB pulses per information symbol) plus either pure random (non-repeating) dithering/polarity shifting codes, or repeating pseudorandom codes in addition to the information modulation, which in general may modulate both the pulse position and pulse amplitude (including polarity). The general PSD expression for such a UWB signal is derived in Annex 3B, using the new method developed here. The results are also derived independently in Annexes 3C and 3D for verification.

Chapter 3 provides some simple examples of PSD calculation, with the accompanying graphs, which illustrate how selection of different parameters affects the signal power level in a particular frequency band. As is clearly seen from both the general PSD results and from the examples, the UWB PSD in general consists of both discrete tones at specific frequencies, and a "continuous" component (watts per Hz), which is noise-like.

Chapter 4 develops mathematical models for the PSD of a UWB signal in which the pulse repetition frequency (PRF) is modulated by a known time-function or a random

[1] To the knowledge of the authors, this is a new result, not available in the public technical literature.

process with known statistics. It is assumed that the pulse rate deviation is small compared to the average pulse rate. Exact and approximate PSD expressions are developed for the specific case of a swept PRF, whereby the PRF is modulated by a "sawtooth" wave. Finally, an expression is derived for the PSD of a UWB signal that is PRF-modulated by a random process. It is shown that in the "wideband" case (the RMS pulse rate deviation is significantly larger than the bandwidth of the modulating process), the PSD consists of spectral envelopes that have the same shape as the probability density function (PDF) of the modulating process, and are centered on frequencies that are harmonics of the average PRF. The width (in frequency) of each of these envelopes is proportional to its center frequency, and the height (in watts/Hz) is inversely proportional to the center frequency. On frequencies between these spectral envelopes, there is negligible power from the UWB signal, which demonstrates that by appropriately managing the timing of the UWB signal, it is possible to avoid generating interference into specific bands.

Chapter 5 discusses in detail the UWB signal as seen by a narrowband receiver. For a typical receiver architecture, the limiting bandwidth will be that of the intermediate frequency (IF) sections. The IF bandwidth usually is roughly the same as the signal bandwidth. The effective UWB interference as seen by the demodulator or detector stage of the receiver is the output of the final IF stage, which can be modeled as a bandpass-filtered version of the UWB signal. Chapter 5 develops mathematical models for this IF-output UWB interference signal in both the time domain and the frequency domain, including expressions for baseband-equivalent in-phase and quadrature components, which often are useful for performance analysis. An algorithm for simulating the IF output interference envelope is described and example results are shown.

The temporal and statistical characteristics of the IF output interference depend on the relationship between the average UWB pulse rate and the IF bandwidth, as well as the position modulation and dithering of the UWB pulses. The IF output in response to a single pulse is the aggregate IF impulse response, which has a settling time that varies inversely with the IF bandwidth. If the pulse rate is less than the IF bandwidth, then the IF response will settle between successive pulses, and the IF response to the UWB signal will be a sequence of IF impulse responses, the timing of which will be the same as the UWB signal timing. On the other hand, if the pulse rate is significantly greater than the IF bandwidth, then the IF output will be the sum of multiple overlapping impulse responses, and the envelope power will depend on the phase relationships among these overlapping responses. If they are all in phase and add constructively, then the receiver center frequency is a harmonic of the pulse rate, and the receiver output is a constant level (there is a tone in the UWB signal spectrum at the receiver center frequency). If the overlapping pulses are randomly phased relative to one another, then the IF output signal varies and appears noise-like.

Chapters 6, 7, and 8 develop models for the effect of UWB interference on fixed-frequency digital receivers. Chapter 6 pertains to coherently-detected phase-shift keying (PSK), Chapter 7 to coherently-detected frequency-shift keying (FSK), and Chapter 8 to non-coherently-detected FSK. The effects of combined UWB interference and Gaussian

noise on the bit error rate (BER) are explored, for different UWB pulse rates (relative to the receiver IF bandwidth), and also for the case in which the UWB interference consists of a single CW tone within the receiver passband. Results are presented in terms of the time-average UWB interference power within the IF bandwidth. If the pulse rate is greater than the IF bandwidth and the pulse position is randomly dithered, the BER does not appear to be very sensitive to the pulse rate, for a given average in-band UWB interference power, and the effect on BER is similar to that of Gaussian noise (although at low BERs the Gaussian noise is worse due to its unlimited peak-to-average ratio). If the interference is a CW tone, the effect on the BER depends on the frequency of the tone, but is less severe than that of Gaussian noise with the same average power.

If the pulse rate is less than or equal to the IF bandwidth, the BER is nearly constant as the signal to interference ratio (SIR) increases, then drops sharply to zero as the SIR becomes greater than some threshold value. That SIR threshold is inversely proportional to the pulse rate. This is because the energy per pulse is inversely proportional to the ratio of the pulse rate to the IF bandwidth, for constant average UWB interference power. For a range of SIR below this threshold, low pulse-rate UWB interference affects the receiver more severely than Gaussian noise, compared on the basis of average in-band noise or interference power. For both coherent and non-coherent FSK, that threshold is 6 dB when the pulse rate equals the IF bandwidth.

Chapter 9 analyzes the effect of UWB interference on an FM receiver. The results are stated in terms of the impact on the baseband signal to noise ratio (SNR). With tone interference, the impact depends on the frequency of the tone and can be more or less severe than that of Gaussian noise. With a pulse rate greater than the IF bandwidth and dithering, the effect of the UWB signal on the FM receiver will be comparable to that of Gaussian noise. With a low pulse rate, the effect is the same as Gaussian noise when the ratio of the carrier (desired signal) power to the average in-band UWB interference is above a threshold. However, the threshold varies inversely with the ratio of the pulse rate to the IF bandwidth. Note that this is analogous to the SIR threshold for digital receivers described above. As the pulse rate decreases, the threshold increases. If the pulse rate is equal to the IF bandwidth, the threshold is about 6 dB, just as it is with FSK.

1.3. Summary of Conclusions and Next Steps

The main purpose of this report is to document the fundamental models which have been developed to analyze the effect of UWB interference on narrowband receivers. The results presented here for those receivers suggest that the average UWB interference within the receiver IF bandwidth is the primary factor that determines the impact, as would be expected. The exact impact will vary according to the characteristics of the UWB interference as seen by the receiver: tone-like, noise-like, or pulse-like.

The general models developed here can be applied to specific receivers of interest by setting their parameters accordingly. This will allow comparison of modeling and testing results. Additional next steps include extension of these models to situations that cannot be readily tested, such as aggregate interference from multiple UWB transmitters. Other areas for further work include development of models for frequency-hopping receivers,

UWB signal design techniques, and UWB receiver techniques for robust operation in the presence of multiple narrowband interference sources.

Chapter 2: OVERVIEW OF THE UWB SIGNAL AND ITS INTERFERENCE TO NARROWBAND RECEIVERS

2.1. The General UWB Signal Model

The UWB signal of interest here is a sequence of very short pulses. If the basic pulse waveform is $p(t)$, the UWB signal can be described as

$$w(t) = \sum a_k p(t - T_k) \tag{2-1}$$

where T_k and a_k are the transmit time and amplitude modulation of the k^{th} pulse, respectively. For analysis, it is often useful to define

$$d(t) \equiv \sum_k a_k \delta(t - T_k) \qquad D(f) = \sum_k a_k e^{-j2\pi f T_k} \tag{2-2}$$

where $\delta(t)$ is the Dirac delta function. The UWB signal is then

$$w(t) = p(t) * d(t) \tag{2-3}$$

where $*$ denotes convolution.

The Fourier transform of the UWB signal is

$$W(f) = P(f)D(f) = P(f)\sum_k a_k e^{-j2\pi f T_k} \tag{2-4}$$

Since the $\{a_k\}$ and $\{T_k\}$ are in general random, the UWB signal must be modeled as a random process, and a more useful frequency-domain description of the UWB signal is the power spectral density (PSD), which represents the average power-per-Hz as a function of frequency. The PSD of a process $w(t)$ is denoted here by $S_w(f)$, and has units of watts/Hz. In the case of the UWB signal,

$$S_w(f) = |P(f)|^2 S_d(f) \tag{2-5}$$

The term $|P(f)|^2$ is the magnitude of the Fourier transform of the pulse waveform $p(t)$:

$$P(f) = \int_{-\infty}^{\infty} p(t) e^{-j2\pi ft} dt \tag{2-6}$$

and $|P(f)|^2$ represents the *energy spectral density* (ESD) of a single pulse, in units of joules/Hz. The PSD of the UWB signal therefore can be represented as the product of two components: the ESD of the pulse itself, which provides the overall large-scale "shape" of the spectrum, and the PSD of the process $d(t)$, which determines the fine structure that depends on how the pulse is modulated in amplitude and repeated in time.

2.2. Pulse Repetition Frequency, Average Power, and Effective Bandwidth

In many cases the UWB timing structure consists of intervals or "frames" of duration *T*, with one pulse transmitted in each frame. The position of the pulse within the frame may vary, according to pulse-position modulation and/or pseudorandom "dithering" of the pulse position. Hence,

$$T_k = kT + \varepsilon_k \tag{2-7}$$

where ε_k includes the combined effects of pulse position modulation (PPM) and dithering. The average pulse repetition frequency (PRF) is then $\overline{R} = 1/T$.

The energy in a single pulse is

$$E_p = \int_{-\infty}^{\infty} |P(f)|^2 df \qquad \text{joules} \tag{2-8}$$

and the total average power of the UWB signal is

$$\overline{P}_w = \left\langle a_k^2 \right\rangle \overline{R} E_p \text{ watts} \tag{2-9}$$

An equivalent rectangular UWB pulse bandwidth can be defined as

$$B_p = \frac{E_p}{2|P(f)|^2_{\max}} \qquad \text{Hz} \tag{2-10}$$

where the factor of 2 in the denominator reflects the two-sided definition (positive and negative frequencies) of $P(f)$. It should be noted that since the pulse waveform $p(t)$ is real (has no imaginary component), $P(f)$ is conjugate-symmetric; that is $P(-f) = P^*(f)$; therefore, $|P(f)| = |P(-f)|$.

2.3. UWB Signal Applied to a Narrowband Receiver

Of primary interest here is the effect of a UWB signal on a narrowband receiver. Typically, such a receiver will use a dual-conversion superheterodyne architecture, and the output of the final intermediate-frequency (IF) stage is the input to the detector or demodulator which recovers the baseband signal or data. Also, there usually will be an automatic gain control (AGC) in the receive chain to avoid overloading IF/baseband circuitry, which is necessary because of the large dynamic range of received radio signals.

The interfering UWB signal will be processed through this same receive chain, so the interference into the detector/demodulator stage can be represented as the output of a bandpass filter centered on the RF carrier frequency f_0. Since most radios can tune over a range of frequency channels, the front-end RF bandwidth is usually relatively wide compared to the signal bandwidth, and the effective filtering that acts on the UWB signal will be dominated by the IF filtering, which typically has same bandwidth as the signal. The transfer function of the filter acting on the UWB signal therefore is denoted $H_{IF}(f)$. In the frequency domain, the filter output in response to the UWB signal is

$$G(f) = H_{IF}(f)W(f) \tag{2-11}$$

where $g(t)$ is the output waveform and $G(f)$ is its Fourier transform. Note that $g(t)$ is a bandpass signal with nominal center frequency f_0 (see Figure 2-1).

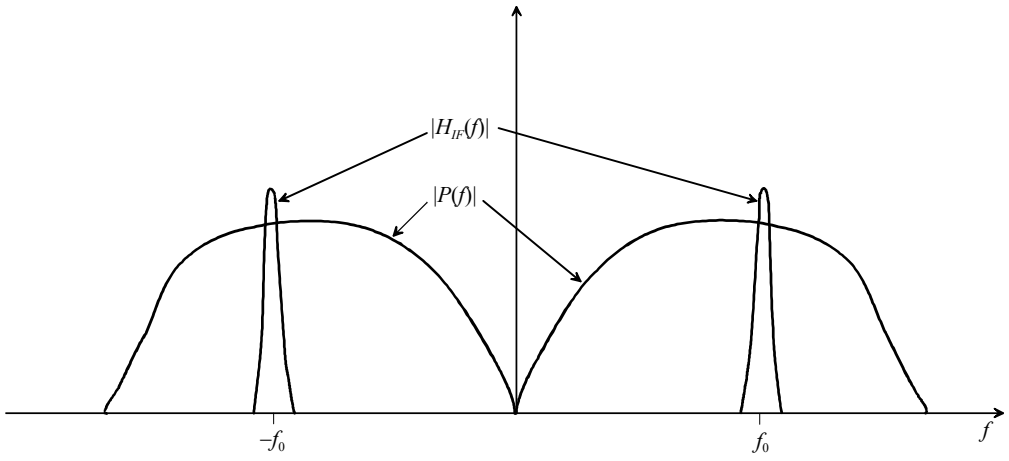

Figure 2-1: *Illustration of UWB pulse ESD and narrowband filter frequency response*

If, as is normally expected to be the case, the bandwidth of the UWB pulse far exceeds the channel bandwidth of the victim receiver, the exact shape of the pulse is not important, because the response of the receiver IF to a single pulse will effectively be the impulse response of the IF, denoted $h_{IF}(t)$, which is the inverse Fourier transform of $H_{IF}(f)$. Stated another way, $P(f)$ is essentially constant over the receiver channel passband. Given that, the independence of $g(t)$ on the pulse waveform can be seen as follows.

The Fourier transform of $g(t)$ is

$$G(f) = H_{IF}(f)W(f) = H_{IF}(f)P(f)D(f) \tag{2-12}$$

Typically, the bandwidth of the pulse spectrum $P(f)$ far exceeds that of $H_{IF}(f)$, and $P(f)$ is essentially constant over the passband of $H_{IF}(f)$, in which case

$$G(f) \cong \begin{cases} H_{IF}(f)P(f_0)D(f) & f \geq 0 \\ H_{IF}(f)P(-f_0)D(f) & f < 0 \end{cases} \tag{2-13}$$

Since $h_{IF}(t)$ and $p(t)$ are real (have no imaginary component), $H_{IF}(f)$ and $P(f)$ are conjugate-symmetric; that is, $H_{IF}(-f) = H_{IF}^*(f)$ and $P(-f) = P^*(f)$. In general, $P(f)$ is complex: $P(f) = |P(f)|e^{j\psi(f)}$. Letting $\psi_0 = \psi(f_0)$,

$$G(f) \cong \begin{cases} H_{IF}(f)|P(f_0)|e^{j\psi_0}D(f) & f \geq 0 \\ H_{IF}(f)|P(f_0)|e^{-j\psi_0}D(f) & f < 0 \end{cases} \tag{2-14}$$

Finally, letting

$$H_{IF\psi}(f) \equiv \begin{cases} e^{j\psi_0}H_{IF}(f) & f \geq 0 \\ e^{-j\psi_0}H_{IF}(f) & f < 0 \end{cases} \tag{2-15}$$

then

$$G(f) \cong H_{IF\psi}(f)|P(f_0)|D(f) \tag{2-16}$$

Taking the inverse transform gives

$$g(t) \cong |P(f_0)| h_{IF\psi}(t) * d(t) = |P(f_0)| \sum_k a_k h_{IF\psi}(t - T_k) \tag{2-17}$$

The envelope of the impulse response $h_{IF\psi}(t)$ is the same as that of the actual response $h_{IF}(t)$ but the phase of the underlying oscillatory response will be shifted by ψ_0 radians. However, for interference analysis, the constant phase shift ψ_0 has no effect on the end results, and it can be ignored without loss of generality.

Finally, the PSD of the IF output is

$$S_g(f) \cong |P(f_0)|^2 |H_{IF}(f)|^2 S_d(f) \tag{2-18}$$

If is therefore clear that the response of the narrowband receiver to the UWB signal depends on the ESD of the UWB pulse at the center frequency of the receiver, and the pulse modulation/dithering as described by the pulse repetition sequence $d(t)$. A detailed temporal description of the pulse waveform is not important. All that is necessary is that the pulse ESD magnitude at the receiver center frequency, which can be measured using a spectrum analyzer.

2.4. Other Representations of the Effective UWB Interference

The actual signal into the detector or demodulator will not be an RF signal with center frequency f_0, but rather a frequency-shifted version. For some receiver types, it is the envelope of $g(t)$ that is of interest, and for other types, the equivalent low-pass inphase and quadrature components, denoted $x(t)$ and $y(t)$ are most applicable, where $g(t)$ can be written in bandpass form as

$$g(t) = x(t)\cos 2\pi f_0 t - y(t)\sin 2\pi f_0 t \tag{2-19}$$

The necessary temporal and spectral relationships among $g(t)$, $x(t)$, and $y(t)$ are developed in detail in Chapter 5. The envelope and phase of $g(t)$ are

$$a_g(t) = \sqrt{x^2(t) + y^2(t)} \qquad \theta(t) = \tan^{-1} y(t)/x(t) \tag{2-20}$$

and, in terms of that envelope,

$$g(t) = a_g(t)\cos[2\pi f_0 t + \theta(t)] \tag{2-21}$$

The envelope power of $g(t)$ is

$$P_g(t) = \frac{a_g^2(t)}{2} \tag{2-22}$$

Clearly, given $x(t)$ and $y(t)$, which can be derived from $g(t)$, a frequency-shifted version of the signal (reflecting down-conversion to a center frequency f_c) is easily constructed as

$$g_c(t) = x(t)\cos 2\pi f_c t - y(t)\sin 2\pi f_c t \tag{2-23}$$

2.5. Temporal Characteristics of the IF Output Interference

The response to a single pulse occurring at time T_k is $h_{IF}(t - T_k)$. If B_{IF} is the IF filter bandwidth, the duration of the filter impulse response is inversely proportional to B_{IF}. If the average pulse rate $\overline{R}$ is significantly less than B_{IF}, then the IF filter "settles" between pulses, and the response to the UWB interference is a sequence of individual impulse responses. However, if $\overline{R} > B_{IF}$, then there is overlap between the responses to successive pulses and the net result will depend on the phase relationships among the successive responses. For example, if pulses are evenly spaced in time with rate *R* and the center frequency f_0 of the channel is an integer multiple of *R*, then the successive responses are perfectly in phase and add constructively. If *R* is sufficiently greater than B_{IF}, then the IF output is a single tone of frequency f_0 and constant power level.

This case can also be considered in terms of the frequency domain. With a constant pulse rate with no amplitude modulation, the spectrum of the UWB signal consists only of CW tones at frequencies that are integer multiples of *R*. If the receiver bandwidth is less than *R*, it can capture at most one of the tones. The IF filter achieves its maximum response if its center frequency coincides with one of the tones. If a tone is within the passband but not at the center frequency, it still appears at the IF output but at a reduced level, corresponding to the receiver IF filter rolloff.

If $\overline{R} >> B_{IF}$ and the pulse position is varied, the IF output is the sum of multiple overlapping impulse responses with different (possibly random) phase relationships. In the limit, if the pulse position is randomly varied uniformly over the UWB frame, the IF output appears noise-like and in fact the distributions of the low-pass components $x(t)$ and $y(t)$ approach Gaussian distributions.

The next two chapters discuss the UWB PSD, and following that, Chapter 5 develops detailed expressions for the IF filter output, including an algorithm for simulating the output in the time domain.

Chapter 3: ANALYSIS OF UWB POWER SPECTRAL DENSITY

3.1. Introduction

In analyzing UWB interference effects, the power spectral density (PSD) is of central importance, since the distribution of power over the bandwidth of the UWB pulse depends not only on the shape of the pulse spectrum itself, but on how the pulses are amplitude-modulated and positioned in time. If the PSD is understood, it may be possible to reduce or eliminate interference from the UWB signal to selected narrowband channels.

PSD is usually defined as the Fourier transform of the autocorrelation of a wide-sense stationary (WSS) random process. From the perspective of physical meaning, a more useful definition is that PSD is the average power per Hz as a function of frequency. That is, if $w(t)$ represents the UWB signal, then its PSD $S_w(f)df$ is the average power that would be seen at frequency f by a filter of infinitesimally narrow bandwidth *df*.

By definition, the mean and autocorrelation of a WSS process are time-independent. That is, if $z(t)$ is stationary, then $\langle z(t)\rangle = \mu_z$ and $R_z(t+\tau,t) = \langle z(t+\tau)z^*(t)\rangle = R_z(\tau)$. In general, a UWB signal may be cyclostationary rather than stationary, meaning that the mean and autocorrelations are periodic functions of time with some period *T*:

$$\langle w(t)\rangle = \langle w(t+T)\rangle \qquad R_w(t+\tau,t) = R_w(t+T+\tau,t+T) \tag{3-1}$$

To compute the PSD of a cyclostationary process, a time-average must be taken over the period *T*. This is consistent with the view of PSD as the *average* power per unit bandwidth. The time-average mean and autocorrelation can be written as

$$\overline{\mu}_w = \frac{1}{T}\int_t^{t+T} \langle w(\xi)\rangle d\xi \qquad \overline{R}_w(\tau) = \frac{1}{T}\int_t^{t+T} R_w(\xi+\tau,\xi)d\xi \tag{3-2}$$

where the overbar denotes time-averaging and $\langle\cdot\rangle$ signifies expectation.

The PSD is then

$$S_w(f) = \int_{-\infty}^{\infty} \overline{R}_w(\tau)e^{-j2\pi f\tau}d\tau \tag{3-3}$$

Consider the UWB signal

$$w(t) = \sum a_k p(t - T_k) \tag{3-4}$$

As in Chapter 2, it is useful to define

$$d(t) \equiv \sum_k a_k \delta(t - T_k) \tag{3-5}$$

so that

$$w(t) = p(t) * d(t) \tag{3-6}$$

and

$$S_w(f) = |P(f)|^2 S_d(f). \tag{3-7}$$

It therefore suffices to determine $S_d(f)$. To do so, it is possible to determine the autocorrelation, perform the specified time-averaging and expectation, and take the Fourier transform, and there are numerous variations on this approach in the literature (see e.g., [3], [7] which are explored in detail in Annexes 3C and 3D, respectively). However, there is a simpler (and more intuitively appealing) approach that can be used, based on the following reasoning.

Consider a process $z(t)$ and define

$$Z(f,t) = \int_{-\infty}^{t} z(\tau) e^{-j2\pi f\tau} d\tau . \tag{3-8}$$

The accumulated energy spectral density (ESD) at time *t* is $|Z(f,t)|^2$, in joules/Hz, so the instantaneous power spectral density at time *t* is $\frac{d}{dt}|Z(f,t)|^2$, watts/Hz, which is clearly a random process for a given *f*. If $z(t)$ is stationary, then its PSD is therefore

$$S_z(f) = \left\langle \frac{d}{dt}|Z(f,t)|^2 \right\rangle \tag{3-9}$$

which is independent of *t* for $z(t)$ stationary.

If $z(t)$ is cyclostationary, then time-averaging over one period *T* must be performed, giving:

$$S_z(f) = \left\langle \overline{\frac{d}{dt}\left|Z(f,t)\right|^2} \right\rangle = \frac{1}{T}\left\langle \left|Z(f,t+T)\right|^2 - \left|Z(f,t)\right|^2 \right\rangle \tag{3-10}$$

which is independent of *t* for $z(t)$ cyclostationary with period *T*.

Although these relationships are intuitively apparent, in that the PSD is the average rate of change of the energy spectral density, they are formally proven in Annex 3A. As demonstrated below, using these relationships simplifies the mechanics of calculating the PSD for UWB signals, compared to other approaches. To demonstrate, $S_d(f)$ is computed for a basic UWB signal using this approach.

With $d(t) = \sum_k a_k \delta(t - T_k)$,

$$D(f,t) = \sum_k a_k \int_{-\infty}^{t} \delta(\tau - T_k) e^{-j2\pi f\tau} d\tau = \sum_k a_k e^{-j2\pi f t_k} U(t - T_k) \tag{3-11}$$

and the time-dependent energy spectral density is

$$\begin{aligned} \left|D(f,t)\right|^2 &= \sum_k a_k e^{-j2\pi f T_k} U(t - T_k) \sum_n a_n^* e^{j2\pi f T_n} U(t - T_n) \\ &= \sum_k \sum_l a_k a_{k+l}^* e^{j2\pi f (T_{k+l} - T_k)} U(t - T_k) U(t - T_{k+l}) \end{aligned} \tag{3-12}$$

Since

$$U(t - T_k) U(t - T_{k+l}) = \begin{cases} U(t - T_k) & l \le 0 \\ U(t - T_{k+l}) & l \ge 0 \end{cases}, \tag{3-13}$$

the ESD is:

$$\begin{aligned} \left|D(f,t)\right|^2 = \sum_k \left|a_k\right|^2 U(t - T_k) &+ \sum_{l<0} \sum_k a_k a_{k+l}^* e^{j2\pi f (T_{k+l} - T_k)} U(t - T_k) \\ &+ \sum_{l>0} \sum_k a_k a_{k+l}^* e^{j2\pi f (T_{k+l} - T_k)} U(t - T_{k+l}) \end{aligned}. \tag{3-14}$$

Taking the time derivative gives

$$\frac{d}{dt}\left|D(f,t)\right|^2 = \sum_k |a_k|^2 \delta(t-T_k) + \sum_{l<0}\sum_k a_k a_{k+l}^* e^{j2\pi f(T_{k+l}-T_k)}\delta(t-T_k) + \sum_{l>0}\sum_k a_k a_{k+l}^* e^{j2\pi f(T_{k+l}-T_k)}\delta(t-T_{k+l}) \tag{3-15}$$

The next step is to perform expectation and if necessary, time-averaging. In many cases, the sequences $\{a_k\}$ and $\{T_k\}$ are stationary, in which case the autocorrelation $\left\langle a_k a_{k+l}^* e^{j2\pi f(T_{k+l}-T_k)}\right\rangle$ is independent of *k* (a function of *l* only), and

$$\begin{aligned}\left\langle a_k a_{k+l}^* e^{j2\pi f(T_{k+l}-T_k)}\delta(t-T_k)\right\rangle &= \left\langle a_k a_{k+l}^* e^{j2\pi f(T_{k+l}-T_k)}\right\rangle\left\langle\delta(t-T_k)\right\rangle \\ \left\langle a_k a_{k+l}^* e^{j2\pi f(T_{k+l}-T_k)}\delta(t-T_{k+l})\right\rangle &= \left\langle a_k a_{k+l}^* e^{j2\pi f(T_{k+l}-T_k)}\right\rangle\left\langle\delta(t-T_{k+l})\right\rangle\end{aligned} \tag{3-16}$$

Letting $\gamma_k(f) = a_k e^{-j2\pi f T_k}$ and defining $R_{\gamma(f)}[l] = \left\langle \gamma_k(f)\gamma_{k+l}^*(f)\right\rangle$

$$\left\langle \frac{d}{dt}\left|D(f,t)\right|^2\right\rangle = \sum_{l\le 0} R_{\gamma(f)}[l]\left\langle\sum_k \delta(t-T_k)\right\rangle + \sum_{l>0} R_{\gamma(f)}[l]\left\langle\sum_k \delta(t-T_{k+l})\right\rangle \tag{3-17}$$

If there are restrictions on T_k relative to the nominal UWB frame boundary, then $\left\langle\sum_k \delta(t-T_k)\right\rangle$ is dependent on *t* and time-averaging is necessary, and

$$\overline{\left\langle\sum_k \delta(t-T_k)\right\rangle} = \frac{1}{T} \tag{3-18}$$

which is the average pulse rate. If T_k is unrestricted, then $\left\langle\sum_k \delta(t-T_k)\right\rangle = \frac{1}{T}$ without time-averaging. In either case,

$$S_d(f) = \frac{1}{T}\sum_l R_{\gamma(f)}[l] \tag{3-19}$$

If the $\{a_k\}$ and/or $\{T_k\}$ are stationary, then the autocorrelation requires averaging over *k*; that is, $R_{\gamma(f)}[l] = \left\langle \overline{\gamma_k(f)\gamma_{k+l}^*(f)} \right\rangle$ where the overbar indicates averaging over *k*.

3.2. Application to the Poisson Process

It is useful to test this expression on a well-known process. Consider a Poisson process

$$z(t) = \sum_k \delta(t - T_k) \tag{3-20}$$

with average rate λ. The PDF of the time between successive pulse is $\lambda e^{-\lambda t}$, and PDF for the time between pulse *k* and pulse $k + l$ is the Erlang PDF, given by

$$p_{\Delta t_l}(t) = \frac{\lambda^l}{(l-1)!} t^{l-1} e^{-\lambda t} \quad t \geq 0 \tag{3-21}$$

With $a_k = 1, \ \forall k$, the PSD is

$$\begin{aligned} S_z(f) &= \lambda\left(1 + \sum_{l<0}\left\langle e^{j2\pi f\Delta t_l}\right\rangle + \sum_{l>0}\left\langle e^{j2\pi f\Delta t_l}\right\rangle\right) = \lambda\left(1 + \sum_{l=1}^{\infty}\left\langle e^{-j2\pi f\Delta t_l}\right\rangle + \left\langle e^{j2\pi f\Delta t_l}\right\rangle\right) \\ &= \lambda\left(1 + \sum_{l=1}^{\infty}\int_0^{\infty}\frac{\lambda^l}{(l-1)!}t^{l-1}e^{-\lambda t}e^{-j2\pi ft}dt + \int_0^{\infty}\frac{\lambda^l}{(l-1)!}t^{l-1}e^{-\lambda t}e^{j2\pi ft}dt\right) \\ &= \lambda\left(1 + \int_0^{\infty}e^{-\lambda t}e^{-j2\pi ft}\sum_{l=1}^{\infty}\frac{\lambda^l}{(l-1)!}t^{l-1}dt + \int_0^{\infty}e^{-\lambda t}e^{j2\pi ft}\sum_{l=1}^{\infty}\frac{\lambda^l}{(l-1)!}t^{l-1}dt\right) \end{aligned} \tag{3-22}$$

Since $\sum_{l=1}^{\infty}\frac{\lambda^l}{(l-1)!}t^{l-1} = \lambda\sum_{l=0}^{\infty}\frac{(\lambda t)^l}{l!} = \lambda e^{\lambda t}$, the PSD is

$$S_z(f) = \lambda + \lambda^2\left(\int_0^{\infty}e^{-j2\pi ft}dt + \int_0^{\infty}e^{j2\pi ft}dt\right) = \lambda + \lambda^2\int_{-\infty}^{\infty}e^{j2\pi ft}dt = \lambda + \lambda^2\delta(f), \tag{3-23}$$

which agrees with results derived elsewhere using a different approach (see [1], p. 321).

3.3. Application to a Fixed-Frame UWB Signal

If the UWB frame duration is *T*, the transmit time of the k^{th} pulse can be expressed as

$$T_k = kT + \varepsilon_k \tag{3-24}$$

Letting $c_k(f) = a_k e^{-j2\pi f\varepsilon_k}$, it clear that $\gamma_k(f) = c_k(f)e^{-j2\pi fkT}$. With

$$R_c[l] \equiv \left\langle c_k(f)c_{k+l}^*(f)\right\rangle \tag{3-25}$$

the power spectral density of the UWB signal is

$$S_w(f) = \frac{|P(f)|^2}{T}\sum_l R_c[l]e^{j2\pi flT} \tag{3-26}$$

The PSD generally consists of both a continuous and a discrete component. These can be extracted from the above expression by expressing the modulation term $c_k(f)$ in terms of its mean value $\mu_c(f)$ and a zero-mean (centered) process $\tilde{c}_k(f) = c_k(f) - \mu_c(f)$. If $\tilde{c}_k(f)$ is white; that is, $\left\langle \tilde{c}_k(f)\tilde{c}_{k+l}^*(f)\right\rangle = \sigma_c^2(f)\delta[l]$, then $R_c[l] = |\mu_c(f)|^2 + \sigma_c^2(f)\delta[l]$ and the PSD is

$$\begin{aligned} S_w(f) &= \frac{1}{T}|P(f)|^2\left\{R_c[0] + |\mu_c(f)|^2\sum_{l\neq 0}e^{j2\pi flT}\right\} \\ &= \frac{1}{T}|P(f)|^2\left\{\sigma_c^2(f) + |\mu_c(f)|^2\sum_{l}e^{j2\pi flT}\right\} \\ &= |P(f)|^2\left\{\frac{\sigma_c^2(f)}{T} + \frac{|\mu_c(f)|^2}{T^2}\sum_k \delta\left(f - \frac{k}{T}\right)\right\} \end{aligned} \tag{3-27}$$

where the final equality follows from the Poisson sum formula. The first term represents the continuous component of the PSD, and the second term the discrete component (spectral lines).

Letting $b_k(f) = e^{-j2\pi f\varepsilon_k}$, it is clear that $c_k(f) = a_k b_k(f)$, and that $\left\langle |c_k(f)|^2\right\rangle = \left\langle |a_k|^2\right\rangle$. As above, it is convenient to define $\tilde{a}_k = a_k - \mu_a$ and $\tilde{b}_k(f) = b_k(f) - \mu_b(f)$. If a_k and $b_k(f)$ are uncorrelated ($\left\langle \tilde{a}_k\tilde{b}_k^*(f)\right\rangle = 0$), then the PSD can be expressed as

$$S_w(f) = |P(f)|^2\left\{\frac{\left\langle |a_k|^2\right\rangle - |\mu_a|^2|\mu_b(f)|^2}{T} + \frac{|\mu_a|^2|\mu_b(f)|^2}{T^2}\sum_k\delta\left(f - \frac{k}{T}\right)\right\} \tag{3-28}$$

Note that the continuous component has minima at frequencies with discrete components, and that if $\mu_a = 0$, then the discrete component vanishes.

This expression is easily modified to include the effects of any frame-by-frame pseudorandom amplitude modulation and dithering using

$$w(t) = \sum_k \alpha_k a_k p(t - kT - \Delta_k - \varepsilon_k) \tag{3-29}$$

where the $\{\alpha_k\}$ and $\{\varepsilon_k\}$ represent the effects of randomizing of the amplitude and position, respectively, and the $\{a_k\}$ and $\{\Delta_k\}$ account for amplitude and pulse-position modulation, respectively. In that case, the above development applies but with $c_k(f) = \alpha_k a_k e^{-j2\pi f(\Delta_k + \varepsilon_k)}$, and the statistical properties of both the modulation and pseudorandom effects can be incorporated into the final PSD expression.

3.4. UWB PSD Examples

To illustrate the application of the expressions developed above, some examples are useful. The intent here is not to be exhaustive, but to demonstrate the process by which the PSD is computed for a specific case. For these examples, it is assumed that there is no amplitude modulation, but that the pulse is position-modulated and pseudorandomly dithered. The UWB signal used is therefore

$$w(t) = \sum_k p(t - kT - \Delta_k - \varepsilon_k) \tag{3-30}$$

3.4.1. UWB Pulse Model

The pulse waveform $p(t)$ has a Fourier transform $P(f)$ and an energy spectral density (ESD) $|P(f)|^2$ joules/Hz. As an example, the first derivative of the Gaussian monocycle is [2]:

$$p(t) = 6 p_{\max} \sqrt{\frac{e\pi}{3}} \frac{t}{\tau} e^{-6\pi(t/\tau)^2} \tag{3-31}$$

which is shown in Figure 3-1. This might represent the output of the UWB antenna, which acts as a high-pass filter.

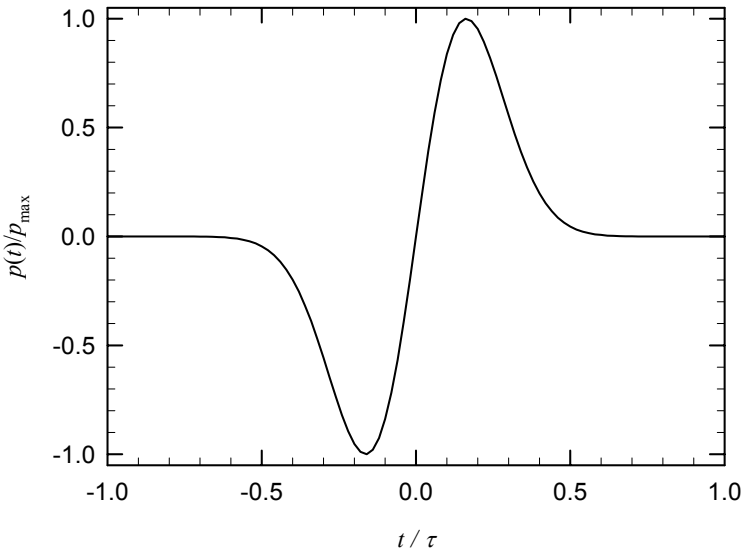

Figure 3-1: *Example of a basic UWB pulse waveform*

Its Fourier transform is

$$P(f) = -j\frac{p_{\max} f\tau^2}{3}\sqrt{\frac{e\pi}{2}}e^{-(f\tau)^2\pi/6} \tag{3-32}$$

and the two-sided energy spectral density is:

$$|P(f)|^2 = p_{\max}^2 f^2\tau^4\,\frac{e\pi}{18}e^{-(f\tau)^2\pi/3}. \tag{3-33}$$

The maximum occurs when $f_m = \frac{1}{\tau}\sqrt{\frac{3}{\pi}}$, so $|P(f)|^2_{\max} = |P(f_m)|^2 = \frac{p_{\max}^2\tau^2}{6}$, and the ESD can be expressed as:

$$|P(f)|^2 = |P(f)|^2_{\max}\cdot a(f) \tag{3-34}$$

where

$$a(f) = (f\tau)^2\,\frac{e\pi}{3}e^{-(f\tau)^2\pi/3}. \tag{3-35}$$

Figure 3-2 shows $\frac{|P(f)|^2}{|P(f)|^2_{\max}}$ for $\tau = 0.5$ ns.

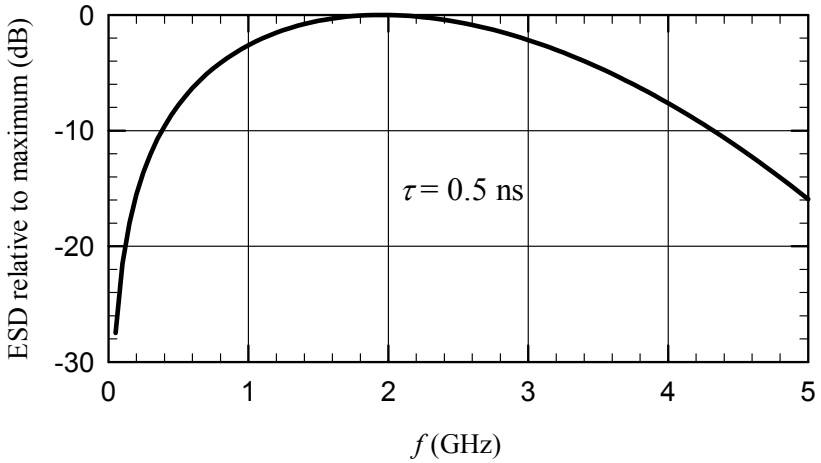

Figure 3-2: *Energy spectral density of the basic pulse of Figure 3-1.*

The total energy in the pulse is

$$E_p = \int_{-\infty}^{\infty} |P(f)|^2 \, df = \frac{p_{\max}^2 e \tau}{4\sqrt{3}} = \frac{e\sqrt{3}}{2\tau} |P(f)|_{\max}^2 \tag{3-36}$$

The average pulse repetition frequency (PRF) is $R = 1/T$ Hz, so the total power in the UWB signal is $\left\langle |a_n|^2 \right\rangle R \cdot E_p$ watts, where $\langle \cdot \rangle$ denotes averaging.

It is also useful to define an equivalent "rectangular" bandwidth for the UWB pulse as:

$$B_{uwb} = \frac{E_p}{2|P(f)|_{\max}^2} = \frac{e\sqrt{3}}{4\tau} = \frac{1.18}{\tau} \tag{3-37}$$

The factor of 2 in the denominator is because $P(f)$ is two-sided (defined for $-\infty < f < \infty$). For $\tau = 0.5\,\text{ns}$, $B_{uwb} = 2.36\,\text{GHz}$.

3.4.2. PSD Calculations

The continuous and discrete components of the PSD are, respectively:

$$S_{wc}(f) = R|P(f)|^2 \left(\left\langle |a_n|^2 \right\rangle - |\mu_a|^2 |\mu_b(f)|^2 \right) \quad \text{watts/Hz} \tag{3-38}$$

$$S_{wd}(f) = R^2 |P(f)|^2 |\mu_a|^2 |\mu_b(f)|^2 \sum_{k=-\infty}^{\infty} \delta(f - kR) \text{ watts/Hz} \quad (3\text{-}39)$$

where $\mu_a = \langle a_n \rangle$ and $\mu_b(f) = \left\langle e^{j2\pi f \Delta_n} \right\rangle$. Note that Δ_n includes shifts in pulse position due to both modulation and dithering. Also note that if the mean value of the amplitude is zero (i.e., $\mu_a = 0$), the discrete component vanishes and there are no spectral lines. On the other hand, if there is no modulation or dithering, the continuous component vanishes and the spectrum consists only of discrete tones.

Note that the continuous PSD is proportional to the pulse rate *R*, and that the power in each discrete spectral component is proportional to R^2, and that the spectral lines occur at multiples of *R*. The detailed fine structure of the PSD is determined by the statistics of the amplitude modulation and position-shifting terms.

The PSD in these expressions represents the *average* power per Hz over a time interval *T*. This averaging is necessary to eliminate the time variable in the expressions, because the UWB signal is *cyclostationary* due to the repetitive frame structure.

The value of these expressions is that they allow the UWB signal generator parameters to be determined that will give a desired UWB spectrum. They also allow the average power output of a narrowband filter with a specified center frequency and impulse response to be calculated.

3.4.3. Numerical Results

To illustrate how these expressions are applied, assume $a_n = 1$, that the time offset due to modulation is ±Δ, and that the time hopping code can place the nominal pulse position at $m\varepsilon_c$, where $0 \le m \le M-1$ and ε_c is the granularity of the code-controlled pulse position. The pulse position is therefore restricted to the interval $(M-1)\varepsilon_c + 2\Delta$, giving the constraint $(M-1)\varepsilon_c + 2\Delta \le T$.

The pulse can appear at positions $\pm\Delta$, $\varepsilon_c \pm \Delta$, $2\varepsilon_c \pm \Delta$, . . . , $(M-1)\varepsilon_c \pm \Delta$, for a total of 2*M* possible positions. If these positions are assumed equally-likely, then:

$$E\left\{e^{j2\pi f \varepsilon_k}\right\} = \frac{1}{2M} \sum_{m=0}^{M-1} \left[e^{j2\pi f (m\varepsilon_c + \Delta)} + e^{j2\pi f (m\varepsilon_c - \Delta)}\right] = \frac{\cos(2\pi f \Delta)}{M} \sum_{m=0}^{M-1} e^{j2\pi f m \varepsilon_c} \quad (3\text{-}40)$$

Since $\sum_{m=0}^{M-1} z^m = \frac{z^M - 1}{z - 1}$, this becomes:

$$E\left\{e^{j2\pi f\varepsilon_k}\right\}=\frac{\cos(2\pi f\Delta)}{M}\frac{e^{j2\pi fM\varepsilon_c}-1}{e^{j2\pi f\varepsilon_c}-1}=\cos(2\pi f\Delta)\frac{\sin(\pi fM\varepsilon_c)}{M\sin(\pi f\varepsilon_c)}e^{j\pi f(M-1)\varepsilon_c} \tag{3-41}$$

Similarly,

$$E\left\{e^{-j2\pi f\varepsilon_k}\right\}=\cos(2\pi f\Delta)\frac{\sin(\pi fM\varepsilon_c)}{M\sin(\pi f\varepsilon_c)}e^{-j\pi f(M-1)\varepsilon_c}\,. \tag{3-42}$$

The continuous PSD component therefore is

$$S_{wc}(f)=R\left|P(f)\right|^2\left\{1-\left[\cos 2\pi f\Delta\frac{\sin(\pi fM\varepsilon_c)}{M\sin(\pi f\varepsilon_c)}\right]^2\right\} \tag{3-43}$$

and the power in the n^{th} discrete spectral component is

$$P_n=R^2\left|P(nR)\right|^2\left[\cos(2\pi n\Delta/T)\frac{\sin(\pi nM\varepsilon_c/T)}{M\sin(\pi n\varepsilon_c/T)}\right]^2 \tag{3-44}$$

A few simple examples serve to show the effect of the parameters on the UWB signal spectrum. A 10 MHz average pulse rate is assumed, with a total signal power of 10 dBm. This is based on the assumed maximum output power of 20 dBm at a rate of 100 MHz. Since the maximum pulse energy is fixed, $P_{uwb}=100R_{MHz}/100$, or the average total power output is equal to the average pulse rate in MHz, assuming no amplitude modulation. Also, for these examples, no PPM is assumed ($\Delta=0$). The spectra are shown in terms of the power output of a filter with a bandwidth of 1 MHz, which is adequate to resolve the spectrum at a 10 MHz pulse rate. This is roughly analogous to the result of sweeping a 1-MHz resolution filter across the band with a spectrum analyzer, with power averaging.

In the first case, it is assumed that $\varepsilon_c=10$ ns, the minimum bin resolution of the MSSI UWB emulator, and that $M=10$, since the UWB frame is 100 ns in this case. It was assumed that pulses are randomly placed on one of the ten 10-ns bins in each frame, per the above derivation. Figure 3-3 shows the result. Note that the spectral lines are 100 MHz apart rather than 10 MHz apart, due to the dithering (100 MHz = $1/\varepsilon_c$). Figure 3-4 shows an expanded view. As would be expected from the relationships developed above, the continuous component is minimized at frequencies where there are spectral lines.

If ε_c is reduced to 2 ns and M is correspondingly increased to 50, then the spectrum shown in Figure 3-5 results. Note that the spectral lines are now 500 MHz apart.

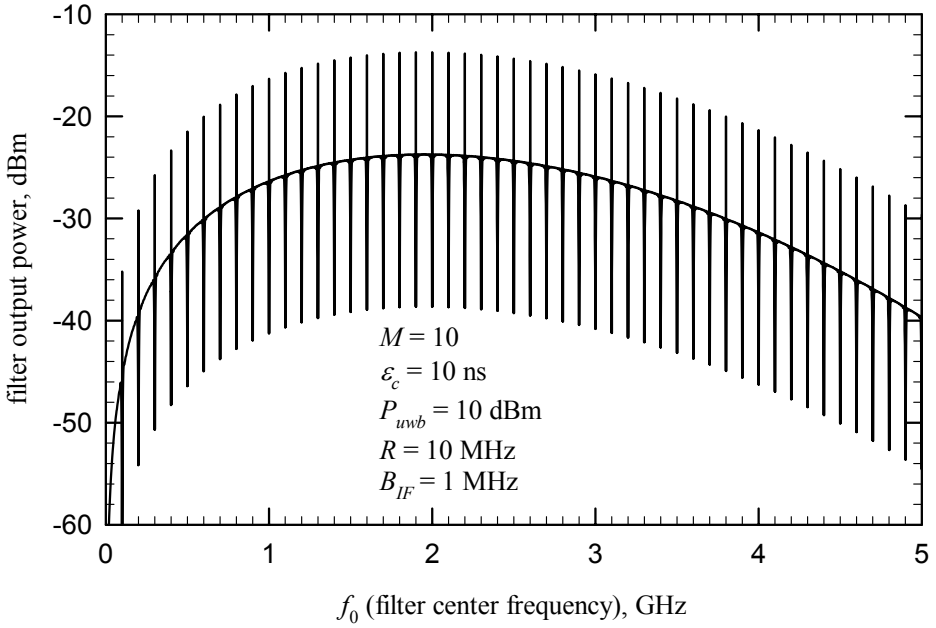

Figure 3-3: *UWB PSD example, as seen through a 1-MHz resolution filter*

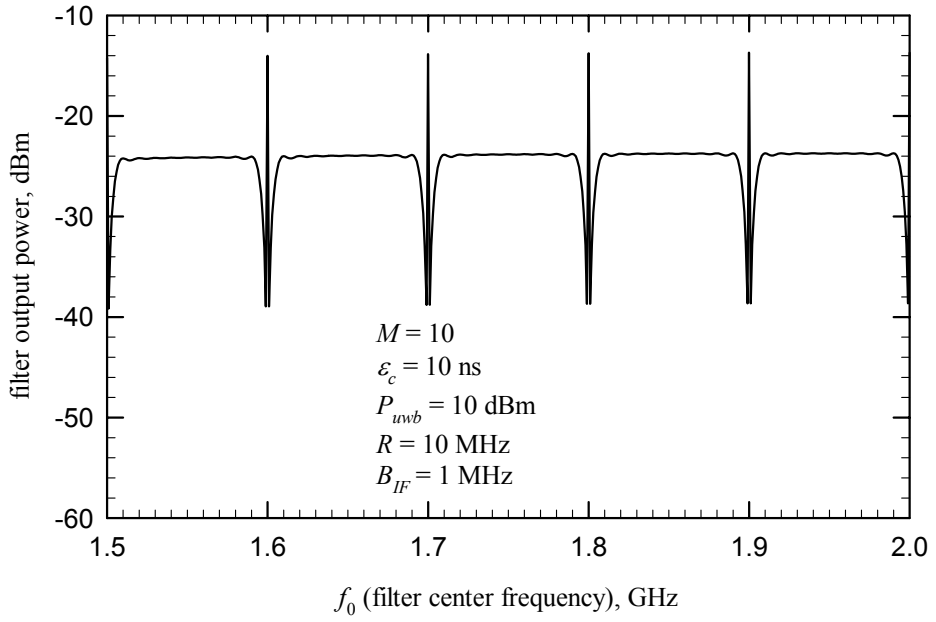

Figure 3-4: *Closeup view of Figure 3-3*

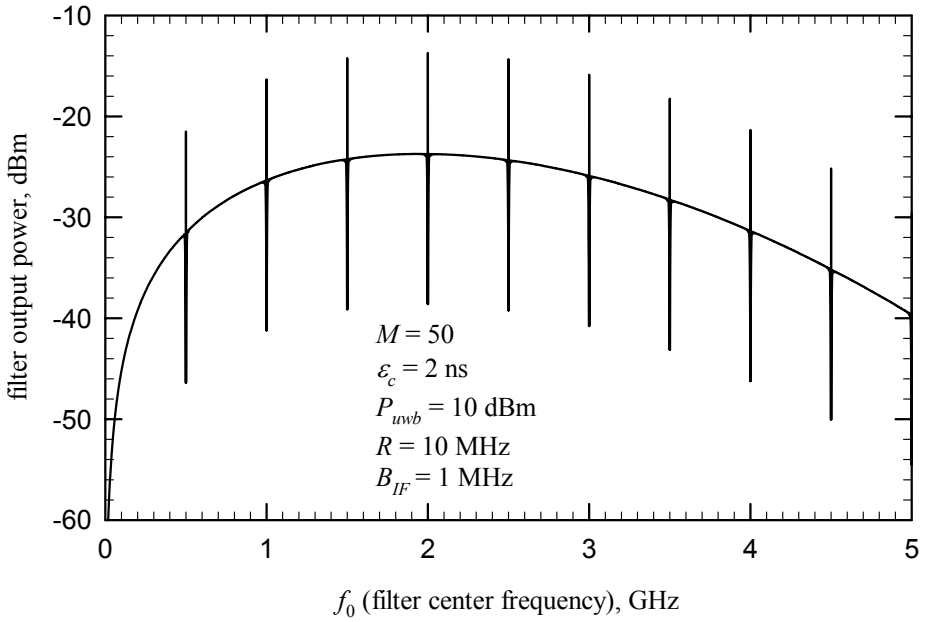

Figure 3-5: *UWB spectrum with a 2-ns dithering code resolution*

If ε_c is maintained at 2 ns but M is reduced to 10, the result is as shown in Figure 3-6, with an expanded view in Figure 3-7. Note that now there are lines every 10 MHz, but the large discrete components still occur every 100 MHz. If PPM is added, with a deviation of $\Delta = 0.2$ ns, the result is shown in Figure 3-8. The difference between Figure 3-8 and Figure 3-6 is the term $\cos^2 2\pi f\Delta$, which has nulls at 1.25 GHz and 3.75 GHz for $\Delta = 0.2$ ns, as shown in Figure 3-9. This term reduces the discrete components near those frequencies.

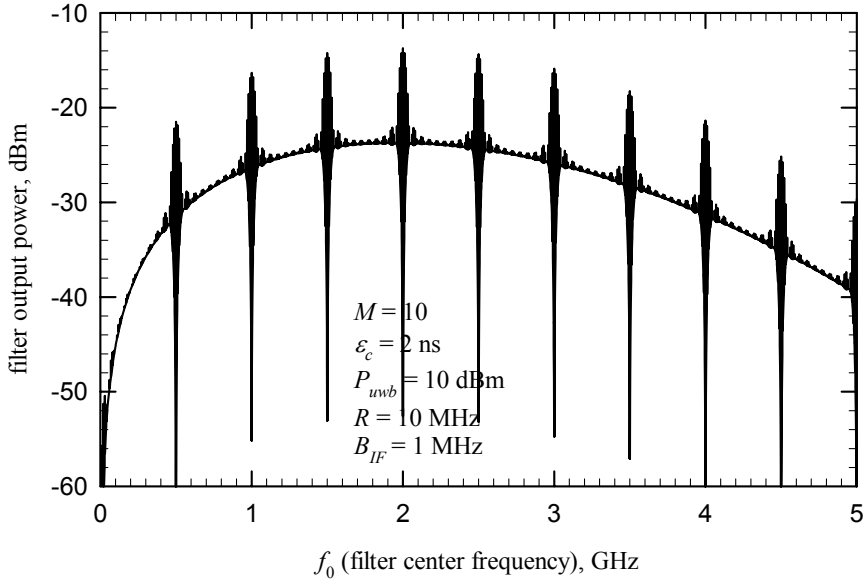

Figure 3-6: *Effect of dithering over only 20% of the UWB frame, with a 2-ns code resolution*

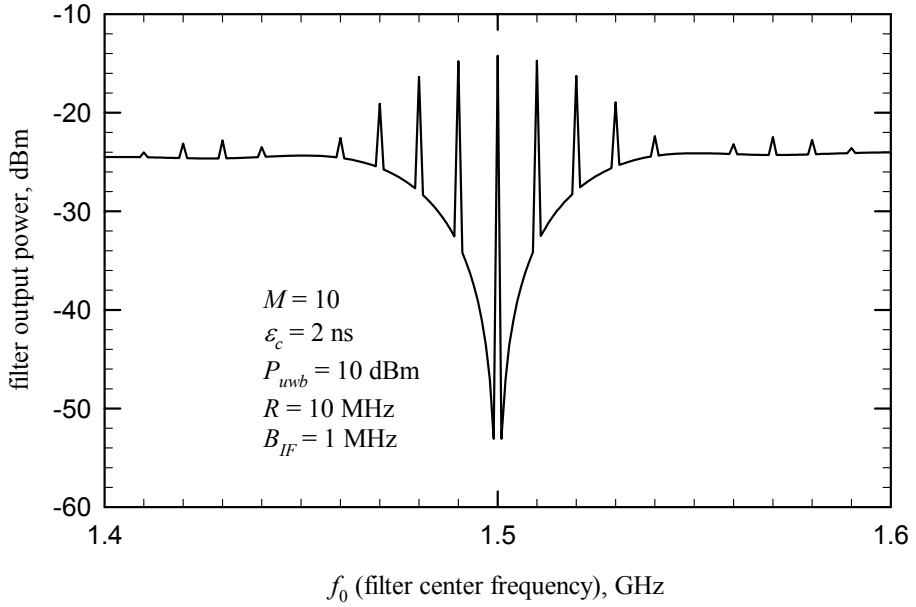

Figure 3-7: *Closeup of the case shown in Figure 3-6.*

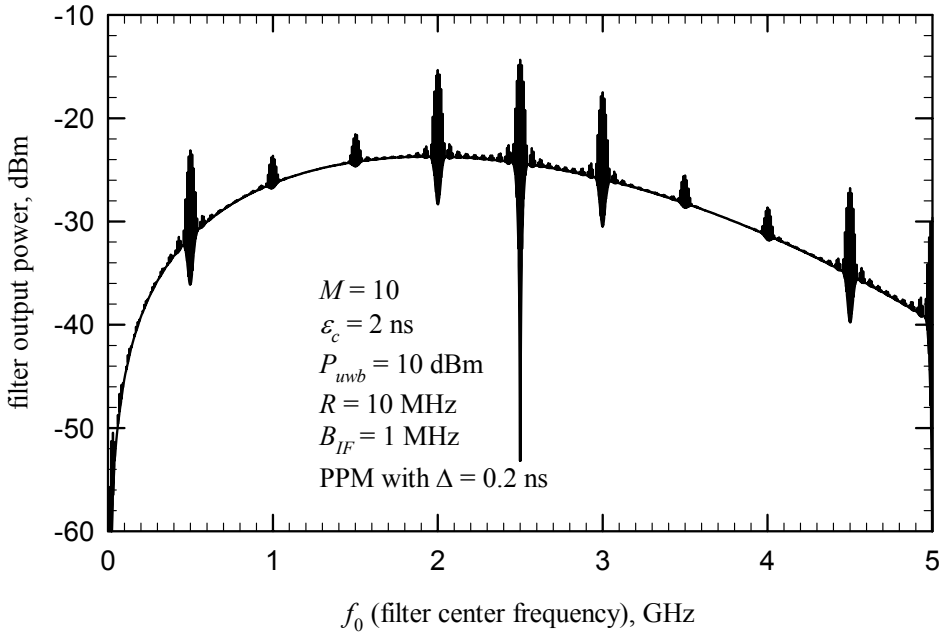

Figure 3-8: *Effect of adding PPM with 0.2-ns deviation*

To summarize, dithering with granularity ε_c produces relatively large spectral lines separated by $\Delta f = 1/\varepsilon_c$. There generally will be smaller spectral lines separated by $1/R$, but these are suppressed by dithering over the entire frame; that is $M\varepsilon_c = 1/R$. If dithering is applied over only a fraction of the frame, then these smaller lines are only partially suppressed. In the limit, with no dithering, they are not suppressed at all.

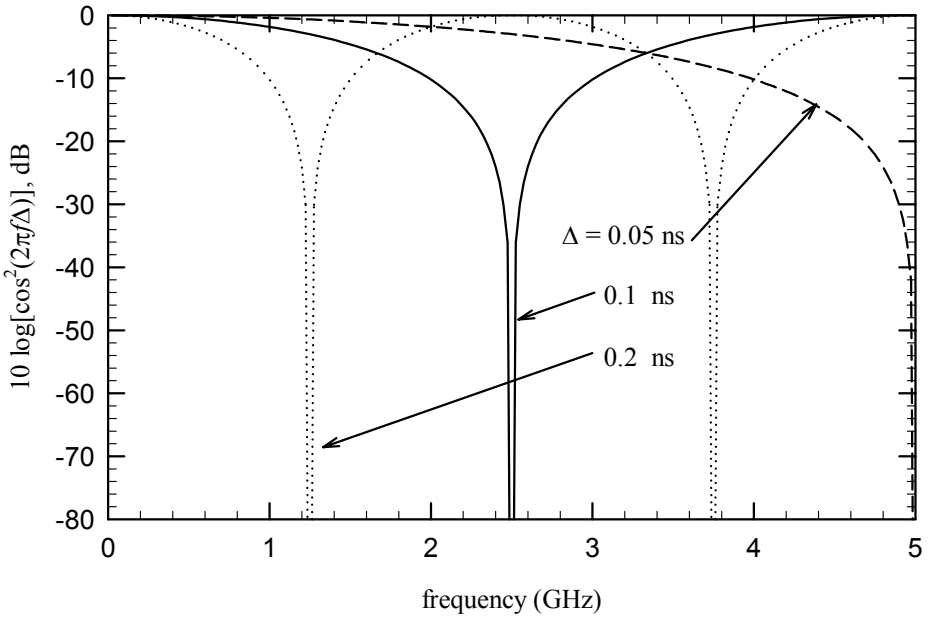

Figure 3-9: *The PPM multiplier* $\cos^2 2\pi f\Delta$

Finally, the term $\left[\frac{\sin(\pi f M\varepsilon_c)}{M\sin(\pi f\varepsilon_c)}\right]^2$ is important to understand. Figure 3-10 shows this term for $M = 25$ and $\varepsilon_c = 2$ ns. The function is periodic with maxima occurring at odd multiples of $1/2\varepsilon_c$. The function is 1 at these maxima (easily verified using L'Hopital's rule).

Figure 3-10: *Example of the time-hopping multiplier* $\left[\frac{\sin(\pi f M\varepsilon_c)}{M\sin(\pi f\varepsilon_c)}\right]^2$ *(dB) vs. frequency.*

Figure 3-11 shows the term $1-\left[\cos 2\pi f\Delta \dfrac{\sin(\pi fM\varepsilon_c)}{M\sin(\pi f\varepsilon_c)}\right]^2$, which is the multiplier for the continuous portion of the spectrum.

Figure 3-11: *The multiplier* $1-\left[\cos 2\pi f\Delta \dfrac{\sin(\pi fM\varepsilon_c)}{M\sin(\pi f\varepsilon_c)}\right]^2$ *for the continuous PSD component.*

Figure 3-12 shows the spectral lines $\left[\cos(2\pi n\Delta/T)\dfrac{\sin(\pi nM\varepsilon_c/T)}{M\sin(\pi n\varepsilon_c/T)}\right]^2\delta\left(f-\dfrac{n}{T}\right)$. Note that the continuous spectrum (Figure 3-11) has minima where the spectral lines are strongest.

Figure 3-12: *Discrete spectral components of the PSD.*

3.5. Uniform Random Pulse Position

In the above examples, it was assumed that the pulse position was limited to a finite number of discrete positions relative to the UWB frame boundary. Here, it is assumed that the pulse can appear anywhere within an interval $[-\alpha/2, +\alpha/2]$, and its position is uniformly-distributed within that interval, then the probability density function of the pulse position is

$$f_{\varepsilon_k}(\varepsilon) = \frac{1}{\alpha}, \quad -\frac{\alpha}{2} \le \varepsilon \le \frac{\alpha}{2} \tag{3-45}$$

and

$$\begin{aligned} E\left\{e^{j2\pi f\varepsilon_k}\right\} &= \frac{1}{\alpha}\int_{-\alpha/2}^{\alpha/2} e^{j2\pi f\varepsilon}\,d\varepsilon = \frac{1}{2j\pi f\alpha}\left(e^{j\pi f\alpha} - e^{j\pi f\alpha}\right) \\ &= \frac{\sin(\pi f\alpha)}{\pi f\alpha} = \operatorname{sinc}(\pi f\alpha) \end{aligned} \tag{3-46}$$

The same result applies to $E\left\{e^{-j2\pi f\varepsilon_k}\right\}$. Therefore, the continuous PSD component is

$$S_p^c(f) = \frac{1}{T}\phi_v(f)\left[1 - \text{sinc}^2(\pi f\alpha)\right], \tag{3-47}$$

and the power in the spectral component at frequency n/T is

$$P_n = \frac{1}{T^2}\phi_v\left(\frac{n}{T}\right)\text{sinc}^2\left(\pi\frac{n}{T}\alpha\right). \tag{3-48}$$

Note that if $\alpha = T$; that is, the pulse can appear anywhere in the UWB frame, then the spectral lines vanish except at $f = 0$. If $\alpha = aT, a < 1$, then

$$P_n = \frac{1}{T^2}\phi_v\left(\frac{n}{T}\right)\text{sinc}^2(\pi na). \tag{3-49}$$

While in general there will be spectral lines, the multiplier $\text{sinc}^2(\pi na)$ decays rapidly with frequency. The line frequencies are $f_n = n/T$, so if $T = 100$ ns , then $n = 100 f_{\text{GHz}}$. For example, at 1 GHz, the multiplier is $\text{sinc}^2(100\pi a)$. To show the effect of the $\text{sinc}^2(\pi na)$ multiplier term, Figure 3-13 shows $1/(\pi na)^2$ in dB vs. frequency. Since $\text{sinc}^2(\pi na) = \sin^2(\pi na)/(\pi na)^2$, the curves in Figure 3-13 represent an upper bound on the $\text{sinc}^2(\pi na)$ term, which oscillates as a function of frequency.

Figure 3-13: *Upper bound on the multiplier* $\text{sinc}^2(\pi na)$ *vs. frequency.*

Note that the previous "discrete" position case approaches this "continuous" pulse position case if $\Delta = 0$, $M\varepsilon_c = \alpha$, and $M \to \infty$.

3.6. Generalized UWB Signal Model

While the model developed above is fairly simple, it does not account for the possibility of multi-frame information symbols or finite-length pseudorandom dithering codes that repeat. A more general UWB signal model is

$$w(t) = \sum_n a_n v_n(t - nT - \Delta_n) \tag{3-50}$$

where a_n and Δ_n represent the amplitude and position modulation, respectively, for the n^{th} symbol and $v_n(t)$ is non-zero only for $0 \le t \le t_v$, with $t_v + \Delta_{\max} \le T$. In general,

$$v_n(t) = \sum_{m=0}^{M-1} \alpha_{n,m} p(t - mT_f - \varepsilon_{n.m}) \tag{3-51}$$

where T_f is the UWB frame interval, $\varepsilon_{n,m}$ and $\alpha_{n,m}$ are respectively the dithering delay and amplitude for frame *m* of waveform *n*, and $p(t)$ is the elemental pulse waveform. Note that $T = MT_f$. The Fourier transform of $v_n(t)$ is

$$V_n(f) = \sum_{m=0}^{M-1} P(f)\beta_{n,m} e^{-j2\pi m T_f} \tag{3-52}$$

where $\beta_{n,m} = \alpha_{n,m} e^{-j2\pi\varepsilon_{n,m}}$.

The $\{\varepsilon_{n,m}\}$ and $\{\alpha_{n,m}\}$ can be modeled as random or deterministic, as appropriate. The latter case pertains to a finite-length pseudorandom dithering code, which can be described as

$$q(t) = \sum_{n=0}^{N-1} v_n(t - nT) \tag{3-53}$$

In this case, $v_n(t) = v_{N+n}(t)$ and $q(t) = q(t + NT) = q(t + NMT_f)$.

Also note that

$$Q(f) = \sum_{n=0}^{N-1} V_n(f) e^{-j2\pi fnT} \tag{3-54}$$

and

$$|Q(f)|^2 = \sum_{n=0}^{N-1}\sum_{m=0}^{N-1} V_n(f) V_m^*(f) e^{j2\pi(m-n)fT} \tag{3-55}$$

3.7. PSD of the Generalized UWB Signal

There are two cases that must be considered. The first is that of a non-periodic (random) dithering code. In this case, the $\{\alpha_{n,m}\}$ and $\{\varepsilon_{n,m}\}$ are modeled as random. As shown in Annex 3B, the PSD in this case is

$$S_w(f) = \frac{1}{T}\sum_l R_c[l] R_V[l] e^{j2\pi flT} \tag{3-56}$$

where $R_V[l] \equiv \langle V_n(f) V_{n+l}^*(f) \rangle$.

With a periodic dithering code, the process has a period of *NT*, and as shown in Annex 3B, the general expression for the PSD is:

$$S_w(f) = \frac{1}{NT}\sum_l R_c[l] e^{j2\pi flT} \sum_{k=0}^{N-1} V_n(f) V_{n+l}^*(f) \tag{3-57}$$

Both of these cases are developed in more detail below.

3.8. Detailed Development

3.8.1. Case 1: Periodic Dithering Code

Assuming as above that $R_c[l] = |\mu_c(f)|^2 + \sigma_c^2(f)\delta[l]$, the PSD is

$$S_w(f) = \frac{1}{NT}\left[\sigma_c^2(f)\sum_{n=0}^{N-1}|V_n(f)|^2 + |\mu_c(f)|^2 \sum_l e^{j2\pi flT}\sum_{n=0}^{N-1} V_n(f) V_{n+l}^*(f)\right] \tag{3-58}$$

The second term can be put into a more useful form using $\sum_{i=-\infty}^{\infty} g[i] = \sum_{k=-\infty}^{\infty}\sum_{m=0}^{N-1} g[m-kN]$:

$$\begin{aligned}
&\sum_l e^{j2\pi flT}\sum_{n=0}^{N-1}V_n(f)V_{n+l}^*(f)=\sum_{n=0}^{N-1}V_n(f)\sum_l e^{j2\pi flT}V_{n+l}^*(f)\\
&=\sum_{n=0}^{N-1}V_n(f)\sum_i e^{j2\pi f(i-n)T}V_i^*(f)=\sum_{n=0}^{N-1}V_n(f)\sum_{k=-\infty}^{\infty}\sum_{m=0}^{N-1}e^{j2\pi f(m-kN-n)T}V_{m+kN}^*(f)\\
&=\sum_{n=0}^{N-1}V_n(f)\sum_{k=-\infty}^{\infty}e^{-j2\pi fkNT}\sum_{m=0}^{N-1}e^{j2\pi f(m-n)T}V_{m+kN}^*(f)\\
&=\sum_{n=0}^{N-1}\sum_{m=0}^{N-1}V_n(f)V_m^*(f)e^{j2\pi f(m-n)T}\sum_{k=-\infty}^{\infty}e^{-j2\pi fkNT}\\
&=\frac{1}{NT}\sum_{n=0}^{N-1}\sum_{m=0}^{N-1}V_n(f)V_m^*(f)e^{j2\pi f(m-n)T}\sum_{k=-\infty}^{\infty}\delta\left(f-\frac{k}{NT}\right)
\end{aligned} \tag{3-59}$$

where the final equality uses the Poisson sum formula.

Recalling that $|Q(f)|^2=\sum_{n=0}^{N-1}\sum_{m=0}^{N-1}V_n(f)V_m^*(f)e^{j2\pi(m-n)fT}$ gives the PSD as

$$S_w(f)=\frac{1}{NT}\sigma_c^2(f)\sum_{n=0}^{N-1}|V_n(f)|^2+\left(\frac{1}{NT}\right)^2|\mu_c(f)|^2|Q(f)|^2\sum_k\delta\left(f-\frac{k}{NT}\right) \tag{3-60}$$

The continuous and discrete components therefore are:

$$\begin{aligned}
S_{w,C}(f)&=\frac{1}{NT}\sigma_c^2(f)\sum_{n=0}^{N-1}|V_n(f)|^2\\
S_{w,D}(f)&=\left(\frac{1}{NT}\right)^2|\mu_c(f)|^2|Q(f)|^2\sum_k\delta\left(f-\frac{k}{NT}\right)
\end{aligned} \tag{3-61}$$

Note that, as in the simpler case, if the modulation term is zero-mean ($\mu_c(f)=0$), the discrete component vanishes. As in (3-28), if a_n and $b_n(f)$ are uncorrelated, then (3-61) can be written as:

$$\begin{aligned}
S_{w,C}(f)&=\frac{1}{NT}\left[\left\langle|a_n|^2\right\rangle-|\mu_a|^2|\mu_b(f)|^2\right]\sum_{n=0}^{N-1}|V_n(f)|^2\\
S_{w,D}(f)&=\left(\frac{1}{NT}\right)^2|\mu_a|^2|\mu_b(f)|^2|Q(f)|^2\sum_k\delta\left(f-\frac{k}{NT}\right)
\end{aligned} \tag{3-62}$$

3.8.2. Case 2: Random Dithering Code

With a random dithering code

$$R_V[l] = \left\langle V_n(f) V_{n+l}^*(f) \right\rangle = |P(f)|^2 \sum_{m=0}^{M-1} e^{-j2\pi f m T_f} \sum_{k=0}^{M-1} e^{j2\pi f k T_f} \left\langle \beta_{n,m}(f) \beta_{n+l,k}^*(f) \right\rangle \tag{3-63}$$

Letting $\tilde{\beta}_{n,m}(f) = \beta_{n,m}(f) - \mu_\beta(f)$, where $\mu_\beta(f) = \left\langle \beta_{n,m}(f) \right\rangle$, and assuming that $\beta_{n,m}(f)$ and $\beta_{n+l,k}(f)$ are uncorrelated if $l \neq 0$ or $m \neq k$, then

$$\left\langle \beta_{n,m}(f) \beta_{n+l,k}^*(f) \right\rangle = \left| \mu_\beta(f) \right|^2 + \sigma_\beta^2 \delta[l] \delta[m-k] \tag{3-64}$$

For $l \neq 0$,

$$\begin{aligned} R_V[l \neq 0] &= \left\langle V_n(f) V_{n+l}^*(f) \right\rangle = |P(f)|^2 \left| \mu_\beta(f) \right|^2 \sum_{m=0}^{M-1} e^{-j2\pi f m T_f} \sum_{k=0}^{M-1} e^{j2\pi f k T_f} \\ &= |P(f)|^2 \left| \mu_\beta(f) \right|^2 \left(\frac{\sin \pi f M T_f}{\sin \pi f T_f} \right)^2 \end{aligned} \tag{3-65}$$

If $l = 0$, then

$$\begin{aligned} R_V[0] &= \left\langle |V_n(f)|^2 \right\rangle = |P(f)|^2 \left[M\sigma_\beta^2(f) + \left| \mu_\beta(f) \right|^2 \sum_{m=0}^{M-1} e^{-j2\pi f m T_f} \sum_{k=0}^{M-1} e^{j2\pi f k T_f} \right] \\ &= |P(f)|^2 \left[M\sigma_\beta^2(f) + \left| \mu_\beta(f) \right|^2 \left(\frac{\sin \pi f M T_f}{\sin \pi f T_f} \right)^2 \right] \end{aligned} \tag{3-66}$$

Therefore,

$$R_V[l] = |P(f)|^2 \left[\delta[l] M\sigma_\beta^2(f) + \left| \mu_\beta(f) \right|^2 \left(\frac{\sin \pi f M T_f}{\sin \pi f T_f} \right)^2 \right] \tag{3-67}$$

The PSD therefore is:

$$S_w(f) = \frac{1}{T}\sum_l R_c[l]R_V[l]e^{j2\pi flT} = \frac{1}{T}|P(f)|^2 R_c[0]\left[M\sigma_\beta^2(f) + |\mu_\beta(f)|^2\left(\frac{\sin \pi fMT_f}{\sin \pi fT_f}\right)^2\right]$$
$$+ \frac{1}{T}|P(f)|^2|\mu_\beta(f)|^2\left(\frac{\sin \pi fMT_f}{\sin \pi fT_f}\right)^2 \sum_{l\neq 0} R_c[l]e^{j2\pi flT}$$
$$= \frac{1}{T}|P(f)|^2\left\{R_c[0]M\sigma_\beta^2(f) + |\mu_\beta(f)|^2\left(\frac{\sin \pi fMT_f}{\sin \pi fT_f}\right)^2 \sum_l R_c[l]e^{j2\pi flT}\right\} \quad (3\text{-}68)$$

With $R_c[l] = |\mu_c(f)|^2 + \sigma_c^2(f)\delta[l]$, this becomes:

$$S_w(f) = \frac{1}{T}|P(f)|^2\left\{R_c[0]M\sigma_\beta^2(f) + \sigma_c^2(f)|\mu_\beta(f)|^2\left(\frac{\sin \pi fMT_f}{\sin \pi fT_f}\right)^2\right\}$$
$$+ \frac{1}{T}|P(f)|^2|\mu_c(f)|^2|\mu_\beta(f)|^2\left(\frac{\sin \pi fMT_f}{\sin \pi fT_f}\right)^2 \sum_l e^{j2\pi flT} \quad (3\text{-}69)$$

Finally, applying the Poisson sum formula gives:

$$S_w(f) = \frac{1}{T}|P(f)|^2\left\{R_c[0]M\sigma_\beta^2(f) + \sigma_c^2(f)|\mu_\beta(f)|^2\left(\frac{\sin \pi fMT_f}{\sin \pi fT_f}\right)^2\right\}$$
$$+ \frac{1}{T^2}|P(f)|^2|\mu_c(f)|^2|\mu_\beta(f)|^2\left(\frac{\sin \pi fMT_f}{\sin \pi fT_f}\right)^2 \sum_k \delta\left(f - \frac{k}{T}\right) \quad (3\text{-}70)$$

Annex 3A

Proof of ESD Derivative and ESD Difference Techniques for PSD Calculation

Consider a random process $y(t)$ that starts at time t_0. Its Fourier transform, observed at time *t*, is:

$$Y(f,t) \equiv \int_{t_0}^{t} y(\tau) e^{-j2\pi f\tau} d\tau \,. \tag{3A-1}$$

Clearly, $Y(f,t)$ is a random process, since it is derived from the process $y(t)$. The accumulated energy spectral density at time t is:

$$|Y(f,t)|^2 = Y(f,t)Y^*(f,t) = \int_{t_0}^{t} dt_2 \int_{t_0}^{t} y(t_1) y^*(t_2) e^{-j2\pi f(t_1-t_2)} dt_1 \,. \tag{3A-2}$$

Defining the autocorrelation as $R_y(t,\tau) = \langle y(t) y^*(t-\tau) \rangle$, which applies to both stationary and cyclostationary processes, the expected value of $|Y(f,t)|^2$ is:

$$\left\langle |Y(f,t)|^2 \right\rangle = \int_{t_0}^{t} dt_2 \int_{t_0}^{t} R_y(t_1, t_1 - t_2) e^{-j2\pi f(t_1-t_2)} dt_1 \,. \tag{3A-3}$$

Substituting $\tau = t_1 - t_2$ and $\xi = t_1 + t_2$ (see Figure 3A-1), the area element in the new coordinate system is

$$d\tau d\xi = \left| \frac{\partial\tau}{\partial t_1}\frac{\partial\xi}{\partial t_2} - \frac{\partial\tau}{\partial t_2}\frac{\partial\xi}{\partial t_1} \right| dt_1 dt_2 = 2 dt_1 dt_2 \,, \tag{3A-4}$$

and (3A-3) becomes:

$$\left\langle |Y(f,t)|^2 \right\rangle = \frac{1}{2} \int_{t_0 - t}^{t - t_0} e^{-j2\pi f\tau} d\tau \int_{2t_0 + |\tau|}^{2t - |\tau|} R_y\left(\frac{\xi + \tau}{2}, \tau \right) d\xi \,. \tag{3A-5}$$

Without loss of generality, $t_0 = -\infty$, giving

$$\left\langle \left|Y(f,t)\right|^2 \right\rangle = \frac{1}{2}\int_{-\infty}^{\infty} e^{-j2\pi f\tau}\, d\tau \int_{-\infty}^{2t-|\tau|} R_y\left(\frac{\xi+\tau}{2},\tau\right) d\xi \tag{3A-6}$$

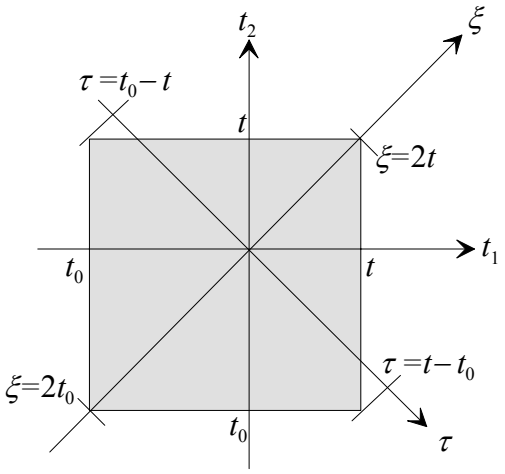

Figure 3A-1: *Coordinate transformation*

If $y(t)$ is stationary, then the autocorrelation is a function of τ only, and

$$\left\langle \left|Y(f,t)\right|^2 \right\rangle = \frac{1}{2}\int_{-\infty}^{\infty} R_y(\tau) e^{-j2\pi f\tau}\, d\tau \int_{-\infty}^{2t-|\tau|} d\xi \tag{3A-7}$$

In that case,

$$\frac{d}{dt}\left\langle \left|Y(f,t)\right|^2 \right\rangle = \int_{-\infty}^{\infty} R_y(\tau) e^{-j2\pi f\tau}\, d\tau = S_y(f) \tag{3A-8}$$

where $S_y(f)$ is the power spectral density of $y(t)$.

Now consider a cyclostationary process $x(t)$ with period *T*, meaning that $R_x(t,\tau) = R_x(t+kT,\tau)$, where *k* is any integer. Then from (A-6),

$$\frac{d}{dt}\left\langle \left|X(f,t)\right|^2 \right\rangle = \frac{1}{2}\int_{-\infty}^{\infty} e^{-j2\pi f\tau}\, \frac{d}{dt}\left\{ \int_{-\infty}^{2t-|\tau|} R_x\left(\frac{\xi+\tau}{2},\tau\right) d\xi \right\} d\tau\,. \tag{3A-9}$$

Since

$$\frac{d}{dt}\left\{\int_{-\infty}^{2t-|\tau|} R_x\left(\frac{\xi+\tau}{2},\tau\right)d\xi\right\} = \begin{cases} 2R_x(t,\tau) & \tau \geq 0 \\ 2R_x(t+\tau,\tau) & \tau \geq 0 \end{cases}, \tag{3A-10}$$

and

$$R_x^*(t,\tau) = R_x(t-\tau,-\tau), \tag{3A-11}$$

(3A-9) becomes

$$\frac{d}{dt}\left\langle |X(f,t)|^2 \right\rangle = \int_0^\infty \left[R_x(t,\tau)e^{-j2\pi f\tau} + R_x^*(t,\tau)e^{j2\pi f\tau}\right]d\tau \tag{3A-12}$$

Note that $\frac{d}{dt}\left\langle |X(f,t)|^2 \right\rangle \neq \int_{-\infty}^{\infty} R_x(t,\tau)e^{-j2\pi f\tau}\,d\tau$, which in general has an imaginary component, since $R_x(t,\tau) \neq R_x^*(t,-\tau)$, and therefore cannot represent a power spectrum.

The PSD of a cyclostationary process generally is represented as a time-average over one period, that is,

$$S_x(f) = \frac{1}{T}\int_t^{t+T} du \int_{-\infty}^{\infty} R_x(u,\tau)e^{-j2\pi f\tau}d\tau = \int_{-\infty}^{\infty} \overline{R_x}(\tau)e^{-j2\pi f\tau}d\tau \tag{3A-13}$$

where $\overline{R_x}(\tau) = \frac{1}{T}\int_t^{t+T} R_x(u,\tau)du$ is the time-average autocorrelation function. From (3A-11), $\overline{R_x^*}(\tau) = \overline{R_x}(-\tau)$ and

$$\begin{aligned} \frac{1}{T}\int_t^{t+T}\left\{\frac{d}{du}\left\langle |X(f,u)|^2\right\rangle\right\}du &= \frac{1}{T}\int_t^{t+T}\left\{\int_0^\infty \left[R_x(u,\tau)e^{-j2\pi f\tau} + R_x^*(u,\tau)e^{j2\pi f\tau}\right]d\tau\right\}du \\ &= \frac{1}{T}\int_0^\infty \left[\overline{R_x}(\tau)e^{-j2\pi f\tau} + \overline{R_x}(-\tau)e^{j2\pi f\tau}\right]d\tau = \frac{1}{T}\int_{-\infty}^{\infty}\overline{R_x}(\tau)e^{-j2\pi f\tau}d\tau \\ &= S_x(f) \end{aligned} \tag{3A-14}$$

Therefore,

$$S_x(f) = \frac{1}{T}\int_t^{t+T}\left\{\frac{d}{du}\left\langle |X(f,u)|^2\right\rangle\right\}du = \frac{1}{T}\left\{\left\langle |X(f,t+T)|^2\right\rangle - \left\langle |X(f,t)|^2\right\rangle\right\} \tag{3A-15}$$

Annex 3B

Derivation of the PSD for the Generalized UWB Signal using the ESD Difference Method

This Annex derives expressions for the power spectral density of the generalized UWB signal

$$w(t) = \sum_n a_n v_n(t - nT - \Delta_n) \tag{3B-1}$$

where the $\{a_n\}$ (amplitude modulation) and $\{\Delta_n\}$ (position modulation) terms generally are modeled as discrete processes with prescribed statistical properties, and the waveform $v(t)$ is non-zero for $0 \le t \le t_v$ only, with $t_v + \Delta_{\max} \le T$.

In this case, $v_n(t)$ is a dithering "sub-code", defined as

$$v_n(t) = \sum_{m=0}^{M-1} \alpha_{n,m} p(t - mT_f - \varepsilon_{n.m}) \tag{3B-2}$$

As shown in Annex 3A, with $W(f,t) \equiv \int_{-\infty}^{t} w(\tau) e^{-j2\pi f\tau} d\tau$, the PSD can be expressed as

$$S_w(f) = \frac{1}{T}\left\{\left\langle |W(f,t+T)|^2 \right\rangle - \left\langle |W(f,t)|^2 \right\rangle\right\} \tag{3B-3}$$

For the UWB signal,

$$\begin{aligned} W(f,t) &= \int_{-\infty}^{t} \sum_n a_n v_n(\tau - nT - \Delta_n) e^{-j2\pi f\tau} d\tau \\ &= \sum_n a_n e^{-j2\pi fnT} e^{-j2\pi f\Delta_n} V_n(f, t - nT - \Delta_n) = \sum_n a_c e^{-j2\pi fnT} V_n(f, t - nT - \Delta_n) \end{aligned} \tag{3B-4}$$

where $V_n(f,t) = \int_{-\infty}^{t} v_n(\tau) e^{-j2\pi f\tau} d\tau$ and $c_n = a_n e^{-j2\pi f\Delta_n}$.

Since $v_n(t)$ is limited to the time interval $0 \le t \le t_v$, $V_n(f, mT - \Delta) = V_n(f)$ if $mT - \Delta \ge t_v$, or $mT \ge t_v + \Delta$. Given the specified constraint $t_v + \Delta_{\max} \le T$, this means

that $V_n(f, mT-\Delta) = V_n(f)$ for $m \geq 1$. Hence, $V_n(f, mT-\Delta) = V_n(f)U[m-1]$, where $U[m]$ is the discrete step function, defined as

$$U[m] = \begin{cases} 1, & m \geq 0 \\ 0, & m < 0 \end{cases} \tag{3B-5}$$

Therefore,

$$W(f,(k+1)T) = \sum_n c_n V_n(f) e^{-j2\pi f n T} U[k-n] \tag{3B-6}$$

and the corresponding energy spectral density at time $(k+1)T$ is:

$$|W(f,(k+1)T)|^2 = \sum_n \sum_m c_n c_m^* V_n(f) V_m^*(f) e^{j2\pi f(m-n)T} U[k-n]U[k-m]. \tag{3B-7}$$

Letting $R_c[m-n] = \langle c_n c_m^* \rangle$, $R_V[m-n] = \langle V_n(f) V_m^*(f) \rangle$, and $l = m-n$, the average ESD at time $(k+1)T$ is

$$\left\langle |W(f,(k+1)T)|^2 \right\rangle = \sum_l R_c[l] R_V[l] e^{j2\pi f l T} \sum_n U[k-n]U[k-n-l], \tag{3B-8}$$

and from the PSD is

$$\begin{aligned} S_w(f) &= \frac{1}{T}\left\{ \left\langle |W(f,(k+1)T)|^2 \right\rangle - \left\langle |W(f,kT)|^2 \right\rangle \right\} \\ &= \frac{1}{T} \sum_l R_c[l] R_V[l] e^{j2\pi f l T} \sum_n U[k-n]U[k-n-l] - U[k-1-n]U[k-1-n-l] \end{aligned} \tag{3B-9}$$

Noting that $U[k-n]U[k-n-l] = U[l]U[k-n-l] + U[-l-1]U[k-n]$, and that $U[k-n] - U[k-1-n] = \delta[k-n]$ where $\delta[n]$ is the Kronecker delta function, the PSD becomes:

$$\begin{aligned} S_w(f) &= \frac{1}{T} \sum_l R_c[l] R_V[l] e^{j2\pi f l T} \sum_n U[l]\delta[k-n-l] + U[-l-1]\delta[k-n] \\ &= \frac{1}{T} \sum_l R_c[l] R_V[l] e^{j2\pi f l T} \left(U[l] + U[-1-l] \right) \\ &= \frac{1}{T} \sum_l R_c[l] R_V[l] e^{j2\pi f l T} \end{aligned} \tag{3B-10}$$

Note that if $v_n(t) = v(t)$ then $R_V[l] = |V(f)|^2$ and $S_w(f) = \frac{1}{T}|V(f)|^2 \sum_l R_c[l] e^{j2\pi flT}$.

In the simplest case, if $v(t) = p(t)$, then $S_w(f) = \frac{1}{T}|P(f)|^2 \sum_l R_c[l] e^{j2\pi flT}$, which is the same as the result derived previously for the basic UWB signal format.

With a periodic dithering code, the process has a period of *NT*, and the PSD is:

$$\begin{aligned} S_w(f) &= \frac{1}{NT}\left\{\left\langle |W(f,(K+N)T)|^2 \right\rangle - \left\langle |W(f,KT)|^2 \right\rangle\right\} \\ &= \frac{1}{NT}\sum_{k=K}^{K+N-1}\left\langle |W(f,(k+1)T)|^2 \right\rangle - \left\langle |W(f,kT)|^2 \right\rangle \end{aligned} \tag{3B-11}$$

Following (10), the PSD is

$$\begin{aligned} S_w(f) &= \frac{1}{NT}\sum_l R_c[l] e^{j2\pi flT} \\ &\times \sum_{k=K}^{K+N-1}\sum_n V_n(f) V_{n+l}^*(f)\left(U[l]\delta[k-n-l] + U[-l-1]\delta[k-n]\right) \\ &= \frac{1}{NT}\sum_l R_c[l] e^{j2\pi flT} U[l]\sum_{k=K}^{K+N-1} V_{k-l}(f) V_k^*(f) + U[-l-1]\sum_{k=K}^{K+N-1} V_k(f) V_{k+l}^*(f) \end{aligned} \tag{3B-12}$$

Since $V_k(f) = V_{k+mN}(f)$,

$$\sum_{k=K}^{K+N-1} V_{k-l}(f) V_k^*(f) = \sum_{k=K}^{K+N-1} V_k(f) V_{k+l}^*(f) = \sum_{k=0}^{N-1} V_n(f) V_{n+l}^*(f) \tag{3B-13}$$

for any integer *m*, and the PSD reduces to:

$$S_w(f) = \frac{1}{NT}\sum_l R_c[l] e^{j2\pi flT} \sum_{k=0}^{N-1} V_n(f) V_{n+l}^*(f) \tag{3B-14}$$

Annex 3C

Analysis of Generalized UWB PSD Using the Method of Romme and Piazzo [3]

Part I: Model Development

Introduction

Earlier works on the Power Spectral Density (PSD) of Ultra-Wideband (UWB) waveforms did not consider the effect of pulse repetition per information symbol (which results in integration gain) and the periodicity of the pseudo-random time-hopping (TH) code (see e.g., [4]). However, the treatment in [3] is the most general reported thus far in that it accounts for both of the above-mentioned UWB waveform parameters. Therefore, following the methodology sketched in [3], this Annex verifies the main result reported therein by providing a more detailed and rigorous derivation of the PSD for a general UWB waveform. The generalized PSD expression accounts for the following parameters:

1. Arbitrary UWB pulse shape and repetition discipline
2. Amenable to PAM and PPM modulation schemes or a combination thereof
3. Arbitrary TH code with a finite period
4. Pulse repetitions per data symbol (integration gain)

The generalized PSD expression derived in this report may be viewed as more of methodology to compute the PSD rather than an expression, which explicitly shows the dependence of the UWB waveform parameters on the power spectrum. Therefore, to gain insight into the effect of various parameters on the spectra, it is necessary to perform simulations using this result. Since there is value in showing analytically the influence of the various parameters, in Part II of this Annex, the dependence of the PSD on the waveform parameters and the code and modulation statistics will be explicitly shown. The analytical treatment in Part II uses the generalized PSD expression derived here as the starting point.

UWB Waveform Model

This section presents the UWB signal model in terms of the waveform parameters. This model will form the basis for the PSD derivation that follows in the next section. Since the largest periodicity is due to that of the TH code, it is this period that will be used to form a synthetic waveform comprising of many elementary UWB pulses as shown in Figure 3C-1. A period of the TH code, denoted by T_{TH}, is assumed to contain N_s equally sized bins of duration T_s such that $N_s T_s \le T_{TH}$. Each T_s contains one information symbol. Hence, the symbol rate is $1/T_s$. Further, each information symbol is comprised of multiple frames or elementary UWB monocycles that are all modulated by the same data symbol. The number of monocycles per data symbol is denoted as N_s and is equal to the integration gain. Each monocycle can occur in a frame of size T_f. Again, the frame structure is subject to the constraint $N_s T_f \le T_s$. The average pulse repetition

frequency (PRF) is given by $1/T_f$. For a monocycle of width T_p, the duty cycle is defined as T_p/T_f. Within the ith frame of N_s frame repetitions, the position of a monocycle is determined by the TH code chip, $c_{j,i}$, where the index j refers to the jth symbol within the TH period. The code chip can take values from 0 to $N_c - 1$ with granularity T_c such that $N_c T_c \le T_f$.

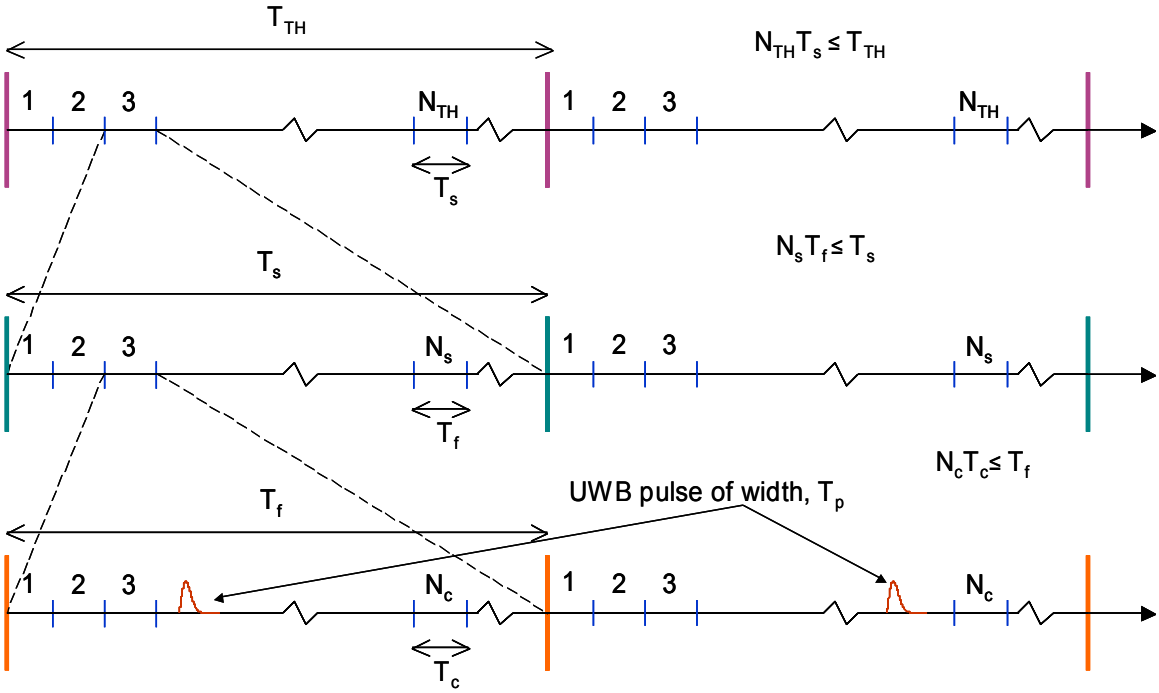

Figure 3C-1: *Structure of the UWB Waveform.*

When PPM is employed, the position is additionally determined by the data symbol, b_j^k, where k refers to the kth time-hopping period. The granularity of the position-based modulation is denoted by T_d. To accommodate pulse amplitude modulation (PAM) schemes, such as BPSK or OOK, the basic waveform has a multiplication factor a_j^k where j and k are as defined before. Given these definitions, the synthesized waveform whose duration is equal to that of the periodicity of the TH code is given as

$$s_k(t) = \sum_{j=1}^{N_{TH}} \sum_{i=1}^{N_s} a_j^k \delta(t - b_j^k T_d - c_{j,i} T_c - iT_f - jT_s) \qquad \text{(3C1-1)}$$

With the above description of the composite waveform, some observations are in order. Each waveform, $s_k(t)$ contains $N_{TH} N_s$ elementary UWB pulses. The selection of a particular waveform depends on the values of N_{TH} information symbols and $N_{TH} N_s$ TH code chips. For an M-ary modulation scheme, the total number of waveforms equals $M^{N_{TH}} N_c^{N_s N_{TH}}$.

Finally, the UWB signal is represented as a concatenation of time-shifted waveforms, $s_k(t)$:

$$y(t) = \sum_k s_{d_k}(t - kT_{TH} - \Theta) \tag{3C1-2}$$

where Θ is a random variable (RV) independent of d_k and with a distribution uniform in $(0, T_{TH})$. The purpose of the random variable Θ is to account for the arbitrary time origin. Each of the waveforms may be thought of as a mapping from an I.I.D. sequence **d** where each element d_k can take 1 of $M^{N_{TH}} N_c^{N_s N_{TH}}$ values with a certain probability distribution depending on the distribution of the data symbols and the code chips.
Note that the pulse shape for the model in (3C1-1) is assumed to be an impulse function (Dirac-delta). However this does not limit the generality of the PSD derivation in that the PSD for any arbitrary pulse shape, $v(t)$, is obtained from the one using the impulse function by appropriately filtering it.

PSD Derivation
In order to compute the spectrum, the autocorrelation of $y(t)$ is first derived, and it is thereby shown that the UWB signal, as modeled in (3C1-2), results in a correlation–stationary process. Then, the PSD is readily obtained by taking the Fourier Transform (FT) of the autocorrelation function.

With that high-level sketch, we begin the derivation of the autocorrelation function for the UWB signal as follows

$$\begin{aligned} R^y(t,\tau) &= E\left\{y(t)y^*(t-\tau)\right\} \\ &= E\left\{\sum_k \sum_h s_{d_k}(t - kT_{TH} - \Theta) s^*_{d_k}(t - \tau - hT_{TH} - \Theta)\right\} \end{aligned} \tag{3C1-3}$$

In (3C1-3), the expectation is over the variables d_k and Θ, where d_k is a function of the sequence of code chips and data symbols.

Performing the averaging over Θ only, (3C1-3) yields

$$\begin{aligned} R^y(t,\tau) &= E\left\{\sum_k \sum_h \left\langle s_{d_k}(t - kT_{TH} - \Theta) s^*_{d_h}(t - \tau - hT_{TH} - \Theta)\right\rangle_\Theta\right\} \\ &= \frac{1}{T_{TH}} E\left\{\sum_k \sum_h \int_0^{T_{TH}} s_{d_k}(t - kT_{TH} - \Theta) s^*_{d_h}(t - \tau - hT_{TH} - \Theta) d\Theta\right\} \end{aligned} \tag{3C1-4}$$

Now, the expectation within the summation operation in (3C1-4) may be decomposed into two cases depending on whether the constituents of the double summation are like-terms or cross-terms:

1. Expectation over two independent RVs, d_k and d_h
2. Expectation over one RV d_k

Further, for convenience, we introduce two RVs p and q which are independent and distributed like d_k and d_h. Then, separating the summation term in (3C1-4) into the two cases described above, the autocorrelation is expressed as

$$\begin{aligned} R^y(t,\tau) &= \frac{1}{T_{TH}} E\left\{ \sum_k \int_0^{T_{TH}} s_p(t - kT_{TH} - \Theta) s_p^*(t - \tau - kT_{TH} - \Theta) d\Theta \right\} \\ &+ \frac{1}{T_{TH}} E\left\{ \sum_k \sum_{h \neq k} \int_0^{T_{TH}} s_p(t - kT_{TH} - \Theta) s_q^*(t - \tau - hT_{TH} - \Theta) d\Theta \right\} \\ &= R_1(t,\tau) + R_2(t,\tau) \end{aligned} \tag{3C1-5}$$

where, $R_1(t,\tau)$ and $R_2(t,\tau)$ denote the 1st and 2nd terms of the right hand side (RHS) of , respectively.

Now, focusing on the 1st term and setting $u = kT_{TH} + \Theta$, we have

$$\begin{aligned} R_1(t,\tau) &= \frac{1}{T_{TH}} E\left\{ \sum_{k=-\infty}^{\infty} \int_{kT_{TH}}^{(k+1)T_{TH}} s_p(t-u) s_p^*(t-\tau-u) du \right\} \\ &= \frac{1}{T_{TH}} E\left\{ \int_{-\infty}^{-\infty} s_p(t-u) s_p^*(t-\tau-u) du \right\} \end{aligned} \tag{3C1-6}$$

Again setting $t - u = q$, (3C1-6) becomes

$$\begin{aligned} R_1(t,\tau) &= \frac{1}{T_{TH}} E\left\{ \int_{-\infty}^{-\infty} s_p(q) s_p^*(q-\tau) dq \right\} \\ &= \frac{1}{T_{TH}} E\left\{ R_p(\tau) \right\} \end{aligned} \tag{3C1-7}$$

The term $R_k(x)$ is the deterministic autocorrelation function, which is defined as $\int_{-\infty}^{\infty} s_k(y)s_k^*(y-x)dy$ [4]. Also, note that the RHS of (3C1-7) depends only on τ, and henceforth, the dependency on t will be dropped for the like-term component of the stochastic autocorrelation function defined in (3C1-3).

Next, we focus on the cross-term component of the stochastic autocorrelation function given as

$$R_2(t,\tau) = \frac{1}{T_{TH}} E\left\{ \sum_k \sum_{h \neq k} \int_0^{T_{TH}} s_p(t - kT_{TH} - \Theta) s_q^*(t - \tau - hT_{TH} - \Theta) d\Theta \right\} \tag{3C1-8}$$

Setting $u = kT_{TH} + \Theta$, (3C1-8) becomes

$$\begin{aligned} R_2(t,\tau) &= \frac{1}{T_{TH}} E\left\{ \sum_k \int_{kT_{TH}}^{(k+1)T_{TH}} s_p(t-u) \sum_{h \neq k} s_q^*(t - \tau - (h-k)T_{TH} - u) du \right\} \\ &= \frac{1}{T_{TH}} E\left\{ \sum_{h \neq k} \int_{-\infty}^{\infty} s_p(t-u) s_q^*(t - \tau - (h-k)T_{TH} - u) du \right\} \end{aligned} \tag{3C1-9}$$

Again setting $t - u = q$, (3C1-9) becomes

$$\begin{aligned} R_2(t,\tau) &= \frac{1}{T_{TH}} E\left\{ \sum_{h \neq k} \int_{-\infty}^{-\infty} s_p(q) s_q^*(q - (\tau + (h-k)T_{TH})) dq \right\} \\ &= \frac{1}{T_{TH}} E\left\{ \sum_{h \neq k} R_{p,q}(\tau - (h-k)T_{TH}) \right\} \\ &= \frac{1}{T_{TH}} E\left\{ \sum_{l \neq 0} R_{p,q}(\tau - lT_{TH}) \right\} \end{aligned} \tag{3C1-10}$$

The term $R_{k,h}(x)$ is the deterministic cross-correlation function, which is defined as $\int_{-\infty}^{\infty} s_k(y)s_h^*(y-x)dy$ [4]. Since the RHS of (10) depends only on $\tau - lT_{TH}$, the dependency on t will be dropped for the cross-term component of the stochastic autocorrelation function defined in (3C1-3).

Substituting (3C1-7) and (3C1-10) in (3C1-5), we have

$$E\{y(t)y^*(t-\tau)\} = R^y(\tau) = \frac{1}{T_{TH}} E\{R_p(\tau)\} + \frac{1}{T_{TH}} \sum_{l\neq 0} E\{R_{p,q}(\tau - lT_{TH})\}$$
$$= \frac{1}{T_{TH}} E\{R_p(\tau)\} - \frac{1}{T_{TH}} E\{R_{p,q}(\tau)\} + \frac{1}{T_{TH}} \sum_{l} E\{R_{p,q}(\tau - lT_{TH})\} \quad (3C1\text{-}11)$$

The bottom expression in (3C1-11) shows that the autocorrelation of $y(t)$ depends only on τ, and hence, $y(t)$ is correlation-stationary. Therefore, the PSD of $y(t)$ is obtained by taking the Fourier transform of the RHS in (3C1-11).

It is shown in Note 1 at the end of this Annex that the Fourier transform of the cross-correlation and auto-correlation functions are given as

$$F_\tau\left(R_{k,h}(\tau)\right) = S_k(f)S_h^*(f)$$
$$F_\tau\left(R_{k,k}(\tau)\right) = \left|S_k(f)\right|^2 \quad (3C1\text{-}12)$$

Applying the above Fourier transform property to (3C1-11), we have

$$P_y(f) = \frac{1}{T_{TH}} \left(E\left\{\left|S_p(f)\right|^2\right\} - E\{S_p(f)S_q^*(f)\}\right)$$
$$+ \frac{1}{T_{TH}} E\{S_p(f)S_q^*(f)\} \sum_l e^{-j2\pi f l T_{TH}} \quad (3C1\text{-}13)$$

where $S_p(f)$ is the Fourier Transform of $s_p(t)$ as defined in (3C1-1).
Then, using Poisson's sum formula for the last term in (3C1-13), it follows that

$$P_y(f) = \frac{1}{T_{TH}} \left(E\left\{\left|S_p(f)\right|^2\right\} - E\{S_p(f)S_q^*(f)\}\right)$$
$$+ \frac{1}{T_{TH}^2} E\{S_p(f)S_q^*(f)\} \sum_{n=-\infty}^{\infty} \delta\left(f - \frac{n}{T_{TH}}\right) \quad (3C1\text{-}14)$$

The above expression is the PSD for UWB pulses whose shape is defined by the Dirac delta function. Now, for the general case of an arbitrary UWB pulse shape, the PSD is readily obtained from the PSD expression in (3C1-14) using the following property of a linear time invariant (LTI) filter.

$$Y(f) = \left|H(f)\right|^2 X(f) \quad (3C1\text{-}15)$$

where, $X(f)$ and $Y(f)$ are the input and output power spectral densities, respectively, of a filter whose transfer function is given as $H(f)$.

Therefore, using (3C1-14) and (3C1-15), the UWB PSD for an arbitrary pulse shape, $v(t)$, is given as

$$S(f) = \frac{|V(f)|^2}{T_{TH}} \left(E\left\{ |S_p(f)|^2 \right\} - E\left\{ S_p(f) S_q^*(f) \right\} \right) + \frac{1}{T_{TH}^2} \sum_{n=-\infty}^{\infty} \left| V\left(\frac{n}{T_{TH}} \right) \right|^2 E\left\{ S_p(f) S_q^*(f) \right\} \delta\left(f - \frac{n}{T_{TH}} \right) \quad \text{(3C1-16)}$$

where $S_p(f)$ is the Fourier Transform of the UWB waveform defined in the p th period of the TH code and is explicitly defined in (3C1-1). In the above PSD expression, T_{TH} is the period of the time-hopping code.

The above expression shows that a portion of the signal power given by $\frac{1}{T_{TH}} \int_{-\infty}^{\infty} E\left\{ S_p(f) S_q^*(f) \right\} df$ is removed from the continuous portion of the spectrum and appears as a set of spectral lines at multiples of the TH code repetition frequency, $1/T_{TH}$. Note that the integrand is the Fourier transform of the average cross-correlation function. Hence, smaller the cross-correlation function, the smaller the strength of the spectral lines. This observation suggests that the packet and higher layer framing structure should be so designed to keep the packet redundancy minimal from one code period to the next to reduce spectral lines. Since these issues fall outside the main focus of this report, they will be relegated to future investigations.

Conclusions

This first part derives a general expression for the power spectral density (PSD) of UWB waveforms taking account the following:

1. Arbitrary UWB pulse shape and repetition discipline
2. Amenable to PAM and PPM modulation schemes or a combination thereof
3. Arbitrary TH code with a finite period
4. Pulse repetitions per data symbol (integration gain)

It is shown that the PSD basically depends on the auto- and cross-correlation of the spectrum of the UWB waveform defined within a code period. The UWB PSD exhibits spectral lines that appear at integer multiples of the code repetition frequency which is defined as the reciprocal of the TH code period. Further, it is observed that power contained in the spectrum of the cross-correlation function of the composite waveform is removed from the continuous portion of the PSD and appears as spectral lines.

Part 2: Detailed UWB PSD Analysis

Introduction

This work uses the generalized power spectral density (PSD) results in Part I and recasts them explicitly in terms of the statistics/spectrum of the time-hopping (TH) code and modulation. The main result developed in Part 1, which is used in this report is summarized as follows.

If the UWB waveform is represented as $y(t) = \sum_k s_k(t - kT_{TH} - \Theta)$, where $s_k(t)$ represents the waveform in the k th TH code cycle of period T_{TH} and Θ is a random variable (RV) independent of d_k and with a distribution uniform in $(0, T_{TH})$, then the PSD is given as

$$P_y(f) = \frac{1}{T_{TH}}\left[\left\langle |S_p(f)|^2 \right\rangle - \left\langle S_p(f) S_q^*(f) \right\rangle\right] + \frac{1}{T_{TH}^2}\left\langle S_p(f) S_q^*(f) \right\rangle \sum_{n=-\infty}^{\infty} \delta\left(f - \frac{n}{T_{TH}}\right) \quad \text{(3C2-1a)}$$

where $S_p(f)$ is the Fourier Transform of the UWB waveform in the p th period of the TH code.

PSD Analysis

If the waveform $s_k(t)$ represents the k th code cycle, with each elementary pulse (in general) amplitude- and position-modulated, then

$$s_k(t) = \sum_{m=1}^{N_{TH}} \sum_{n=1}^{N_s} a_m^k \delta\left(t - mT_s - b_m^k T_d - c_{m,n} T_c - nT_f\right) \quad \text{(3C2-1b)}$$

where the parameters are as defined in Part I above.

With the above definitions in place, we derive $\left\langle |S_p(f)|^2 \right\rangle$ and $\left\langle S_p(f) S_q^*(f) \right\rangle$ in terms of the statistics of the modulation symbols and the TH code, which will then be substituted in the (3C2-1a) to get the generalized PSD.

The Fourier transform (FT) of this waveform is written as

$$S_k(f) = \sum_{m=1}^{N_{TH}} a_m^k D_m(f) e^{-j2\pi f b_m^k T_d} e^{-j2\pi f m T_s} \quad \text{(3C2-2)}$$

where $D_m(f)$ is the FT of the m th sub-TH code and is defined below. The code spectrum is derived below in terms of the spectrum of the m th sub-TH code.
The TH code is first defined as

$$d(t) = \sum_{m=1}^{N_{TH}} \sum_{n=1}^{N_s} \delta\left(t - mT_s - c_{m,n}T_c - nT_f\right) \tag{3C2-3}$$

Then, the Fourier transform of the TH code is obtained as

$$D(f) = \sum_{m=1}^{N_{TH}} D_m(f) e^{-j2\pi fmT_s} \tag{3C2-4}$$

where $D_m(f)$, which is the Fourier transform of the m th sub-TH code, is given as

$$D_m(f) = \sum_{n=1}^{N_s} e^{-j2\pi fc_{m,n}T_c} e^{-j2\pi fnT_f} \tag{3C2-5}$$

With the above definitions in place, we derive $\left\langle \left|S_p(f)\right|^2 \right\rangle$ and $\left\langle S_p(f)S_q^*(f) \right\rangle$ in terms of the statistics of the modulation symbols and the TH code, which will then be substituted in the equation below (result from Part 1) to get the generalized PSD.

$$\begin{aligned} P_y(f) &= \frac{1}{T_{TH}} \left[\left\langle \left|S_p(f)\right|^2 \right\rangle - \left\langle S_p(f)S_q^*(f) \right\rangle \right] \\ &+ \frac{1}{T_{TH}^2} \left\langle S_p(f)S_q^*(f) \right\rangle \sum_{n=-\infty}^{\infty} \delta\left(f - \frac{n}{T_{TH}} \right) \end{aligned} \tag{3C2-6}$$

Using (3C2-2), $\left\langle \left|S_p(f)\right|^2 \right\rangle$ is obtained as

$$\begin{aligned} \left\langle \left|S_p(f)\right|^2 \right\rangle &= \sum_{m1=1}^{N_{TH}} \sum_{m2=1}^{N_{TH}} \left\langle a_{m1}^p \left(a_{m2}^p\right)^* \right\rangle \left\langle e^{-j2\pi f b_{m1}^p T_d} e^{j2\pi f b_{m2}^p T_d} \right\rangle \\ &\times \left\langle D_{m1}(f) D_{m2}^*(f) \right\rangle e^{-j2\pi f(m1-m2)T_s} \end{aligned} \tag{3C2-7}$$

The expression in (3C2-7) implicitly assumes independence among the TH code, and the amplitude and position modulation symbols. Now, the correlation statistics of the modulation symbols in (7) take on only two values depending on whether $m1 = m2$ or $m1 \neq m2$.

$$\begin{aligned}\left\langle \left|S_p(f)\right|^2 \right\rangle &= R_0^a \sum_{m=1}^{N_{TH}} \left\langle \left|D_m(f)\right|^2 \right\rangle + R_\Delta^a R_\Delta^b(f) \sum_{m1=1}^{N_{TH}} \sum_{m2\neq m1}^{N_{TH}} \left\langle D_{m1}(f) D_{m2}^*(f) \right\rangle e^{-j2\pi f(m1-m2)T_s} \\ &= R_0^a \sum_{m=1}^{N_{TH}} \left\langle \left|D_m(f)\right|^2 \right\rangle \\ &+ R_\Delta^a R_\Delta^b(f) \left[\sum_{m1=1}^{N_{TH}} \sum_{m2}^{N_{TH}} \left\langle D_{m1}(f) D_{m2}^*(f) \right\rangle e^{-j2\pi f(m1-m2)T_s} - \sum_{m=1}^{N_{TH}} \left\langle \left|D_m(f)\right|^2 \right\rangle \right]\end{aligned} \tag{3C2-8}$$

where,

$$\begin{aligned} R_0^a &= \left\langle a_m^p \left(a_m^p\right)^* \right\rangle = \left\langle \left|a_m^p\right|^2 \right\rangle, \forall\, p, m \\ R_\Delta^a &= \left\langle a_{m1}^p \left(a_{m2}^q\right)^* \right\rangle, m1 \neq m2 \text{ or } p \neq q \\ R_\Delta^b(f) &= \left\langle e^{-j\omega\, b_{m1}^p T_d} \right\rangle \left\langle e^{j\omega\, b_{m2}^q T_d} \right\rangle, m1 \neq m2 \text{ or } p \neq q \end{aligned} \tag{3C2-9}$$

It is also implied in (3C2-9) that the correlation functions[2] are independent of $m1$ and $m2$.

Similarly, $\left\langle S_p(f) S_q^*(f) \right\rangle$ is derived as

$$\begin{aligned}\left\langle S_p(f) S_q^*(f) \right\rangle &= \sum_{m1=1}^{N_{TH}} \sum_{m2=1}^{N_{TH}} \left\langle a_{m1}^p \left(a_{m2}^q\right)^* \right\rangle \left\langle e^{-j2\pi f\, b_{m1}^p T_d} e^{j2\pi f\, b_{m2}^q T_d} \right\rangle \\ &\quad \times \left\langle D_{m1}(f) D_{m2}^*(f) \right\rangle e^{-j2\pi f(m1-m2)T_s} \\ &= R_\Delta^a R_\Delta^b(f) \sum_{m1=1}^{N_{TH}} \sum_{m2=1}^{N_{TH}} \left\langle D_{m1}(f) D_{m2}^*(f) \right\rangle e^{-j2\pi f(m1-m2)T_s}\end{aligned} \tag{3C2-10}$$

Substituting (3C2-8) and (3C2-10) in (3C2-6), we get

$$P_y(f) = \frac{A_0(f)}{T_{TH}} \left[R_0^a - R_\Delta^a R_\Delta^b(f) \right] + \frac{A(f) R_\Delta^a R_\Delta^b(f)}{T_{TH}^2} \sum_{k=-\infty}^{\infty} \delta\left(f - \frac{k}{T_{TH}} \right) \tag{3C2-11a}$$

where

$$\begin{aligned} A(f) &= \sum_{m1=1}^{N_{TH}} \sum_{m2=1}^{N_{TH}} \left\langle D_{m1}(f) D_{m2}^*(f) \right\rangle e^{-j2\pi f(m1-m2)T_s} = \left\langle \left|D(f)\right|^2 \right\rangle \\ A_0(f) &= \sum_{m=1}^{N_{TH}} \left\langle \left|D_m(f)\right|^2 \right\rangle \end{aligned} \tag{3C2-11b}$$

[2] Strictly speaking, $R_\Delta^b(f)$ is the product of the characteristic function of $b_m^p T_d$ and $-b_m^p T_d$.

The PSD expression in (3C2-11a) is still quite general (except for the assumption about the modulation statistics in (3C2-9)), and shows the effect of the TH code spectrum on the UWB PSD. It is seen from (11a) that the continuous portion is affected only by the sub-TH code spectrum whereas the discrete component is affected by the spectrum of the entire code.

Next, we make some assumptions of the TH code statistics that shows the effect of holding the modulation constant for N_s pulses. This step is required since N_s is buried in the sub-code spectrum as defined in (3C2-5).

Define $R_{\Delta}^{c}(f)$ as:

$$R_{\Delta}^{c}(f) = \left\langle e^{-j2\pi fc_{m1,n1}T_c} e^{j2\pi fc_{m2,n2}T_c} \right\rangle, \forall\ m1 \neq m2 \text{ or } n1 \neq n2 \qquad \text{(3C2-12)}$$

with $R_{\Delta}^{c}(f)$ being independent of code chip location.

Based on definitions in (3C2-11b), $A(f)$ can be decomposed as

$$A(f) = A_0(f) + A_{\Delta}(f)$$
where (3C2-13)
$$A_{\Delta}(f) = \sum_{m1=1}^{N_{TH}} \sum_{m2 \neq m1}^{N_{TH}} \left\langle D_{m1}(f) D_{m2}^{*}(f) \right\rangle e^{-j2\pi f(m1-m2)T_s}$$

Using (3C2-11b) and (3C2-12), $A_0(f)$ can be expressed in terms of $R_{\Delta}^{c}(f)$ as

$$
\begin{aligned}
A_0(f) &= \sum_{m=1}^{N_{TH}} \left\langle \left| D_m(f) \right|^2 \right\rangle \\
&= \sum_{m=1}^{N_{TH}} \sum_{n1=1}^{N_s} \sum_{n2=1}^{N_s} \left\langle e^{-j2\pi f c_{m,n1} T_c} e^{j2\pi f c_{m,n2} T_c} \right\rangle e^{-j2\pi f (n1-n2) T_f} \\
&= \sum_{m=1}^{N_{TH}} \left[N_s + R_\Delta^c(f) \sum_{n1=1}^{N_s} \sum_{n2 \neq n1}^{N_s} e^{-j2\pi f (n1-n2) T_f} \right] \\
&= \sum_{m=1}^{N_{TH}} \left[N_s + R_\Delta^c(f) \left\{ \sum_{n1=1}^{N_s} \sum_{n2=1}^{N_s} e^{-j2\pi f (n1-n2) T_f} - N_s \right\} \right] \\
&= N_{TH} \left[N_s + R_\Delta^c(f) \left\{ \left(\frac{\sin(\pi f N_s T_f)}{\sin(\pi f T_f)} \right)^2 - N_s \right\} \right]
\end{aligned}
\tag{3C2-14}
$$

Similarly, $A_\Delta(f)$ can be expressed in terms of $R_\Delta^c(f)$. We begin with the definition of $A_\Delta(f)$ in (3C2-13) , and is repeated below as

$$
A_\Delta(f) = \sum_{m1=1}^{N_{TH}} \sum_{m2 \neq m1}^{N_{TH}} \left\langle D_{m1}(f) D_{m2}^*(f) \right\rangle e^{-j2\pi f (m1-m1) T_s}
\tag{3C2-15}
$$

Now, we evaluate $\left\langle D_{m1}(f) D_{m2}^*(f) \right\rangle$ when $m1 \neq m2$ as follows

$$
\begin{aligned}
\left\langle D_{m1}(f) D_{m2}^*(f) \right\rangle_{m1 \neq m2} &= \sum_{n1=1}^{N_s} \sum_{n2=1}^{N_s} \left\langle e^{-j2\pi f c_{m1,n1} T_c} e^{j2\pi f c_{m2,n2} T_c} \right\rangle e^{-j2\pi f n1 T_f} e^{j2\pi f n2 T_f} \\
= R_\Delta^c(f) \sum_{n1=1}^{N_s} \sum_{n2=1}^{N_s} e^{-j2\pi f n1 T_f} e^{j2\pi f n2 T_f} &= R_\Delta^c(f) \left(\frac{\sin(\pi f N_s T_f)}{\sin(\pi f T_f)} \right)^2
\end{aligned}
\tag{3C2-16}
$$

Substituting (3C2-16) in (3C2-15), $A_\Delta(f)$ is expressed as

$$
\begin{aligned}
A_\Delta(f) &= R_\Delta^c(f) \left(\frac{\sin(\pi f N_s T_f)}{\sin(\pi f T_f)} \right)^2 \sum_{m1=1}^{N_{TH}} \sum_{m2 \neq m1}^{N_{TH}} e^{-j2\pi f (m1-m1) T_s} \\
&= R_\Delta^c(f) \left(\frac{\sin(\pi f N_s T_f)}{\sin(\pi f T_f)} \right)^2 \left[\sum_{m1=1}^{N_{TH}} \sum_{m2=1}^{N_{TH}} e^{-j2\pi f (m1-m1) T_s} - N_{TH} \right] \\
&= R_\Delta^c(f) \left(\frac{\sin(\pi f N_s T_f)}{\sin(\pi f T_f)} \right)^2 \left[\left(\frac{\sin(\pi f N_{TH} T_s)}{\sin(\pi f T_s)} \right)^2 - N_{TH} \right]
\end{aligned}
\tag{3C2-17}
$$

Finally, combining (3C2-14) and (3C2-17), $A(f)$ is obtained as follows

$$A(f) = N_{TH}N_s - R_\Delta^c(f)\left[N_{TH}N_s - \left(\frac{\sin(\pi fN_{TH}T_s)}{\sin(\pi fT_s)}\frac{\sin(\pi fN_sT_f)}{\sin(\pi fT_f)}\right)^2\right] \quad \text{(3C2-18)}$$

Substituting (3C2-14) and (3C2-18) in (3C2-11), we get

$$P_y(f) = \frac{N_{TH}N_s}{T_{TH}}\left[1 - R_\Delta^c(f)\left\{1 - \frac{1}{N_s}\left(\frac{\sin(\pi fN_sT_f)}{\sin(\pi fT_f)}\right)^2\right\}\right]\left(R_0^a - R_\Delta^a R_\Delta^b(f)\right)$$
$$+ \frac{N_{TH}N_s}{T_{TH}^2}\left(1 - R_\Delta^c(f)\left[1 - \frac{1}{N_{TH}N_s}\left(\frac{\sin(\pi fN_{TH}T_s)}{\sin(\pi fT_s)}\frac{\sin(\pi fN_sT_f)}{\sin(\pi fT_f)}\right)^2\right]\right)R_\Delta^a R_\Delta^b(f) \quad \text{(3C2-19)}$$
$$\times \sum_{k=-\infty}^{\infty}\delta\left(f - \frac{k}{T_{TH}}\right)$$

Next, we derive the PSD for certain special cases where the integration gain and TH period can take the values unity or infinity.

Effect of Code Length and Integration Gain

Case I: TH code of infinite length

Assume that the TH code never repeats or equivalently, has a period of infinite duration. This is represented as

$$\left.\begin{matrix} T_{TH} \to \infty \\ N_{TH} \to \infty \end{matrix}\right\}, \text{such that } \frac{T_{TH}}{N_{TH}} = T_s = N_sT_f \quad \text{(3C2-20)}$$

Substituting the above conditions in (3C2-19), we get

$$P_y(f) = P_{1,\infty}(f) + P_{2,\infty}(f) \quad \text{(3C2-21a)}$$

where

$$P_{1,\infty}(f)=\frac{1}{T_f}\left(1-R_\Delta^c(f)\left[1-\frac{1}{N_s}\left(\frac{\sin(\pi fN_sT_f)}{\sin(\pi fT_f)}\right)^2\right]\right)\left(R_0^a-R_\Delta^aR_\Delta^b(f)\right)$$

$$P_{2,\infty}(f)=\left(\frac{1}{T_f}-R_\Delta^c(f)\left[\frac{1}{T_f}-\lim_{N_{TH}\to\infty}\frac{1}{N_{TH}T_s}\left(\frac{\sin(\pi fN_{TH}T_s)}{\sin(\pi fT_s)}\right)^2\left(\frac{\sin(\pi fN_sT_f)}{\sin(\pi fT_f)}\right)^2\right]\right) \quad \text{(3C2-21b)}$$

$$\times R_\Delta^aR_\Delta^b(f)\lim_{T_{TH}\to\infty}\frac{1}{T_{TH}}\sum_{k=-\infty}^{\infty}\delta\left(f-\frac{k}{T_{TH}}\right)$$

Now, from the results derived in Note 2, we have

$$\lim_{N_{TH}\to\infty}\frac{1}{N_{TH}T_s}\left(\frac{\sin(\pi fN_{TH}T_s)}{\sin(\pi fT_s)}\right)^2=\frac{1}{T_s^2}\sum_{n=-\infty}^{\infty}\delta\left(f-\frac{n}{T_s}\right)$$
$$\lim_{T_{TH}\to\infty}\frac{1}{T_{TH}}\sum_{k=-\infty}^{\infty}\delta\left(f-\frac{k}{T_{TH}}\right)=1 \quad \text{(3C2-22)}$$

Substituting these results in $P_{2,\infty}(f)$ as defined in (3C2-21b),

$$P_{2,\infty}(f)=\frac{\left(1-R_\Delta^c(f)\right)R_\Delta^aR_\Delta^b(f)}{T_f}+\frac{R_\Delta^c(f)R_\Delta^aR_\Delta^b(f)}{\left(N_sT_f\right)^2}\left(\frac{\sin(\pi fN_sT_f)}{\sin(\pi fT_f)}\right)^2$$
$$\times\sum_{n=-\infty}^{\infty}\delta\left(f-\frac{n}{N_sT_f}\right) \quad \text{(3C2-23)}$$

From, (3C2-21) and (3C2-23), the PSD is finally obtained as

$$P_y(f)=\frac{R_\Delta^c(f)\left\{\left(R_0^a-R_\Delta^aR_\Delta^b(f)\right)D(N_s,T_f)-N_sR_0^a\right\}+N_sR_0^a(f)}{N_sT_f}$$
$$+\frac{R_\Delta^c(f)R_\Delta^aR_\Delta^b(f)}{\left(N_sT_f\right)^2}D(N_s,T_f)\sum_{n=-\infty}^{\infty}\delta\left(f-\frac{n}{N_sT_f}\right) \quad \text{(3C2-24a)}$$

where,

$$D(N_s,T_f)=\left(\frac{\sin(\pi fN_sT_f)}{\sin(\pi fT_f)}\right)^2 \quad \text{(3C2-24b)}$$

Sub-case I: $N_s = 1 \Rightarrow$ **Unity integration gain**

This is the case in which one pulse is modulated by one information symbol. Substituting $N_s = 1$ in (3C2-24), we get

$$P_y(f) = \frac{\left[R_0^a - R_\Delta^a R_\Delta^b(f) R_\Delta^c(f)\right]}{T_f} + \frac{R_\Delta^a R_\Delta^b(f) R_\Delta^c(f)}{T_f^2} \sum_{n=-\infty}^{\infty} \delta\left(f - \frac{n}{T_f}\right) \tag{3C2-25}$$

Sub-case II: $N_s \to \infty \Rightarrow$ **Infinite integration gain**

Similarly letting $N_s \to \infty$ in (3C2-24) and using the results in (3C2-22), we get

$$P_y(f) = R_0^a \left(\frac{\left(1 - R_\Delta^c(f)\right)}{T_f} + \frac{R_\Delta^c(f)}{T_f^2} \sum_{n=-\infty}^{\infty} \delta\left(f - \frac{n}{T_f}\right) \right) \tag{3C2-26}$$

The PSD expression shows that the modulation no longer affects the PSD. This is intuitively satisfying since infinite pulses are now modulated by the same information symbol effectively removing any variation in the pulse sequence due to the modulation symbols. Additionally, if there is no time-hopping (i.e., $R_\Delta^c(f)$=1), the above expression indicates that the continuous component would disappear with all of the power appearing only as spectral lines.

Case II: N_{TH} **= 1** $\Rightarrow$ **Code repeats every symbol**

In this case, $N_{TH} = 1$ or $T_{TH} = T_s$, i.e., the TH code repeats itself from one symbol duration to the next. Substituting $N_{TH} = 1$ in (3C2-19), and using results in (3C2-22), we get

$$P_y(f) = P_{1,1}(f) + P_{2,1}(f) \tag{3C2-27a}$$

where

$$\begin{aligned} P_{1,1}(f) &= \frac{1}{T_f}\left\{1 - R_\Delta^c(f)\left(1 - \frac{D(N_s, T_f)}{N_s}\right)\right\}\left(R_0^a - R_\Delta^a R_\Delta^b(f)\right) \\ P_{2,1}(f) &= \frac{1}{T_f}\left\{1 - R_\Delta^c(f)\left(1 - \frac{D(N_s, T_f)}{N_s}\right)\right\} R_\Delta^a R_\Delta^b(f) \frac{1}{T_s} \sum_{n=-\infty}^{\infty} \delta\left(f - \frac{n}{T_s}\right) \end{aligned} \tag{3C2-27b}$$

Sub-case I: $N_s = 1 \Rightarrow$ **Unity integration gain**

This is the case where one pulse is modulated by one information symbol. Substituting $N_s = 1$ in (3C2-27), we get

$$P_y(f) = \frac{\left[R_0^a - R_\Delta^a R_\Delta^b(f)\right]}{T_f} + \frac{R_\Delta^a R_\Delta^b(f)}{T_f^2} \sum_{n=-\infty}^{\infty} \delta\left(f - \frac{n}{T_f}\right) \tag{3C2-28}$$

In this case the code repeats every pulse, and hence, effectively removes any time dithering. Therefore, the PSD should not be affected by the TH code as is borne out in the expression in (3C2-28).

Sub-case II: $N_s \to \infty \Rightarrow$ **Infinite integration gain**

Similarly letting $N_s \to \infty$ in (3C2-27) and using the results in (3C2-22), we get

$$P_y(f) = R_0^a \left(\frac{\left(1 - R_\Delta^c(f)\right)}{T_f} + \frac{R_\Delta^c(f)}{T_f^2} \sum_{n=-\infty}^{\infty} \delta\left(f - \frac{n}{T_f}\right) \right) \tag{3C2-29}$$

Again, similar to the case of infinite length TH code and infinite integration gain, the effect of modulation from the PSD vanishes. On the other hand, since there is a random code chip for each pulse among the N_s pulses used to represent one modulation symbol, the effect of. $N_s \to \infty$ is essentially that of an infinite code length. Hence, this expression is the same as that of the corresponding sub-case when $N_{TH} \to \infty$ (see (3C2-26)).
In conclusion, from (3C2-25)-(3C2-26) and (3C2-28)-(3C2-29), the effect of integration gain and length of TH code on the PSD may be summarized as follows:

Effect of TH code length: Note that in an absolute sense, the code length is unity implies that the same chip is used every pulse. But setting $N_{TH} = 1$ only implies that the code repeats every symbol, which may consists of multiple pulses depending on the integration gain. Therefore, using the above definition, the unit length code case is only achieved by setting both N_s and N_{TH} equal to one. The infinite code length case, on the other hand, is given by setting N_s or N_{TH} equal to infinity. In summary, the unit length case is given by (3C2-28) and the infinite length case is given by (3C2-25)-(3C2-26) and (3C2-29). Comparing these equations, it is seen that unit length is equivalent to no coding at all. Infinite length code, on the other hand, removes power proportional to the non-zero lag code-correlation from the continuous component and converts it to spectral lines. Since the non-zero lag code-correlation of a code is designed to be small, it follows that the benefits of time hopping are maximized when codes of large length are used.

Effect of integration gain: The effect of integration is observed by comparing the expressions for N_s =1 and $N_s = \infty$ for a fixed code length. Hence, comparing (3C2-23) and (3C2-26) or (3C2-28) and (3C2-29), it is seen that as integration gain increases, the effect of modulation statistics on the PSD vanishes. Hence, control of the PSD through

modulation becomes ineffective if large integration gain is required for UWB communications.

Effect of Modulation Statistics

In this section, the effect of modulation (a_k and b_k) statistics on the PSD are explicitly shown.

Let $a_k = x_k + \mu_a$, where x_k is a zero-mean random component. Then, from (3C2-9), $R_0^a = E\{a_k^2\}$ and $R_\Delta^a = E\{x_k x_n\} + \mu_a^2, k \neq n$. If x_k and x_n are uncorrelated for $n \neq k$, then $R_\Delta^a = \mu_a^2$. Similarly, let $p_k = e^{-j\omega b_k T_d} = y_k + \mu_b$.

Then, again from (3C2-9), $R_\Delta^b(f) = E\{p_k p_n^*\} = E\{y_k y_n^*\} + |\mu_b(f)|^2$. If, as before, y_k and y_n are uncorrelated for $n \neq k$, then $R_\Delta^b(f) = |\mu_b(f)|^2$.

Substituting, R_0^a, $R_\Delta^a(f)$ and $R_\Delta^b(f)$ in (3C2-19), we get

$$P_y(f) = \frac{N_{TH} N_s}{T_{TH}} \left[1 - R_\Delta^c(f) \left\{ 1 - \frac{1}{N_s} \left(\frac{\sin(\pi f N_s T_f)}{\sin(\pi f T_f)} \right)^2 \right\} \right] \left(\langle a^2 \rangle - \mu_a^2 |\mu_b(f)|^2 \right)$$
$$+ \frac{N_{TH} N_s}{T_{TH}^2} \left(1 - R_\Delta^c(f) \left[1 - \frac{1}{N_{TH} N_s} \left(\frac{\sin(\pi f N_{TH} T_s)}{\sin(\pi f T_s)} \frac{\sin(\pi f N_s T_f)}{\sin(\pi f T_f)} \right)^2 \right] \right) \mu_a^2 |\mu_b(f)|^2 \qquad \text{(3C2-30)}$$
$$\times \sum_{k=-\infty}^{\infty} \delta\left(f - \frac{k}{T_{TH}} \right)$$

From (3C2-30), it is seen that when zero-mean amplitude modulation is used, the spectral lines vanish. Zero-mean amplitude modulation also implies the loss of the ability to shape the remaining smooth portion of the spectrum through position modulation. That is if hybrid modulation (example, combining BPSK and PPM) were employed to eliminate spectral lines, modulation parameters can no longer be used to shape the continuous portion of the spectrum. Also, if the characteristic function of the position modulation, $\{b_m T_d\}$, is zero at integer multiples of the code repetition frequency ($1/T_{TH}$), then the spectral lines again vanish completely.

Conclusions

This Annex derives analytical expressions for the power spectral density (PSD) of UWB waveforms in terms of the properties of the key UWB waveform parameters. Specifically, it is shown that the PSD is affected by properties of the time-hopping (TH) code, statistical properties of the modulation scheme and the integration gain embedded in the UWB waveform. For codes with a finite period, it is shown that spectral lines appear at integer multiples of the code repetition frequency defined as the reciprocal of

the TH code period. It is seen that the benefits of good code design (low non-zero lag correlation) are maximized when using codes of large length. Conversely, the power of the TH code to tailor the spectrum diminishes as the periodicity of the code decreases. The PSD is also affected by the integration gain. When the integration gain is low, the PSD can be controlled by the modulation scheme. This dependence of the PSD on the modulation vanishes as the integration gain becomes very large. It is shown that for zero-mean modulation such as BPSK, the spectral lines vanish completely. However, along with the elimination of the spectral lines, the ability to control the continuous portion of the spectrum is also lost. In the case of pulse position modulation, it is shown that the spectra lines vanish if the characteristic function of the position modulation exhibits nulls at the TH code repetition frequency. However, as mentioned earlier, this control of the spectrum using the modulation becomes ineffective when large integration gains are required for the UWB communications system.

NOTE 1
Derivation of Fourier Transform of the Correlation Functions

Define a general cross-correlation function as

$$R_{x,y}(\tau) = \int_{-\infty}^{\infty} x(t) y^*(t-\tau) dt$$

The goal is to find the Fourier Transform (FT) of the cross-correlation function as defined above. The FT of $R_{x,y}(\tau)$ is derived as follows:

$$S_{x,y}(f) = F_\tau\left(R_{x,y}(\tau)\right) = \int_{-\infty}^{\infty}\left[\int_{-\infty}^{\infty} x(t) y^*(t-\tau) dt\right] e^{-j2\pi f\tau} d\tau$$

$$= \int_{-\infty}^{\infty} x(t)\left[\int_{-\infty}^{\infty} y^*(t-\tau) e^{-j2\pi f\tau} d\tau\right] dt$$

$$= \int_{-\infty}^{\infty} x(t)\left[\int_{-\infty}^{\infty} y(t-\tau) e^{j2\pi f\tau} d\tau\right]^* dt$$

$$\overset{t-\tau=u}{=} \int_{-\infty}^{\infty} x(t)\left[\int_{-\infty}^{\infty} y(u) e^{-j2\pi f u} du\right]^* e^{-j2\pi f t} dt$$

$$= \int_{-\infty}^{\infty} x(t)\left[Y(f)\right]^* e^{-j2\pi f t} dt$$

$$= X(f) Y^*(f)$$

Using the above result, the FT of the auto-correlation function is obtained as

$$S_x(f) = F_\tau\left(R_x(\tau)\right) = X(f) X^*(f) = \left|X(f)\right|^2$$

NOTE 2
Proofs of Results used in the Text

1. Proof of $\lim_{N\to\infty}\frac{1}{NT}\left(\frac{\sin(\pi fNT)}{\sin(\pi fT)}\right)^2=\frac{1}{T^2}\sum_{n=-\infty}^{\infty}\delta\left(f-\frac{n}{T}\right)$

Let $G_N(f)=\frac{1}{NT}\left(\frac{\sin(\pi fNT)}{\sin(\pi fT)}\right)^2=\sum_{n=-\infty}^{\infty}a_n e^{-j2\pi fnT}$ where the RHS is the Fourier series representation. The period of $G_N(f)$ is $1/T$ Hz. The coefficients are

$$a_n=T\int_{-\frac{1}{2T}}^{\frac{1}{2T}}G_N(f)e^{j2\pi fnT}df$$

Let $b_n=\lim_{N\to\infty}a_n=\lim_{N\to\infty}T\int_{-\frac{1}{2T}}^{\frac{1}{2T}}G_N(f)df=\lim_{N\to\infty}\frac{1}{\pi NT}\int_{-\frac{\pi}{2}}^{\frac{\pi}{2}}\left(\frac{\sin Nx}{\sin x}\right)^2dx$

From [6], $\int_0^{\pi/2}\left(\frac{\sin ax}{\sin x}\right)^2dx=\frac{a\pi}{2}-\frac{1}{2}\sin\pi a\left[2a\beta(a)-1\right]$ where

$\beta(x)=\int_0^1\frac{t^x-1}{1+t}dt$ $\quad \mathrm{Re}\,x>0$ from [6] p. 947, 8.371(1)

Hence $b_n=\frac{1}{T}$ and $\lim_{N\to\infty}G_N(f)=\frac{1}{T}\sum_{n=-\infty}^{\infty}e^{-j2\pi fnT}=\frac{1}{T^2}\sum_{n=-\infty}^{\infty}\delta\left(f-\frac{n}{T}\right)$

where the last equality is from Poisson's sum formula.

2. Proof of $\lim_{T\to\infty}\frac{1}{T}\sum_{k=-\infty}^{\infty}\delta\left(f-\frac{k}{T}\right)=1$

In general, $\int_a^b f(x)dx=\lim_{\Delta x\to 0}\Delta x\sum_{k=k_a}^{k_b}f(k\Delta x)$, where $k_a=\frac{a}{\Delta x}$ and $k_b=\frac{b}{\Delta x}$.

To evaluate $\lim_{T\to\infty}\frac{1}{T}\sum_{k=-\infty}^{\infty}V(f)\delta\left(f-\frac{k}{T}\right)$, let $Z(\xi)=V(f)\delta(f-\xi)$ and $\Delta f=\frac{1}{T}$, where $V(f)=1$.

Then,

$$\lim_{T\to\infty}\frac{1}{T}\sum_{k=-\infty}^{\infty}V(f)\delta\left(f-\frac{k}{T}\right)=\lim_{\Delta f\to 0}\Delta f\sum_{k=-\infty}^{\infty}Z(k\Delta f)=\int_{-\infty}^{\infty}Z(\xi)d\xi$$

$$=\int_{-\infty}^{\infty}V(f)\delta(f-\xi)d\xi=V(f)=1$$

Annex 3D

UWB PSD using the method of Simon, Hinedi, and Lindsey [7]

The UWB signal can be represented as:

$$x(t) = \sum_n a_n v(t - nT - \Delta_n) \tag{3D-1}$$

Its autocorrelation is:

$$\begin{aligned} R_x(t,\tau) &= E\{x(t)x^*(t+\tau)\} \\ &= \sum_n \sum_m R_a(n,m) E\{v(t - nT - \Delta_n)v^*(t - mT - \Delta_m + \tau)\} \end{aligned} \tag{3D-2}$$

where $R_a(n,m) = E\{a_n a_m^*\}$.

With $v(t) = \int_{-\infty}^{\infty} V(f) e^{j2\pi ft} df$ this becomes

$$\begin{aligned} R_x(t,\tau) = \sum_n \sum_m R_a(n,m) \int_y \int_z E\{e^{-j2\pi y\Lambda_n} e^{+j2\pi z\Delta_m}\} V(y) V^*(z) \\ \times e^{-j2\pi ynT} e^{+j2\pi zmT} e^{j2\pi(y-z)t} e^{-j2\pi z\tau} dz\, dy \end{aligned} \tag{3D-3}$$

Averaging over T gives

$$\begin{aligned} R_x(\tau) = \langle R_x(t,\tau) \rangle_t = \sum_n \sum_m R_a(n,m) \int_y \int_z E\{e^{-j2\pi y\Lambda_n} e^{+j2\pi z\Delta_m}\} V(y) V^*(z) \\ \times e^{-j2\pi ynT} e^{+j2\pi zmT} \left\langle e^{j2\pi(y-z)t} \right\rangle_t e^{-j2\pi z\tau} dz\, dy \end{aligned} \tag{3D-4}$$

and taking the Fourier transform over τ gives the PSD as

$$S_x(f) = \int_{-\infty}^{\infty} R_x(\tau) e^{-j2\pi f\tau} d\tau = \sum_n \sum_m R_a(n,m) \int_y \int_z E\left\{e^{-j2\pi y\Lambda_n} e^{+j2\pi z\Delta_m}\right\} V(y) V^*(z) \\ \times e^{-j2\pi ynT} e^{+j2\pi zmT} \left\langle e^{j2\pi(y-z)t} \right\rangle_t \left(\int_{-\infty}^{\infty} e^{-j2\pi(f+z)\tau} d\tau \right) dz\, dy \tag{3D-5}$$

Since $\int_{-\infty}^{\infty} e^{-j2\pi(f+z)\tau} d\tau = \delta(f+z)$,

$$S_x(f) = \sum_n \sum_m R_a(n,m) \int_y E\left\{e^{-j2\pi y\Lambda_n} e^{-j2\pi f\Delta_m}\right\} \\ \times V(y) V^*(-f) e^{-j2\pi ynT} e^{-j2\pi fmT} \left\langle e^{j2\pi(y+f)t} \right\rangle_t dy \tag{3D-6}$$

multiplying by $e^{-j2\pi fnT} e^{+j2\pi fnT}$ gives

$$S_x(f) = \sum_n \sum_m R_a(n,m) \int_y E\left\{e^{-j2\pi y\Lambda_n} e^{-j2\pi f\Delta_m}\right\} V(y) V^*(-f) \\ \times e^{-j2\pi(y+f)nT} e^{-j2\pi f(m-n)T} \left\langle e^{j2\pi(y+f)t} \right\rangle_t dy \tag{3D-7}$$

This expression can be used as a point of departure for several different cases, depending on whether or not the $\{a_n\}$ and/or the $\{\Delta_n\}$ are cyclostationary. The simplest case is if neither are. In that case, $R_a(n,m) = R_a(m-n)$ and $E\left\{e^{-j2\pi y\Lambda_n} e^{-j2\pi f\Delta_m}\right\}$ can be denoted as $R_\Delta(m-n, y, f)$. The time average is taken over the frame interval *T*, giving

$$\left\langle e^{j2\pi(y+f)t} \right\rangle_t = \frac{1}{T} \int_{-T/2}^{T/2} e^{j2\pi(y+f)t} dt = \frac{\sin \pi(y+f)T}{\pi(y+f)T} \tag{3D-8}$$

and therefore

$$S_x(f) = \sum_n \sum_m R_a(m-n) \int_y E\left\{e^{-j2\pi y\Lambda_n} e^{-j2\pi f\Delta_m}\right\} V(y) V^*(-f) \\ \times e^{-j2\pi(y+f)nT} e^{-j2\pi f(m-n)T} \frac{\sin \pi(y+f)T}{\pi(y+f)T} dy \tag{3D-9}$$

Letting $l = m - n$, this becomes

$$S_x(f) = \sum_l R_a(l) e^{-j2\pi flT} \int_y V(y) V^*(-f) \frac{\sin \pi (y+f)T}{\pi (y+f)T} R_\Delta(l, y, f) \sum_n e^{-j2\pi (y+f)nT} \, dy \qquad \text{(3D-10)}$$

From the Poisson sum formula, $\sum_n e^{-j2\pi (y+f)nT} = \frac{1}{T} \sum_k \delta\left(y + f - \frac{k}{T} \right)$ giving

$$S_x(f) = \frac{1}{T} \sum_l R_a(l) e^{-j2\pi flT} V^*(-f) \sum_k V\left(\frac{k}{T} - f \right) \frac{\sin \pi kT}{\pi kT} R_\Delta\left(l, \frac{k}{T} - f, f \right) \qquad \text{(3D-11)}$$

but $\frac{\sin \pi kT}{\pi kT} = 0$ for $k \neq 0$, hence:

$$\begin{aligned} S_x(f) &= \frac{1}{T} \sum_l R_a(l) e^{-j2\pi flT} V^*(-f) V(-f) R_\Delta(l, -f, f) \\ &= \frac{1}{T} |V(f)|^2 \sum_l R_a(l) e^{-j2\pi flT} R_\Delta(l, -f, f) \end{aligned} \qquad \text{(3D-12)}$$

Letting $b_n(f) = e^{+j2\pi f \Delta_n}$ and $R_{b(f)}(l) = E\{ b_n(f) b_{n+l}^*(f) \} = R_\Delta(l, -f, f)$ gives:

$$S_x(f) = \frac{1}{T} |V(f)|^2 \sum_l R_a(l) e^{-j2\pi flT} R_{b(f)}(l). \qquad \text{(3D-13)}$$

Letting $a_n = \alpha_n + \mu_a$, with $\overline{\alpha}_n = 0$ and $\mu_a = \overline{a}_n$ gives $R_a(l) = R_\alpha(l) + |\mu_a|^2$. Similarly, $b_n(f) = \beta_n(f) + \mu_b(f)$ and $R_{b(f)}(l) = R_{\beta(f)}(l) + |\mu_\beta(f)|^2$. Note that $R_{\beta(f)}(0) = 1$.

Assuming that $R_\alpha(l) = R_{\beta(f)}(l) = 0, l \neq 0$, the PSD is

$$\begin{aligned} S_x(f) &= \frac{1}{T} |V(f)|^2 \left[R_a(0) + |\mu_a|^2 |\mu_b(f)|^2 \sum_{l \neq 0} e^{-j2\pi flT} \right] \\ &= \frac{1}{T} |V(f)|^2 \left[R_a(0) - |\mu_a|^2 |\mu_b(f)|^2 + |\mu_a|^2 |\mu_b(f)|^2 \sum_l e^{-j2\pi flT} \right] \end{aligned} \qquad \text{(3D- 14)}$$

Since $\sum_l e^{-j2\pi flT} = \frac{1}{T}\sum_k \delta\left(f - \frac{k}{T}\right)$,

$$S_x(f) = \frac{1}{T}|V(f)|^2\left[R_a(0) - |\mu_a|^2|\mu_b(f)|^2 + |\mu_a|^2|\mu_b(f)|^2\frac{1}{T}\sum_k \delta\left(f - \frac{k}{T}\right)\right] \tag{3D-15}$$

and the continuous and discrete components of the PSD are

$$S_x^c(f) = \frac{1}{T}|V(f)|^2\left[R_a(0) - |\mu_a|^2|\mu_b(f)|^2\right] \tag{3D-16}$$

$$S_x^d(f) = \frac{1}{T^2}|V(f)|^2|\mu_a|^2|\mu_b(f)|^2\sum_k \delta\left(f - \frac{k}{T}\right) \tag{3D-17}$$

where $|\mu_b(f)|^2 = \left|E\left\{e^{j2\pi f\Delta_n}\right\}\right|^2$. Note that Δ_n includes shifts in pulse position due to both modulation and dithering.

Effect of Finite-Length Dithering Code

Assume now that the $\{\Delta_n\}$ represent pulse position shifts due to modulation only, and that a periodic dithering of pulse position is also imposed, giving a total signal of

$$x(t) = \sum_n a_n v(t - nT - \Delta_n - \varepsilon_n) \tag{3D-18}$$

where ε_n is the pulse position shift due to the dithering code.

The dithering code itself can be represented as

$$d(t) = \sum_{n=1}^{N} \delta(t - nT - \varepsilon_n) \tag{3D-19}$$

with

$$D(f) = \sum_{n=1}^{N} e^{-j2\pi fnT}e^{-j2\pi f\varepsilon_n}\ . \tag{3D-20}$$

In this case, the $\{\varepsilon_n\}$ are predefined, not random. The energy spectrum is

$$|D(f)|^2 = \sum_{n=1}^{N}\sum_{m=1}^{N} e^{j2\pi f(n-m)T} e^{j2\pi f(\varepsilon_n-\varepsilon_m)} \tag{3D-21}$$

The PSD of the dithered UWB sequence becomes:

$$\begin{aligned} S_x(f) = \sum_n \sum_m R_a(n,m) \int_y e^{-j2\pi y\varepsilon_n} e^{-j2\pi f\varepsilon_m} E\left\{e^{-j2\pi y\Lambda_n} e^{-j2\pi f\Delta_m}\right\} V(y)V^*(-f) \\ \times e^{-j2\pi(y+f)nT} e^{-j2\pi f(m-n)T} \left\langle e^{j2\pi(y+f)t} \right\rangle_t dy \end{aligned} \tag{3D- 22}$$

As before, letting $l = m - n$ and $R_\varepsilon(n,l,y,f) = e^{-j2\pi y\varepsilon_n} e^{-j2\pi f\varepsilon_{n+l}}$, this becomes

$$\begin{aligned} S_x(f) = \sum_l R_a(l) e^{-j2\pi flT} \int_y V(y)V^*(-f) R_\Delta(l,y,f) \left\langle e^{j2\pi(y+f)t} \right\rangle_t \\ \times \sum_n R_\varepsilon(n,l,y,f) e^{-j2\pi(y+f)nT} dy \end{aligned} \tag{3D-23}$$

Noting that $\sum_{n=-\infty}^{\infty} g(n) = \sum_{k=-\infty}^{\infty}\sum_{n=1}^{N} g(n+kN)$ and $R_\varepsilon(n,l,y,f) = R_\varepsilon(n+kN,l,y,f)$, the inner sum can be written as

$$\begin{aligned} \sum_n R_\varepsilon(n,l,y,f) e^{-j2\pi(y+f)nT} &= \sum_{n=1}^{N}\sum_{k=-\infty}^{\infty} R_\varepsilon(n+kN,l,y,f) e^{-j2\pi(y+f)(n+kN)T} \\ &= \sum_{n=1}^{N} R_\varepsilon(n,l,y,f) e^{-j2\pi(y+f)nT} \sum_{k=-\infty}^{\infty} e^{-j2\pi(y+f)kNT} \\ &= \sum_{n=1}^{N} R_\varepsilon(n,l,y,f) e^{-j2\pi(y+f)nT} \frac{1}{NT} \sum_k \delta\left(y+f-\frac{k}{NT}\right) \end{aligned} \tag{3D-24}$$

where the final equality follows from the Poisson sum formula. Substituting and integrating over *y* gives:

$$S_x(f)=\frac{1}{NT}\sum_l R_a(l)e^{-j2\pi flT}V^*(-f)\sum_k V\left(\frac{k}{NT}-f\right)R_\Delta\left(l,\frac{k}{NT}-f,f\right)$$
$$\times\sum_{n=1}^{N}R_\varepsilon\left(n,l,\frac{k}{NT}-f,f\right)e^{-j2\pi kn/N}\left\langle e^{j2\pi(k/NT)t}\right\rangle_t \qquad \text{(3D-25)}$$

The time average must be taken over NT, the period of the dithering sequence:

$$\left\langle e^{j2\pi(k/NT)t}\right\rangle_t=\frac{1}{NT}\int_{-NT/2}^{NT/2}e^{j2\pi(k/NT)t}dt=\frac{\sin\pi k}{\pi k}=0,\ k\neq 0 \qquad \text{(3D-26)}$$

and with $R_\Delta(l,-f,f)=R_{b(f)}(l)$ as before, the PSD becomes

$$\begin{aligned}S_x(f)&=\frac{1}{NT}\sum_l R_a(l)e^{-j2\pi flT}V^*(-f)V(-f)R_{b(f)}(l)\sum_{n=1}^{N}R_\varepsilon(n,l,-f,f)\\&=\frac{1}{NT}|V(f)|^2\sum_l R_a(l)e^{-j2\pi flT}R_{b(f)}(l)\sum_{n=1}^{N}R_\varepsilon(n,l,-f,f)\\&=\frac{1}{NT}|V(f)|^2\sum_l R_a(l)e^{-j2\pi flT}R_{b(f)}(l)\sum_{n=1}^{N}e^{j2\pi f\varepsilon_n}e^{-j2\pi f\varepsilon_{n+l}}\end{aligned} \qquad \text{(3D-27)}$$

Assuming as before that $R_a(l)=|\mu_a|^2$ and $R_{b(f)}(l)=|\mu_b(f)|^2$ for $l\neq 0$ yields the continuous and discrete components as

$$\begin{aligned}S_x^c(f)&=\frac{1}{NT}|V(f)|^2\left[NR_a(0)R_{b(f)}(0)-N|\mu_a|^2|\mu_b(f)|^2\right]\\&=\frac{1}{T}|V(f)|^2\left[R_a(0)R_{b(f)}(0)-|\mu_a|^2|\mu_b(f)|^2\right]\end{aligned} \qquad \text{(3D-28)}$$

$$S_x^d(f)=\frac{1}{NT}|V(f)|^2|\mu_a|^2|\mu_b(f)|^2\sum_l e^{-j2\pi flT}\sum_{n=1}^{N}e^{j2\pi f\varepsilon_n}e^{-j2\pi f\varepsilon_{n+l}} \qquad \text{(3D-29)}$$

The discrete component can be expressed in a more useful form by recognizing that:

$$\sum_l e^{-j2\pi flT}\sum_{n=1}^{N}e^{j2\pi f\varepsilon_n}e^{-j2\pi f\varepsilon_{n+l}}=\sum_{n=1}^{N}e^{j2\pi f\varepsilon_n}\sum_l e^{-j2\pi flT}e^{-j2\pi f\varepsilon_{n+l}} \qquad \text{(3D-30)}$$

letting $l = m - n$ gives

$$\begin{aligned}\sum_m e^{-j2\pi f(m-n)T} e^{-j2\pi f\varepsilon_m} &= \sum_{k=-\infty}^{\infty}\sum_{m=1}^{N} e^{-j2\pi f(Nk+m-n)T} e^{-j2\pi f\varepsilon_{kN+m}} \\ &= \sum_{k=-\infty}^{\infty} e^{-j2\pi fNkT}\sum_{m=1}^{N} e^{-j2\pi f(m-n)T} e^{-j2\pi f\varepsilon_m} \\ &= \left[\sum_{m=1}^{N} e^{-j2\pi f(m-n)T} e^{-j2\pi f\varepsilon_m}\right]\frac{1}{NT}\left[\sum_{k=-\infty}^{\infty}\delta\left(f-\frac{k}{NT}\right)\right]\end{aligned} \tag{3D-31}$$

Hence,

$$\begin{aligned}&\sum_l e^{-j2\pi flT}\sum_{n=1}^{N} e^{j2\pi f\varepsilon_n} e^{-j2\pi f\varepsilon_{n+l}} \\ &= \frac{1}{NT}\left[\sum_{n=1}^{N}\sum_{m=1}^{N} e^{j2\pi f(n-m)T} e^{j2\pi f\varepsilon_n} e^{-j2\pi f\varepsilon_m}\right]\left[\sum_{k=-\infty}^{\infty}\delta\left(f-\frac{k}{NT}\right)\right] \\ &= \frac{1}{NT}\left|D(f)\right|^2\sum_{k=-\infty}^{\infty}\delta\left(f-\frac{k}{NT}\right)\end{aligned} \tag{3D-32}$$

and

$$\begin{aligned}S_x^d(f) &= \left(\frac{1}{NT}\right)^2\left|V(f)\right|^2\left|\mu_a\right|^2\left|\mu_b(f)\right|^2\left|D(f)\right|^2\sum_{k=-\infty}^{\infty}\delta\left(f-\frac{k}{NT}\right) \\ &= \left(\frac{1}{NT}\right)^2\left|\mu_a\right|^2\sum_{k=-\infty}^{\infty}\left|V\left(\frac{k}{NT}\right)\right|^2\left|\mu_b\left(\frac{k}{NT}\right)\right|^2\left|D\left(\frac{k}{NT}\right)\right|^2\delta\left(f-\frac{k}{NT}\right)\end{aligned} \tag{3D-33}$$

Integration Gain

Now assume that

$$x(t) = \sum_n a_n v_n(t - nT - \Delta_n) \tag{3D-34}$$

where $v_n(t)$ represents a dithering sub-code:

$$v_n(t) = \sum_{m=1}^{M} p(t - mT_f - \varepsilon_{n,m}) \tag{3D-35}$$

where $T = MT_f$ and $p(t)$ now represents the basic UWB pulse waveform and $\varepsilon_{n,m}$ is the pulse position offset for the m^{th} chip in the n^{th} sub-code. The total dithering code is

$$d(t) = \sum_{k=1}^{N} v_k(t - kT) \tag{3D-36}$$

so $v_n(t) = v_{n+N}(t)$ and $d(t) = d(t + NT) = d(t + NMT_f)$.

Also note that

$$D(f) = \sum_{k=1}^{N} V_k(f) e^{-jkT} \tag{3D-37}$$

and

$$|D(f)|^2 = \sum_{n=1}^{N}\sum_{m=1}^{N} V_n(f) V_m^*(f) e^{j2\pi(m-n)fT} \tag{3D-38}$$

This is a generalization of the previous case. The PSD is

$$\begin{aligned} S_x(f) = \sum_n \sum_m R_a(n,m) \int_y E\left\{e^{-j2\pi y\Lambda_n} e^{-j2\pi f\Delta_m}\right\} V_n(y) V_m^*(-f) \\ \times e^{-j2\pi(y+f)nT} e^{-j2\pi f(m-n)T} \left\langle e^{j2\pi(y+f)t} \right\rangle_t dy \end{aligned} \tag{3D-39}$$

Letting $l = m - n$, this becomes

$$S_x(f) = \sum_l R_a(l) e^{-j2\pi flT} \int_y R_\Delta(l, y, f) \left\langle e^{j2\pi(y+f)t} \right\rangle_t \sum_n V_n(y) V_{n+l}^*(-f) e^{-j2\pi(y+f)nT} dy \tag{3D-40}$$

As above, the inner sum can be written as

$$\begin{aligned}\sum_n V_n(y)V_{n+l}^*(-f)e^{-j2\pi(y+f)nT} &= \sum_{n=1}^{N}\sum_{k=-\infty}^{\infty} V_{n+kN}(y)V_{n+kN+l}^*(-f)e^{-j2\pi(y+f)(n+kN)T} \\ &= \sum_{n=1}^{N} V_n(y)V_{n+l}^*(-f)e^{-j2\pi(y+f)nT}\sum_{k=-\infty}^{\infty} e^{-j2\pi(y+f)kNT} \\ &= \sum_{n=1}^{N} V_n(y)V_{n+l}^*(-f)e^{-j2\pi(y+f)nT}\frac{1}{NT}\sum_k \delta\left(y+f-\frac{k}{NT}\right)\end{aligned} \tag{3D-41}$$

where the final equality follows from the Poisson sum formula. Substituting and integrating over y gives:

$$\begin{aligned}S_x(f) &= \frac{1}{NT}\sum_l R_a(l)e^{-j2\pi flT}\sum_k R_\Delta\left(l,\frac{k}{NT}-f,f\right) \\ &\times\sum_{n=1}^{N} V_n\left(\frac{k}{NT}-f\right)V_{n+l}^*(-f)e^{-j2\pi kn/N}\left\langle e^{j2\pi(k/NT)t}\right\rangle_t\end{aligned} \tag{3D-42}$$

The time average must again be taken over NT, the period of the dithering sequence:

$$\left\langle e^{j2\pi(k/NT)t}\right\rangle_t = \frac{\sin\pi k}{\pi k} = 0,\ k\neq 0 \tag{3D-43}$$

and with $R_\Delta(l,-f,f) = R_{b(f)}(l)$ as before, the PSD becomes

$$S_x(f) = \frac{1}{NT}\sum_l R_a(l)e^{-j2\pi flT}R_{b(f)}(l)\sum_{n=1}^{N} V_n(-f)V_{n+l}^*(-f) \tag{3D-44}$$

With $R_a(l) = |\mu_a|^2$ and $R_{b(f)}(l) = |\mu_b(f)|^2$ for $l\neq 0$ the continuous and discrete components are

$$S_x^c(f) = \frac{1}{NT}\sum_{n=1}^{N}|V_n(f)|^2\left[R_a(0)R_{b(f)}(0) - |\mu_a|^2|\mu_b(f)|^2\right] \tag{3D-45}$$

$$S_x^d(f) = \frac{1}{NT}|\mu_a|^2|\mu_b(f)|^2\sum_l e^{-j2\pi flT}\sum_{n=1}^{N} V_n(-f)V_{n+l}^*(-f) \tag{3D-46}$$

to put the discrete component into a more useful form,

$$\begin{aligned}
&\sum_l e^{-j2\pi flT}\sum_{n=1}^{N}V_n(-f)V_{n+l}^*(-f)=\sum_{n=1}^{N}V_n(-f)\sum_l V_{n+l}^*(-f)e^{-j2\pi flT}\\
&=\sum_{n=1}^{N}V_n(-f)\sum_m V_m^*(-f)e^{-j2\pi f(m-n)T}=\sum_{n=1}^{N}V_n(-f)\sum_{k=-\infty}^{\infty}\sum_{m=1}^{N}V_{m+Nk}^*(-f)e^{-j2\pi f(m+Nk-n)T}\\
&=\sum_{n=1}^{N}V_n(-f)\sum_{k=-\infty}^{\infty}e^{-j2\pi fNkT}\sum_{m=1}^{N}V_m^*(-f)e^{-j2\pi f(m-n)T}\\
&=\frac{1}{NT}\left[\sum_{n=1}^{N}\sum_{m=1}^{N}V_n(-f)V_m^*(-f)e^{-j2\pi f(m-n)T}\right]\left[\sum_{k=-\infty}^{\infty}\delta\left(f-\frac{k}{NT}\right)\right]\\
&=\frac{1}{NT}|D(f)|^2\sum_{k=-\infty}^{\infty}\delta\left(f-\frac{k}{NT}\right)
\end{aligned} \tag{3D- 47}$$

and

$$S_x^d(f)=\frac{1}{(NT)^2}|\mu_a|^2|\mu_b(f)|^2|D(f)|^2\sum_{k=-\infty}^{\infty}\delta\left(f-\frac{k}{NT}\right) \tag{3D-48}$$

Summary

In the most general case analyzed here, there are *M* frames or code chips per modulation symbol and *N* modulation symbols per code length. The frame duration is T_f, so the total code duration is NMT_f.

It was assumed in the above that the basic pulse waveform shape was included in the definition of the sub-codes; i.e.,

$$v_n(t)=\sum_{m=1}^{M}p\left(t-mT_f-\varepsilon_{n,m}\right) \tag{3D-49}$$

and therefore the pulse spectrum is not explicitly shown in the resulting expressions. However, the sub-codes could be defined as

$$v_n(t)=\sum_{m=1}^{M}\delta\left(t-mT_f-\varepsilon_{n,m}\right) \tag{3D-50}$$

and the resulting continuous and discrete components of the PSD become

$$S_x^c(f) = \frac{|P(f)|^2}{NMT_f} \sum_{n=1}^{N} |V_n(f)|^2 \left[R_a(0) - |\mu_a|^2 |\mu_b(f)|^2 \right] \tag{3D-51}$$

$$S_x^d(f) = \frac{|P(f)|^2}{(NMT_f)^2} |\mu_a|^2 |\mu_b(f)|^2 |D(f)|^2 \sum_{k=-\infty}^{\infty} \delta\left(f - \frac{k}{NMT_f} \right) \tag{3D-52}$$

Observations

The amplitude and position-modulation terms always appear together. Defining

$$c_n(f) = a_n b_n(f) = a_n e^{+j2\pi f \Delta_n}, \tag{3D-53}$$

it is clear that $R_{c(f)}(0) = E\{c_n(f) c_n^*(f)\} = R_a(0)$, and that if a_n and $b_n(f)$ are uncorrelated (that is, $E\{a_n b_n(f)\} - \mu_a \mu_b(f) = 0$), then $|\mu_c(f)|^2 = |\mu_a|^2 |\mu_b(f)|^2$ (they were assumed uncorrelated in the derivation). In that case, with $\sigma_c^2(f) = R_{c(f)}(0) - |\mu_c(f)|^2$

$$S_x^c(f) = \frac{|P(f)|^2}{NMT_f} \sum_{n=1}^{N} |V_n(f)|^2 \sigma_c^2(f) \tag{3D-54}$$

$$S_x^d(f) = \frac{|P(f)|^2}{(NMT_f)^2} |\mu_c(f)|^2 |D(f)|^2 \sum_{k=-\infty}^{\infty} \delta\left(f - \frac{k}{NMT_f} \right) \tag{3D-55}$$

However, even if a_n and $b_n(f)$ are correlated, the result is the same as can be seen by defining in the derivation

$$R_\Delta(m-n, y, f) = E\left\{ a_n e^{-j2\pi y \Delta_n} a_m^* e^{-j2\pi f \Delta_m} \right\} \tag{3D-56}$$

and removing the term $R_a(m-n)$, giving

$$\begin{aligned} S_x(f) &= \frac{1}{NT} \sum_l e^{-j2\pi f l T} \sum_k R_\Delta\left(l, \frac{k}{NT} - f, f \right) \\ &\times \sum_{n=1}^{N} V_n\left(\frac{k}{NT} - f \right) V_{n+l}^*(-f) e^{-j2\pi k n/N} \left\langle e^{j2\pi (k/NT) t} \right\rangle_t \end{aligned} \tag{3D-57}$$

which leads to the above results. Thus, the PSD can be expressed in terms of a single complex modulation symbol that accounts for both amplitude and position modulation.

Clearly, if the modulation symbol is zero-mean, the discrete component vanishes.

In the above expressions, the PSD was expressed in terms of the spectra of the dithering code and sub-codes, as if these are deterministic. If they are random, then expectations must be taken over these spectra.

Chapter 3 References

[1] A. Papoulis, *Probability, Random Variables, and Stochastic Processes,* third edition, McGraw-Hill, 1991, p. 321.

[2] Alan Petroff and Paul Withington, "Time Modulated Ultra-Wideband (TM-UWB) Overview," presented at Wireless Symposium/Portable by Design, Feb. 25, 2000, San Jose, CA.

[3] J. Romme and L. Piazzo, "On the Power Spectral Density of Time-Hopping Impulse Radio," *IEEE Conf. on UWB Systems and Technologies (UWBST) 2002*, Baltimore, Maryland, May 20-23, 2002.

[4] M. Z. Win, "Spectral density of random time-hopping spread spectrum UWB signals with uniform timing jitter," *Proc. MILCOM*, Vol. 2, 1999.

[5] J. G. Proakis and M. Salehi, *Communications Systems Engineering*, Prentice-Hall, Upper Saddle River, NJ.

[6] I. S. Gradshteyn and I. M. Ryzhik, *Table of Integrals, Series, and Products,* Academic Press, New York, 1980.

[7] M. K. Simon, S. M. Hinedi, and W. C. Lindsey, *Digital Communication Techniques – Signal Design and Detection*, Prentice-Hall, Upper Saddle River, NJ, 1995.

Chapter 4: THE PSD OF A UWB SIGNAL WITH PULSE REPETITION FREQUENCY (PRF) MODULATION

4.1. Introduction

Up to this point, it has been assumed that the UWB pulse position in the frame is varied on a frame-by-frame basis under the control of a combination of modulation and random or pseudorandom dithering processes, and that the pulse positions in successive frames (or blocks of frames, if multi-frame modulation symbols are used) are generally independent. Further, the average pulse rate or pulse repetition frequency (PRF) is constant.

With PRF modulation, the pulse rate itself is varied systematically by a specified modulating waveform, or by a random process with known statistics. This section develops the mathematical foundation needed to understand the characteristics of a UWB signal that is PRF-modulated. Basic relationships are developed first. Following that, the PSD of a swept-PRF signal is derived and example results are presented. Finally, an expression is derived for the PSD of a UWB signal that is PRF-modulated by a random process (e.g., an information-bearing signal).

4.2. General Relationships for PRF Modulation

If the timing-dependent component of UWB signal is expressed as the impulse sequence

$$d(t) = \sum_n \delta(t - T_n) \tag{4-1}$$

then the apparent instantaneous pulse rate can be defined as

$$r_n = \frac{1}{T_n - T_{n-1}} \tag{4-2}$$

In a sense, therefore, any dithering or pulse position modulation represents modulation of the PRF. However, the PRF is varying at a rate that is on the same order as the frame rate (i.e., the average PRF itself), and average PRF (with the average taken over a small number of frames) is time-invariant.

Conversely, "PRF modulation" imposes a systematic variation of the pulse rate according to some $r(t)$, which is either known explicitly or is a random process with known first- and second-order statistics. The problem here is to find the PSD of $d(t)$, given $r(t)$ if it

is deterministic, or the statistics of $r(t)$, if it is random. In the detailed development below, these two cases will be treated separately.

For the distinction between PRF modulation and conventional dithering to be meaningful, it generally will be assumed that the variation in the pulse rate is slow relative to the instantaneous rate. This means that if $\Delta T_n \equiv T_n - T_{n-1}$, then

$$\left| 1 - \frac{\Delta T_{n-1}}{\Delta T_n} \right| << 1. \tag{4-3}$$

4.3. Determining the Pulse Transmit Times

For some time-varying pulse rate $r(t)$, the relationship between *n* and T_n is

$$n = \int_{t_0}^{T_n} r(t)dt \tag{4-4}$$

where t_0 is the start time of the signal and *n* is the number of pulses generated since that time. This is easily seen with an analogy to a body traveling a straight line with a time-varying velocity $v(t)$ mph. The distance covered in time T_x is $x = \int_{t_0}^{T_x} v(t)dt$. If there are markers at 1-mile intervals, corresponding to integer values of *x*, then the time required to reach the n^{th} mile marker is T_n and is analogous to the time at which the n^{th} pulse is transmitted.

Note that if $z(t) = \sum_{n=n_0}^{\infty} U(t - T_n)$, where $U(t)$ is the Heaviside step function, then $n = z(T_n)$, so

$$\int_{T_{n0}}^{T_n} r(t)dt = \sum_{n=n_0}^{\infty} U(t - T_n) \tag{4-5}$$

Also, $d(t) = \frac{d}{dt} z(t)$, so $\langle z(t) \rangle = \left\langle \int_{T_{n0}}^{t} r(\alpha)d\alpha \right\rangle = \bar{r} \cdot (t - T_{n_0})$. Therefore,

$$\langle d(t) \rangle = \frac{d}{dt} z(t) = \bar{r} \tag{4-6}$$

For purposes of analysis and simulation, it often will be necessary to determine the $\{T_n\}$ corresponding to some particular PRF modulating function $r(t)$. In general, a closed-form expression for the $\{T_n\}$ may be difficult to derive even if the function $r(t)$ is deterministic and known explicitly. To see this, let $\zeta(t) \equiv \int r(t)dt$. From (4-4),

$$n = \zeta(T_n) - \zeta(t_0) \tag{4-7}$$

giving

$$T_n = \zeta^{-1}[n + \zeta(t_0)] \tag{4-8}$$

Thus, unless a closed-form expression for $\left[\int r(t)dt\right]^{-1}$ can be found, the $\{T_n\}$ must be found by recursion. An example of a case in which a closed-form expression can be found is that swept PRF, which is analyzed in detail below.

4.4. Recursive Solution for the Pulse Transmit Times

If a closed-form expression for the $\{T_n\}$ cannot be found, then a recursive approach can be used as described here. It is assumed that $r(t)$ is known.

In the interval $\{T_n, T_{n+1}\}$, the average rate is

$$\bar{r}_{n,n+1} = \frac{1}{T_{n+1} - T_n} \int_{T_n}^{T_{n+1}} r(t)dt = \frac{1}{T_{n+1} - T_n} \tag{4-9}$$

Invoking the assumption of slow variation of $r(t)$, this gives

$$r_n = r(T_n) \cong \bar{r}_{n,n+1}(t) = \frac{1}{T_{n+1} - T_n} \tag{4-10}$$

and the recursion relation is

$$T_{n+1} = T_n + \frac{1}{r(T_n)} \tag{4-11}$$

where $r(T_n)$ is determined from the known relationship $r(t)$.

4.5. Periodic PRF-Modulating Functions

If $r(t)$ is deterministic and periodic with period T, then

$$d(t) = \sum_k v(t - kT) \tag{4-12}$$

where $v(t)$ is a finite-duration sequence:

$$v(t) = \sum_{n=0}^{M-1} \delta(t - T_n), \tag{4-13}$$

and the PSD of $d(t)$ is

$$S_d(f) = \frac{1}{T^2} |V(f)|^2 \sum_k \delta\left(f - \frac{k}{T}\right). \tag{4-14}$$

The problem therefore reduces to that of finding the Fourier transform of $v(t)$, which is simply

$$V(f) = \sum_{n=0}^{M-1} e^{-j2\pi f T_n} . \tag{4-15}$$

The $\{T_n\}$ are determined from $r(t)$ either in closed form (if possible) or recursively as above.

The total number of pulses in the finite-duration sequence $v(t)$ is

$$M = \int_0^T r(t) dt \tag{4-16}$$

This imposes the condition that $\int_0^T r(t)dt$ must be an integer. Also, the condition that $r(t)$ must be slowly-varying relative to the average pulse rate can be expressed as

$$\left|\frac{1}{\Delta T_n} - \frac{1}{\Delta T_{n-1}}\right| << \left|\frac{1}{\Delta T_n}\right|. \tag{4-17}$$

4.6. Properties of the PRF Modulating Function

The PRF modulating function $r(t)$ can be written as

$$r(t) = \bar{r} + \tilde{r}(t) \tag{4-18}$$

where $\bar{r}$ is the average pulse rate and $\tilde{r}(t)$ is the zero-mean time-varying component. There are two general cases: $\tilde{r}(t)$ can be a deterministic signal of duration *T* which is continuously repeated, forming a periodic waveform with period *T*, or $\tilde{r}(t)$ may be an aperiodic stochastic (random) process. Figure 4-1 shows an illustrative PRF modulating function. As is explained in detail below, there are three important parameters: the mean PRF $\bar{r}$, some measure of the pulse rate deviation, which is illustrated in Figure 4-1 as Δr, and the rate-of-change or bandwidth $B_{\tilde{r}}$ of the varying component of modulating function. Relationships among these parameters are developed below.

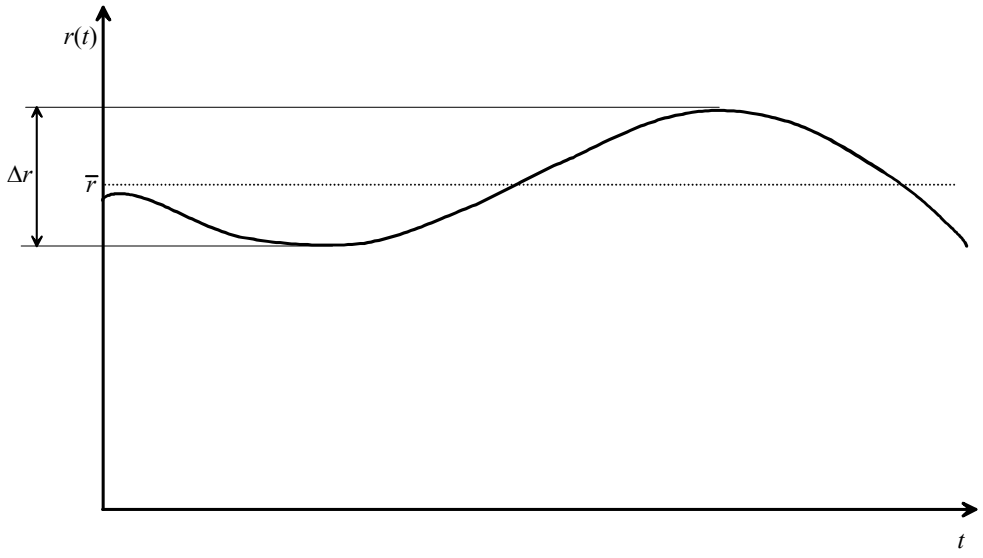

Figure 4-1: *Illustrative example of a PRF modulating function.*

Not surprisingly, there is a strong parallel between PRF modulation and conventional analog FM, for which the instantaneous frequency can be written as $f_i = f_0 + \tilde{f}(t)$, where $\tilde{f}(t)$ gives the time variation of the frequency imposed by the modulation. The FM signal is $A\cos[2\pi f_0 t + \phi(t)]$ where A is the amplitude and $\phi(t)$ is the instantaneous phase, with $\tilde{f}(t) = \frac{1}{2\pi}\frac{d\phi(t)}{dt}$.

With PRF modulation, the average rate $\bar{r}$ is analogous to the nominal FM carrier frequency f_0, and the time-varying component of the pulse rate $\tilde{r}(t)$ plays the same role as $\tilde{f}(t)$ in the FM case. The total cumulative phase $\phi(t)$ of an FM signal is analogous to $n(t) = \text{int}\left(\int_{t_0}^{t} \tilde{r}(\tau)d\tau\right)$, which represents the total number of pulse that have been transmitted at time t.

With FM, the range of frequency variation is usually orders of magnitude less than the carrier; that is, $\left|\tilde{f}(t)\right|_{\max} << f_0$. With PRF modulation, this condition corresponds to the requirement that

$$\left|\tilde{r}(t)\right|_{\max} << \bar{r} \tag{4-19}$$

An important parameter in FM is the *modulation index*, which is the ratio of the frequency deviation to the bandwidth of the modulating signal. In rough terms, *wideband FM* means that the modulation index is much greater than 1.

A modulation index also can be defined for PRF modulation as follows. For a deterministic signal of duration T, the RMS value of $\tilde{r}(t)$ is

$$\sigma_{\tilde{r}} = \sqrt{\frac{1}{T}\int_0^T \tilde{r}^2(t)dt} \tag{4-20}$$

and for a stochastic signal it is

$$\sigma_{\tilde{r}} = \sqrt{\left\langle \tilde{r}^2(t) \right\rangle}. \tag{4-21}$$

The modulation index can be defined as $\sigma_{\tilde{r}}/B_{\tilde{r}}$, where $B_{\tilde{r}}$ is the bandwidth of $\tilde{r}(t)$. If $\tilde{r}(t)$ is a deterministic waveform with Fourier transform $\tilde{R}(f)$, then the total energy in a single cycle of $\tilde{r}(t)$ is

$$E_{\tilde{r}} = \int_{-\infty}^{\infty} \left|\tilde{R}(f)\right|^2 df = \int_0^T \tilde{r}^2(t)dt = T\sigma_{\tilde{r}}^2 \tag{4-22}$$

Letting $\dot{\tilde{r}}(t) = d\tilde{r}(t)/dt$, the Fourier transform of $\dot{\tilde{r}}(t)$ is $-j2\pi f\tilde{R}(f)$, so the total energy in $\dot{\tilde{r}}(t)$ is

$$E_{\dot{\tilde{r}}} = 4\pi^2 \int_{-\infty}^{\infty} f^2 \left|\tilde{R}(f)\right|^2 df = T\sigma_{\dot{\tilde{r}}}^2 \tag{4-23}$$

One reasonable definition of bandwidth is

$$B_{\tilde{r}} = \sqrt{\frac{\int_{-\infty}^{\infty} f^2 \left|\tilde{R}(f)\right|^2 df}{\int_{-\infty}^{\infty} \left|\tilde{R}(f)\right|^2 df}} = \frac{\sigma_{\dot{\tilde{r}}}}{2\pi\,\sigma_{\tilde{r}}} \tag{4-24}$$

Similarly, if $\tilde{r}(t)$ is stochastic with PSD $S_{\tilde{r}}(f)$, then the average power in $\tilde{r}(t)$ is

$$\overline{P}_{\tilde{r}} = \int_{-\infty}^{\infty} S_{\tilde{r}}(f)df = \left\langle \tilde{r}^2(t) \right\rangle = \sigma_{\tilde{r}}^2 \tag{4-25}$$

The PSD of $\dot{\tilde{r}}(t)$ is $4\pi^2 f^2 S_{\tilde{r}}(f)$, so the average power in $\dot{\tilde{r}}(t)$ is

$$\overline{P}_{\dot{\tilde{r}}} = 4\pi^2 \int_{-\infty}^{\infty} f^2 S_{\dot{\tilde{r}}}(f)df = \left\langle \dot{\tilde{r}}(t) \right\rangle = \sigma_{\dot{\tilde{r}}}^2 \tag{4-26}$$

and the bandwidth is

$$B_{\tilde{r}} = \sqrt{\frac{\int_{-\infty}^{\infty} f^2 S_{\tilde{r}} df}{\int_{-\infty}^{\infty} S_{\tilde{r}} df}} = \frac{\sigma_{\dot{\tilde{r}}}}{2\pi\sigma_{\tilde{r}}} \tag{4-27}$$

The modulation index for PRF modulation therefore can be defined as

$$\beta_{prfm} = \frac{\sigma_{\tilde{r}}}{B_{\tilde{r}}} = 2\pi\frac{\sigma_{\tilde{r}}^2}{\sigma_{\dot{\tilde{r}}}} \tag{4-28}$$

Note that β_{prfm} is dimensionless, since $\sigma_{\tilde{r}}$ has the dimension of Hz (pulses/sec), and $\sigma_{\dot{\tilde{r}}}$ has the dimension of Hz^2.

It generally is assumed in the following analyses that $\beta_{prfm} >> 1$, which is analogous to the wideband FM case.

4.7. PSD of a Swept PRF Signal

The PSD for a swept PRF signal can be determined analytically. Figure 4-2 shows the PRF vs. time for a single sweep cycle, where the sweep interval is *T*, the average rate is $\bar{r}$, and the pulse rate varies linearly from $\bar{r} - r_d$ to $\bar{r} + r_d$ over the sweep interval as shown. The periodic modulating waveform is therefore a "sawtooth" as shown in Figure 4-3.

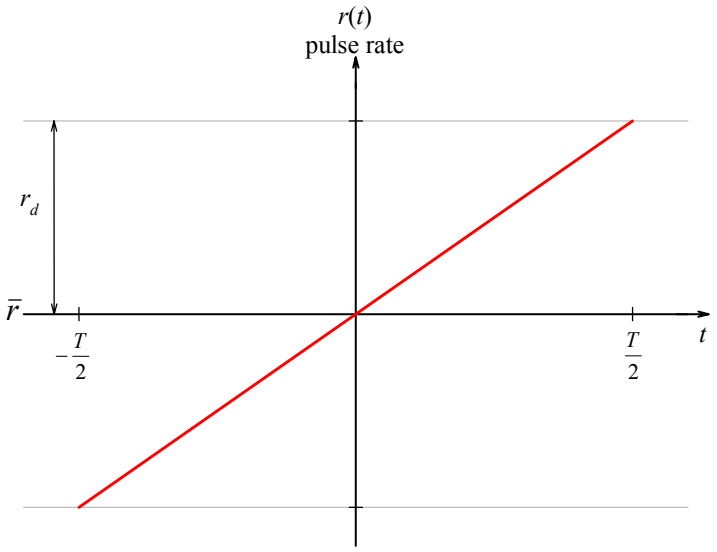

Figure 4-2: *PRF vs. time for a single cycle of a swept-PRF signal*

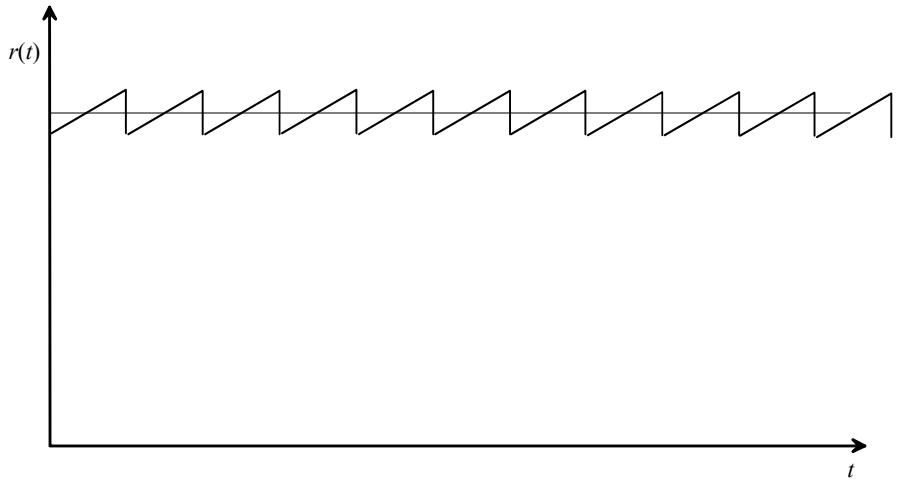

Figure 4-3: *Swept PRF modulating waveform*

The pulse rate is

$$r(t) = \bar{r} + at \quad -\frac{T}{2} < t \le \frac{T}{2} \tag{4-29}$$

with $a = 2r_d/T$.

A single cycle of the swept-PRF UWB signal (with each pulse idealized as an impulse) can be represented as:

$$v(t) = \sum_{n=-M+1}^{M} \delta(t - T_n), \tag{4-30}$$

and T_n is related to *n* by

$$\begin{aligned} n &= \int_{-T/2}^{T_n} r(t)dt - M = \bar{r}T_n + \int_{-T/2}^{T_n} at\,dt \\ &= \bar{r}T_n + \frac{a}{2}\left(T_n^2 - \frac{T^2}{4}\right) \end{aligned} \tag{4-31}$$

Note that T_{-M} corresponds to the final pulse of the previous cycle, which occurs at $t = -T/2$. Substituting $n = M$, with the arbitrary constraint $T_M = T/2$, gives $M = \bar{r}\,T/2$, or $\bar{r} = 2M/T$ as would be expected. Applying the quadratic formula yields

$$T_n = \frac{-\bar{r} + \sqrt{\bar{r}^2 + 2a\left(n + T^2/4\right)}}{a} \tag{4-32}$$

and $V(f) = \sum_{n=-M+1}^{M} e^{-j2\pi f T_n}$.

4.7.1. Parameter Selection and Constraints

Since $\bar{r}T/2$ must be an integer, $\bar{r}$ and T cannot be chosen completely arbitrarily. The factor of 2 is due to the definition of $v(t)$ in this case as having an even number of pulses. Without this constraint, $\bar{r}T$ would be required to be an integer.

The time-varying component of the PRF modulating function is

$$\tilde{r}(t) = at \quad -\frac{T}{2} < t \le \frac{T}{2} \tag{4-33}$$

which has an average power of

$$\sigma_{\tilde{r}}^2 = \frac{1}{T}\int_{-T/2}^{T/2} (at)^2\, dt = \frac{a^2T^2}{12} \tag{4-34}$$

so $\sigma_{\tilde{r}} = \frac{aT}{2\sqrt{3}}$. Since $\dot{\tilde{r}}(t) = a$, $\sigma_{\dot{\tilde{r}}} = a$, the bandwidth of $\tilde{r}(t)$ is $B_{\tilde{r}} = \sqrt{3}/\pi T$, and the modulation index is

$$\beta_{prfm} = \frac{\pi a T^2}{6} = \frac{\pi r_d T}{3} \cong r_d T \tag{4-35}$$

Thus, the "wideband" condition is $r_d >> 1/T$ in this case.

With $\frac{1}{\Delta T_n} - \frac{1}{\Delta T_{n-1}} = \Delta r_n$ and $a = \frac{\Delta r_n}{\Delta T_n}$, the "slow variation" condition translates to $\Delta r_n << r_n$. Dividing both sides by ΔT_n gives $a << r_n^2 \ \forall n$, so the requirement on *a* is $a << r_{\min}^2$, with $r_{\min} = \bar{r} - r_d$.

4.7.2. Analytic Approximations for Swept PRF

In the case of a swept PRF, it is possible to develop both rough and fairly accurate analytic expressions for $V(f)$, which provide insights beyond what is gained by simple brute-force computation of the spectrum. To do so, it is convenient to define the nominal UWB "frame" interval as $T_f \equiv 1/\bar{r}$, and to represent T_n as

$$T_n = nT_f + \varepsilon_n \tag{4-36}$$

Hence,

$$\varepsilon_n = -\frac{r_d}{\bar{r}}\left(\frac{T_n^2}{T} - \frac{T}{4}\right) = -\frac{r_d}{\bar{r}}\left[\frac{(nT_f + \varepsilon_n)^2}{T} - \frac{T}{4}\right] \tag{4-37}$$

Rearranging and substituting gives

$$\varepsilon_n\left[1 + \frac{r_d}{\bar{r}}\left(\frac{n}{M} + \frac{\varepsilon_n}{T}\right)\right] = \frac{r_d}{\bar{r}}\left(\frac{T}{4} - \frac{n^2T_f^2}{T}\right) \tag{4-38}$$

From (4-38), it is clear that $\varepsilon_M = \varepsilon_{-M} = 0$ (as would be expected, since the final pulse in the cycle was constrained to occur at $t = T/2$), and that $\varepsilon_{n\max} = \varepsilon_0 = \frac{r_d}{\bar{r}} \cdot \frac{T}{4}$. Thus, for $r_d/\bar{r} << 1$,

$$\varepsilon_n \cong \frac{r_d}{\bar{r}}\left(\frac{T}{4} - \frac{n^2T_f^2}{T}\right) \tag{4-39}$$

The Fourier transform of $v(t)$ is

$$V(f) = P(f)\sum_{n=-M+1}^{M} e^{-j2\pi fT_n} = P(f)\sum_{n=-M+1}^{M} e^{-j2\pi fnT_f} \cdot e^{-j2\pi f\varepsilon_n} \tag{4-40}$$

Defining $\varphi(f) = P(f)e^{-j2\pi f\frac{r_d}{\bar{r}}\frac{T}{4}}$ and $\alpha = \frac{r_d}{\bar{r}T} = \frac{r_d}{2M}$,

$$\begin{aligned} V(f) &= \varphi(f) \sum_{n=-M+1}^{M} e^{-j2\pi f\left(nT_f - \alpha n^2 T_f^2\right)} \\ &= \varphi(f) \sum_{n=-M+1}^{M} \int_{-\infty}^{\infty} e^{-j2\pi f\left(t-\alpha t^2\right)} \delta\left(t - nT_f\right) dt \\ &= \varphi(f) \int_{-\infty}^{\infty} e^{-j2\pi f\left(t-\alpha t^2\right)} \sum_{n=-M+1}^{M} \delta\left(t - nT_f\right) dt \end{aligned} \tag{4-41}$$

With $p_T(t) = \begin{cases} 1 & -T/2 < t \le T/2 \\ 0 & \text{otherwise} \end{cases}$, (see Figure 4-4), (4-41) becomes

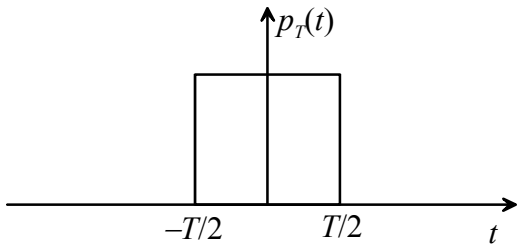

Figure 4-4: *The rectangular pulse* $p_T(t)$

$$V(f) = \varphi(f) \int_{-\infty}^{\infty} p_T(t) e^{-j2\pi f\left(t-\alpha t^2\right)} \sum_{n=-\infty}^{\infty} \delta\left(t - nT_f\right) dt \tag{4-42}$$

From the Poisson sum formula, $\sum_{n=-\infty}^{\infty} \delta\left(t - nT_f\right) = \frac{1}{T_f} \sum_{n} e^{j2\pi nt/T_f}$, giving

$$V(f) = \varphi(f) \cdot \frac{1}{T_f} \sum_{n} \int_{-\infty}^{\infty} p_T(t) e^{-j2\pi\left(f - n/T_f\right)t} \, e^{j2\pi f \alpha t^2} dt \tag{4-43}$$

The integral is of the form $\int_{-\infty}^{\infty} g(t) e^{j\beta t^2} e^{-j\omega t} dt$, with $\beta = 2\pi f\alpha$, $\omega = 2\pi\left(f - n/T_f\right)$ and $g(t) = p_T(t)$. This integral represents the transform of an amplitude-modulated linear FM signal. Papoulis [1] (pp. 263-271) provides an approximate solution, as well as an exact solution for the specific case in which $g(t)$ is a rectangular waveform as is the case here.

4.7.3. Approximate First-Order Solution

The approximate solution is:

$$\int_{-\infty}^{\infty} g(t) e^{j\beta t^2} e^{-j\omega t} dt \approx \sqrt{\frac{j\pi}{\beta}} e^{-j\omega^2/4\beta} g\left(\frac{\omega}{2\beta}\right) \tag{4-44}$$

Substituting for β and ω gives

$$V(f) \approx \frac{\varphi(f)}{T_f} \sqrt{\frac{j}{2f\alpha}} \sum_n e^{-j\pi\left(f - n/T_f\right)^2/2\pi f\alpha} p_T\left(\frac{f - n/T_f}{2f\alpha}\right) \tag{4-45}$$

The summand is non-zero for

$$\left|\frac{f - n/T_f}{2f\alpha}\right| \le \frac{T}{2} \tag{4-46}$$

or, with $\alpha = r_d/\bar{r}T$,

$$\frac{n/T_f}{1 + r_d/\bar{r}} \le f \le \frac{n/T_f}{1 - r_d/\bar{r}} \tag{4-47}$$

The width of the rectangular window for index *n* in the frequency domain is

$$\frac{n}{T_f}\left(\frac{1}{1 - r_d/\bar{r}} - \frac{1}{1 + r_d/\bar{r}}\right) = \frac{2n}{T_f} \frac{r_d/\bar{r}}{1 - \left(r_d/\bar{r}\right)^2} \cong \frac{2n}{T_f} \frac{r_d}{\bar{r}} = 2nr_d \tag{4-48}$$

The approximation assumes that $r_d << \bar{r}$. Hence,

$$p_T\left(\frac{f - n/T_f}{2f\alpha}\right) \cong p_{2nr_d}\left(f - \frac{n}{T_f}\right) \tag{4-49}$$

which is shown in Figure 4-5.

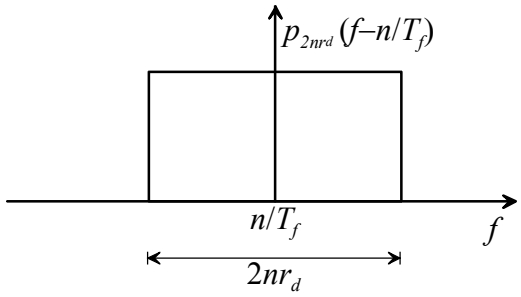

Figure 4-5: *Frequency domain window for index n.*

The centers of these frequency-domain windows are separated by $\bar{r}$ Hz. Therefore, the windows do not overlap if $|n| < \bar{r}/2r_d$, a condition corresponds to frequencies less than $\bar{r}^2/r_d$. If the bandwidth of the pulse waveform is less than this, then the windows do not overlap within the pulse bandwidth and the energy spectral density of $v(t)$ is:

$$|V(f)|^2 \approx \frac{|P(f)|^2}{2T_f^2 f\alpha} \sum_n p_{2nr_d}\left(f - \frac{n}{T_f}\right) = \frac{|P(f)|^2}{2T_f\alpha} \sum_n \frac{1}{fT_f} p_{2nr_d}\left(f - \frac{n}{T_f}\right) \tag{4-50}$$

Again invoking the assumption that $r_d << r$, the width of each rectangular frequency component is small relative to its center frequency, so

$$\frac{1}{fT_f} p_{2nr_d}\left(f - \frac{n}{T_f}\right) \cong \frac{1}{n} p_{2nr_d}\left(f - \frac{n}{T_f}\right) \tag{4-51}$$

With this approximation and the fact that $\alpha = r_d/2M$, the ESD is

$$|V(f)|^2 \approx M\bar{r}|P(f)|^2 \sum_n \frac{1}{nr_d} p_{2nr_d}\left(f - \frac{n}{T_f}\right) \tag{4-52}$$

Thus, the approximate ESD consists of rectangular components centered at frequencies that are integer multiples of the average pulse rate $\bar{r}$.

4.7.4. Power and Energy

As a sanity check on the approximate solution, the average signal power and the total energy per sweep can be computed in the time and frequency domains and compared. To simplify the comparison, it is assumed that the UWB pulse has a rectangular spectrum

with one-sided bandwidth B_p which spans N rectangular components on the positive frequency axis (excluding the zero-frequency component). Thus, $B_p = \bar{r}(N + 1/2)$, and it is assumed that $2Nr_d < \bar{r}$ so there is no overlap. The component at frequency $n\bar{r}$ has a width of $2nr_d$ and a magnitude $M\bar{r}|P(f)|^2 / nr_d$, and therefore an energy of $E_n = 2M\bar{r}|P(f)|^2$, so the components have equal energy in this approximate representation since $|P(f)|$ is assumed constant across the pulse passband. The total energy in $v(t)$ is therefore

$$E_v = (2N+1)E_n = 4B_p M|P(f)|^2 \tag{4-53}$$

The total energy can also be calculated in the time domain for comparison. If the energy in each UWB pulse is E_p, then the total energy of the 2*M*-pulse sequence $v(t)$ is $E_v = 2ME_p$. Since $E_p = 2B_p|P(f)|^2$, it follows that $E_v = 4B_p M|P(f)|^2$.

When the sweep pattern is repeated every *T* seconds, the total power is

$$\overline{P}_{tot} = \bar{r}E_p = \frac{E_v}{T} \tag{4-54}$$

The power spectrum is a set of discrete tones separated by $1/T$ Hz. The power in the tone at frequency k/T is

$$P\left(\frac{k}{T}\right) = \frac{1}{T^2}\left|V\left(\frac{k}{T}\right)\right|^2 . \tag{4-55}$$

Since the n^{th} rectangular component of $V(f)$ spans $2nr_d$ Hz, it includes $2nr_d T$ tones. The power in each tone is

$$P_n = \frac{1}{T^2} \cdot \frac{M\bar{r}|P(f)|^2}{nr_d} \tag{4-56}$$

with $\bar{r}|P(f)|^2 = \overline{P}_{tot}/2B_p$ this becomes

$$P_n = \frac{1}{T^2} \cdot \frac{M\overline{P}_{tot}}{2B_p n r_d} \tag{4-57}$$

The total power of the tones within the n^{th} rectangular component therefore is

$$P_{n\Sigma} = 2nr_d T P_n = \frac{M\overline{P}_{tot}}{B_p T} \tag{4-58}$$

With $2N+1$ components, the total power is then $\frac{M\overline{P}_{tot}}{B_p T} \cdot (2N+1) = \frac{2M\overline{P}_{tot}}{\bar{r}T} = \overline{P}_{tot}$, since $\bar{r}T = 2M$.

Also note that $P_{n\Sigma} = \frac{2M\bar{r}|P(f)|^2}{T} = \frac{E_n}{T}$ as would be expected.

The above simple calculations serve to verify that the approximate solution for the PSD of a swept PRF signal is accurate with respect to total energy and average power.

4.7.5. Example

As an example, the power spectrum for a swept-PRF signal was computed both numerically and also using a rough first-order approximation (as a sanity check), for an average rate of $\bar{r} = 100$ MHz, a sweep rate of 100 kHz (10 μs sweep time), a pulse rate deviation of $r_d = 2$ MHz, and a total average power of 1 watt (so the results can easily be adjusted to any desired total power). For simplicity, the pulse waveform was assumed to have a rectangular spectrum, flat from 0 Hz to 1.05 GHz. This idealized assumption was made to avoid any spectral shaping due to the pulse itself, so that the shaping due to the PRF modulation can be clearly seen.

Since this waveform has a period of 10 μs, the spectrum consists of discrete tones separated by 100 kHz. The power in each tone is controlled by the energy spectral density of a single 10-μs sweep. The resulting (one-sided) spectrum "envelope" is shown in Figure 4-6, with a close-up of a portion of the spectrum in Figure 4-7.

The computation and plotting resolution is 100 kHz in both cases. What is shown represents the power of a tone at the corresponding frequency. The individual tones are shown explicitly on the expanded scales in Figure 4-8 and Figure 4-9.

Note that the power is confined to regions which are centered on harmonics of the average pulse rate (100 MHz in this case). With the rough first-order analytic model used, these regions are approximated as rectangular bins. The width of the bin centered

on the n^{th} harmonic is $2nr_d$ Hz, or in this case $4n$ MHz, and the height is $P_n = \dfrac{\overline{P}_{tot}\bar{r}}{2TB_p r_d n}$, where $\overline{P}_{tot}$ is the average transmit power and B_p is the (one-sided) pulse bandwidth. Therefore, the total power within each bin is $\overline{P}_{tot}\bar{r}/B_p$. There is also a single tone at $f = 0$ with a power of $\overline{P}_{tot}\bar{r}/2B_p$.

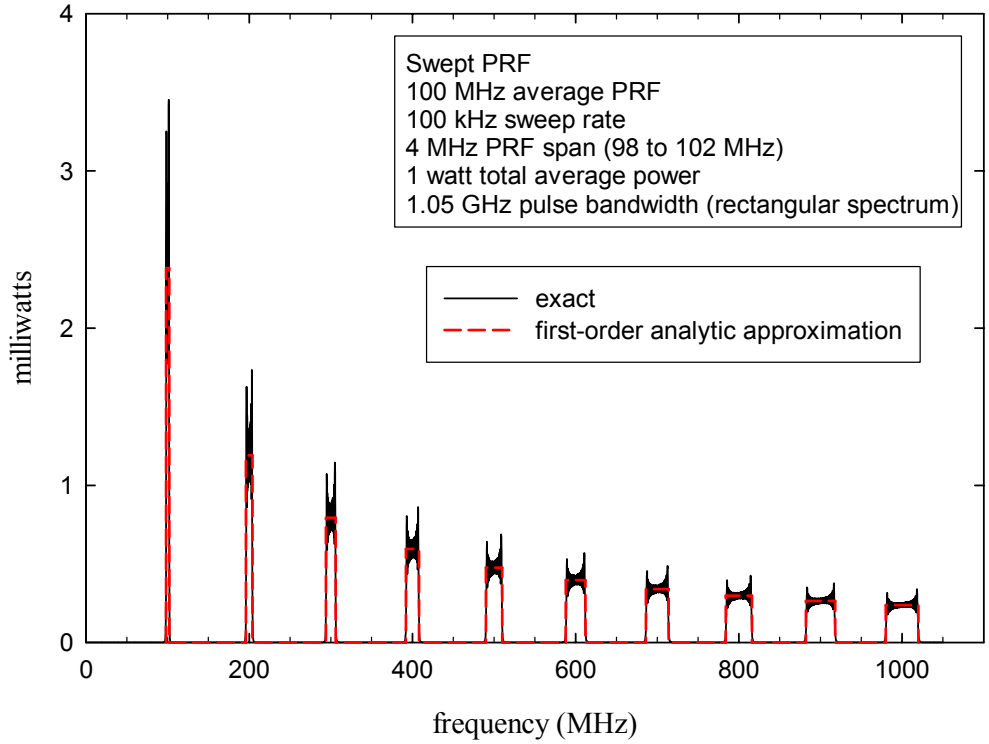

Figure 4-6: *Example PSD of a swept PRF signal.*

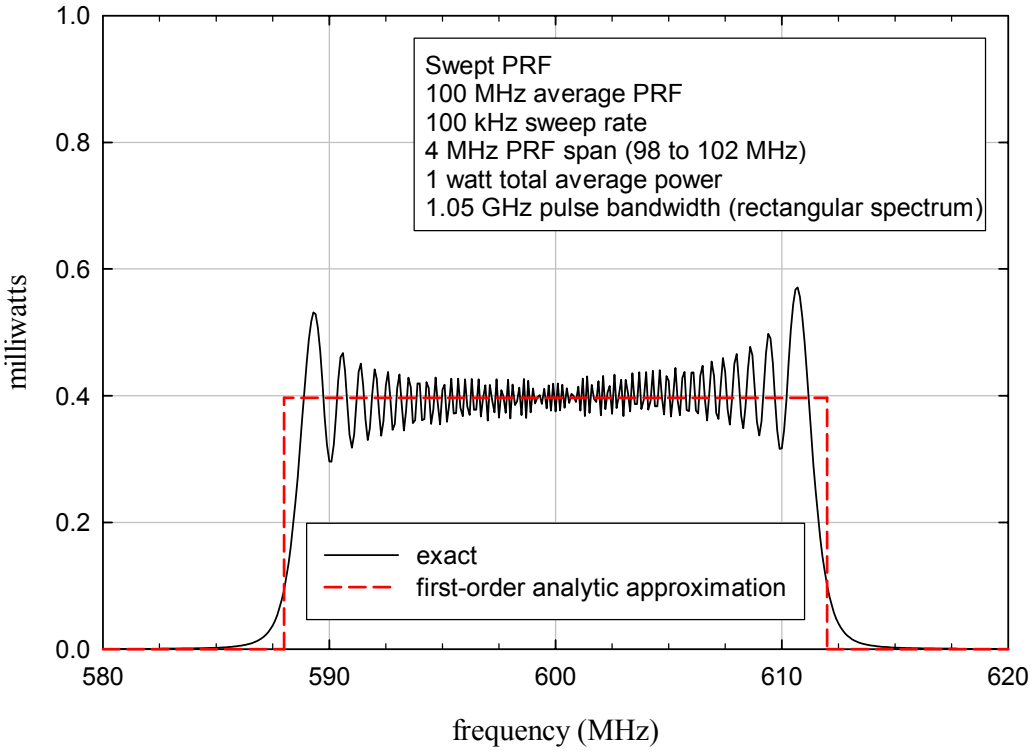

Figure 4-7: *Closeup view of a segment of Figure 4-6.*

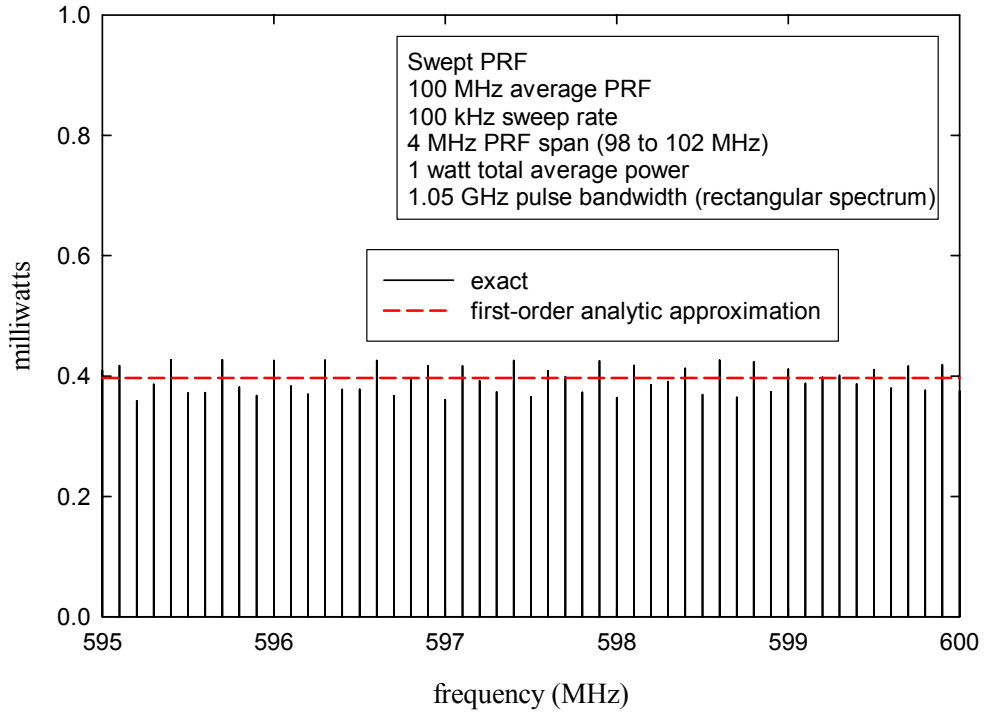

Figure 4-8: *Individual tones of the swept PRF signal.*

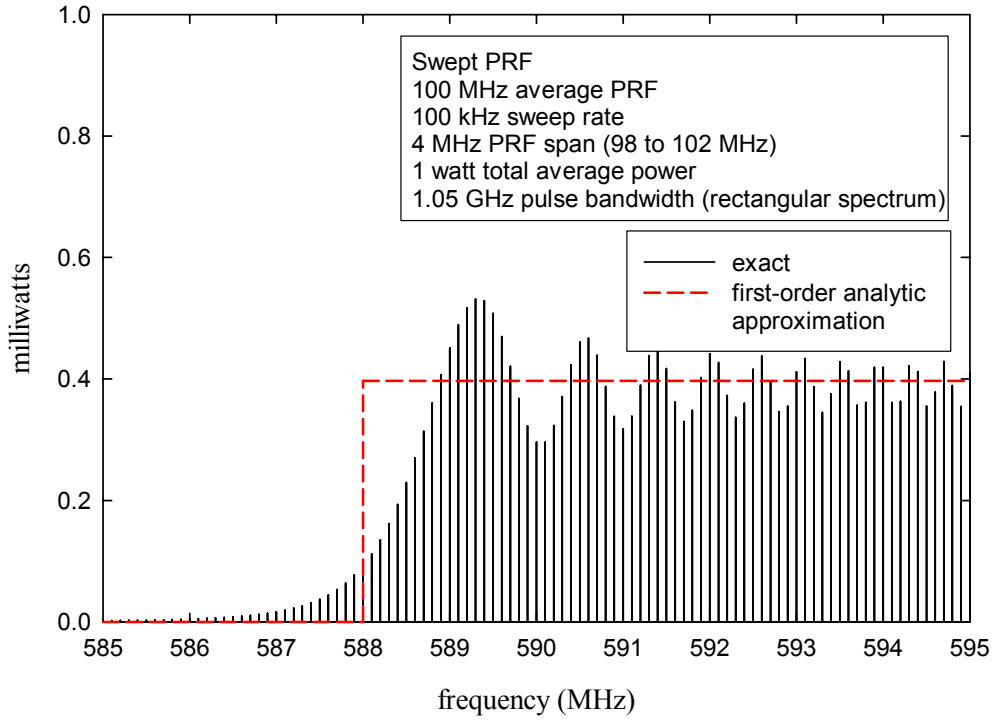

Figure 4-9: *Individual tones of the swept PRF signal.*

Observations

The power spectrum as presented here represents what would be seen by a filter of infinitesimally narrow bandwidth (and infinitely long integration time). A spectrum analyzer observing the swept PRF signal using a resolution bandwidth less than the sweep rate (100 kHz in this case), would show approximately the same thing, although each tone would be replaced by the frequency response of the resolution filter.
Without the PRF modulation, the spectrum would consist of tones at harmonics of the PRF (100 MHz in this case). Conceptually, sweeping the PRF at a rate that is very low relative to the average pulse rate (100 kHz vs. 100 MHz in this case) effectively moves these tones between the minimum and maximum PRF (98 and 102 MHz in this case). The n^{th} harmonics of the minimum and maximum are $98n$ and $102n$ MHz, respectively, and therefore the effective frequency range over which power is spread is proportional to n as seen in the results. However, the total power is the same as the power in the original n^{th} harmonic tone without the PRF modulation. Therefore, the power in the spectrum representing the swept n^{th} harmonic must vary inversely with n. Since the PRF is uniformly-distributed between is minimum and maximum values, spectral envelopes that are roughly rectangular are not surprising.

4.8. Refined Analytic Solution using Fresnel Integrals

As shown by Papoulis, the exact solution to the summand in (4-43) is

$$\int_a^b e^{j\beta t^2} e^{-j\omega t} dt = \sqrt{\frac{\pi}{2\beta}} \left[K\left(\frac{2\beta b - \omega}{\sqrt{2\beta\pi}} \right) - K\left(\frac{2\beta a - \omega}{\sqrt{2\beta\pi}} \right) \right] e^{-j\omega^2/4\beta} \tag{4-59}$$

with

$$K(x) = \int_0^x e^{j\pi t^2/2} dt = C(x) + jS(x) \tag{4-60}$$

where

$$C(x) = \int_0^x \cos\frac{\pi}{2} t^2 dt \qquad S(x) = \int_0^x \sin\frac{\pi}{2} t^2 dt \tag{4-61}$$

are the Fresnel integrals, as shown in Figure 4-10.

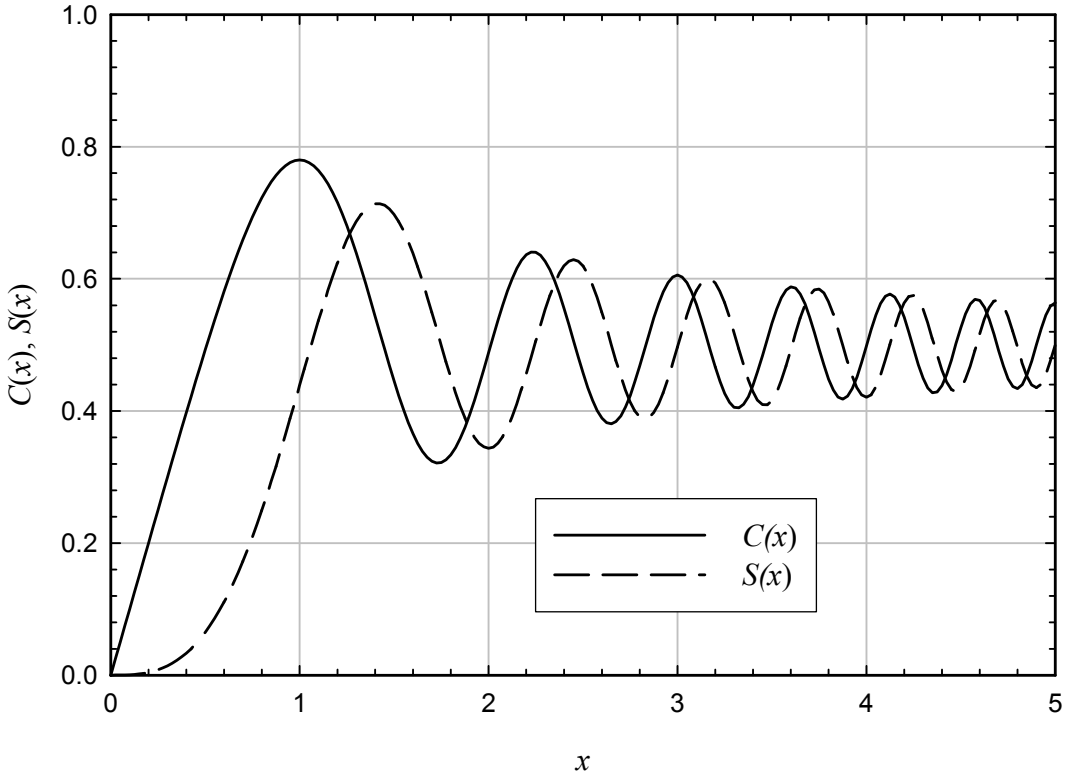

Figure 4-10: *The Fresnel integrals*

In this case, $\beta = 2\pi f\alpha$, $\omega = 2\pi\left(f - n/T_f\right)$ as above, $a = -T/2$, and $b = T/2$. Letting

$$V(f) = \varphi(f) \cdot \frac{1}{T_f} \sum_n y_n \tag{4-62}$$

where $\varphi(f) = P(f) e^{-j2\pi f \frac{r_d}{\bar{r}} \frac{T}{4}}$ and

$$\begin{aligned} y_n &= \int_{-\infty}^{\infty} p_T(t) e^{-j2\pi(f - n/T_f)t} \, e^{j2\pi f \alpha t^2} \, dt = \int_{-T/2}^{T/2} e^{-j2\pi(f - n/T_f)t} \, e^{j2\pi f \alpha t^2} \\ &= \sqrt{\frac{1}{4f\alpha}} \left[K(x_1) - K(x_2) \right] e^{-j\omega^2/4\beta} \end{aligned} \tag{4-63}$$

where

$$\begin{aligned} x_1 &= \frac{2\pi f \alpha T - 2\pi(f - n/T_f)}{2\pi\sqrt{f\alpha}} = \frac{f(\alpha T - 1) + n/T_f}{\sqrt{f\alpha}} \\ x_2 &= \frac{-2\pi f \alpha T - 2\pi(f - n/T_f)}{2\pi\sqrt{f\alpha}} = \frac{-f(\alpha T + 1) + n/T_f}{\sqrt{f\alpha}} \end{aligned} \tag{4-64}$$

Thus,

$$y_n = \sqrt{\frac{1}{4f\alpha}} \left[C(x_1) + jS(x_1) - C(x_2) - jS(x_2) \right] e^{-j\omega^2/4\beta} \tag{4-65}$$

and

$$|y_n|^2 = \frac{1}{4f\alpha} \left\{ \left[C(x_1) - C(x_2) \right]^2 + \left[S(x_1) - S(x_2) \right]^2 \right\} \tag{4-66}$$

Substituting for $\alpha = \frac{r_d}{2M}$ and letting

$$x_h = -x_2 = \frac{f \cdot \left(1 + \frac{r_d}{\bar{r}}\right) - \frac{n}{T_f}}{\sqrt{f r_d / 2M}}$$
$$x_l = -x_1 = \frac{f \cdot \left(1 - \frac{r_d}{\bar{r}}\right) - \frac{n}{T_f}}{\sqrt{f r_d / 2M}} \tag{4-67}$$

gives

$$|y_n(f)|^2 = \frac{M}{2 f r_d}\left\{[C(x_h) - C(x_l)]^2 + [S(x_h) - S(x_l)]^2\right\} \tag{4-68}$$

Note that if $f = n/T_f$,

$$x_h = \frac{f\, r_d/\bar{r}}{\sqrt{f r_d/2M}} = \frac{\sqrt{2Mf r_d}}{\bar{r}} = \sqrt{2Mn\, r_d/\bar{r}} = \sqrt{nTr_d} \tag{4-69}$$

and $x_l = -x_h$, so assuming that $Tr_d >> 1$,

$$\left|y_n\left(\frac{n}{T_f}\right)\right|^2 = \frac{MT_f}{2nr_d}\left\{[2C(x_h)]^2 + [2S(x_h)]^2\right\} \cong 2\frac{MT_f}{2nr_d} = \frac{MT_f}{nr_d} \tag{4-70}$$

where the approximation follows from the fact that $C(x)$ and $S(x)$ approach 0.5 for large x.

Assuming no overlap of spectral windows, the ESD of $v(t)$ becomes

$$|V(f)|^2 = \frac{|P(f)|^2}{T_f^2}\sum_n |y_n(f)|^2 \tag{4-71}$$

Note that $\left|V\left(\frac{n}{T_f}\right)\right|^2 = |P(f)|^2 \frac{M\bar{r}}{nr_d}$, which is the same as with the first-order approximation.

Computationally, if the spectral windows do not overlap, then it is not necessary to sum over n. Rather, for each value of n, values of $|V(f)|^2$ are computed for frequencies over the range $n\bar{r} - M/T < f \le n\bar{r} + M/T$ with a frequency increment of $1/T$. Each point therefore represents a single calculation rather than a sum over $2M$ calculations as in the exact case. An example result is shown in Figure 4-11, with an expanded view in Figure 4-12. The match to the exact results is close, but not perfect, presumably due to approximation for ε_n that was used to obtain the linear FM form for the analytic expressions.

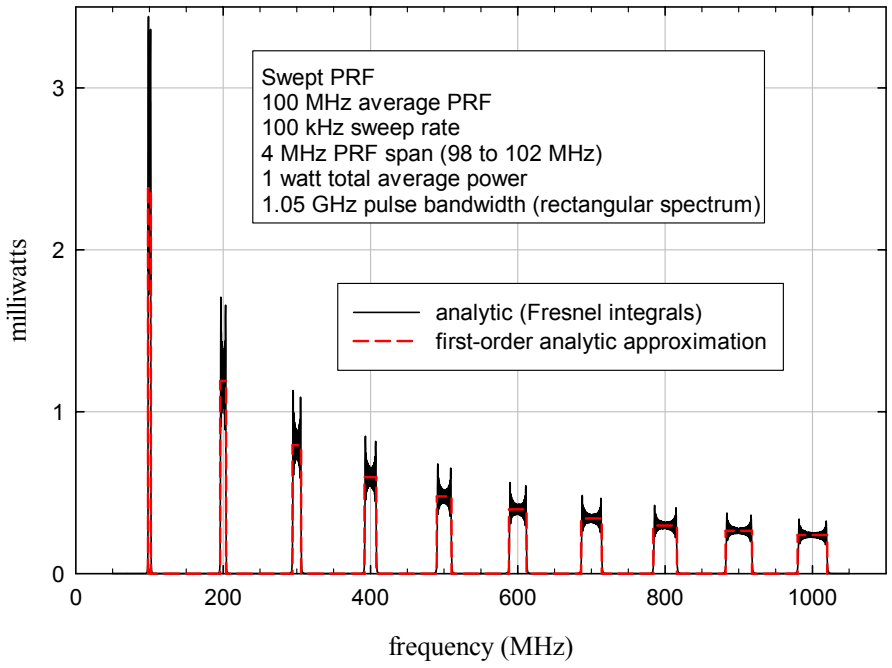

Figure 4-11: *PSD of the swept PRF signal computed using Fresnel integrals.*

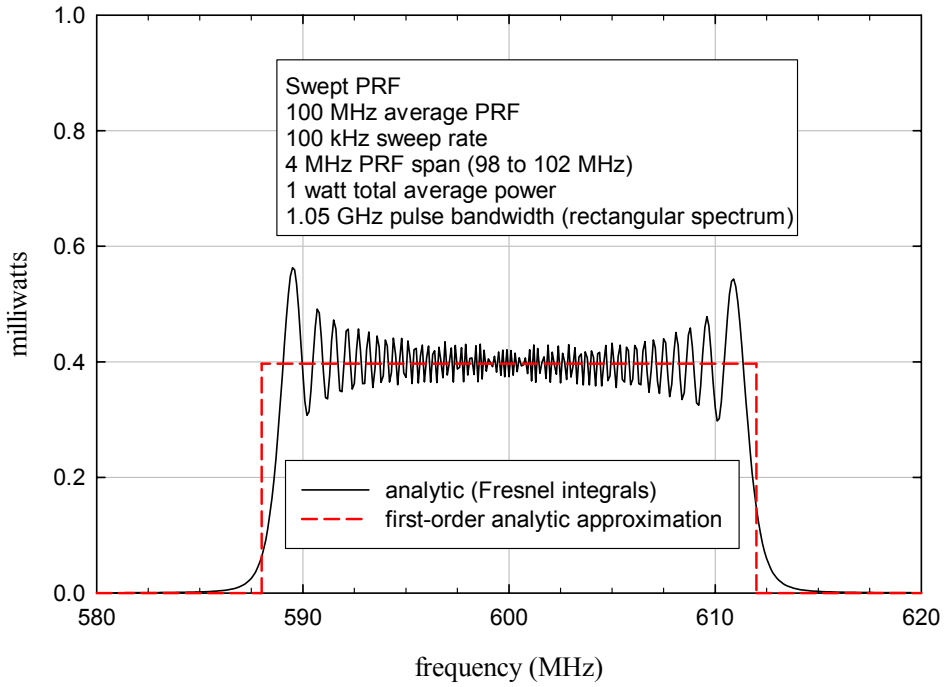

Figure 4-12: *Closeup view of a segment of Figure 4-11.*

4.9. PRF Modulation by a Random Process

The above analysis assumed that the PRF was modulated by a known signal. It is also useful to derive an expression for the PSD when the modulating function is a random process with known probability density function (PDF) and autocorrelation. Such an expression is developed here, subject to certain conditions which are specified.

As before, let $d(t)=\sum_n \delta(t-T_n)$ where the $\{T_n\}$ are controlled by a pulse rate modulating function $r(t)$, which is this case is a stationary random process. With $T_n = nT + \varepsilon_n$, the PSD is

$$S_d(f)=\frac{1}{T}\sum_l \left\langle e^{j2\pi f(\varepsilon_{n+l}-\varepsilon_n)}\right\rangle e^{j2\pi flT} \tag{4-72}$$

and the average pulse rate is $\bar{r}=\frac{1}{T}$. As before, $r(t)=\bar{r}+\tilde{r}(t)$, where $\tilde{r}(t)$ is a zero-mean process. Since $n=\int_{t_0}^{T_n} r(t)dt$ where t_0 is the start time of the process $x(t)$,

$$l = \int_{T_n}^{T_{n+l}} r(t)dt = \bar{r}(T_{n+l} - T_n) + \int_{t_n}^{T_{n+l}} \tilde{r}(t)dt \,. \qquad (4\text{-}73)$$

Substituting

$$T_{n+l} - T_n = lT + \varepsilon_{n+l} - \varepsilon_n \qquad (4\text{-}74)$$

gives

$$\varepsilon_{n+l} - \varepsilon_n = -T \int_{T_n}^{T_{n+l}} \tilde{r}(t)dt \,. \qquad (4\text{-}75)$$

If $r(t)$ is slowly-varying relative to the pulse rate, then $\tilde{r}(T_n) \cong \tilde{r}(T_{n+l})$ for $|T_{n+l} - T_n| \le \tau_{\tilde{r}}$, where $\tau_{\tilde{r}}$ depends on the autocovariance of $\tilde{r}(t)$. Applying this condition and letting $\tilde{r}_n \equiv r(T_n) \cong r(T_{n+l})$ gives $\varepsilon_{n+l} - \varepsilon_n \cong -T\tilde{r}_n(lT + \varepsilon_{n+l} - \varepsilon_n)$ or

$$\varepsilon_{n+l} - \varepsilon_n = -lT \frac{\tilde{r}_n}{\bar{r} + \tilde{r}_n} \qquad (4\text{-}76)$$

Therefore,

$$lT + \varepsilon_{n+l} - \varepsilon_n = lT\left(1 - \frac{\tilde{r}_n}{\bar{r} + \tilde{r}_n}\right) = lT\frac{\bar{r}}{\bar{r} + \tilde{r}_n} = \frac{l}{\bar{r} + \tilde{r}_n} \,. \qquad (4\text{-}77)$$

If $p_{\tilde{r}}(\alpha)$ is the probability density function (PDF) of $\tilde{r}_n$ then

$$\left\langle e^{j2\pi f(lT + \varepsilon_{n+l} - \varepsilon_n)} \right\rangle \cong \left\langle e^{j2\pi fl/(\bar{r} + \tilde{r}_n)} \right\rangle = \int_{\alpha} e^{j2\pi fl/(\bar{r} + \alpha)} p_{\tilde{r}}(\alpha)d\alpha \,. \qquad (4\text{-}78)$$

For $|l| > \frac{\tau_{\tilde{r}}}{T}$, the integral approaches zero if $\sigma_{\tilde{r}} >> \frac{1}{\tau_{\tilde{r}}}$. This can be seen as follows. Assuming $|\tilde{r}|_{\max} << \bar{r}$, then $\varepsilon_{n+l} - \varepsilon_n \cong -lT(\tilde{r}/\bar{r})$ and:

$$\left\langle e^{j2\pi f(\varepsilon_{n+l} - \varepsilon_n)} \right\rangle \cong \left\langle e^{j2\pi flT(\tilde{r}/\bar{r})} \right\rangle . \qquad (4\text{-}79)$$

Substituting $lT = \tau_{\tilde{r}}$ and $x = \tilde{r}_n / \sigma_{\tilde{r}}$ (so that $\sigma_x = 1$) gives

$$\left\langle e^{j2\pi f(\varepsilon_{n+l}-\varepsilon_n)} \right\rangle \cong \int_\beta e^{j2\pi f \tau_{\tilde{r}} \sigma_{\tilde{r}} (\beta/\bar{r})} p_x(\beta) d\beta = \Phi_x\left(-2\pi f \tau_{\tilde{r}} \sigma_{\tilde{r}} / \bar{r}\right), \tag{4-80}$$

where $\Phi_x(\omega) = \int_x e^{j\omega\beta} p_x(\beta) d\beta$ is the characteristic function of *x*, and $\omega = -2\pi f \tau_{\tilde{r}} \sigma_{\tilde{r}} / \bar{r}$. Clearly, $\Phi_x(0) = 1$, and as $\omega \to \infty$, $\Phi(\omega) \to 0$, so $|\Phi(\omega)| < \Phi_0$ for $|\omega| > \omega_0$ (see [1], pp. 94-96) which translates to the condition $2\pi f \tau_{\tilde{r}} \sigma_{\tilde{r}} / \bar{r} > \omega_0$ to ensure that $|\Phi(\omega)| < \Phi_0$. Since ω_0 is on the order of 1, then

$$\sigma_{\tilde{r}} >> \frac{1}{\tau_{\tilde{r}}} \cdot \frac{1}{fT} \tag{4-81}$$

ensures that $\left\langle e^{j2\pi f(\varepsilon_{n+l}-\varepsilon_n)} \right\rangle \cong 0$ for $lT > \tau_{\tilde{r}}$, in which case

$$\begin{aligned} &\sum_l \left\langle e^{j2\pi f(\varepsilon_{n+l}-\varepsilon_n)} \right\rangle e^{j2\pi flT} \cong \sum_l \left\langle e^{j2\pi fl/(\bar{r}+\tilde{r}_n)} \right\rangle = \sum_l \int_\alpha e^{j2\pi fl/(\bar{r}+\alpha)} p_{\tilde{r}}(\alpha) d\alpha \\ &= \int_\alpha (\bar{r}+\alpha) \sum_k \delta[f - k(\bar{r}+\alpha)] p_{\tilde{r}}(\alpha) d\alpha \\ &= \sum_k \frac{f}{k^2} p_{\tilde{r}}\left(\frac{f}{k} - \frac{1}{T}\right) \end{aligned} \tag{4-82}$$

In other words, the spectral lines are replaced by spectral envelopes that are scaled versions of the PDF of $\tilde{r}(t)$. Note that the "spread" of the k^{th} component is proportional to *k*, so at high frequencies, distinct copies of the PDF may not be discernible.

At this point, an example is useful. Let *x* be uniformly-distributed:

$$p_x(\beta) = \begin{cases} 1/2x_{\max}, & |x| \le x_{\max} \\ 0, & |x| > x_{\max} \end{cases} \tag{4-83}$$

Since $\bar{x} = 0$, $\sigma_x^2 = \int \beta^2 p_x(\beta) d\beta = x_{\max}^2 / 3$. By definition, $\sigma_x = 1$, so $x_{\max} = \sqrt{3}$. The characteristic function is

$$\Phi_x(\omega) = \int e^{j\omega\beta} p_x(\beta) d\beta = \frac{\sin(\omega x_{\max})}{\omega x_{\max}} = \frac{\sin(\omega\sqrt{3})}{\omega\sqrt{3}} \tag{4-84}$$

Since $|\Phi(\omega)| \le 1/\omega\sqrt{3}$, $|\omega_0| = 1/\sqrt{3}|\Phi_0|$ in this case, and for $|lT| > \tau_{\tilde{r}}$,

$$|\Phi(\omega)| < \frac{1}{2\sqrt{3}\pi fT\tau_{\tilde{r}}\sigma_{\tilde{r}}} \cong \frac{1}{10fT} \cdot \frac{1}{\tau_{\tilde{r}}\sigma_{\tilde{r}}} \tag{4-85}$$

With a UWB signal, relevant values of fT will typically be greater than 1 due to the filtering of the pulse by the UWB transmit antenna. If the lowest frequency of practical interest is the second harmonic of the average pulse repetition rate ($fT = 2$), then $|\Phi(\omega)| < 0.01$ if $\sigma_{\tilde{r}} > 5/\tau_{\tilde{r}}$. This is analogous to wideband FM in the analog case (the frequency deviation is at least several times greater than the bandwidth of the modulating signal).

As a second example, assume that *x* is Gaussian with $\sigma_x = 1$, in which case $\Phi_x(\omega) = e^{-\omega^2/2}$. Again with $\omega = -2\pi fT\tau_{\tilde{r}}\sigma_{\tilde{r}}$ and $fT = 2$, $|\Phi(\omega)| < 0.01$ if $\tau_{\tilde{r}}\sigma_{\tilde{r}} > 0.242$, so the wideband requirement is not even necessary in this case.

Chapter 4 References

[1] A. Papoulis, *Signal Analysis*, McGraw-Hill, 1977.

Chapter 5: UWB INTERFERENCE AS SEEN BY A NARROWBAND RECEIVER

5.1. Introduction

Of primary interest in the current phase of the program is how UWB interference will affect "narrowband" receivers. In this context, "narrowband" refers to the controlling bandwidth of the received signal relative to the UWB pulse bandwidth. With a typical radio receiver architecture, the controlling bandwidth is often that of the concatenated intermediate frequency (IF) stages. Figure 5-1 shows a high-level block diagram of a typical dual-conversion receiver. In general, the RF block may include a low-noise amplifier (LNA), an RF filter and a duplexer or antenna switching circuitry.

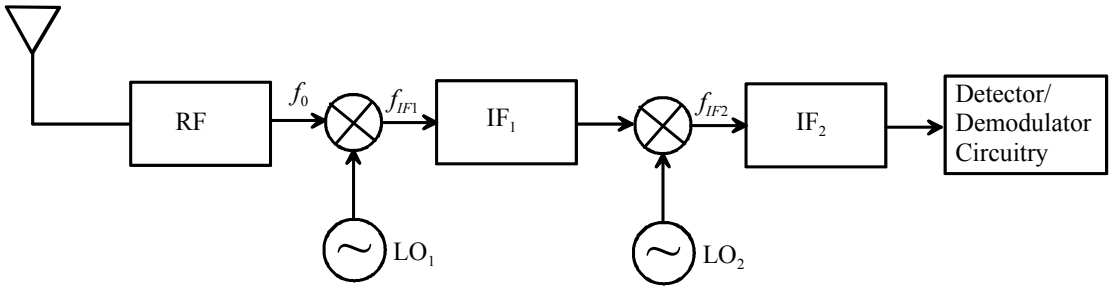

Figure 5-1: *Illustrative dual-conversion radio receiver architecture*

The RF signal, with center frequency f_0, is mixed with first local oscillator (LO) and down-converted to the first IF, then typically passed through an IF amplifier and filter. With a dual-conversion receiver, another down-conversion to a second IF follows, and the second IF signal then is processed by the demodulator or detector functions. Not shown is the automatic gain control (AGC) loop, which typically would adjust the gain of the amplifiers to avoid overload.

Radios typically access multiple channels, so the RF (front end) bandwidth is often much greater than the IF bandwidth, which corresponds to the bandwidth of a single channel. Therefore, in a UWB interference situation, the controlling bandwidth is the narrowest IF bandwidth, which should effectively be the same as the signal bandwidth. In most cases of practical interest, the signal bandwidth of the victim receiver will be orders of magnitude less than the UWB pulse bandwidth. Even a radar with a 20-MHz bandwidth is narrowband compared to a UWB pulse with a bandwidth of 1 or 2 GHz.

The analysis here assumes that linearity holds. While it is possible for an interfering RF signal to be sufficiently powerful to drive the LNA or first mixer into non-linear operation, causing effects such as third-order intermodulation products, such interference levels are in most cases far above the interference required to cause observable receiver

performance degradation. Therefore, the initial analysis will concentrate on interference levels required to compromise performance.[3]

Assuming linearity, the effective UWB interference as seen by the demodulator or detector stages following the final IF stage can be modeled as the output of a filter with center frequency f_0, which is the RF center frequency of a particular channel, and transfer characteristic $H_{IF}(f)$, which represents the aggregate IF frequency response, but centered at f_0 as shown in Figure 5-2, along with the output signal $g(t)$. The bandwidth of $H_{IF}(f)$ is denoted B_{IF} as shown.

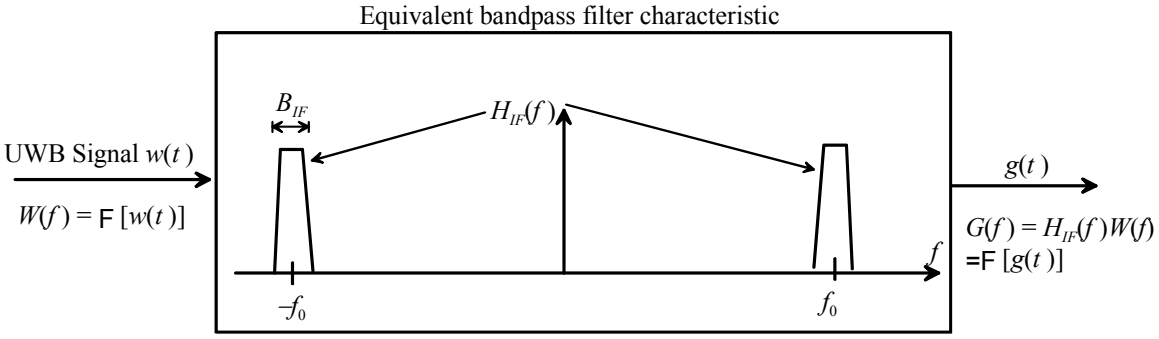

Figure 5-2: *UWB-to-narrowband interference model*

Note that $H_{IF}(f)$ is a fictitious filter, in that it does not exist in an actual receiver; it has the frequency response of the cascaded receive chain (typically dominated by the IF filtering), but a center frequency of the actual RF signal being received. Similarly, $g(t)$ is a fictitious signal, being the result of a UWB signal passed through a fictitious filter. However, $g(t)$ differs from the actual interference at the final IF output by only its center frequency; the actual interference at the demodulator/detector input would be a down-converted version of $g(t)$. What $g(t)$ actually represents is the bandpass-filtered UWB signal.

In the time domain, each UWB pulse effectively acts as an impulse input to the filter $H_{IF}(f)$, so the filter output in response to each UWB pulse is a scaled, time-shifted version of the filter impulse response $h_{IF}(t)$ as shown in Figure 5-3. What is actually shown in the *envelope* of the impulse response, denoted $h_{if}(t)$. As will be seen, the impulse response is the carrier f_0 amplitude-modulated by the envelope $h_{if}(t)$.

[3] It must be kept in mind, however, that because of the fact that UWB signals (1) are wideband; and (2) can include discrete tones of relatively high power, it is conceivable that front-end effects could occur in situations that leave a particular channel unaffected.

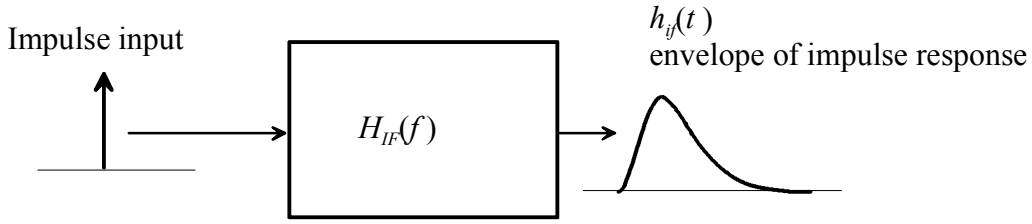

Figure 5-3: *Response of receiver IF to a single UWB pulse*

The actual UWB signal is a sequence of pulses, and the IF response will be a sequence of impulse responses as shown in Figure 5-4. If response envelopes overlap, the composite output signal will depend on the phase relationships among the successive responses. If the pulse rate is low compared to the IF bandwidth, there will be no significant overlap.

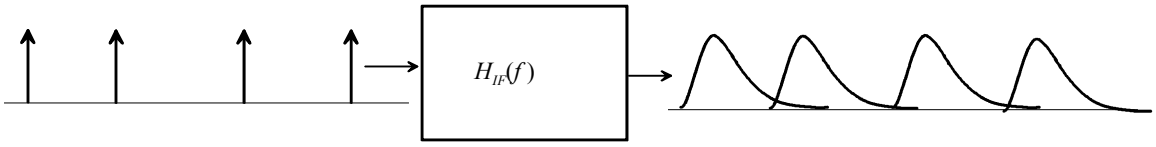

Figure 5-4: *Response of receiver IF to a pulse sequence*

The usefulness of this interference model will become apparent as the analysis develops. The following subsections develop expressions for the interference $g(t)$ in both the frequency and time domains.

5.2. Baseband-Equivalent Interference Representation

This section summarizes the baseband-equivalent model used for the bandpass UWB interference as seen by the victim receiver. Detailed derivations and references are provided in Annex 5A.

5.2.1. General Relationships

From Figure 5-2, the Fourier transform of the bandpass-filtered UWB signal is

$$G(f) = W(f)H_{IF}(f) \tag{5-1}$$

Since $H_{IF}(f)$ is bandpass, $g(t)$ is zero-mean.

$H_{IF}(f)$ can be expressed in terms of its baseband equivalent response, denoted $H_{if}(f)$, and its center frequency f_0 as (see [1], p. 153):

$$H_{IF}(f) = H_{if}(f - f_0) + H_{if}^*(-f - f_0) \tag{5-2}$$

For analysis, it is often useful to represent the bandpass process $g(t)$ in terms of baseband quadrature components $x(t)$ and $y(t)$:

$$g(t) = x(t)\cos 2\pi f_0 t - y(t)\sin 2\pi f_0 t \tag{5-3}$$

The envelope of the IF output interference is $\sqrt{x^2(t) + y^2(t)}$.

Annex 5A develops in detail the relationships among $H_{if}(f)$ and the spectra and power spectral densities of $w(t)$, $g(t)$, $x(t)$, and $y(t)$. As shown, the Fourier transforms of $x(t)$ and $y(t)$ are related to that of the UWB signal $w(t)$ and $H_{if}(f)$ by

$$\begin{aligned} X(f) &= W(f_0 + f)H_{if}(f) + W^*(f_0 - f)H_{if}^*(-f) \\ Y(f) &= \frac{1}{j}W(f_0 + f)H_{if}(f) - \frac{1}{j}W^*(f_0 - f)H_{if}^*(-f) \end{aligned} \tag{5-4}$$

Assuming $x(t)$ and $y(t)$ are zero-mean, stationary, and satisfy the conditions $R_x(\tau) = R_y(\tau)$ and $R_{xy}(\tau) = -R_{yx}(\tau)$, then as shown in Annex 5A, the PSD relationships are, as illustrated in Figure 5-5,

$$\begin{aligned} S_x(f) = S_y(f) &= S_w(f_0 + f)\left|H_{if}(f)\right|^2 + S_w(f_0 - f)\left|H_{if}(-f)\right|^2 \\ &= S_g(f_0 + f)U(f_0 + f) + S_g(f_0 - f)U(f_0 - f) \end{aligned} \tag{5-5}$$

Note that $S_x(f)$ and $S_y(f)$ are symmetric about $f = 0$, even if the positive and negative frequency components of $S_g(f)$ are not symmetric about f_0 and $-f_0$, respectively.

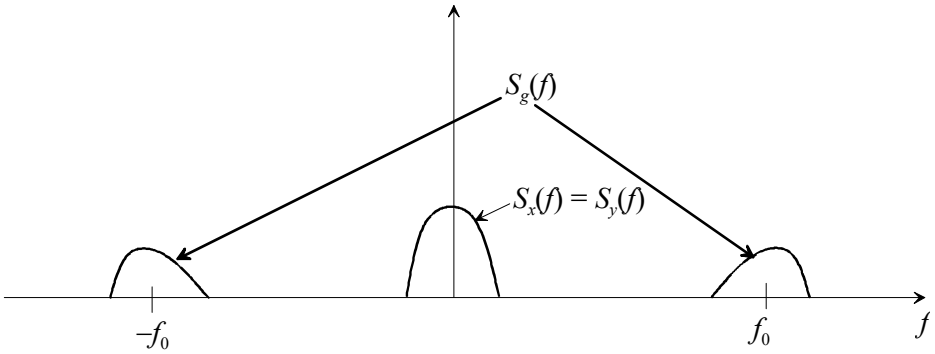

Figure 5-5: *Relationships among the spectra of the bandpass UWB interference and the baseband-equivalent components*

The total average IF output power due to the UWB interference is:

$$\overline{p}_x = \overline{p}_y = \int S_x(f)df = \int S_y(f)df = \int S_g(f)df = \overline{p}_g \tag{5-6}$$

as would be expected, since $\overline{p}_g = \dfrac{\overline{p}_x + \overline{p}_y}{2}$.

5.2.2. Example: A Single CW Tone within the IF Passband

As a simple but relevant example, consider a case in which $W(f)$ has a single discrete spectral component at frequency f_1 within the receiver passband.[4] The UWB signal as seen by the receiver therefore is

$$w_H(t) = A\cos(2\pi f_1 t + \theta) \tag{5-7}$$

and its Fourier transform is

$$W_H(f) = \frac{A}{2}\left[e^{j\theta}\delta(f - f_1) + e^{-j\theta}\delta(f + f_1)\right] \tag{5-8}$$

In the frequency domain, the effective interference is

$$G(f) = \frac{A}{2}\left[H_{IF}(f_1)e^{j\theta}\delta(f - f_1) + H_{IF}(-f_1)e^{-j\theta}\delta(f + f_1)\right] \tag{5-9}$$

Let ϕ represent the phase of $H_{IF}(f_1)$; that is, $H_{IF}(f_1) = |H_{IF}(f_1)|e^{j\phi}$. Since $h_{IF}(t)$ is real, $H_{IF}(f)$ is conjugate-symmetric; i.e., $H_{IF}(-f) = H_{IF}^*(f)$. Therefore $H_{IF}(-f_1) = |H_{IF}(f_1)|e^{-j\phi}$, and the time-domain interference waveform is

$$\begin{aligned} g(t) &= \frac{A}{2}|H_{IF}(f_1)|\left[e^{j(\theta+\phi)}e^{j2\pi f_1 t} + e^{-j(\theta+\phi)}e^{-j2\pi f_1 t}\right] \\ &= A|H_{IF}(f_1)|\cos(2\pi f_1 t + \theta + \phi) \end{aligned} \tag{5-10}$$

Letting $\Delta f = f_1 - f_0$ and noting that $H_{IF}(f_1) = H_{if}(\Delta f)$, the baseband equivalent components are

[4] The receiver "passband" here refers to the bandwidth of a single channel (i.e., the IF bandwidth) rather than the RF front-end bandwidth.

$$\begin{aligned} x(t) &= A\left|H_{if}(\Delta f)\right|\cos(2\pi\Delta f t + \theta + \phi) \\ y(t) &= A\left|H_{if}(\Delta f)\right|\sin(2\pi\Delta f t + \theta + \phi) \end{aligned} \tag{5-11}$$

Since $\left|H_{if}(\Delta f)\right| = \left|H_{IF}(f_1)\right|$, it can be seen that $g(t) = \mathrm{Re}\left\{e^{j2\pi f_0 t}\left[x(t) + jy(t)\right]\right\}$ $= x(t)\cos 2\pi f_0 t - y(t)\sin 2\pi f_0 t$ as expected.

Note that if $f_1 = f_0$, $\Delta f = 0$ and

$$\begin{aligned} x(t) &= A\left|H_{if}(\Delta f)\right|\cos(\theta + \phi) \\ y(t) &= A\left|H_{if}(\Delta f)\right|\sin(\theta + \phi) \end{aligned} \tag{5-12}$$

which are time-invariant. In that case, $x(t)$ and $y(t)$ are not zero-mean and in general do not have equal average power.

The respective PSDs, shown in Figure 5-6 are

$$S_g(f) = \frac{A^2}{4}\left|H_{IF}(f_1)\right|^2\left[\delta(f - f_1) + \delta(f + f_1)\right] \tag{5-13}$$

$$S_x(f) = S_y(f) = \frac{A^2}{4}\left|H_{if}(\Delta f)\right|^2\left[\delta(f - \Delta f) + \delta(f + \Delta f)\right] \tag{5-14}$$

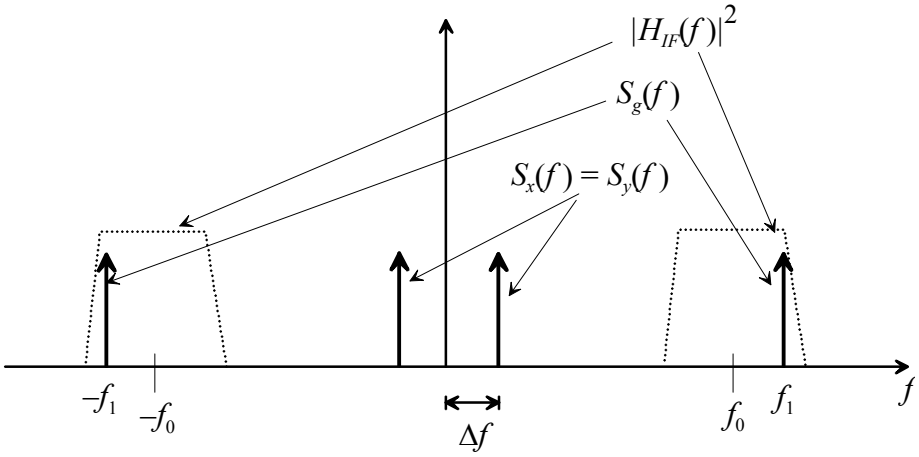

Figure 5-6: *Power spectra for single-tone interference*

5.3. Narrowband Receiver Response to the UWB Pulse Sequence

The preceding section summarized the general relationships among the UWB signal $w(t)$, its bandpass-filtered version $g(t)$, and the baseband-equivalent inphase and quadrature components $x(t)$ and $y(t)$. In this section, expressions are developed specifically for the pulsed UWB signal format.

Recall that the UWB signal can be represented as

$$w(t) = \sum_k a_k p(t - T_k) \tag{5-15}$$

where $p(t)$ is the pulse waveform, a_k is the relative amplitude of the k^{th} pulse, and T_k is the transmit time of the k^{th} pulse.

With

$$d(t) \equiv \sum_k a_k \delta(t - T_k) \tag{5-16}$$

where $\delta(t)$ is the Dirac delta function, the UWB signal can be expressed as

$$w(t) = p(t) * d(t) \tag{5-17}$$

where $*$ denotes convolution. If the IF filter frequency response is $H_{IF}(f)$, then the transform of its response $g(t)$ to the UWB signal is:

$$G(f) = H_{IF}(f)W(f) = H_{IF}(f)P(f)D(f) = H_{IF}(f)P(f)\sum_k a_k e^{-j2\pi f T_k} \tag{5-18}$$

In terms of the baseband-equivalent frequency response $H_{if}(f)$,

$$G(f) = P(f)\left\{H_{if}(f - f_0) + H_{if}^*(-f - f_0)\right\}\sum_k a_k e^{-j2\pi f T_k} \tag{5-19}$$

In general, $P(f)$ is complex and can be written in terms of its magnitude and phase as $P(f) = |P(f)|e^{j\psi(f)}$. Since $p(t)$ is real, $P(f)$ is conjugate-symmetric; that is, $P(-f) = P^*(f)$, so $\psi(-f) = -\psi(f)$. Therefore,

$$G(f) = |P(f)| \left\{ H_{if}(f - f_0) e^{j\psi(f)} + H_{if}^*(-f - f_0) e^{-j\psi(f)} \right\} \sum_k a_k e^{-j2\pi f T_k} \tag{5-20}$$

Typically, the bandwidth of the pulse spectrum $P(f)$ far exceeds that of $H_{IF}(f)$, and $P(f)$ is essentially constant over the passband of $H_{IF}(f)$, in which case

$$G(f) \cong |P(f_0)| \left\{ H_{if}(f - f_0) e^{j\psi_0} + H_{if}^*(-f - f_0) e^{-j\psi_0} \right\} \sum_k a_k e^{-j2\pi f T_k} \tag{5-21}$$

where $\psi_0 = \psi(f_0)$.

The IF filter response to the pulse arriving at time T_k is

$$G_k(f) \cong a_k |P(f_0)| \left\{ H_{if}(f - f_0) e^{j\psi_0} + H_{if}^*(-f - f_0) e^{-j\psi_0} \right\} e^{-j2\pi f T_k} \tag{5-22}$$

Taking the inverse Fourier transform yields:

$$\begin{aligned} g_k(t) &= a_k |P(f_0)| \left\{ h_{if}(t - T_k) e^{j2\pi f_0 (t - T_k)} e^{j\psi_0} + h_{if}^*(t - T_k) e^{-j2\pi f_0 (t - T_k)} e^{-j\psi_0} \right\} \\ &= 2a_k |P(f_0)| \operatorname{Re}\left\{ h_{if}(t - T_k) e^{j(\psi_0 - 2\pi f_0 T_k)} e^{j2\pi f_0 t} \right\} \end{aligned} \tag{5-23}$$

which can be written as

$$g_k(t) = x_k(t) \cos 2\pi f_0 t - y_k(t) \sin 2\pi f_0 t \tag{5-24}$$

where

$$\begin{aligned} x_k(t) &= 2a_k |P(f_0)| \operatorname{Re}\left\{ h_{if}(t - T_k) e^{j(\psi_0 - 2\pi f_0 T_k)} \right\} \\ y_k(t) &= 2a_k |P(f_0)| \operatorname{Im}\left\{ h_{if}(t - T_k) e^{j(\psi_0 - 2\pi f_0 T_k)} \right\} \end{aligned} \tag{5-25}$$

In general, $h_{if}(t)$ is complex, and can be written as $h_{if}(t) = |h_{if}(t)| e^{j\theta(t)}$, giving

$$\begin{aligned} x_k(t) &= 2a_k |P(f_0)| |h_{if}(t - T_k)| \cos[\theta(t - T_k) + \psi_0 - 2\pi f_0 T_k] \\ y_k(t) &= 2a_k |P(f_0)| |h_{if}(t - T_k)| \sin[\theta(t - T_k) + \psi_0 - 2\pi f_0 T_k] \end{aligned}. \tag{5-26}$$

The IF response to the entire UWB pulse sequence is

$$g(t) = \sum_k g_k(t) = x(t)\cos 2\pi f_0 t - y(t)\sin 2\pi f_0 t \tag{5-27}$$

where

$$\begin{aligned} x(t) &= \sum_k x_k(t) \\ y(t) &= \sum_k y_k(t) \end{aligned} \tag{5-28}$$

Note that if $H_{if}(f)$ is conjugate-symmetric, then $h_{if}(t)$ is real, and $\theta(t) = 0$.

To check the spectra of $x(t)$ and $y(t)$ against the general expressions summarized above and developed in Annex 5A, they can be written as

$$\begin{aligned} x_k(t) &= a_k \left| P(f_0) \right| \left\{ h_{if}(t - T_k) e^{-j2\pi f_0 T_k} e^{j\psi_0} + h_{if}^*(t - T_k) e^{j2\pi f_0 T_k} e^{-j\psi_0} \right\} \\ y_k(t) &= a_k \left| P(f_0) \right| \left\{ h_{if}(t - T_k) e^{-j2\pi f_0 T_k} e^{j\psi_0} - h_{if}^*(t - T_k) e^{j2\pi f_0 T_k} e^{-j\psi_0} \right\} \end{aligned} \tag{5-29}$$

giving

$$\begin{aligned} X_k(f) &= a_k \left| P(f_0) \right| \left\{ H_{if}(f) e^{-j2\pi (f_0 + f) T_k} e^{j\psi_0} + H_{if}^*(-f) e^{j2\pi (f_0 - f) T_k} e^{-j\psi_0} \right\} \\ Y_k(f) &= \frac{a_k}{j} \left| P(f_0) \right| \left\{ H_{if}(f) e^{-j2\pi (f_0 + f) T_k} e^{j\psi_0} - H_{if}^*(-f) e^{j2\pi (f_0 - f) T_k} e^{-j\psi_0} \right\} \end{aligned} \tag{5-30}$$

and

$$\begin{aligned} X(f) &= \left\{ H_{if}(f) P(f_0) \sum_k a_k e^{-j2\pi (f_0 + f) T_k} + H_{if}^*(-f) P(-f_0) \sum_k a_k e^{j2\pi (f_0 - f) T_k} \right\} \\ Y(f) &= \frac{1}{j} \left\{ H_{if}(f) P(f_0) \sum_k a_k e^{-j2\pi (f_0 + f) T_k} - H_{if}^*(-f) P(-f_0) \sum_k a_k e^{j2\pi (f_0 - f) T_k} \right\} \end{aligned} \tag{5-31}$$

Since

$$W(f) = P(f) \sum_k a_k e^{-j2\pi f T_k} , \tag{5-32}$$

It is clear that

$$\begin{aligned} X(f) &= H_{if}(f)W(f_0+f)+H_{if}^*(-f)W^*(f_0-f) \\ Y(f) &= \frac{1}{j}\left[H_{if}(f)W(f_0+f)-H_{if}^*(-f)W^*(f_0-f)\right] \end{aligned} \tag{5-33}$$

which agree with (5-4).

If $h_{if}(t)$ is real, then $\theta(t)=0$. If it is assumed that $\psi(f_0)=0$ and $a_k=1\ \forall k$ then:

$$\begin{aligned} x(t) &= 2|P(f_0)|\sum_k h_{if}(t-T_k)\cos 2\pi f_0 T_k \\ y(t) &= -2|P(f_0)|\sum_k h_{if}(t-T_k)\sin 2\pi f_0 T_k \end{aligned} \tag{5-34}$$

5.4. Simulating the Filtered UWB Interference

While the average UWB interference power at the receiver IF output can be obtained by integrating the PSD of $g(t)$, that calculation provides no information about the temporal or statistical properties of the interference. Since those properties can affect the impact of the UWB interference on the detector/demodulator stages following the IF, they need to be understood.

As explained above, the IF response to the UWB pulse sequence is a sequence of IF impulse responses. The duration of each response is inversely proportional to the IF bandwidth. If the pulse rate is low relative to the IF bandwidth, then each response has time to settle before the next pulse arrives, and total IF response is simply a sequence of individual impulse responses, with relative timing the same as that of the UWB pulses.

If the pulse rate exceeds the IF bandwidth, responses will overlap. The resulting signal will depend on the phase relationships among the overlapping components. If the pulse rate is constant (no dithering), then there will be spectral lines at frequencies that are harmonics of the pulse rate. If f_0 happens to coincide with one of those harmonics, then all of the individual IF output responses will be in phase, and the IF output will be constant. On the other hand, if the pulse position is dithered and the average rate exceeds the IF bandwidth, then the IF output can appear noise-like, and under certain conditions will be nearly Gaussian.

Although the qualitative relationships summarized above are useful, sometimes a quantitative understanding of the IF output is necessary, beyond the average power that is provided by the PSD. It therefore is useful to have the capability to simulate the IF output associated with a particular UWB signal, for several reasons:

- Simulation can be used to verify the analytic PSD calculations outlined in Chapter 3.

- Specific simulated IF output waveforms (e.g., envelope vs. time) can be generated as input to simulations of the demodulator/detector stage.
- The statistical properties of the IF output signal can be extracted from simulations. For example, the distributions of the baseband components can be compared to the Gaussian distribution.

The goal of the simulation is to generate the in-phase and quadrature baseband components:

$$\begin{aligned} x(t) &= 2\left|P(f_0)\right| \sum_k a_k \left|h_{if}(t-T_k)\right| \cos\left[\theta(t-T_k)+\psi_0 - 2\pi f_0 T_k\right] \\ y(t) &= 2\left|P(f_0)\right| \sum_k a_k \left|h_{if}(t-T_k)\right| \sin\left[\theta(t-T_k)+\psi_0 - 2\pi f_0 T_k\right] \end{aligned} \tag{5-35}$$

To do so, first define:

$$\begin{aligned} c(t) &= \sum_{k=-\infty}^{\infty} a_k \left|h_{if}(t-T_k)\right| \cos\left[\theta(t-T_k)+\psi(f_0)-2\pi f_0 T_k\right] \\ s(t) &= \sum_{k=-\infty}^{\infty} a_k \left|h_{if}(t-T_k)\right| \sin\left[\theta(t-T_k)+\psi(f_0)-2\pi f_0 T_k\right] \end{aligned} \tag{5-36}$$

so the envelope output power is

$$p_g(t) = \frac{x^2(t)+y^2(t)}{2} = 2\left|P(f_0)\right|^2\left[c^2(t)+s^2(t)\right] \tag{5-37}$$

and

$$g(t) = \sqrt{2p_g(t)}\cos\left[2\pi f_0 t + \tan^{-1}\frac{s(t)}{c(t)}\right] \tag{5-38}$$

5.4.1. Key Parameters

The simulation sampling rate must be high enough to capture the IF filter response with reasonable resolution. This translates to the constraint:

$$R_S \geq J_{\min} B_{IF} \tag{5-39}$$

where R_S is the simulation sample rate, B_{IF} is the effective IF bandwidth, and $J_{\min}$ is the minimum number of samples per IF filter time constant. Letting K_S represent the number of simulation samples per UWB frame, with an average pulse rate of *R*, $R_S = K_S R$ so:

$$K_S \geq J_{\min} \frac{B_{IF}}{R} \tag{5-40}$$

Adding the constraint $K_S \geq 1$ (i.e., there must be at least one sample per UWB frame) gives the sampling rate as:

$$K_S = \left\lceil J_{\min} \frac{B_{IF}}{R} \right\rceil \tag{5-41}$$

where $\lceil \cdot \rceil$ denotes the smallest integer greater than or equal to the argument.

Therefore, if $B_{IF} << R$, then $R_S = R$ (one sample per UWB frame); conversely, if $B_{IF} >> R$, then $R_S = J_{\min} B_{IF}$. Thus, the constraint on the sampling rate depends on the relationship between the IF bandwidth and the pulse rate.

The IF impulse response has significant magnitude for some time interval $T_{IF} = K_{T_{IF}} / B_{IF}$ (for an *n*-pole filter, $K_{T_{IF}}$ is on the order of 2), so each sample of the IF output must account for the additive effect of RT_{IF} UWB pulses. Each simulation sample is therefore the sum of *L* delayed and weighted IF impulse response samples, where

$$L = \left\lceil \frac{RK_{T_{IF}}}{B_{IF}} \right\rceil \tag{5-42}$$

With these parameters, the simulated in-phase and quadrature components are

$$\begin{aligned} c_n &= \sum_{l=1}^{L} a_l h_{if}(n\Delta t - t_l) \cos\left[\theta(n\Delta t - t_l) + \psi(f_0) - 2\pi f_0 t_l\right] \\ s_n &= \sum_{l=1}^{L} a_l h_{if}(n\Delta t - t_l) \sin\left[\theta(n\Delta t - t_l) + \psi(f_0) - 2\pi f_0 t_l\right] \end{aligned} \tag{5-43}$$

where *n* is the sample index, $\Delta t = 1/R_S$ is the simulation sample interval, and t_L is

the arrival time of the most recent UWB pulse, t_{L-1} is the time of the pulse prior to that, etc.

5.4.2. Normalization

To make the simulation as general as possible, the baseband-equivalent impulse response $h_{if}(t)$ can be normalized to unity bandwidth using

$$h_{if}(t) = B_{IF} h_1(B_{IF} t) = B_{IF} \left| h_1(B_{IF} t) \right| e^{j\theta_1(B_{IF} t)} \tag{5-44}$$

where $h_1(t)$ has a bandwidth of 1. It is easily seen that $H_{if}(f) = H_1(f/B_{IF})$, and $\int_{-\infty}^{\infty} \left| h_{if}(t) \right|^2 dt = B_{IF} \int_{-\infty}^{\infty} \left| h_1(t) \right|^2 dt$. Equivalently, $\int_{-\infty}^{\infty} \left| H_{if}(f) \right|^2 df = B_{IF} \int_{-\infty}^{\infty} \left| H_1(f) \right|^2 df$.

Normalizing the time scale with $\tau = B_{IF} t$ gives the sample times as $n\Delta\tau$, where $\Delta\tau = B_{IF}/R_S$, and the pulse arrival times as $\tau_l = B_{IF} t_l$. The normalized baseband components of the filter output then are:

$$\begin{aligned} c_{1n} &= \sum_{l=1}^{L} a_l h_{if}(n\Delta\tau - \tau_l) \cos\left[\theta_1(n\Delta\tau - \tau_l) + \psi(f_0) - 2\pi \frac{f_0}{B_{IF}} \tau_l \right] \\ s_{1n} &= \sum_{l=1}^{L} a_l h_{if}(n\Delta\tau - \tau_l) \sin\left[\theta_1(n\Delta\tau - \tau_l) + \psi(f_0) - 2\pi \frac{f_0}{B_{IF}} \tau_l \right] \end{aligned} \tag{5-45}$$

The n^{th} sample of the IF output envelope is then

$$A_n = \sqrt{2} \left| P(f_0) \right| B_{IF} \sqrt{c_{1n}^2 + s_{1n}^2} \tag{5-46}$$

Note that unless the phase of the interference is of interest, $\psi(f_0)$ can be taken as 0.

The simulation parameters can be expressed in terms of the normalized pulse repetition rate $R_1 = R/B_{IF}$ as:

$$K_S = \left\lceil \frac{J_{\min}}{R_1} \right\rceil \tag{5-47}$$

$$L = \lceil K_{T_{IF}} R_1 \rceil \tag{5-48}$$

$$\Delta\tau = \frac{1}{K_S R_1} \tag{5-49}$$

5.4.3. Operation

The core simulation uses an outer loop and an inner loop. The outer loop is indexed to the normalized UWB frame interval $\Delta\tau_{uwb} = B_{IF}/R = 1/R_1$. The inner loop generates K_S time samples for each pass through the outer loop. Let *m* be the index for the outer loop, so $m\Delta\tau_{uwb}$ is the start time of the m^{th} UWB frame. The outer loop generates the pulse position $\tau_m = m\Delta\tau_{uwb} + \delta_m$ and the amplitude modulation a_m according to the specified UWB signal generation algorithm, which is encoded in a subroutine or function. The inner loop then generates K_S time samples. If the inner loop index is k ($0 \le k \le K_S - 1$), then the normalized time is $\tau_{m,k} = m\Delta\tau_{uwb} + k\Delta\tau$, or $\tau_n = n\Delta\tau$ with $n = mK_S + k$. For each sample time in the inner loop, the normalized baseband I/Q components are computed by summing the *L* most recent impulse responses delayed and weighted with the amplitude and phase factors, and the envelope power and amplitude are computed for the n^{th} sample, given the pulse energy spectrum $|P(f)|^2$.

The simulation can operate in different modes. One mode uses a fixed IF filter center frequency f_0, and corresponds to a "zero-span" display on a spectrum analyzer, showing the envelope of the IF output waveform vs. normalized time (or the time scale can be easily converted to real time by dividing by B_{IF}). In this mode, statistics of the I/Q components can be accumulated to yield the means, variances, and distributions of the $\{c_n\}$ and $\{s_n\}$.

The second mode is a "frequency sweep" mode analogous to the display of a spectrum analyzer with a non-zero span. This mode will usually be of interest for $B_{IF} << R$, and can be used to display the power spectral density (PSD) by stepping f_0 over the desired range. The output is the average power out of the IF filter for each value of f_0. This provides a way to verify theoretical PSD analyses, and also a good test of the simulation.

5.4.4. Example IF Filter: the n-pole Filter[5]

To apply the above development, specific expressions are needed for the IF filter impulse response $h_{if}(t)$ and the pulse spectrum $P(f)$. For the IF filter, an *n*-pole filter will be assumed, which has the transfer characteristic:

$$H_{IF}(f) = \frac{1}{\left[1 + j2\pi (f - f_0)/\alpha\right]^n} + \frac{1}{\left[1 + j2\pi (f + f_0)/\alpha\right]^n} \tag{5-50}$$

The corresponding baseband equivalent transfer function and impulse response are

$$H_{if}(f) = \frac{1}{(1 + j2\pi f/\alpha)^n} \qquad h_{if}(t) = \frac{1}{(n-1)!}\alpha^n t^{n-1} e^{-\alpha t}, \quad t \geq 0 \tag{5-51}$$

The *n*-pole filter has some attractive properties for analysis. It is causal and physically-realizable (in fact, it is common to use 4-pole resolution filters in spectrum analyzers). Also, it has a simple closed-form impulse response, and it is symmetric. Therefore, $h_{if}(t)$ is real, so

$$h_{IF}(t) = 2h_{if}(t)\cos 2\pi f_0 t\ . \tag{5-52}$$

The parameter α specifies the filter bandwidth, as can be seen by applying the definition

$$B_{IF} = \frac{\int_{-\infty}^{\infty} \left|H_{if}(f)\right|^2 df}{\left|H_{if}(0)\right|^2} = \frac{\int_{0}^{\infty} \left|H_{IF}(f)\right|^2 df}{\left|H_{IF}(f_0)\right|^2} \tag{5-53}$$

Since $\left|H_{if}(0)\right| = 1$, the bandwidth is

$$B_{IF} = \int_{-\infty}^{\infty} \left|H_{if}(f)\right|^2 df = \frac{\alpha}{2\pi}\int_{-\infty}^{\infty} \frac{dx}{(1 + x^2)^n} = \frac{\alpha}{2\pi}\frac{\Gamma\left(\frac{1}{2}\right)\Gamma\left(n - \frac{1}{2}\right)}{(n-1)!} \tag{5-54}$$

[5] Portions of the material in this subsection are extracted from the Comments of the Wireless Information Networks Forum (WINForum) filed December, 1998 with the FCC in ET Docket 98-153.

where $\Gamma(\cdot)$ is the Gamma function. Since $\Gamma(n+1) = n\Gamma(n)$ and $\Gamma\left(\frac{1}{2}\right) = \sqrt{\pi}$, $\Gamma\left(\frac{1}{2}\right)\Gamma\left(n-\frac{1}{2}\right) = \pi\left[\frac{1}{2}\cdot\frac{3}{2}\cdots\left(n-\frac{3}{2}\right)\right]$. It is useful to define $x_n = \frac{\alpha}{B_{IF}}$ (shown in Table 5-1), which allows the impulse response to be expressed as:

$$h_{if}(t) = \frac{B_{IF}x^n}{(n-1)!}(B_{IF}t)^{n-1}e^{-xB_{IF}t} \tag{5-55}$$

The values for *x* can be checked by verifying that $\int_0^\infty h_{if}^2(t)dt = B_{IF}$.

Table 5-1: *Bandwidth parameter vs. n for the n-pole filter*

n	$x_n = \alpha/B_{IF}$
2	4
3	16/3
4	32/5

The normalized version of $h_{if}(t)$ is

$$h_1(t) = \frac{h_{IF}(t/B_{IF})}{B_{IF}} = \frac{x^n}{(n-1)!}t^{n-1}e^{-xt}. \tag{5-56}$$

Hence, $h_{if}(t) = B_{IF}\cdot h_1(B_{IF}t)$. Note that $\int_0^\infty h_1(t)dt = \int_0^\infty h_{IF}(t)dt = H_{if}(0)$. Figure 5-7 shows $h_{if}(t)/B_{IF}$ vs. $B_{IF}t$.

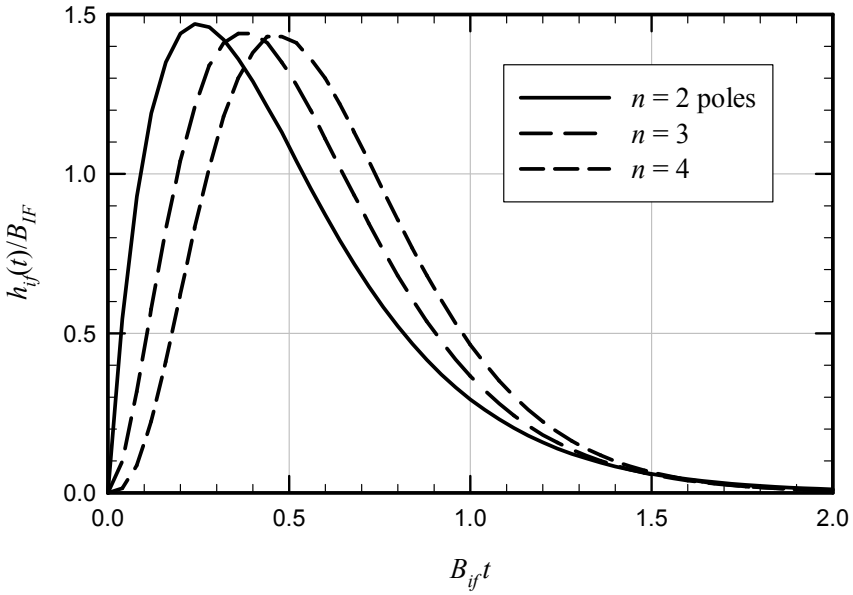

Figure 5-7: *Normalized baseband-equivalent impulse response of n-pole filter*

Note that since $h_{if}(t)$ is real, the *n*-pole filter introduces no phase modulation in the impulse response ($\theta = 0$), and (5-36) becomes

$$\begin{aligned} c(t) &= \sum_{k=-\infty}^{\infty} a_k h_{if}(t - T_k)\cos[\psi(f_0) - 2\pi f_0 T_k] \\ s(t) &= \sum_{k=-\infty}^{\infty} a_k h_{if}(t - T_k)\sin[\psi(f_0) - 2\pi f_0 T_k] \end{aligned} \tag{5-57}$$

5.4.5. Example UWB Pulse: The Gaussian Monocycle

To obtain a meaningful simulation output, the pulse energy spectral density $|P(f)|^2$ must be known, or calculated from known (input) quantities. The most useful inputs are the average pulse rate (which is required in any event), and the total average UWB power. This subsection gives an example of ESD calculation, given the average pulse rate and total power. The "Gaussian monocycle" pulse is used here, but application of this approach to other pulses should be straightforward.

For the "Gaussian monocycle" discussed in Chapter 3,

$$|P(f)|^2 = p_{\max}^2 f^2 \tau^4 \frac{e\pi}{18} e^{-(f\tau)^2 \pi/3} \tag{5-58}$$

where $p_{\max}$ is the peak instantaneous voltage of the time-domain pulse waveform. The maximum energy spectral density, which occurs at the frequency $f_m = \frac{1}{\tau}\sqrt{\frac{3}{\pi}}$, is

$$|P(f)|^2_{\max} = |P(f_m)|^2 = \frac{p^2_{\max}\tau^2}{6}, \tag{5-59}$$

and the ESD can be expressed as

$$|P(f)|^2 = |P(f)|^2_{\max} \cdot a(f) \tag{5-60}$$

where

$$a(f) = (f\tau)^2 \frac{e\pi}{3} e^{-(f\tau)^2\pi/3}. \tag{5-61}$$

The total energy in a single pulse is:

$$E_p = \int_{-\infty}^{\infty} |P(f)|^2 df = \frac{p^2_{\max} e\tau}{4\sqrt{3}} = \frac{e\sqrt{3}}{2\tau}|P(f)|^2_{\max} \quad \text{joules} \tag{5-62}$$

Given the average UWB pulse rate *R*, the total power in the UWB signal is

$$\overline{P}_{UWB} = \left\langle |a_k|^2 \right\rangle R E_p \quad \text{watts} \tag{5-63}$$

Assuming $\left\langle |a_k|^2 \right\rangle = 1$,

$$|P(f)|^2_{\max} = \frac{2\tau E_p}{e\sqrt{3}} = \frac{2\tau \overline{P}_{UWB}}{e\sqrt{3} \cdot R} \tag{5-64}$$

Thus, with the pulse rate and average power as inputs, $|P(f)|^2_{\max}$ can be calculated, and from (5-60) and (5-61), the ESD $|P(f)|^2$ can be calculated for any desired frequency.

To avoid any spectral shaping due to the pulse waveform, a rectangular pulse spectrum of bandwidth B_{uwb} and constant energy spectral density Φ can be used. Thus,

$$|P(f)|^2 = \begin{cases} \Phi & |f| \le B_{uwb} \\ 0 & |f| > B_{uwb} \end{cases} \tag{5-65}$$

and the pulse energy is $E_p = 2\Phi B_{uwb}$. Hence,

$$\Phi = \frac{\overline{P}_{uwb}}{2RB_{uwb}} \tag{5-66}$$

This allows the effects of pulse timing to be separated from those of the shape of the pulse itself, while maintaining consistency between total power and the filter output power at a given frequency.

5.4.6. Simulation Validation

It is useful to test the simulation against a known analytic result to verify operation and correct power scaling. This was done using the same parameters as a case studied in Chapter 3, shown in Figure 3-7, which was calculated analytically using the PSD expressions that were developed.

This case was duplicated using the simulation; the results are shown in Figure 5-8. The center frequency was stepped from 1.4 GHz to 1.6 GHz in 1-MHz steps. At each center frequency a UWB signal consisting of 10,000 pulses was generated, with the pulse in each frame randomly-positioned (i.e., dithering) in one of 10 positions, which are separated by 2 ns. There was no pulse-position modulation. The output of the simulation was the average power at each center frequency. As can be seen, the simulation results agree well with the analysis.

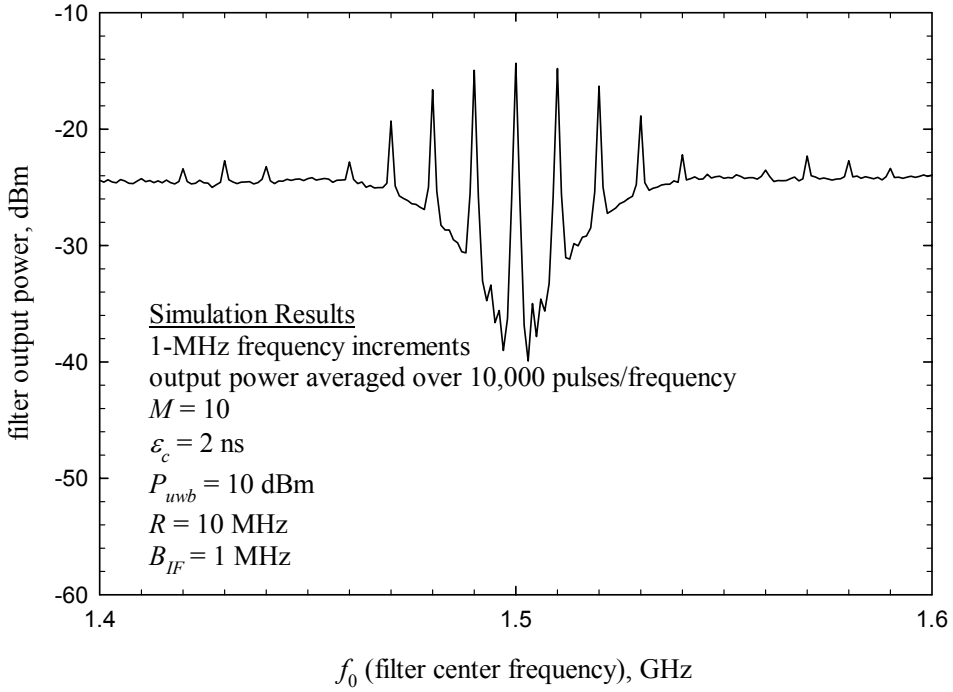

Figure 5-8: *Stepped-frequency simulation – example results*

Figure 5-9 shows the simulation and analytic results superimposed for a direct comparison.

The PSD analysis showed that if the pulse polarity is randomly modulated so that $\overline{a}_k = 0$, the spectral lines will vanish. This is easily verified with the simulation, as shown in Figure 5-10, which used exactly the same settings as Figure 5-8, except that the pulse polarity was randomly varied from frame to frame. As can be seen, the tones are indeed gone.

5.4.7. Simulation Results: Power Output vs. Time

Figure 5-11 shows the 1-MHz bandwidth filter power output vs. time for a center frequency of 1.4 GHz. As can be seen, the signal appears very noise-like. Note that from Figure 5-8, there is no spectral line at 1.4 GHz.

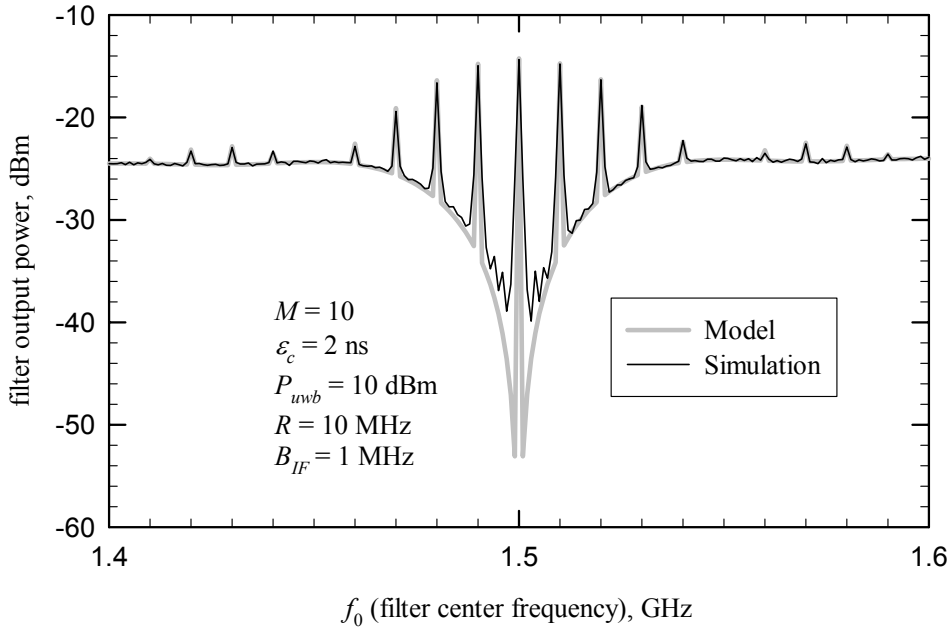

Figure 5-9: *Comparison of example simulation and analysis results*

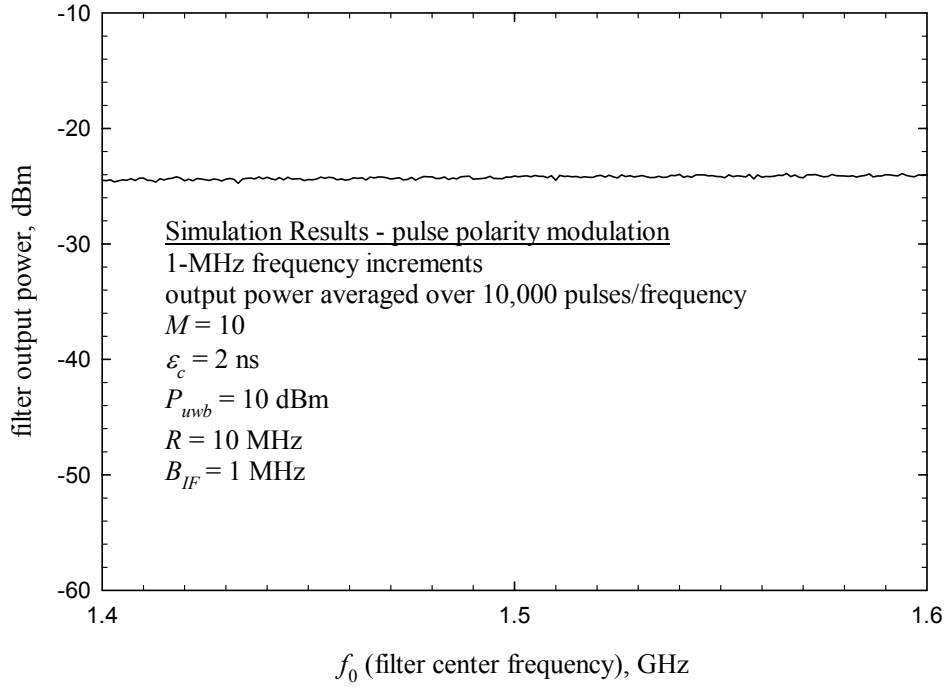

Figure 5-10: *Effect of pulse polarity modulation*

Figure 5-12 shows the results for 1.46 GHz, which has a low-power spectral line, and the signal appears slightly less variable than for 1.4 GHz. However, as can be seen from Figure 5-13, Figure 5-14, Figure 5-15, which show the output for 1.47, 1.48, and 1.50 GHz, respectively, the signal variability decreases markedly as the strength of the tone in the spectral representation increases. In fact, for 1.5 GHz, there is no significant

variation, since the continuous component of the PSD within the 1-MHz filter bandwidth is very small at that center frequency.

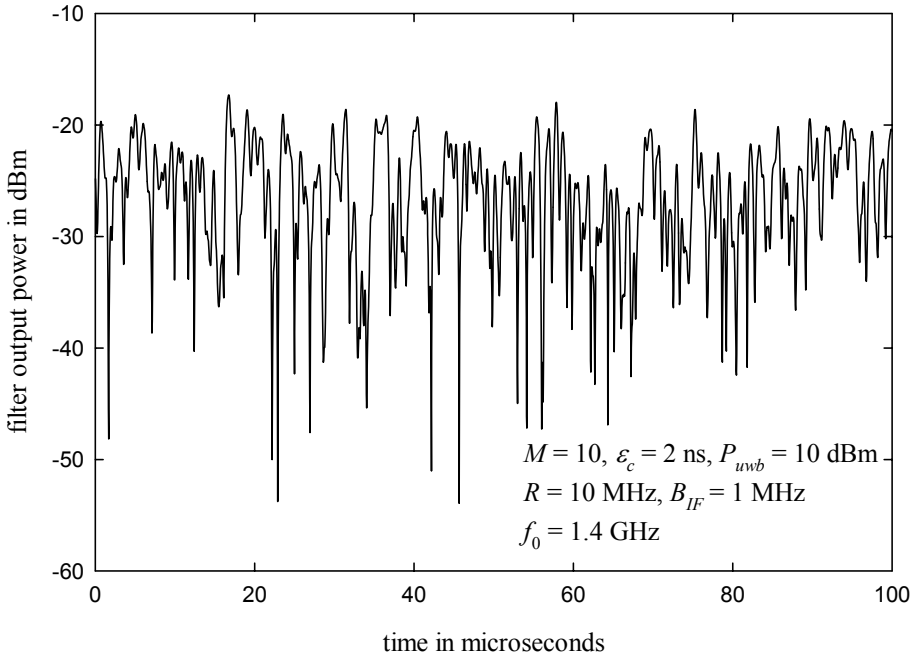

Figure 5-11: *Simulation output for 1.4 GHz*

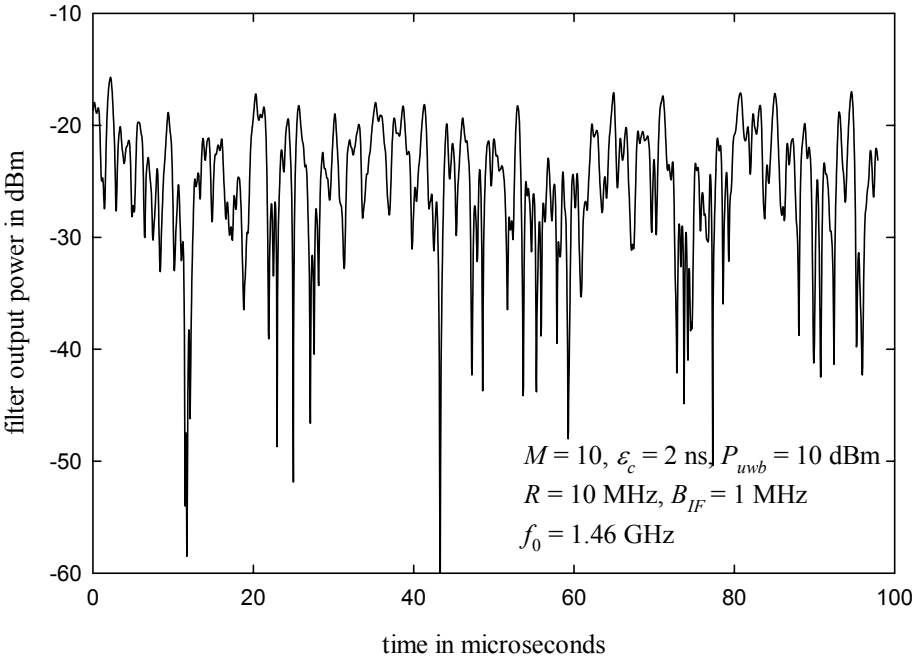

Figure 5-12: *Simulation output for 1.46 GHz, which has a small spectral line*

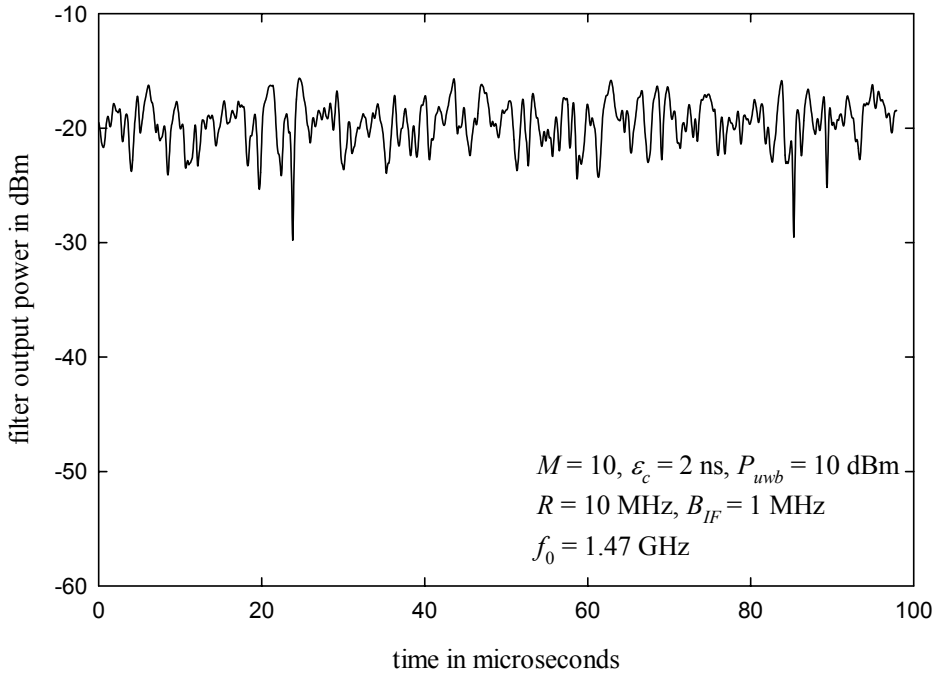

Figure 5-13: *Simulation output for 1.47 GHz*

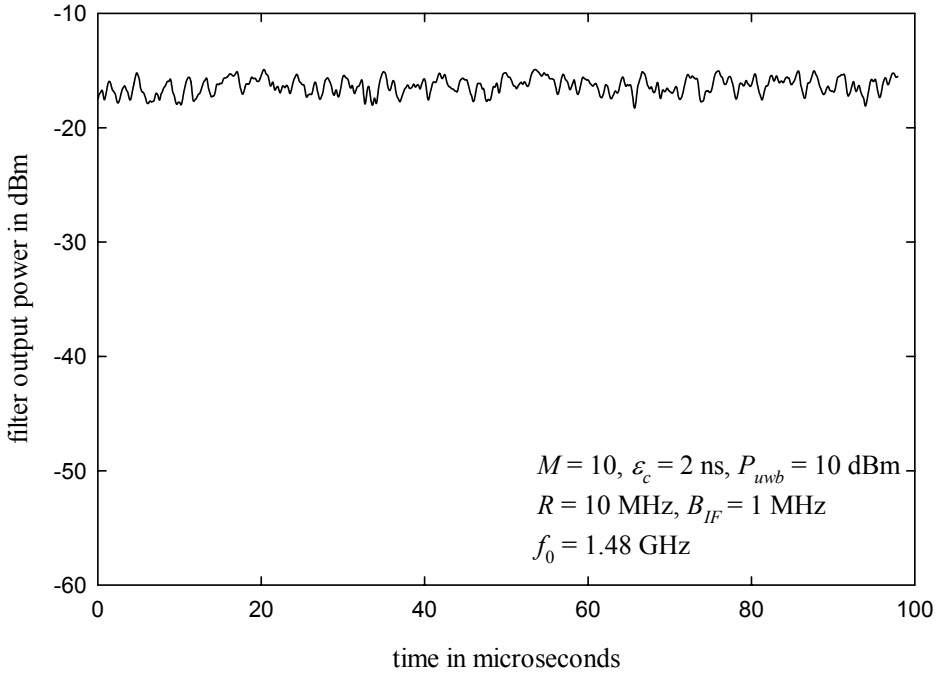

Figure 5-14: *Simulation results for 1.48 GHz*

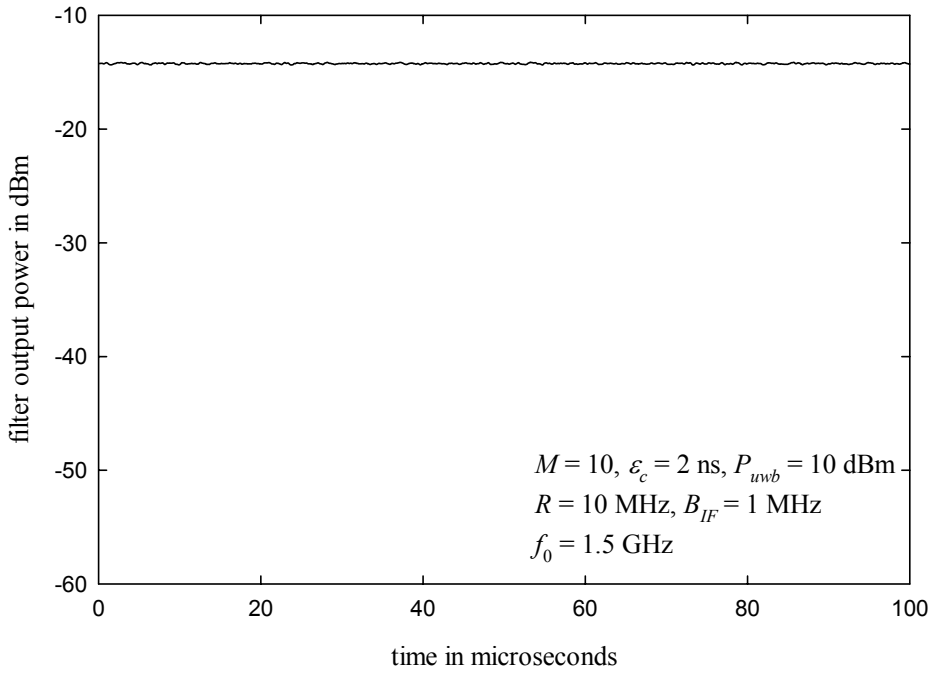

Figure 5-15: *Simulation results for 1.5 GHz*

Annex 5A

General Baseband-Equivalent Representation of a Bandpass-Filtered UWB Signal

From Figure 5-2, the Fourier transform of the bandpass-filtered UWB signal is

$$G(f) = W(f)H_{IF}(f) \tag{5A-1}$$

Since $H_{IF}(f)$ is bandpass, $g(t)$ is zero-mean.

$H_{IF}(f)$ can be expressed in terms of its baseband equivalent response and its center frequency f_0 as (see [1], p. 153):

$$H_{IF}(f) = H_{if}(f - f_0) + H_{if}^*(-f - f_0) \tag{5A-2}$$

For analysis, it is often useful to represent the bandpass process $g(t)$ in terms of baseband quadrature components $x(t)$ and $y(t)$:

$$g(t) = x(t)\cos 2\pi f_0 t - y(t)\sin 2\pi f_0 t \tag{5A-3}$$

To relate $x(t)$ and $y(t)$ to $g(t)$, let

$$Z(f) = 2G(f)U(f) \tag{5A-4}$$

that is, $Z(f)$ is the positive-frequency portion of $G(f)$. As is well-known,

$$z(t) = g(t) + j\hat{g}(t) \tag{5A-5}$$

where $\hat{g}(t)$ is the Hilbert transform of $g(t)$ and $z(t)$ is the analytic part of $g(t)$ [1].

Next define

$$V(f) = Z(f + f_0) \tag{5A-6}$$

which is simply a low pass version of $Z(f)$, and it follows that

$$v(t) = z(t)e^{-j2\pi f_0 t}. \tag{5A-7}$$

Defining

$$v(t) = x(t) + jy(t) \tag{5A-8}$$

where $x(t)$ and $y(t)$ are real low pass processes gives

$$\begin{aligned} g(t) &= \operatorname{Re} z(t) = \operatorname{Re}\left\{v(t)e^{j2\pi f_0 t}\right\} \\ &= x(t)\cos 2\pi f_0 t - y(t)\sin 2\pi f_0 t \end{aligned} \tag{5A-9}$$

which is the desired form.

Since $x(t) = \operatorname{Re} v(t)$ and $y(t) = \operatorname{Im} v(t)$, the Fourier transforms of $x(t)$ and $y(t)$ are

$$\begin{aligned} X(f) &= \frac{1}{2}\int_{-\infty}^{\infty}\left[v(t) + v^*(t)\right]e^{-j2\pi ft}dt = \frac{V(f) + V^*(-f)}{2} \\ Y(f) &= \frac{1}{2j}\int_{-\infty}^{\infty}\left[v(t) - v^*(t)\right]e^{-j2\pi ft}dt = \frac{V(f) - V^*(-f)}{2j} \end{aligned} \tag{5A-10}$$

Clearly, both $X(f)$ and $Y(f)$ are conjugate-symmetric; that is $X(-f) = X^*(f)$ and $Y(-f) = Y^*(f)$ as would be expected, since $x(t)$ and $y(t)$ are real.

Combining (5A-1), (5A-2), and (5A-4) gives

$$Z(f) = 2W(f)H_{if}(f - f_0) \tag{5A-11}$$

and from (5A-6),

$$V(f) = Z(f + f_0) = 2W(f + f_0)H_{if}(f). \tag{5A-12}$$

The transforms of the baseband components therefore are

$$X(f) = W(f_0 + f)H_{if}(f) + W^*(f_0 - f)H_{if}^*(-f)$$
$$Y(f) = \frac{1}{j}W(f_0 + f)H_{if}(f) - \frac{1}{j}W^*(f_0 - f)H_{if}^*(-f) \quad \text{(5A-13)}$$

Power Spectral Density Relationships

For interference analysis, the relationships among the correlation functions and spectra of $x(t)$, $y(t)$, $g(t)$, $\hat{g}(t)$, $z(t)$, and $v(t)$ are of interest. These relationships are developed by Papoulis [2] (pp. 362-367) and will be summarized here for completeness. This summary generally follows that provided by Papoulis, who shows that $g(t)$ is wide-sense stationary (WSS), provided that $x(t)$ and $y(t)$ are zero mean and WSS, and

$$R_x(\tau) = R_y(\tau)$$
$$R_{xy}(\tau) = -R_{yx}(\tau) \quad \text{(5A-14)}$$

where $R_x(\tau) = \langle x(t+\tau)x^*(t)\rangle$ and $R_{xy}(\tau) = \langle x(t+\tau)y^*(t)\rangle$. Note that by definition, $R_{yx}(\tau) = \langle y(t+\tau)x^*(\tau)\rangle = R_{xy}^*(-\tau)$, so from the second condition in (5A-14), $R_{xy}^*(-\tau) = -R_{xy}(\tau)$ that is, $R_{xy}(\tau)$ has odd symmetry whereas $R_x(\tau)$ has even symmetry. In this case, $x(t)$ and $y(t)$ are real, so $R_{xy}(-\tau) = -R_{xy}(\tau)$.

Under the conditions of (5A-14), it is easily shown that

$$R_g(\tau) = R_x(\tau)\cos 2\pi f_0\tau + R_{xy}(\tau)\sin 2\pi f_0\tau$$
$$R_v(\tau) = 2R_x(\tau) - 2jR_{xy}(\tau) \quad \text{(5A-15)}$$

Also, since $\hat{g}(t)$ is the Hilbert transform of $g(t)$,

$$R_g(\tau) = R_{\hat{g}}(\tau)$$
$$R_{g\hat{g}}(\tau) = -R_{\hat{g}g}(\tau) \quad \text{(5A-16)}$$

Thus,

$$R_z(\tau) = 2R_g(\tau) - 2jR_{g\hat{g}}(\tau). \quad \text{(5A-17)}$$

Since $z(t) = e^{j2\pi f_0 t}v(t)$

$$R_z(\tau) = e^{j2\pi f_0\tau}R_v(\tau) \quad \text{(5A-18)}$$

The PSD relationships corresponding to (5A-15), (5A-17), and (5A-18) are

$$\begin{aligned} S_v(f) &= 2S_x(f) - 2jS_{xy}(f) \\ S_z(f) &= 2S_g(f) - 2jS_{g\hat{g}}(f) \\ S_z(f) &= S_v(f - f_0) \end{aligned} \tag{5A-19}$$

$R_{xy}(\tau)$ is real and odd: $R_{xy}(-\tau) = -R_{xy}(\tau)$; hence $S_{xy}(f) = -j\int_{-\infty}^{\infty} R_{xy}(\tau)\sin 2\pi f\tau \, d\tau$ is purely imaginary and odd. That is, $S_{xy}(-f) = -S_{xy}(f)$. Therefore, since $S_x(-f) = S_x(f)$,

$$S_v(f) + S_v(-f) = 4S_x(f) \tag{5A-20}$$

Similarly, $S_{g\hat{g}}(f)$ is imaginary and odd, and $S_g(f)$ is real and even, so

$$S_z(f) + S_z(-f) = 4S_g(f) \tag{5A-21}$$

Hence,

$$\begin{aligned} S_x(f) = S_y(f) &= \frac{1}{4}[S_v(f) + S_v(-f)] \\ &= \frac{1}{4}[S_z(f_0 + f) + S_z(f_0 - f)] \end{aligned} \tag{5A-22}$$

With

$$S_g(f) = S_w(f)\left|H_{IF}(f)\right|^2 = S_w(f)\left\{\left|H_{if}(f - f_0)\right|^2 + \left|H_{if}(-f - f_0)\right|^2\right\} \tag{5A-23}$$

$$S_z(f) = 4S_w(f)\left|H_{if}(f - f_0)\right|^2 \tag{5A-24}$$

Therefore,

$$S_x(f) = S_y(f) = S_w(f_0 + f)\left|H_{if}(f)\right|^2 + S_w(f_0 - f)\left|H_{if}(-f)\right|^2 \tag{5A-25}$$

Similarly, $S_v(f) - S_v(-f) = -4jS_{xy}(f)$, so

$$S_{xy}(f) = \frac{j}{4}\{S_v(f) - S_v(-f)\} = \frac{j}{4}\{S_z(f_0 + f) - S_z(f_0 - f)\} \tag{5A-26}$$

and

$$S_{xy}(f) = j\left\{S_w(f_0+f)\left|H_{if}(f)\right|^2 - S_w(f_0-f)\left|H_{if}(-f)\right|^2\right\} \tag{5A-27}$$

Clearly, $S_{yx}(f) = -S_{xy}(f)$.

Since, from (5A-4), $S_z(f) = 4S_g(f)U(f)$, (5A-22) gives

$$S_x(f) = S_y(f) = S_g(f_0+f)U(f_0+f) + S_g(f_0-f)U(f_0-f) \tag{5A-28}$$

Figure 5A- 1 illustrates the relationships among $S_g(f)$, $S_v(f)$, $S_z(f)$, and $S_x(f)$.

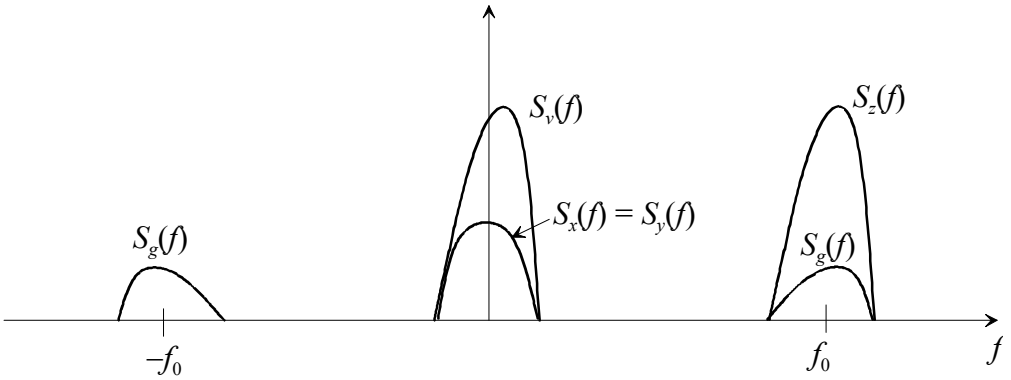

Figure 5A- 1: *Illustrative relationships among PSDs for lowpass and bandpass components*

Note that $S_x(f)$ and $S_y(f)$ are thus symmetric about $f = 0$. Also,

$$\overline{p}_x = \overline{p}_y = \int S_x(f)df = \int S_y(f)df = \int S_g(f)df = \overline{p}_g \tag{5A-29}$$

as would be expected, since $\overline{p}_g = \dfrac{\overline{p}_x + \overline{p}_y}{2}$.

Example: Single Tone within the IF Passband

Consider a case in which, within the IF passband, $W(f)$ has a single discrete spectral component at frequency f_1. Thus,

$$w_H(t) = A\cos(2\pi f_1 t + \theta) \tag{5A-30}$$

and

$$W_H(f) = \frac{A}{2}\left[e^{j\theta}\delta(f-f_1) + e^{-j\theta}\delta(f+f_1)\right] \tag{5A-31}$$

where $w_H(t)$ represents the portion of the UWB signal that falls within the IF passband. In this case,

$$G(f) = \frac{A}{2}\left[H_{IF}(f_1)e^{j\theta}\delta(f - f_1) + H_{IF}(-f_1)e^{-j\theta}\delta(f + f_1)\right] \tag{5A-32}$$

Since $h_{IF}(t)$ is real, $H_{IF}(-f) = H_{IF}^*(f)$. Letting $H_{IF}(f_1) = |H_{IF}(f_1)|e^{j\phi}$ gives

$$G(f) = \frac{A}{2}|H_{IF}(f_1)|\left[e^{j(\theta+\phi)}\delta(f - f_1) + e^{-j\theta(+\phi)}\delta(f + f_1)\right] \tag{5A-33}$$

and

$$\begin{aligned} g(t) &= \frac{A}{2}|H_{IF}(f_1)|\left[e^{j(\theta+\phi)}e^{j2\pi f_1 t} + e^{-j\theta(+\phi)}e^{-j2\pi f_1 t}\right] \\ &= A|H_{IF}(f_1)|\cos(2\pi f_1 t + \theta + \phi) \end{aligned} \tag{5A-34}$$

From (5A-12),

$$\begin{aligned} V(f) &= Ae^{j\theta}H_{if}(f)\delta(f + f_0 - f_1) \\ &= Ae^{j\theta}H_{if}(\Delta f)\delta(f - \Delta f) \end{aligned} \tag{5A-35}$$

where $\Delta f = f_1 - f_0$. Figure 5A- 2 shows $G(f)$, $H_{IF}(f)$, and $V(f)$ for this case.

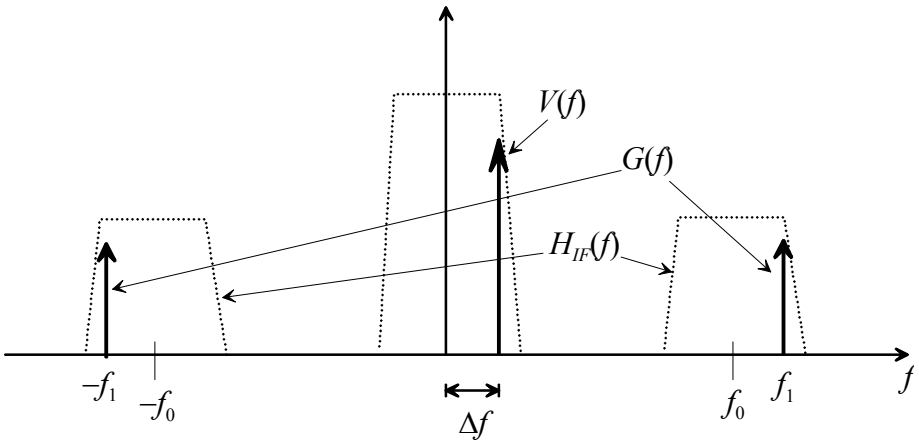

Figure 5A- 2: *Illustration of IF output spectrum for a single tone in the passband*

From (5A-10) and (5A-35),

$$X(f) = \frac{A}{2}\left[e^{j\theta} H_{if}(\Delta f)\delta(f - \Delta f) + e^{-j\theta} H_{if}^{*}(\Delta f)\delta(f + \Delta f)\right]$$
$$Y(f) = \frac{A}{2j}\left[e^{j\theta} H_{if}(\Delta f)\delta(f - \Delta f) - e^{-j\theta} H_{if}^{*}(\Delta f)\delta(f + \Delta f)\right] \quad (5A\text{-}36)$$

and

$$x(t) = \frac{A}{2}\left[e^{j\theta} H_{if}(\Delta f)e^{j2\pi\Delta ft} + e^{-j\theta} H_{if}^{*}(\Delta f)e^{-j2\pi\Delta ft}\right]$$
$$y(t) = \frac{A}{2j}\left[e^{j\theta} H_{if}(\Delta f)e^{j2\pi\Delta ft} - e^{-j\theta} H_{if}^{*}(\Delta f)e^{-j2\pi\Delta ft}\right] \quad (5A\text{-}37)$$

Clearly, $H_{if}(\Delta f) = H_{IF}(f_1)$, so $H_{if}(\Delta f) = \left|H_{if}(\Delta f)\right|e^{j\phi}$ and

$$x(t) = A\left|H_{if}(\Delta f)\right|\cos(2\pi\Delta ft + \theta + \phi)$$
$$y(t) = A\left|H_{if}(\Delta f)\right|\sin(2\pi\Delta ft + \theta + \phi) \quad (5A\text{-}38)$$

Note that if $f_1 = f_0$, $\Delta f = 0$ and

$$x(t) = A\left|H_{if}(\Delta f)\right|\cos(\theta + \phi)$$
$$y(t) = A\left|H_{if}(\Delta f)\right|\sin(\theta + \phi) \quad (5A\text{-}39)$$

which are time-invariant.

Correlations and Power Spectra

The autocorrelations of $x(t)$ and $y(t)$, and their cross-correlation, are:

$$\begin{aligned} R_x(t+\tau,t) &= \langle x(t+\tau)x(t)\rangle \\ &= \frac{A^2}{2}\left|H_{if}(\Delta f)\right|\{\cos 2\pi\Delta f\tau + \cos[2\pi\Delta f(2t+\tau)+2(\theta+\phi)]\} \end{aligned}$$

$$\begin{aligned} R_y(t+\tau,t) &= \langle y(t+\tau)y(t)\rangle \\ &= \frac{A^2}{2}\left|H_{if}(\Delta f)\right|\{\cos 2\pi\Delta f\tau - \cos[2\pi\Delta f(2t+\tau)+2(\theta+\phi)]\} \end{aligned} \qquad \text{(5A-40)}$$

$$\begin{aligned} R_{xy}(t+\tau,t) &= \langle x(t+\tau)y(t)\rangle \\ &= \frac{A^2}{2}\left|H_{if}(\Delta f)\right|\{-\sin 2\pi\Delta f\tau + \sin[2\pi\Delta f(2t+\tau)+2(\theta+\phi)]\} \end{aligned}$$

The UWB signal $w(t)$ is in general cyclostationary, meaning that $R_w(t+\tau,t) = R_w(t+T+\tau,t+T)$. Since power spectral density is the average power per Hz, it is the time-average autocorrelation function that is of interest. In this case, the time-average autocorrelation functions are:

$$\begin{aligned} \overline{R}_x(\tau) &= \overline{R}_y(\tau) = \frac{A^2}{2}\left|H_{if}(\Delta f)\right|\cos 2\pi\Delta f\tau \\ \overline{R}_{xy}(\tau) &= -\frac{A^2}{2}\left|H_{if}(\Delta f)\right|\sin 2\pi\Delta f\tau \end{aligned} \qquad \text{(5A-41)}$$

and the corresponding PSDs are

$$\begin{aligned} S_x(f) &= S_y(f) = \frac{A^2}{4}\left|H_{if}(\Delta f)\right|^2[\delta(f-\Delta f)+\delta(f+\Delta f)] \\ S_{xy}(f) &= \frac{jA^2}{4}\left|H_{if}(\Delta f)\right|^2[\delta(f-\Delta f)-\delta(f+\Delta f)] \end{aligned} \qquad \text{(5A-42)}$$

From (5A-34),

$$\overline{R}_g(\tau) = \frac{A^2}{2}\left|H_{IF}(f_1)\right|^2\cos 2\pi f_1\tau \qquad \text{(5A-43)}$$

and the corresponding PSD is

$$S_g(f) = \frac{A^2}{4}\left|H_{IF}(f_1)\right|^2[\delta(f-f_1)+\delta(f+f_1)] \qquad \text{(5A-44)}$$

Since $f_1 = f_0 + \Delta f$, $H_{IF}(f_1) = H_{if}(\Delta f)$ and

$$\begin{aligned}\overline{R}_g(\tau) &= \frac{A^2}{2}\left|H_{if}(\Delta f)\right|^2 \cos 2\pi(f_0+\Delta f)\tau \\ &= \frac{A^2}{2}\left|H_{if}(\Delta f)\right|^2 \left[\cos 2\pi f_0\tau \cos 2\pi\Delta f\tau - \sin 2\pi f_0\tau \sin 2\pi\Delta f\tau\right] \\ &= \overline{R}_x(\tau)\cos 2\pi f_0\tau + \overline{R}_{xy}(\tau)\sin 2\pi f_0\tau\end{aligned} \tag{5A-45}$$

which is consistent with the general expression in (5A-15). Note also that

$$\begin{aligned}&S_g(f_0+f)U(f_0+f) + S_g(f_0-f)U(f_0-f) \\ &= \frac{A^2}{4}\left|H_{if}(\Delta f)\right|^2\left[\delta(f-\Delta f)+\delta(f+\Delta f)\right] = S_x(f) = S_y(f)\end{aligned} \tag{5A-46}$$

which is consistent with (5A-25) and (5A-28).

Chapter 5 References

[1] J. G. Proakis, *Digital Communications,* 2001, 4th edition, Boston: McGraw-Hill.

[2] A. Papoulis, *Signal Analysis*, 1977, New York: McGraw-Hill.

[3] A. Papoulis, *Probability, Random Variables, and Stochastic Processes*, third edition, 1991, New York: McGraw-Hill.

Chapter 6: UWB INTERFERENCE TO A COHERENT PSK RECEIVER

This Chapter analyzes the bit error rate (BER) performance of a coherent PSK receiver in the presence of UWB interference. The analysis assumes a non-fading channel that is corrupted by additive white Gaussian noise (AWGN). The analytical framework is similar to that used in [1].

A set of canonical models will be used to represent UWB interference in its various forms as seen by a narrowband receiver. These canonical models will allow the treatment of UWB as a source of interference to NB radios for a wide range of operational parameter settings of both the interferer's and the victim's radio systems.

A block diagram of a coherent detection scheme for binary PSK is shown in Figure 6-1. A coherent PSK receiver operates as follows. It consists of a matched filter whose output is sampled every T_s seconds. When this value is positive, a "1" is chosen and when it is negative, a "0" is chosen.

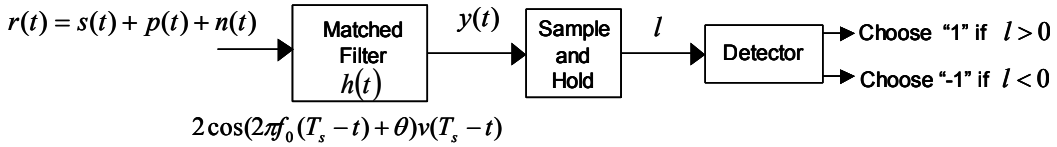

Figure 6-1: *Coherent PSK Receiver*

6.1. System Model

The received waveform at the input to the PSK receiver is given as

$$r(t) = s(t) + p(t) + n(t) \tag{6-1}$$

where $s(t)$, $p(t)$ and $n(t)$ represent the desired narrowband signal, the UWB interference and additive white Gaussian noise (AWGN), respectively.
The desired narrowband (NB) PSK signal is written as

$$s(t) = \sqrt{2P_s}\cos(\omega_0 t + \theta)\sum_{j=-\infty}^{\infty} b_j v(t - jT_s) \tag{6-2}$$

where,

$$v(t - jT_s) = \begin{cases} 1, & jT_s \le t < (j+1)T_s \\ 0, & otherwise \end{cases} \tag{6-3}$$

is a rectangular window function and θ is a random phase term which is uniformly distributed in $[0, 2\pi]$. In (6-2), P_s is the average NB signal power and ω_0 is the carrier frequency. The modulation symbols are denoted by $\{b_j\}$ and can take values ± 1 with equal probability. The symbol period is denoted by T_s and equals reciprocal of the symbol rate, R_s. The noise term, $n(t)$, is modeled as white Gaussian noise with a two-sided power spectral density equal to $N_0 / 2$.

As mentioned earlier, UWB interference as seen by the NB victim receiver will be modeled using two canonical representations. Depending on the specific of the UWB radio, it may or may not appear as spectral lines in the bandwidth of the NB receiver. For the case when lines are not present, UWB is modeled as a time-series of very short (spectrum appears flat to NB receiver) pulses. This will be referred to as the UWB Pulse Model (UPM). The second case, when spectral lines appear, is referred to as the UWB Tone Model (UTM) since lines in the frequency domain represent sinusoids in the time domain.

UWB Pulse Model (UPM)

The UWB waveform, $p(t)$, is given as

$$p(t) = \sqrt{P_u} \sum_k a_k w(t - kT_u - \varepsilon_k) \tag{6-4}$$

where P_u is the average transmit UWB power and $w(t)$ is the UWB pulse shaping function of unit power. For this analysis, it is assumed that the UWB pulse shaping function has the ideal bandpass shape as shown in Figure 6-2. In the figure, B_u is the UWB pulse bandwidth.

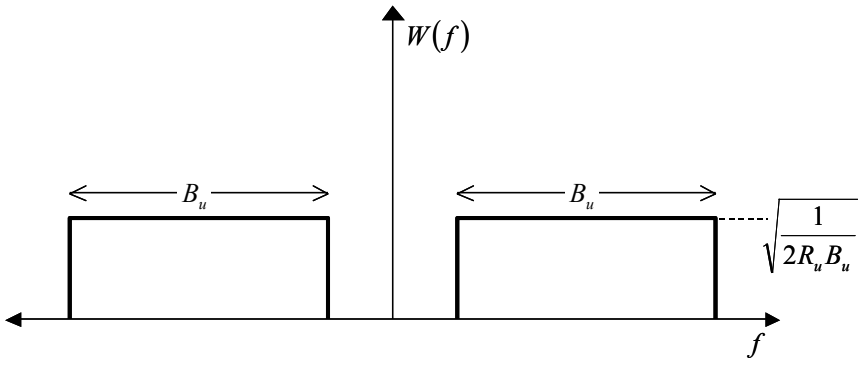

Figure 6-2: *UWB Pulse Shaping Model*

The pulse repetition interval is given by T_u, which is the reciprocal of the average UWB pulse repetition frequency (PRF). UWB amplitude and position-based modulation is modeled through the random variables, a_k and ε_k. It is assumed that any time-dithering

is subsumed in ε_k, and therefore, it may be modeled as uniformly distributed random variable in $[0, \alpha T_u]$, where α is the fractional code-span.

UWB Tone Model (UTM)

The UWB temporal model when it gives rise to spectral lines in the bandwidth of the NB receiver is effectively that of a continuous wave (CW) signal or tone. In this case, the UWB model is given as

$$p(t) = \sqrt{2P_u}\cos((\omega_0 + \Delta\omega_u)t) \tag{6-5}$$

The location of the tone or spectral line may be varied by the frequency shift parameter, $\Delta\omega_u$ with the PSK carrier frequency, ω_0, as the reference point. The average power in this tone is given by P_u and is computed as $\frac{1}{T_s}\int_0^{T_s} p^2(t)dt$. It is assumed that $\omega_0 + \Delta\omega_u >> T_s$.

6.2. BER Analysis

The impulse response of the matched filter is given as

$$h(t) = 2\cos(\omega_0(T_s - t) + \theta)v(T_s - t) \tag{6-6}$$

Note that the signal phase is known and accounted for in the matched filter response for coherent detection. It is also assumed that there is no inter-symbol interference at the filter output at the sampling instant.

The sampled output of the upper branch matched filter is given as

$$\begin{aligned} y(T_s) &= \int_{-\infty}^{\infty} r(\tau)h(T_s - \tau)d\tau \\ &= y_s(T_s) + y_p(T_s) + y_n(T_s) \end{aligned} \tag{6-7}$$

where $y_s(T_s)$, $y_p(T_s)$, and $y_n(T_s)$ represent the sampled matched filter outputs for the desired NB signal, UWB interference signal and noise. Each of these constituents of the matched filter output will now be evaluated separately.

Signal Term

The desired signal term sampled optimally at $(j+1)T_s$ is derived below as follows

$$
\begin{aligned}
y_s(t) &= \int_{-\infty}^{\infty} s(\tau)h(t-\tau)d\tau \\
&= \sum_{j=-\infty}^{\infty} 2\sqrt{2P_s}\int_{-\infty}^{\infty} b_j \cos(\omega_0(\tau - jT_s)+\theta)\cos(\omega_0(T_s-(t-\tau))+\theta)v(\tau - jT_s)v(T_s-(t-\tau))d\tau \\
\therefore\ y_s((j+1)T_s) &= 2\sqrt{2P_s}b_j\int_{-\infty}^{\infty}\cos^2(\omega_0(\tau - jT_s)+\theta)v^2((\tau - jT_s))d\tau \qquad (6\text{-}8) \\
&= 2\sqrt{2P_s}b_j\int_{jT_s}^{(j+1)T_s}\frac{1}{2}[1+\cos(2\omega_0(\tau - jT_s)+\theta)]d\tau \\
&= \sqrt{2P_s}T_s b_j
\end{aligned}
$$

The 2nd term in the integral vanishes due to the high frequency component, $\omega_2 + \omega_1$, which is negligible after integration.

Next, the interference term is evaluated for the two canonical models described earlier.

Interference Term Using UPM

This is readily accomplished by a frequency domain analysis as follows

$$
\begin{aligned}
Y_u(f) &= P(f)H(f) \\
&= \sqrt{\frac{P_u}{2R_uB_u}}\sum_k a_k e^{-j2\pi f(kT_u+\varepsilon_k)}H(f)
\end{aligned} \qquad (6\text{-}9)
$$

Taking the inverse Fourier transform yields the following

$$
\begin{aligned}
y_u(t) &= \sqrt{\frac{P_u}{2R_uB_u}}\sum_k a_k h(t-kT_u-\varepsilon_k) \\
&= \sqrt{\frac{2P_u}{R_uB_u}}\sum_k a_k \cos(\omega_0(T_s-(t-kT_u-\varepsilon_k))+\theta)v(T_s-(t-kT_u-\varepsilon_k))
\end{aligned} \qquad (6\text{-}10)
$$

Therefore, the sampled interference output is obtained as

$$
y_u((j+1)T_s) = \sqrt{\frac{2P_u}{R_uB_u}}\sum_k a_k \cos(\omega_0(kT_u+\varepsilon_k-jT_s)+\theta)v(kT_u+\varepsilon_k-jT_s) \qquad (6\text{-}11)
$$

Interference Term Using UTM

The output of the matched filter for the tone model is evaluated in the time domain as follows

$$
\begin{aligned}
& y_u\left((j+1)T_s\right) = p(t) * h(t)\big|_{t=(j+1)T_s} \\
& = 2\sqrt{2P_u}\int_{-\infty}^{\infty}\cos\left((\omega_0+\Delta\omega_u)\tau\right)\cos\left(\omega_0(\tau-jT_s)+\theta\right)v(\tau-jT_s)d\tau \\
& = \sqrt{2P_u}\int_{0}^{T_s}\cos\left(\Delta\omega_u\tau-\left(\theta-jT_s(\omega_0+\Delta\omega_u)\right)\right)d\tau + \\
& \sqrt{2P_u}\int_{0}^{T_s}\cos\left((2\omega_0+\Delta\omega_u)\tau+\left(\theta+jT_s(\omega_0+\Delta\omega_u)\right)\right)d\tau \\
& = \sqrt{2P_u}T_s\left[\frac{\sin\left(\Delta\omega_u T_s-\left(\theta-jT_s(\omega_0+\Delta\omega_u)\right)\right)+\sin\left(\theta-jT_s(\omega_0+\Delta\omega_u)\right)}{\Delta\omega_u T_s}+\right. \\
& \left.\frac{\sin\left((2\omega_0+\Delta\omega_u)T_s+\left(\theta+jT_s(\omega_0+\Delta\omega_u)\right)\right)-\sin\left(\theta+jT_s(\omega_0+\Delta\omega_u)\right)}{(2\omega_0+\Delta\omega_u)T_s}\right] \\
& \cong \sqrt{2P_u}T_s\left[\frac{\sin\left(\Delta\omega_u T_s-\left(\theta-jT_s(\omega_0+\Delta\omega_u)\right)\right)+\sin\left(\theta-jT_s(\omega_0+\Delta\omega_u)\right)}{\Delta\omega_u T_s}\right]
\end{aligned}
\tag{6-12}
$$

The last step assumes that $2\omega_0+\Delta\omega_u >> 1$.

Finally, the sampled noise output and its statistics are derived.

Noise Term and Statistics

The sampled matched filter output for AWGN for is given as

$$
y_n\left((j+1)T_s\right) = n(t) * h(t)\big|_{t=(j+1)T_s} = 2\int_{-\infty}^{\infty} n(\tau)\cos\left(\omega_0(\tau-jT_s)+\theta\right)v(\tau-jT_s)d\tau \tag{6-13}
$$

Now, the mean and the variance of the sampled noise term are derived.

$$
\begin{aligned}
& \left\langle y_n\left((j+1)T_s\right)\right\rangle = 2\int_{-\infty}^{\infty}\left\langle n(\tau)\right\rangle\cos\left(\omega_0(\tau-jT_s)+\theta\right)v(\tau-jT_s)d\tau = 0 \\
& \left\langle \left(y_n\left((j+1)T_s\right)\right)^2\right\rangle = 4\int_{-\infty}^{\infty}\left[\int_{-\infty}^{\infty}\left\langle n(\tau_1)n(\tau_2)\right\rangle\cos\left(\omega_0(\tau_1-jT_s)+\theta\right)v(\tau_1-jT_s)d\tau_1\right]\times \\
& \cos\left(\omega_0(\tau_2-jT_s)+\theta\right)v(\tau_2-jT_s)d\tau_2 \\
& = 4\int_{-\infty}^{\infty}\left[\int_{-\infty}^{\infty}\delta(\tau_1-\tau_2)\cos\left(\omega_0(\tau_1-jT_s)+\theta\right)v(\tau_1-jT_s)d\tau_1\right]\times \\
& \cos\left(\omega_0(\tau_2-jT_s)+\theta\right)v(\tau_2-jT_s)d\tau_2 \\
& = 4\frac{N_0}{2}\int_{0}^{T_s}\cos^2\left(\omega_0\tau+\theta\right)d\tau = N_0T_s
\end{aligned}
\tag{6-14}
$$

Therefore, the sampled noise output of the matched filter is Gaussian distributed with zero mean with variance, $N_0 T_s$.

Given, the description of all of the constituent terms of the matched filter output, we can now form the decision statistic, and is given as

$$\begin{aligned} +1\ sent: l^{(1)} &= y\big((j+1)T_s\big)\big|_{1\,sent} = A_s + A_u + N \\ -1\ sent: l^{(-1)} &= y\big((j+1)T_s\big)\big|_{-1\,sent} = -A_s + A_u + N \end{aligned} \tag{6-15}$$

where,

$$\begin{aligned} A_s &= y_s\big((j+1)T_s\big) = \sqrt{2P_s}\,T_s \\ A_u &= y_u\big((j+1)T_s\big) \\ N &= y_n\big((j+1)T_s\big) \end{aligned} \tag{6-16}$$

Therefore, the BER for each symbol can be derived by conditioning on the UWB interference terms. Then, using the results in 6-15 and 6-16, the decision statistic, $l^{(1)}$, when $+1$ is sent, is a Gaussian random variable described as

$$\begin{aligned} +1 sent: l^{(1)} &\rightarrow N\left(A_s + A_u, \sigma_N^2\right) \\ -1 sent: l^{(-1)} &\rightarrow N\left(-A_s + A_u, \sigma_N^2\right) \end{aligned}$$

where $A_s = \sqrt{2P_s}\,T_s$ and $\sigma_N^2 = N_0 T_s$. The offset in the mean due to the interference, A_u, is derived for the two canonical modes using expressions 6-16, 6-11 and 6-12. The corresponding conditional PDFs of the decision statistics are shown in Figure 6-3.

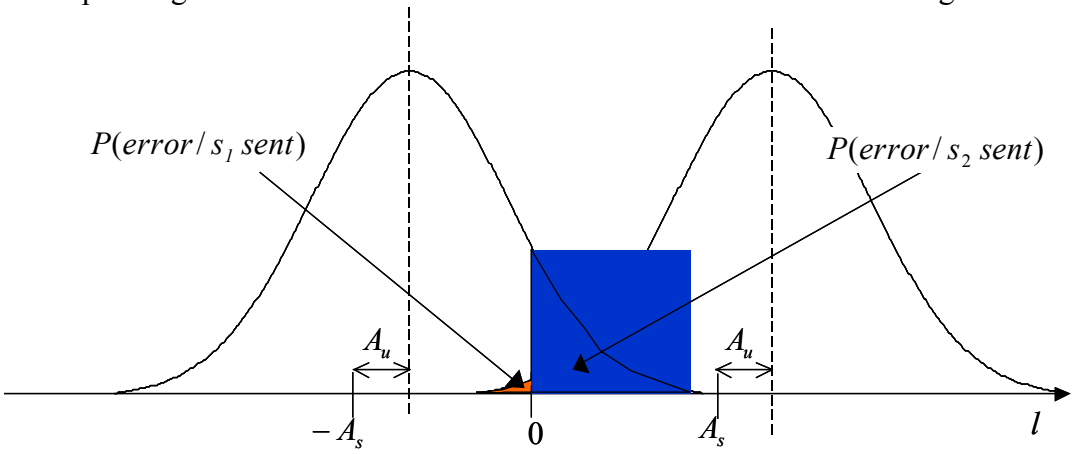

Figure 6-3: *Conditional PDF of decision statistics*

The conditional probability of error for the j the symbol, when $+1$ is sent is derived as

$$P_j(error/(+1sent,\theta,\{a_k\},\varepsilon_k)) = \frac{1}{\sqrt{2\pi\sigma_N^2}}\int_{-\infty}^{0} e^{-(x-A_s-A_u)^2/(2\sigma_N^2)}dx$$
$$= \frac{1}{\sqrt{2\pi}}\int_{(A_s+A_u)/\sigma_N}^{\infty} e^{-y^2/2}dy = \mathrm{Q}\left(\frac{(A_s+A_u)}{\sigma_N}\right) \quad (6\text{-}17)$$

where, $\mathrm{Q}(x)$ is defined as $\frac{1}{\sqrt{2\pi}}\int_x^{\infty} e^{-y^2/2}dy$.

Similarly, the conditional probability of error, when -1 is sent is given as

$$P_j(error/(-1sent,\theta,\{a_k\},\varepsilon_k)) = \mathrm{Q}\left(\frac{(A_s-A_u)}{\sigma_N}\right) \quad (6\text{-}18)$$

Given that both symbols are equally likely, the final BER expression for the j th symbol is given as

$$P_{e,j} = \left\langle \frac{1}{2}\mathrm{Q}\left(\frac{(A_s+A_u)}{\sigma_N}\right) + \frac{1}{2}\mathrm{Q}\left(\frac{(A_s-A_u)}{\sigma_N}\right)\right\rangle_{\theta,\{a_k\},\varepsilon_k} \quad (6\text{-}19)$$

Next, we express the arguments of the $\mathrm{Q}(.)$ function in more physically meaningful terms. The arguments can be split into two terms; the NB signal related term of A_s/σ_N and the UWB interference related term of A_u/σ_N. The 1st term can be expressed as

$$\frac{A_s}{\sigma_N} = \frac{T_s\sqrt{2P_s}}{\sqrt{N_oT_s}} = \frac{\sqrt{2P_sT_s}}{\sqrt{N_o}} = \sqrt{\frac{2E_b}{N_o}} \quad (6\text{-}20)$$

where E_b $(=P_sT_s)$ is the energy per NB symbol.

The 2nd term is handled separately for each canonical UWB interference model.

Error Expression for UPM

Substituting 6-11 in 6-16, we can express the 2nd argument as follows

$$\frac{A_u}{\sigma_N} = \sqrt{\frac{2P_u}{R_uB_u}}\frac{\sum_k a_k\cos(\omega_0(kT_u+\varepsilon_k-jT_s)+\theta)v(kT_u+\varepsilon_k-jT_s)}{\sqrt{N_oT_s}}$$
$$= \frac{T_s\sqrt{2P_s}}{\sqrt{N_oT_s}}\sqrt{\frac{R_s}{R_u}}\sqrt{\frac{(P_u/B_u)R_s}{P_s}}\sum_k a_k\cos(\omega_0(kT_u+\varepsilon_k-jT_s)+\theta)v(kT_u+\varepsilon_k-jT_s) \quad (6\text{-}21)$$
$$= \sqrt{\frac{2E_b}{N_o}}\frac{1}{\sqrt{N_uSIR}}\sum_k a_k\cos(\omega_0(kT_u+\varepsilon_k-jT_s)+\theta)v(kT_u+\varepsilon_k-jT_s)$$

where $N_u = \frac{R_u}{R_s}$ is the average number of UWB pulses per NB symbol period, and SIR is the signal-to-interference ratio within the NB receiver bandwidth, and is given as

$$SIR = \frac{P_s}{(P_u / B_u) R_s}$$

Substituting 6-20 and 6-21 in 6-19, the final BER expression for the j th symbol using the UWB pulse model is given as

$$P_{e,j} = \left\langle \frac{1}{2} \mathrm{Q}\left(\sqrt{\frac{2E_b}{N_o}} (1+\delta) \right) + \frac{1}{2} \mathrm{Q}\left(\sqrt{\frac{2E_b}{N_o}} (1-\delta) \right) \right\rangle_{\theta, \{a_k\}, \varepsilon_k} \tag{6-22}$$

where δ, the interference perturbation factor[6] is given as

$$\delta = \frac{1}{\sqrt{N_u SIR}} \sum_k a_k \cos\left(\omega_0 \left(kT_u + \varepsilon_k - jT_s\right) + \theta\right) v\left(kT_u + \varepsilon_k - jT_s\right) \tag{6-23}$$

Error Expression for UTM

Substituting 6-12 in 6-16, we can express the 2nd argument as follows

$$\frac{A_u}{\sigma_N} = \sqrt{\frac{2E_b}{N_0}} \frac{C}{\sqrt{SIR}} \tag{6-24}$$

where C is defined as

$$C = \left[\frac{\sin\left(\Delta\omega_u T_s - \left(\theta - jT_s\left(\omega_0 + \Delta\omega_u\right)\right)\right) + \sin\left(\theta - jT_s\left(\omega_0 + \Delta\omega_u\right)\right)}{\Delta\omega_u T_s} \right] \tag{6-25}$$

Finally, substituting 6-20 and 6-24 in 6-19, the final BER expression for the j th symbol using the UWB Tone/CW model is given as

$$P_{e,j} = \left\langle \frac{1}{2} \mathrm{Q}\left(\sqrt{\frac{2E_b}{N_o}} (1+\delta) \right) + \frac{1}{2} \mathrm{Q}\left(\sqrt{\frac{2E_b}{N_o}} (1-\delta) \right) \right\rangle_{\theta, \{a_k\}, \varepsilon_k} \tag{6-26}$$

where δ, the interference perturbation factor is given as

$$\delta = C / \sqrt{SIR} \tag{6-27}$$

[6] Other authors investigating the effect of UWB on narrowband radio systems have called it the SNR impairment factor [2].

where the signal-to-interference ratio for the tone interferer case is defined as

$$SIR = \sqrt{\frac{P_s}{P_u}}$$

6.3. Numerical Results

This section presents numerical results for some special cases using the BER analysis developed in the previous section. The case considered here is that of UWB interferer that uses pulse position modulation (PPM) with time-dithering and a fractional code-span of 1.

The coherent PSK radio system is modeled using the following parameter values:

f_0 = 200 MHz

R_s = 50 KHz

The BER is obtained using expressions 6-22 and 6-26, where the conditionality over θ and ε_k are averaged out through Monte Carlo simulations.

Figures 6-4 – 6-8 show the BER results for the UWB interferer using the pulse model. The results are displayed as BER versus $SINR$ and are shown for various values of the PRF to NB symbol rate ratio, N_u, and interference-to-noise ratio, I/N. The interference-to-noise ratio, I/N, is defined as $(E_b/N_0)/SIR$. This allows evaluation of the relative effects of noise and interference. The signal-to-noise plus interference ratio, $SINR$ is computed as $(E_b/N_0)/(1+(I/N))$. The following observations are in order:

Case I (N_u<1)

- At low signal levels (where the signal level is comparable to or lower than the combined interference plus noise level), thermal noise is more detrimental than UWB interference. Note that the BER decreases as I/N increases when SINR is less than 3 dB in figure 6-4.
- At higher signal levels, up to two regions may be observed depending on the ratio of PRF to NB symbol rate ratio. A medium range of signal strength where noise is less detrimental and a high range of signal strength where interference is less detrimental. These two distinct regions are observed in figure 6-6 where the medium range corresponds to SINR in the range 0-6 dB and the high range is where SINR is greater than 6 dB.
- In the interference limited case (see I/N = 30 dB curve), a sharp knee is observed in that, beyond a certain SINR, where there is hardly any thermal noise, the BER quickly falls to zero. This is because there comes a point, where with negligible noise, the UWB pulse energy is never large enough to cause the received signal level to cross the decision threshold and cause an error.
- At very low SINR values, for the interference limited case (I/N = 30 dB curve), the error rate asymptotically equals the probability of a UWB pulse colliding with a NB symbol since whenever it occurs the BER is the maximum of 50 %. Therefore, the asymptotic BER equals $N_u/2$, where N_u equals the probability

that a collision occurs. This is borne out in the results. For example, in figure 6-4, the BER when SINR equals -5 dB is 0.025, which is half of N_u. This is a lower bound on the BER at low SINR since for all other ratios of I/N, the performance only gets worse.

- As a check, the noise limited case is approximated by the curve I/N = -30 dB. The BER for this curve should match the theoretical coherent PSK BER given by $erfc(\sqrt{E_b/N_0})/2$. At 10 dB, the BER from this formula is computed as 3.9×10^{-6}, and matches the simulation result.
- For the low PRF case, shown in figure 6-7, two error rate regions are observed in terms of the effect of the PRF on the BER. At low SINRs, the higher PRF is more detrimental. At high SINRs, the lower PRF exhibits a worse error performance. This is explained as follows. There are two factors that contribute to an error. The first is that of the probability of a collision of a NB symbol with a UWB pulse. Obviously, higher the PRF the more likely is the collision. The second is that of the UWB interference energy per NB symbol which decreases with N_u (for a given total in-band UWB interference power) as seen in 6-21. Given a collision, the probability of an erroneous decision will be based on the interference energy per NB symbol. If the probability of an erroneous decision is high (max of 50 %), as is at low SINR, then fewer the collisions the better since a collision guarantees a coin-flip decision. If on the other hand, the probability of an erroneous decision is small, as is the case at high SINRs, then the average error rate is more sensitive to a high energy collision rather than just any collision. Since the strength of the collision is inversely proportional to N_u (as shown in equation 6-21), at high SINRs, the higher PRF is less detrimental. Table 6-1 shows the required SINR values at a fixed BER of 10^{-4} as a function of N_u for the interference limited case shown in figure 6-7. It is seen that the required SINR for a specified BER is inversely proportional to the UWB PRF. That is, every halving of the UWB PRF requires an additional 3 dB power for the NB radio.

Case II ($N_u \geq 1$)

Figure 6-8 shows the BER versus SINR for the case where the PRF is greater than the NB symbol rate. The following observations are made for this case.

- As the number of UWB pulses per NB symbol increases, the performance becomes less dependent on the actual number of pulses and converges to the noise limited case. For large values of N_u, the effect of UWB pulses depends only on the average interference power seen by the NB receiver and the number of the UWB pulses received in a symbol duration becomes less important.
- It is seen that as the PRF increases, the interference approaches the noise limited case (approximately represented by the curve corresponding to I/N = -30 dB) suggesting the validity of the white Gaussian noise model for high N_u. Note that the validity of this approximation is also a function of the time-dithering applied. In the simulation results shown here, dithering over a 100 % of the code span was assumed.

- It is also seen that the UWB interference is less detrimental than white noise since the peak-to-average ratio for UWB is limited whereas for the noise it is not.

Next, results for the BER performance using the UWB Tone model are discussed. Figure 6-9 shows the BER versus SINR when the UWB spectral line occurs exactly at the carrier frequency of the PSK radio. Figure 6-10 shows the effect of the tone interferer as a function of its location about the carrier frequency of the PSK radio. The following observations are made for UWB interference assuming the Tone model

- From figure 6-9, it is seen that the tone or spectral line is less harmful than white noise of the same power.
- Figure 6-10 shows that the UWB system causes most harm when it places a spectral line exactly at the carrier frequency.
- The BER as a function of location exhibits a "sinc" function behavior about the carrier frequency. This is not surprising since the interference is a tone convolved with a bandpass rectangular filter (assumed NB pulse shaping) resulting in an interferer, which in the frequency domain is a "sinc", centered at the carrier frequency. It follows that the tone is nulled at multiples of R_s Hz about the carrier with the BER at those locations being equal to that of an equivalent AWGN channel.
- At a separation of about 5 times the PSK symbol rate, the interference is negligible since at that point the tone falls outside the passband of the NB receiver.

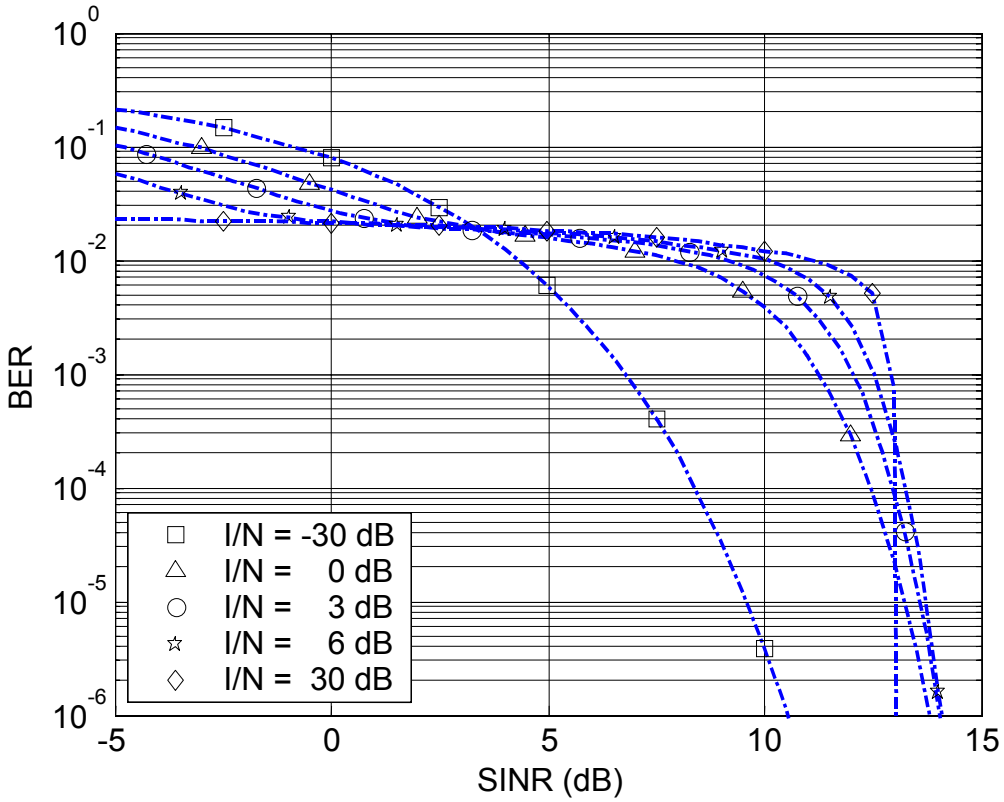

Figure 6-4: *BER performance using UWB Pulse model;* $N_u = 0.05$

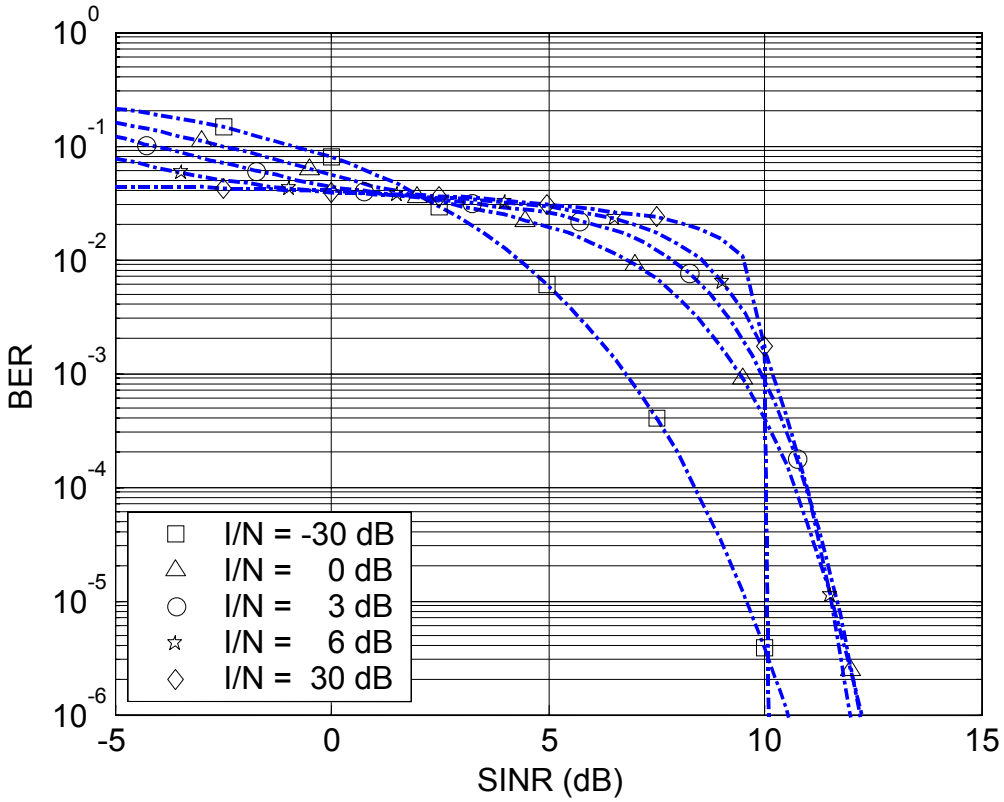

Figure 6-5: *BER performance using UWB Pulse model;* $N_u = 0.1$

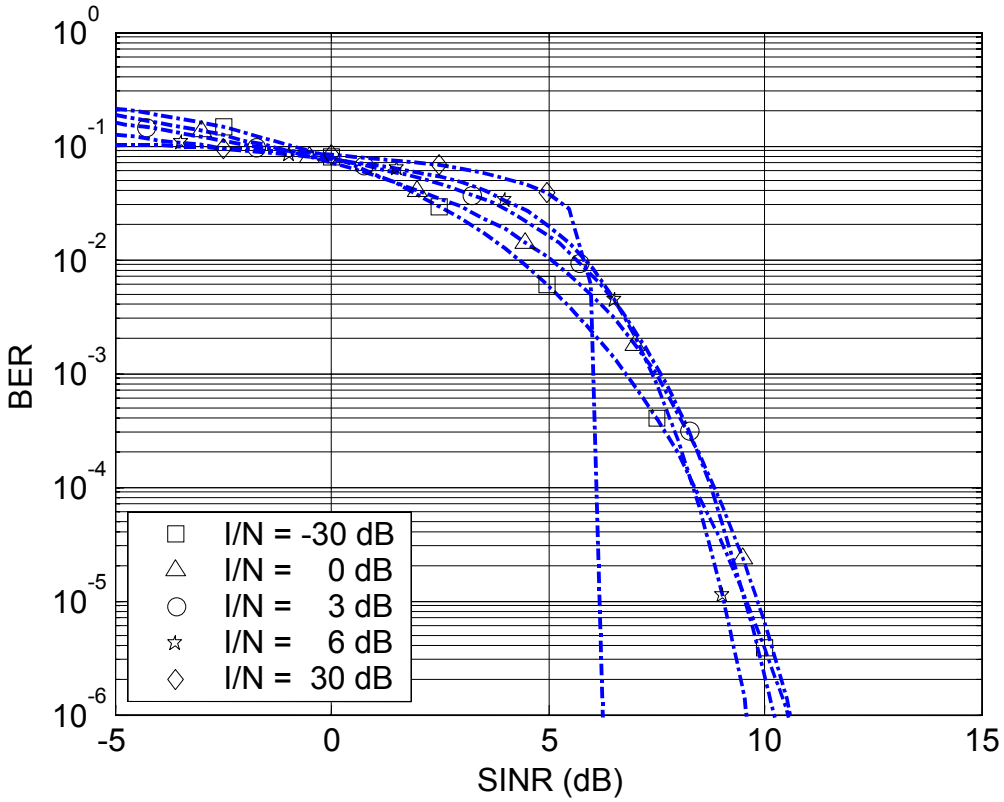

Figure 6-6: *BER performance using UWB Pulse model;* $N_u = 0.25$

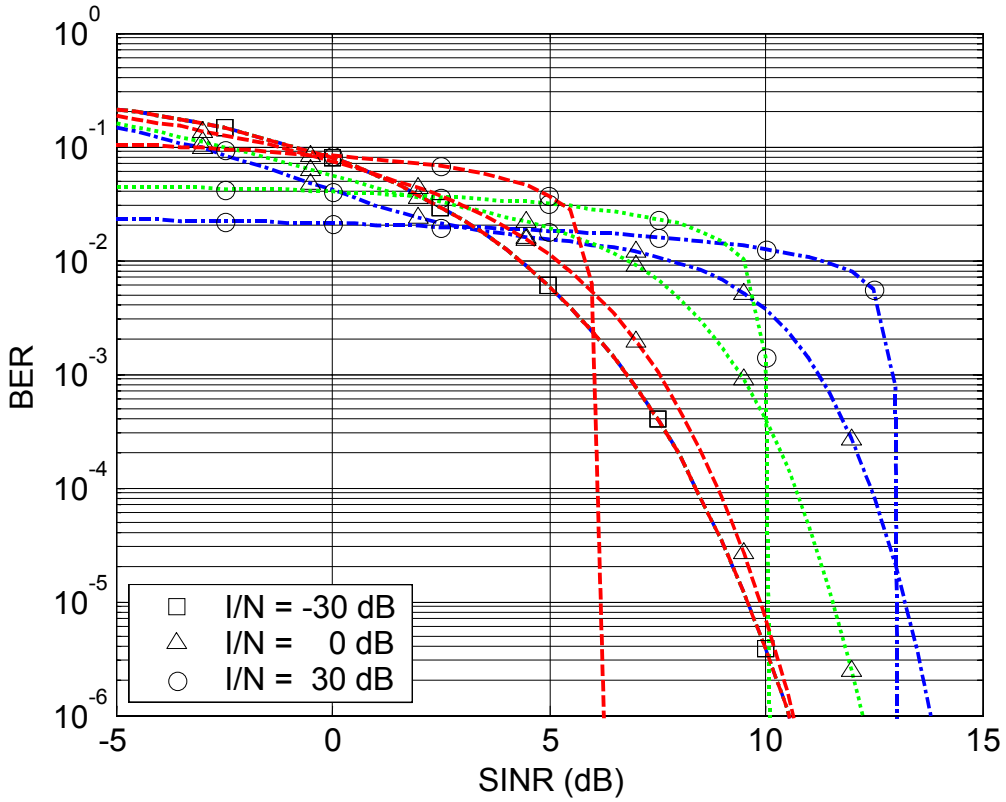

Figure 6-7: *BER performance using UWB Pulse model; Dashed-dotted blue line ($N_u = 0.05$), Dotted green line ($N_u = 0.1$), Dashed red line ($N_u = 0.25$)*

Table 6-1: *SINR Values Extracted from Figure 6-7 for Interference Limited Case ($I/N = 30$ dB)*

N_u	$10\log_{10}(N_u)$	*SINR @ BER of* 10^{-4}
0.05	13 dB	13 dB
0.1	10 dB	10 dB
0.25	6 dB	6 dB

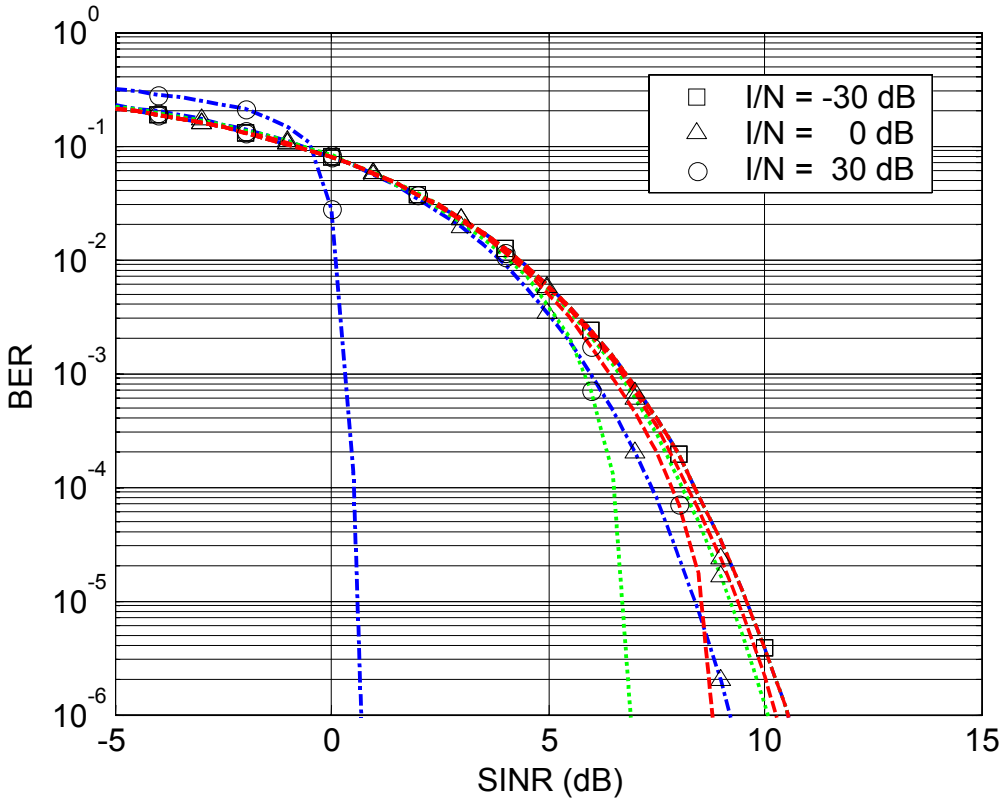

Figure 6-8: *BER performance using UWB Pulse model; Dashed-dotted blue line ($N_u = 1$), Dotted green line ($N_u = 5$), Dashed red line ($N_u = 10$)*

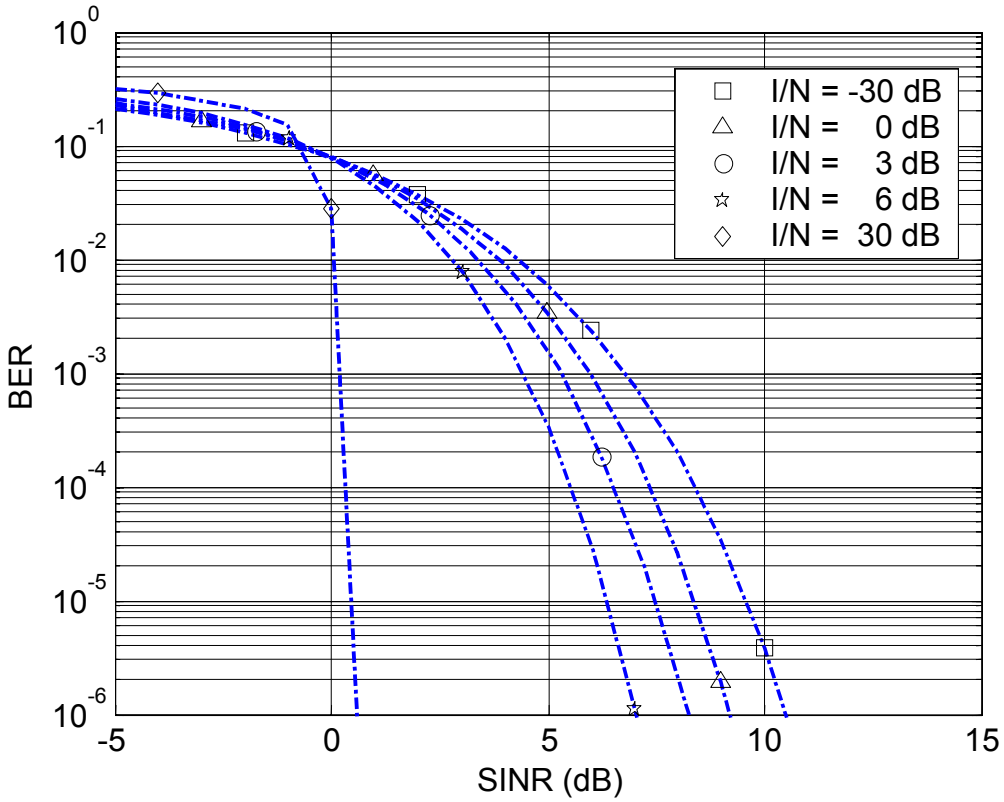

Figure 6-9: *BER using UWB Tone Model; $\Delta\omega_u$ =0 (tone centered at carrier frequency)*

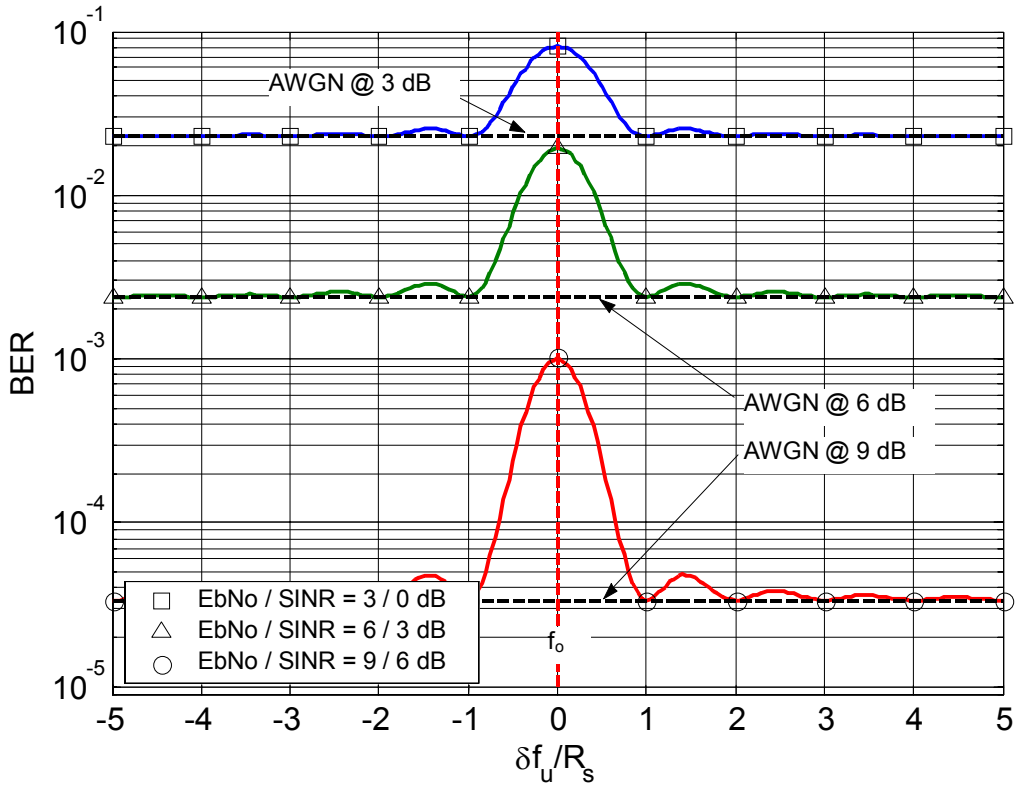

Figure 6-10: *BER using UWB Tone Model; Performance as a function of spectral line location; I/N=0 dB*

6.4. Conclusions

In this chapter, the BER performance of a coherent PSK receiver in the presence of a UWB interferer has been analyzed. The UWB interference has been modeled using a pulse model and a tone model. The latter is used to represent the case where UWB places a spectral line in the bandwidth of the narrowband victim receiver. Using the analytical model, some sample cases were simulated to study the effect of UWB PRF relative to the NB signaling rate, spectral line location and the effect of UWB interference relative to white noise.

Using the UWB pulse model, it is generally seen that UWB interference is less harmful than white noise of the same strength. For the low PRF (that is, when the UWB PRF is less than PSK symbol rate) case, in the low signal strength regime, a higher PRF is more detrimental. Whereas at high signal strengths, a lower PRF poses a greater problem for the NB radio. In fact, it is shown that in the high signal strength regime, the required NB signal strength for a fixed BER and data rate is inversely proportional to the UWB PRF. That is every halving of the UWB PRF requires an additional 3 dB power for the NB radio.

When the PRF is greater than the NB symbol rate, the interference can be approximated by the white Gaussian noise model when dithering over a large code-span is applied. As the number of UWB pulses per NB symbol increases, the performance becomes less dependent on the actual number of pulses and converges to the noise limited case where the effect of UWB pulses depends only on the average interference power seen by the NB receiver and not the number of the UWB pulses received in a symbol duration.

The analysis using the tone model also indicates that the tone or spectral line is less harmful than white noise of the same strength. As expected, the effect of the line is shown to depend on its location. The UWB system causes most harm when it places a spectral line exactly at the carrier frequency. Conversely, it is also seen that when the lines are separated from the carrier frequency by about 3-5 times the NB symbol rate, the interference completely vanishes. Further, it is seen that the BER as a function of the tone location follows the magnitude response of the Fourier transform of the NB pulse shaping with AWGN performance at the nulls of the transform.

Chapter 6 References

[1] J. R. Foerster, “Interference Modeling of Pulse-based UWB Waveforms on Narrowband Systems,” Vehicular Technology Conference, pp. 1931-1934, 2002.
[2] A. Swami, B, Sadler and J. Turner, “On the Coexistence of Ultra-Wideband and Narrowband Radio Systems,” MILCOM 2001, Vol. 1, pp. 16-19, 2001.

Chapter 7: UWB INTERFERENCE TO A COHERENT FSK RECEIVER

This Chapter analyzes the bit error rate (BER) performance of a coherent FSK receiver in the presence of UWB interference. The analysis assumes a non-fading channel that is corrupted by additive white Gaussian noise (AWGN).

A set of canonical models will be used to represent UWB interference in its various forms as seen by a narrowband receiver. These canonical models will allow the treatment of UWB as a source of interference to NB radios for a wide range of operational parameter settings of both the interferer's and the victim's radio systems.

A block diagram of a coherent detection scheme for binary FSK is shown in Figure 7-1. A coherent FSK receiver operates as follows. It consists of two matched filters corresponding to each of the two possible frequencies. The output of the filters are sampled every T_s seconds with the difference of the sampled outputs from the two branches forming the decision statistic. When this value is positive, a "1" is chosen and when it is negative, a "0" is chosen.

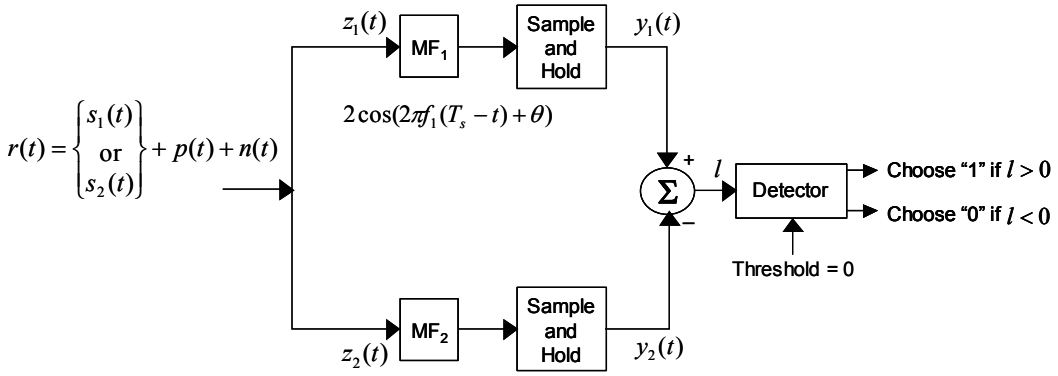

Figure 7-1: *Coherent FSK Receiver*

7.1. System Model

The received waveform at the input to the FSK receiver is given as

$$r(t) = s(t) + p(t) + n(t) \tag{7-1}$$

where $s(t)$, $p(t)$ and $n(t)$ represent the desired narrowband signal, the UWB interference and additive white Gaussian noise (AWGN), respectively.
The desired narrowband (NB) FSK signal is written as

$$s(t) = \sqrt{2P_s} \sum_{j=-\infty}^{\infty} \cos(\omega_i(t - jT_s) + \theta) v(t - jT_s) \tag{7-2}$$

where,

$$v(t - jT_s) = \begin{cases} 1, & jT_s \le t < (j+1)T_s \\ 0, & otherwise \end{cases} \tag{7-3}$$

is a rectangular window function and θ is a random phase term which is uniformly distributed in $[0, 2\pi]$. In (7-2), P_s is the average NB signal power and ω_i is the carrier frequency that can take values ω_1 and ω_2 with equal probability. The symbol period is denoted by T_s and equals reciprocal of the symbol rate, R_s. For simultaneously ensuring waveform orthogonality and phase-continuity, the minimum frequency separation condition is given as $2\Delta\omega = \omega_2 - \omega_1 = 2\pi/T_s = 2\pi R_s$. In FSK parlance, $\Delta\omega$ is referred to as the peak frequency deviation about a nominal carrier frequency, $\omega_0 = (\omega_2 + \omega_1)/2$. The noise term, $n(t)$, is modeled as white Gaussian noise with a two-sided power spectral density equal to $N_0/2$.

As mentioned earlier, UWB interference as seen by the NB victim receiver will be modeled using two canonical representations. Depending on the specific of the UWB radio, it may or may not appear as spectral lines in the bandwidth of the NB receiver. For the case when lines are not present, UWB is modeled as a time-series of very short (spectrum appears flat to NB receiver) pulses. This will be referred to as the UWB Pulse Model (UPM). The second case, when spectral lines appear, is referred to as the UWB Tone Model (UTM) since lines in the frequency domain represent sinusoids in the time domain.

UWB Pulse Model (UPM)

The UWB waveform, $p(t)$, is given as

$$p(t) = \sqrt{P_u} \sum_k a_k w(t - kT_u - \varepsilon_k) \tag{7-4}$$

where P_u is the average transmit UWB power and $w(t)$ is the UWB pulse shaping function of unit power. For this analysis, it is assumed that the UWB waveform has the ideal bandpass shape as shown in. In Figure 7-2, B_u is the UWB pulse bandwidth.

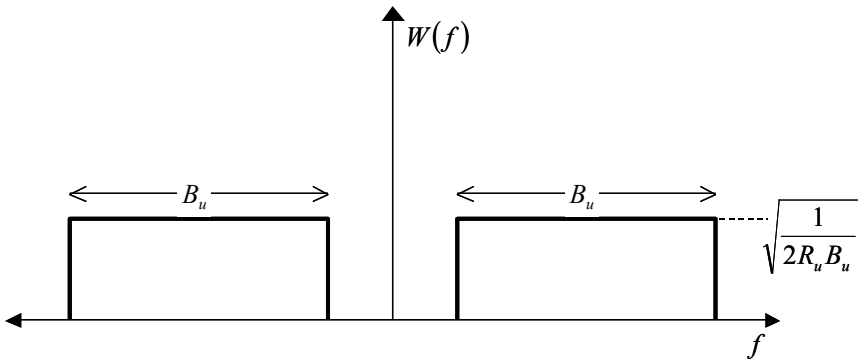

Figure 7-2: *UWB Pulse Shaping Model*

The pulse repetition interval is given by T_u, which is the reciprocal of the average UWB pulse repetition frequency (PRF). UWB amplitude and position-based modulation is modeled through the random variables, a_k and ε_k. It is assumed that any time-dithering is subsumed in ε_k, and therefore, it may be modeled as uniformly distributed random variable in $[0, \alpha T_u]$, where α is the fractional code-span.

UWB Tone Model (UTM)

The UWB temporal model when it gives rise to spectral lines in the bandwidth of the NB receiver is effectively that of a continuous wave (CW) signal or tone. In this case, the UWB model is given as

$$p(t) = \sqrt{2P_u}\cos((\omega_0 + \Delta\omega_u)t) \tag{7-5}$$

The location of the tone or spectral line may be varied by the frequency shift parameter, $\Delta\omega_u$ with the nominal FSK center frequency, ω_0, as the reference point. The average power in this tone is given by P_u and is computed as $\frac{1}{T_s}\int_0^{T_s} p^2(t)dt$. It is assumed that $\omega_0 + \Delta\omega_u >> 2\pi/T_s$.

7.2. BER Analysis

The impulse response of the matched filter of the upper branch or branch 1, which is matched to the signal at frequency, ω_1, is given as

$$h_1(t) = 2\cos(\omega_1(T_s - t) + \theta)v(T_s - t) \tag{7-6}$$

Note that the signal phase is known and accounted for in the matched filter response for coherent detection. It is also assumed that there is no inter-symbol interference at the filter output at the sampling instant.

The sampled output of the upper branch matched filter is given as

$$\begin{aligned} y_1(T_s) &= \int_{-\infty}^{\infty} r(\tau) h_1(T_s - \tau) d\tau \\ &= y_{s,1}(T_s) + y_{p,1}(T_s) + y_{n,1}(T_s) \end{aligned} \tag{7-7}$$

where $y_{s,1}(T_s)$, $y_{p,1}(T_s)$, and $y_{n,1}(T_s)$ represent the sampled matched filter outputs for the desired NB signal, UWB interference signal and noise. Each of these constituents of the matched filter output will now be evaluated separately.

Signal Term

Assuming that s_1 was sent in the j th symbol interval, where s_i is the symbol corresponding to ω_i, the desired signal term sampled optimally at $(j+1)T_s$ is derived below as follows

$$\begin{aligned} y_{s,1}^{(1)}(t) &= \int_{-\infty}^{\infty} s(\tau) h_1(t - \tau) d\tau \\ &= \sum_{j=-\infty}^{\infty} 2\sqrt{2P_s} \int_{-\infty}^{\infty} \cos(\omega_i(\tau - jT_s) + \theta) \cos(\omega_1(T_s - (t - \tau)) + \theta) v(\tau - jT_s) v(T_s - (t - \tau)) d\tau \\ \therefore y_{s,1}^{(1)}((j+1)T_s) &= 2\sqrt{2P_s} \int_{-\infty}^{\infty} \cos^2(\omega_1(\tau - jT_s) + \theta) v^2((\tau - jT_s)) d\tau \\ &= 2\sqrt{2P_s} \int_{jT_s}^{(j+1)T_s} \frac{1}{2}[1 + \cos(2\omega_1(\tau - jT_s) + \theta)] d\tau \\ &= \sqrt{2P_s} T_s \end{aligned} \tag{7-8}$$

Similarly, the output of the lower branch is obtained as

$$\begin{aligned} y_{s,2}^{(1)}((j+1)T_s) &= 2\sqrt{2P_s} \int_{-\infty}^{\infty} \cos(\omega_1(\tau - jT_s) + \theta) \cos(\omega_2(\tau - jT_s) + \theta) v^2(\tau - jT_s) d\tau \\ &= \sqrt{2P_s} \int_{jT_s}^{(j+1)T_s} [\cos((\omega_1 - \omega_2)(\tau - jT_s)) + \cos((\omega_1 + \omega_2)(\tau - jT_s) + 2\theta)] d\tau \\ &= 0 \end{aligned} \tag{7-9}$$

The 1st integral equals zero since $\omega_2 - \omega_1 = 2\pi/T_s$ and the 2nd integral vanishes due to the high frequency component, $\omega_2 + \omega_1$, which is negligible after integration.

Next, the interference term is evaluated for the two canonical models described earlier.

Interference Term Using UPM

This is readily accomplished by a frequency domain analysis as follows

$$\begin{aligned} Y_{u,i}(f) &= P(f)H_i(f) \\ &= \sqrt{\frac{P_u}{2R_uB_u}}\sum_k a_k e^{-j2\pi f(kT_u+\varepsilon_k)}H_i(f) \end{aligned} \tag{7-10}$$

Taking the inverse Fourier transform yields the following

$$\begin{aligned} y_{u,i}(t) &= \sqrt{\frac{P_u}{2R_uB_u}}\sum_k a_k h_i(t-kT_u-\varepsilon_k) \\ &= \sqrt{\frac{2P_u}{R_uB_u}}\sum_k a_k \cos\left(\omega_i\left(T_s-(t-kT_u-\varepsilon_k)\right)+\theta\right)v\left(T_s-(t-kT_u-\varepsilon_k)\right) \end{aligned} \tag{7-11}$$

Therefore, the sampled interference output is obtained as

$$y_{u,i}((j+1)T_s) = \sqrt{\frac{2P_u}{R_uB_u}}\sum_k a_k \cos\left(\omega_i\left(kT_u+\varepsilon_k-jT_s\right)+\theta\right)v\left(kT_u+\varepsilon_k-jT_s\right) \tag{7-12}$$

Interference Term Using UTM

The output of the matched filter for the tone model is evaluated in the time domain separately for each branch as follows

$$
\begin{aligned}
&y_{u,1}\left((j+1)T_s\right) = p(t) * h_1(t)\big|_{t=(j+1)T_s} \\
&= 2\sqrt{2P_u}\int_{-\infty}^{\infty}\cos\left((\omega_0+\Delta\omega_u)\tau\right)\cos\left(\omega_1(\tau-jT_s)+\theta\right)v(\tau-jT_s)d\tau \\
&= \sqrt{2P_u}\int_{0}^{T_s}\cos\left((\Delta\omega+\Delta\omega_u)\tau-\left(\theta-jT_s(\omega_0+\Delta\omega_u)\right)\right)d\tau + \\
&\sqrt{2P_u}\int_{0}^{T_s}\cos\left((\omega_0+\omega_1+\Delta\omega_u)\tau+\left(\theta+jT_s(\omega_0+\Delta\omega_u)\right)\right)d\tau \\
&= \sqrt{2P_u}T_s\left[\frac{\sin\left((\Delta\omega+\Delta\omega_u)T_s-\left(\theta-jT_s(\omega_0+\Delta\omega_u)\right)\right)+\sin\left(\theta-jT_s(\omega_0+\Delta\omega_u)\right)}{(\Delta\omega+\Delta\omega_u)T_s}+\right. \\
&\left.\frac{\sin\left((\omega_0+\omega_1+\Delta\omega_u)T_s+\left(\theta+jT_s(\omega_0+\Delta\omega_u)\right)\right)-\sin\left(\theta+jT_s(\omega_0+\Delta\omega_u)\right)}{(\omega_0+\omega_1+\Delta\omega_u)T_s}\right] \\
&\cong \sqrt{2P_u}T_s\left[\frac{\sin\left((\Delta\omega+\Delta\omega_u)T_s-\left(\theta-jT_s(\omega_0+\Delta\omega_u)\right)\right)+\sin\left(\theta-jT_s(\omega_0+\Delta\omega_u)\right)}{(\Delta\omega+\Delta\omega_u)T_s}\right]
\end{aligned}
\tag{7-13}
$$

The last step assumes that $\omega_0+\omega_1+\Delta\omega_u >> 1$. Similarly, it can be shown that the sampled interference output of branch two is given as

$$
\begin{aligned}
&y_{u,2}\left((j+1)T_s\right) = 2\sqrt{2P_u}\int_{0}^{T_s}\cos\left((\omega_0+\Delta\omega_u)\tau\right)\cos\left(\omega_2\tau+\theta\right)d\tau \\
&= \sqrt{2P_u}T_s\left[\frac{\sin\left((\Delta\omega-\Delta\omega_u)T_s-\left(\theta-jT_s(\omega_0+\Delta\omega_u)\right)\right)-\sin\left(\theta-jT_s(\omega_0+\Delta\omega_u)\right)}{(\Delta\omega-\Delta\omega_u)T_s}+\right. \\
&\left.\frac{\sin\left((\omega_0+\omega_2+\Delta\omega_u)T_s+\left(\theta+jT_s(\omega_0+\Delta\omega_u)\right)\right)-\sin\left(\theta+jT_s(\omega_0+\Delta\omega_u)\right)}{(\omega_0+\omega_2+\Delta\omega_u)T_s}\right] \\
&\cong \sqrt{2P_u}T_s\left[\frac{\sin\left((\Delta\omega-\Delta\omega_u)T_s-\left(\theta-jT_s(\omega_0+\Delta\omega_u)\right)\right)+\sin\left(\theta-jT_s(\omega_0+\Delta\omega_u)\right)}{(\Delta\omega-\Delta\omega_u)T_s}\right]
\end{aligned}
\tag{7-14}
$$

Finally, the sampled noise output and its statistics are derived.

Noise Term and Statistics

The sampled matched filter output for AWGN for the i th branch is given as

$$
y_{n,i}\left((j+1)T_s\right) = n(t) * h_i(t)\big|_{t=(j+1)T_s} = 2\int_{-\infty}^{\infty} n(\tau)\cos\left(\omega_i(\tau-jT_s)+\theta\right)v(\tau-jT_s)d\tau \tag{7-15}
$$

Now, the mean and the variance of the sampled noise term are derived.

$$\begin{aligned}
&\left\langle y_{n,i}\left((j+1)T_s\right)\right\rangle = 2\int_{-\infty}^{\infty}\left\langle n(\tau)\right\rangle \cos\left(\omega_i(\tau - jT_s)+\theta\right)v(\tau - jT_s)d\tau = 0 \\
&\left\langle \left(y_{n,i}\left((j+1)T_s\right)\right)^2\right\rangle = 4\int_{-\infty}^{\infty}\left[\int_{-\infty}^{\infty}\left\langle n(\tau_1)n(\tau_2)\right\rangle \cos\left(\omega_i(\tau_1 - jT_s)+\theta\right)v(\tau_1 - jT_s)d\tau_1\right]\times \\
&\cos\left(\omega_i(\tau_2 - jT_s)+\theta\right)v(\tau_2 - jT_s)d\tau_2 \\
&= 4\int_{-\infty}^{\infty}\left[\int_{-\infty}^{\infty}\delta(\tau_1 - \tau_2)\cos\left(\omega_i(\tau_1 - jT_s)+\theta\right)v(\tau_1 - jT_s)d\tau_1\right]\times \\
&\cos\left(\omega_i(\tau_2 - jT_s)+\theta\right)v(\tau_2 - jT_s)d\tau_2 \\
&= 4\frac{N_0}{2}\int_0^{T_s}\cos^2\left(\omega_i\tau+\theta\right)d\tau = N_0T_s
\end{aligned} \tag{7-16}$$

Therefore, the sampled noise output of branch 1 and branch 2 are Gaussian distributed zero mean with variance, N_0T_s. Further, the noise outputs of the two branches are independent since the bandpass noise processes occupy non-overlapping spectral bands assuming that the frequency separation is greater than the single channel (one FSK symbol) bandwidth.

Given, the description of all of the constituent terms of the matched filter output, we can now form the decision statistic, which is the difference signal of the two branches, and is defined as

$$\begin{aligned}
s_1\ sent: l^{(1)} &= y_1\left((j+1)T_s\right)\big|_{s_1\ sent} - y_2\left((j+1)T_s\right)\big|_{s_1\ sent} = A_s^{(1)} + A_u + N \\
s_2\ sent: l^{(2)} &= y_1\left((j+1)T_s\right)\big|_{s_2\ sent} - y_2\left((j+1)T_s\right)\big|_{s_2\ sent} = -A_s^{(2)} + A_u + N
\end{aligned} \tag{7-17}$$

where,

$$\begin{aligned}
A_s^{(1)} &= y_{s,1}^{(1)}\left((j+1)T_s\right) - y_{s,2}^{(1)}\left((j+1)T_s\right) = \sqrt{2P_s}T_s \\
A_s^{(2)} &= y_{s,1}^{(2)}\left((j+1)T_s\right) - y_{s,2}^{(2)}\left((j+1)T_s\right) = -\sqrt{2P_s}T_s \\
A_u &= y_{u,1}\left((j+1)T_s\right) - y_{u,2}\left((j+1)T_s\right) \\
N &= y_{n,1}\left((j+1)T_s\right) - y_{n,2}\left((j+1)T_s\right)
\end{aligned} \tag{7-18}$$

The last term in 7-18 implies that the random variable N is Gaussian distributed with zero mean and variance $\sigma_N^2 = \left\langle \left(y_{n,1}\left((j+1)T_s\right)\right)^2\right\rangle + \left\langle \left(y_{n,2}\left((j+1)T_s\right)\right)^2\right\rangle = 2N_0T_s$.

Therefore, the BER for each symbol can be derived by conditioning on the UWB interference terms. Then, using the results in 6-15 and 6-16, the decision statistic, $l^{(i)}$, when s_i is sent, is a Gaussian random variable described as

$$s_1 \, sent : l^{(1)} \rightarrow N\left(A_s + A_u, \sigma_N^2\right)$$
$$s_2 \, sent : l^{(2)} \rightarrow N\left(-A_s - A_u, \sigma_N^2\right)$$

where $A_s = \sqrt{2P_s}T_s$ and $\sigma_N^2 = 2N_0T_s$. The offset in the mean due to the interference, A_u, is derived for the two canonical modes using expressions 7-18, 7-12, 7-13 and 7-14. The corresponding conditional PDFs of the decision statistics are shown in Figure 7-3.

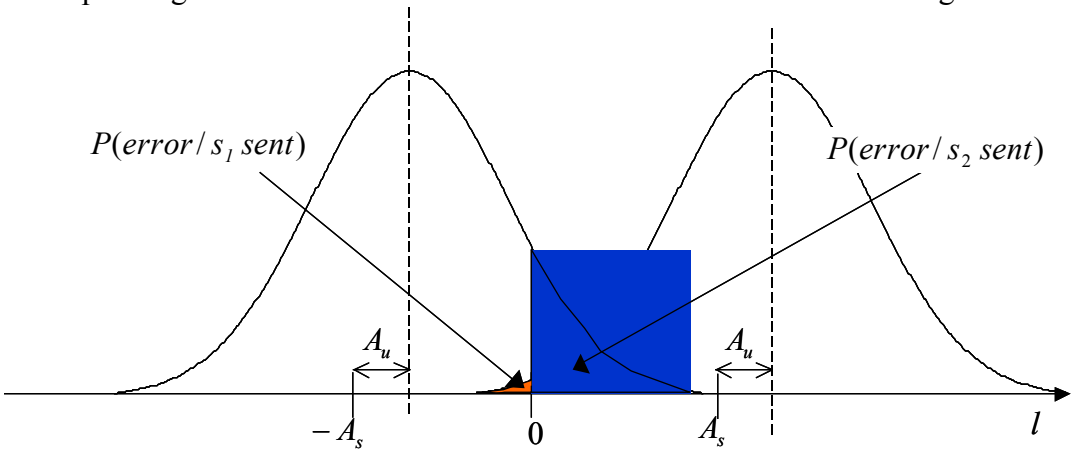

Figure 7-3: *Conditional PDF of decision statistics*

The conditional probability of error for the j the symbol, when s_1 is sent is derived as

$$P_j(error/(s_1 \, sent, \theta, \{a_k\}, \varepsilon_k)) = \frac{1}{\sqrt{2\pi\sigma_N^2}} \int_{-\infty}^{0} e^{-(x - A_s - A_u)^2/(2\sigma_N^2)} dx$$
$$= \frac{1}{\sqrt{2\pi}} \int_{(A_s + A_u)/\sigma_N}^{\infty} e^{-y^2/2} dy = \mathrm{Q}\left(\frac{(A_s + A_u)}{\sigma_N}\right) \tag{7-19}$$

where, $\mathrm{Q}(x)$ is defined as $\frac{1}{\sqrt{2\pi}} \int_x^{\infty} e^{-y^2/2} dy$.

Similarly, the conditional probability of error, when s_2 is sent is given as

$$P_j(error/(s_2 \, sent, \theta, \{a_k\}, \varepsilon_k)) = \mathrm{Q}\left(\frac{(A_s - A_u)}{\sigma_N}\right) \tag{7-20}$$

Given that both symbols are equally likely, the final BER expression for the j th symbol is given as

$$P_{e,j} = \left\langle \frac{1}{2}\mathrm{Q}\left(\frac{(A_s + A_u)}{\sigma_N}\right) + \frac{1}{2}\mathrm{Q}\left(\frac{(A_s - A_u)}{\sigma_N}\right) \right\rangle_{\theta, \{a_k\}, \varepsilon_k} \tag{7-21}$$

Next, we express the arguments of the $\mathrm{Q}(.)$ function in more physically meaningful terms. The arguments can be split into two terms; the NB signal related term of A_s/σ_N and the UWB interference related term of A_u/σ_N. The 1st term can be expressed as

$$\frac{A_s}{\sigma_N} = \frac{T_s\sqrt{2P_s}}{\sqrt{2N_oT_s}} = \frac{\sqrt{P_sT_s}}{\sqrt{N_o}} = \sqrt{\frac{E_b}{N_o}} \tag{7-22}$$

where E_b $(= P_sT)$ is the energy per NB symbol.
The 2nd term is handled separately for each canonical UWB interference model.

Error Expression for UPM
Substituting 7-12 in 7-18, we can express the 2nd argument as follows

$$\begin{aligned}
&\frac{A_u}{\sigma_N} = \sqrt{\frac{2P_u}{R_uB_u}} \times \\
&\frac{\sum_k a_k\left[\cos\left(\omega_1\left(kT_u+\varepsilon_k-jT_s\right)+\theta\right)-\cos\left(\omega_2\left(kT_u+\varepsilon_k-jT_s\right)+\theta\right)\right]v\left(kT_u+\varepsilon_k-jT_s\right)}{\sqrt{2N_oT_s}} \\
&= \frac{T_s\sqrt{2P_s}}{\sqrt{2N_oT_s}}\sqrt{\frac{R_s}{R_u}}\sqrt{\frac{(P_u/B_u)R_s}{P_s}} \times \\
&2\sum_k a_k \sin\left(\omega_0\left(kT_u+\varepsilon_k-jT_s\right)+\theta\right)\sin\left(\Delta\omega\left(kT_u+\varepsilon_k-jT_s\right)\right)v\left(kT_u+\varepsilon_k-jT_s\right) \\
&= \sqrt{\frac{E_b}{N_o}}\frac{2}{\sqrt{N_uSIR}} \times \\
&\sum_k a_k \sin\left(\omega_0\left(kT_u+\varepsilon_k-jT_s\right)+\theta\right)\sin\left(\Delta\omega\left(kT_u+\varepsilon_k-jT_s\right)\right)v\left(kT_u+\varepsilon_k-jT_s\right)
\end{aligned} \tag{7-23}$$

where $N_u = \dfrac{R_u}{R_s}$ is the average number of UWB pulses per NB symbol period, and SIR is the signal-to-interference ratio within the NB receiver bandwidth, and is given as

$$SIR = \frac{P_s}{(P_u/B_u)R_s}$$

Substituting 7-22 and 7-23 in 7-21, the final BER expression for the j th symbol using the UWB pulse model is given as

$$P_{e,j} = \left\langle \frac{1}{2}\mathrm{Q}\left(\sqrt{\frac{E_b}{N_o}}(1+\delta)\right) + \frac{1}{2}\mathrm{Q}\left(\sqrt{\frac{E_b}{N_o}}(1-\delta)\right)\right\rangle_{\theta,\{a_k\},\varepsilon_k} \tag{7-24}$$

where δ, the interference perturbation factor is given as

$$\delta = \frac{2}{\sqrt{N_u SIR}} \sum_k a_k \sin\left(\omega_0\left(kT_u + \varepsilon_k - jT_s\right) + \theta\right) \sin\left(\Delta\omega\left(kT_u + \varepsilon_k - jT_s\right)\right) \times v\left(kT_u + \varepsilon_k - jT_s\right) \tag{7-25}$$

Error Expression for UTM

Substituting 7-13 and 7-14 (approximate values used) in 7-18, we can express the 2nd argument as follows

$$\frac{A_u}{\sigma_N} = \sqrt{\frac{E_b}{N_0}} \frac{\left(C_1 - C_2\right)}{\sqrt{SIR}} \tag{7-26}$$

where C_1 and C_2 are defined as

$$C_1 = \left[\frac{\sin\left(\left(\Delta\omega + \Delta\omega_u\right)T_s - \left(\theta - jT_s\left(\omega_0 + \Delta\omega_u\right)\right)\right) + \sin\left(\theta - jT_s\left(\omega_0 + \Delta\omega_u\right)\right)}{\left(\Delta\omega + \Delta\omega_u\right)T_s}\right]$$
$$C_2 = \left[\frac{\sin\left(\left(\Delta\omega - \Delta\omega_u\right)T_s + \left(\theta - jT_s\left(\omega_0 + \Delta\omega_u\right)\right)\right) - \sin\left(\theta - jT_s\left(\omega_0 + \Delta\omega_u\right)\right)}{\left(\Delta\omega - \Delta\omega_u\right)T_s}\right] \tag{7-27}$$

Finally, substituting 7-22 and 7-26 in 7-21, the final BER expression for the j th symbol using the UWB Tone/CW model is given as

$$P_{e,j} = \left\langle \frac{1}{2} \mathrm{Q}\left(\sqrt{\frac{E_b}{N_o}}\left(1 + \delta\right)\right) + \frac{1}{2} \mathrm{Q}\left(\sqrt{\frac{E_b}{N_o}}\left(1 - \delta\right)\right) \right\rangle_{\theta, \{a_k\}, \varepsilon_k} \tag{7-28}$$

where δ, the interference perturbation factor is given as

$$\delta = \left(C_1 - C_2\right) / \sqrt{SIR} \tag{7-29}$$

where the signal-to-interference ratio for the tone interferer case is defined as

$$SIR = \sqrt{\frac{P_s}{P_u}}$$

7.3. Numerical Results

This section presents numerical results for some special cases using the BER analysis developed in the previous section. The case considered here is that of UWB interferer

that uses pulse position modulation (PPM) with time-dithering and a fractional code-span of 1.

The coherent FSK radio system is modeled using the following parameter values:

f_0 = 200 MHz

$2\Delta f$ = 50 KHz

R_s = 50 KHz

The BER is obtained using expressions 6-22 and 6-26, where the conditionality over θ and ε_k are averaged out through Monte Carlo simulations.

Figures 7-4 – 7-9 show the BER results for the UWB interferer using the pulse model. The results are displayed as BER versus $SINR$ and are shown for various values of the PRF to NB symbol rate ratio, N_u, and interference-to-noise ratio, I/N. The interference-to-noise ratio, I/N, is defined as $(E_b/N_0)/SIR$. This allows evaluation of the relative effects of noise and interference. The signal-to-noise plus interference ratio, $SINR$ is computed as $(E_b/N_0)/(1+(I/N))$. The FSK system shows many of the same qualitative trends as the PSK system with a few differences. The observations made below will include both the similarities as well as the differences.

Case I (N_u<1)

- At low signal levels (where the signal level is comparable to or lower than the combined interference plus noise level), thermal noise is more detrimental than UWB interference. Note that the BER decreases as I/N increases when SINR is less than 7 dB in figure 7-4.
- At higher signal levels, up to two regions may be observed depending on the ratio of PRF to NB symbol rate ratio. A medium range of signal strength where noise is less detrimental and a high range of signal strength where interference is less detrimental. These two distinct regions are observed in figure 7-6 where the medium range corresponds to SINR in the range 2-9 dB and the high range is where SINR is greater than 9 dB.
- In the interference limited case (see I/N = 30 dB curve), a sharp knee is observed in that, beyond a certain SINR, where there is hardly any thermal noise, the BER quickly falls to zero. This is because there comes a point, where with negligible noise, the UWB pulse energy is never large enough to cause the received signal level to cross the decision threshold and cause an error.
- At very low SINR values, for the interference limited case (I/N = 30 dB curve), the error rate asymptotically equals the probability of a UWB pulse colliding with a NB symbol since whenever it occurs the BER is the maximum of 50 %. Therefore, the asymptotic BER equals $N_u/2$, where the N_u is the probability that a collision occurs. This is borne out in the results. For example, in figure 7-4, the BER when SINR equals -10 dB is 0.025 which is half of N_u. This is a lower bound on the BER at low SINR since for all other ratios of I/N, the performance only gets worse.
- As a check, the noise limited case is approximated by the curve I/N = -30 dB. The BER for this curve should match the theoretical coherent FSK BER given by

$erfc(\sqrt{E_b/2N_0})/2$. At 10 dB, the BER from this formula is computed as 7.8 × 10^{-4}, and matches the simulation result.

- For the low PRF case, shown in figure 7-7, two error rate regions are observed in terms of the effect of the PRF on the BER. At low SINRs, the higher PRF is more detrimental. At high SINRs, the lower PRF exhibits a worse error performance. This is explained as follows. There are two factors that contribute to an error. The first is that of the probability of a collision of a NB symbol with a UWB pulse. Obviously, higher the PRF the more likely is the collision. The second is that of the UWB interference energy per NB symbol which decreases with N_u (for a given total in-band UWB interference power) as seen in 7-23. Given a collision, the probability of an erroneous decision will be based on the interference energy per NB symbol. If the probability of an erroneous decision is high (max of 50 %), as is at low SINR, then fewer the collisions the better since a collision guarantees a coin-flip decision. If on the other hand, the probability of an erroneous decision is small, as is the case at high SINRs, then the average error rate is more sensitive to a high energy collision rather than just any collision. Since the strength of the collision is inversely proportional to N_u (as shown in equation 7-23), at high SINRs, the higher PRF is less detrimental. Table 7-1 shows the required SINR values at a fixed BER of 10^{-4} as a function of N_u for the interference limited case shown in figure 7-7. It is seen that the required SINR for a specified BER is inversely proportional to the UWB PRF. That is, every halving of the UWB PRF requires an additional 3 dB power for the NB radio.
- Whereas at high signal strengths, a lower PRF poses a greater problem for the NB radio. In fact, it is shown that in the high signal strength regime, the required NB signal strength for a fixed BER and data rate is inversely proportional to the UWB PRF. That is every halving of the UWB PRF requires an additional 3 dB power for the NB radio.

Case II ($N_u \geq 1$)

Figure 7-8 shows the BER versus SINR for the case where the PRF is greater than the NB symbol rate. The following observations are made for this case.

- As the number of UWB pulses per NB symbol increases, the performance becomes less dependent on the actual number of pulses and converges to the noise limited case. For large values of N_u, the effect of UWB pulses depends only on the average interference power seen by the NB receiver and the number of the UWB pulses received in a symbol duration becomes less important.
- It is seen that as the PRF increases the interference approaches the noise limited case (approximately represented by the curve corresponding to I/N = -30 dB) suggesting the validity of the white Gaussian noise model for high N_u. Note that the validity of this approximation is also a function of the time-dithering applied. In the simulation results shown here, dithering over a 100 % of the code span was assumed.
- It is also seen that the UWB interference is less detrimental than white noise since the peak-to-average ratio for UWB is limited whereas for the noise it is not.

The differences from the PSK case when the UWB pulse model is applied are the following.

- PSK is always superior to FSK by at least 3 dB. PSK is about 3 dB better when either the perturbation is dominated by AWGN or when the UWB interference becomes white Gaussian noise like (for N_u>5). This 3 dB is the same difference between the theoretical AWGN performance of FSK and PSK.
- When the perturbation is dominated by the UWB interference and it is not Gaussian-like, FSK is worse than PSK by about 6 dB. This 6 dB difference comes from the additional factor of 2 appearing in the perturbation factor for the FSK case. Physically, it means that the decision is based on two (one for each branch) looks at the interference as opposed to one look in the PSK case.

Next, results for the BER performance using the UWB Tone model are discussed. Figure 7-9 shows the BER versus SINR when the UWB spectral line occurs at the nominal center frequency of the FSK receiver. Figure 7-11 shows the effect of the tone interferer as a function of its location with respect to the nominal center frequency of the NB FSK radio. The following observations are made for UWB interference assuming the Tone model

- From figure 7-9, it is seen that the tone or spectral line is less harmful than white noise of the same power.
- Figure 7-10 shows that the UWB system causes most harm when it places a spectral line right between the "mark" and "space" tones.
- Like the PSK case, the tone creates an interferer that has a sinc response in the frequency domain for rectangular NB pulse shaping. The difference from the PSK case is that the tone in the FSK receiver produces two sinc functions; one centered at the "mark" frequency and the other at the "space" frequency as shown in figure 7-11. As before, the nulls appear at multiples of the symbol rate, R_s. Note that the normalization factor for the tone offset is the peak frequency deviation, δf, which is equal to $R_s/2$. Obviously, at the nulls, the AWGN BER performance is achieved. Further, if the tones are located at frequencies that are above or below the passband by twice the FSK bandwidth, their effect is negligible.

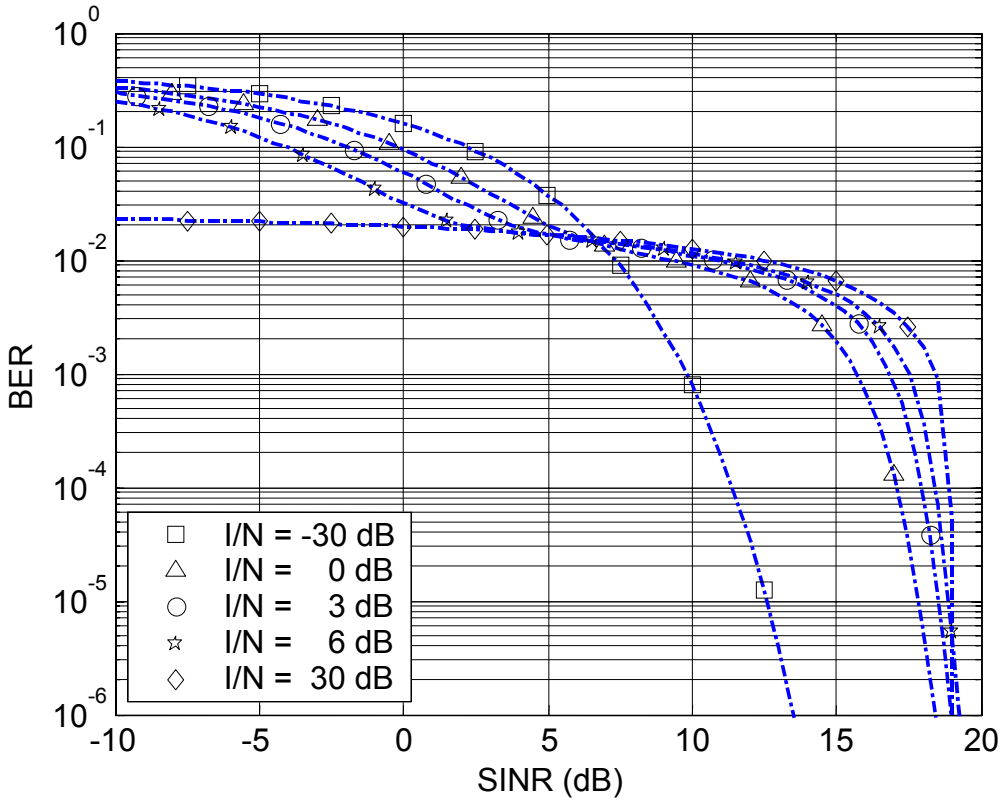

Figure 7-4: *BER performance using UWB Pulse model;* $N_u = 0.05$

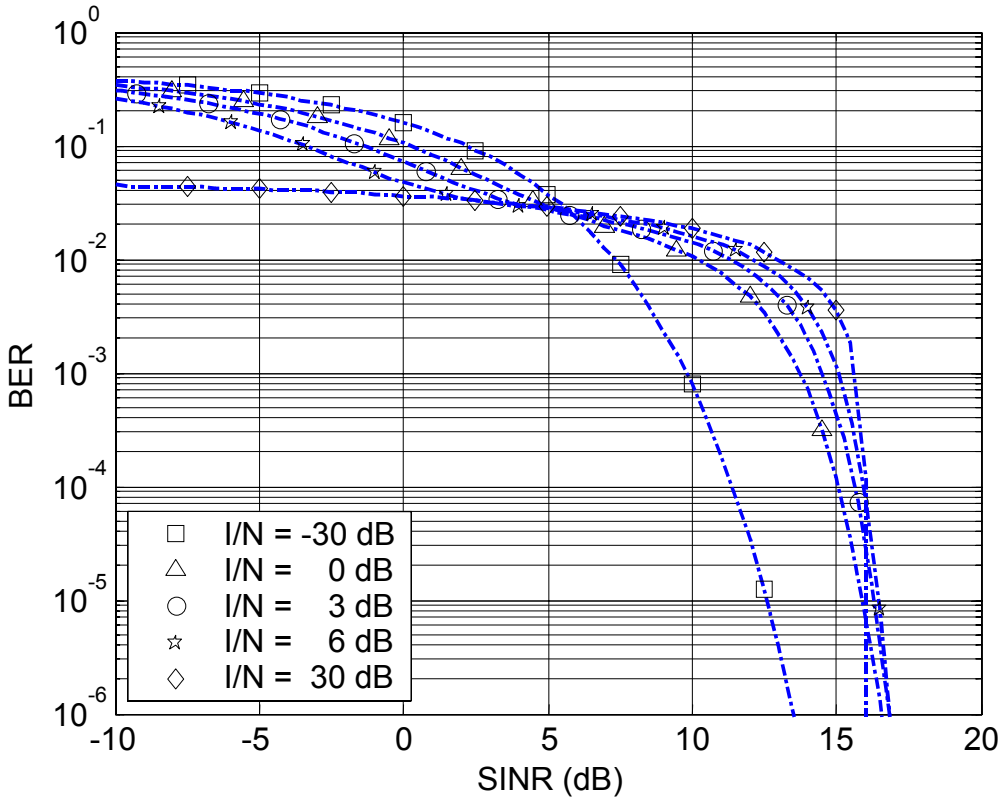

Figure 7-5: *BER performance using UWB Pulse model;* $N_u = 0.1$

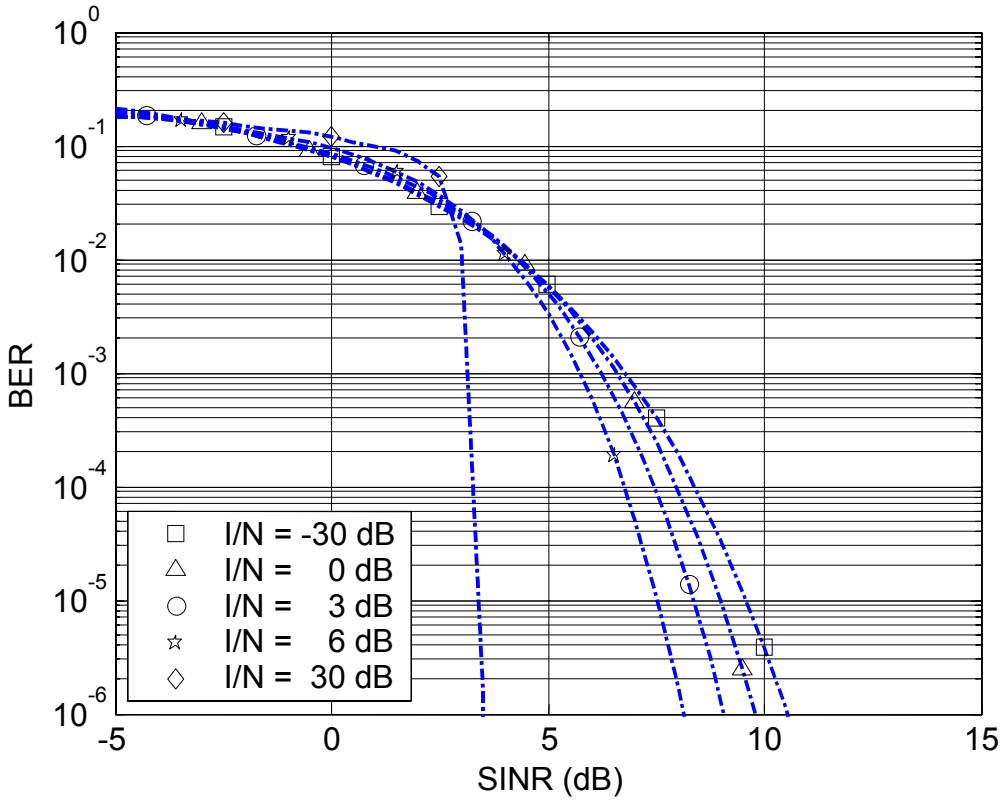

Figure 7-6: *BER performance using UWB Pulse model;* $N_u = 0.5$

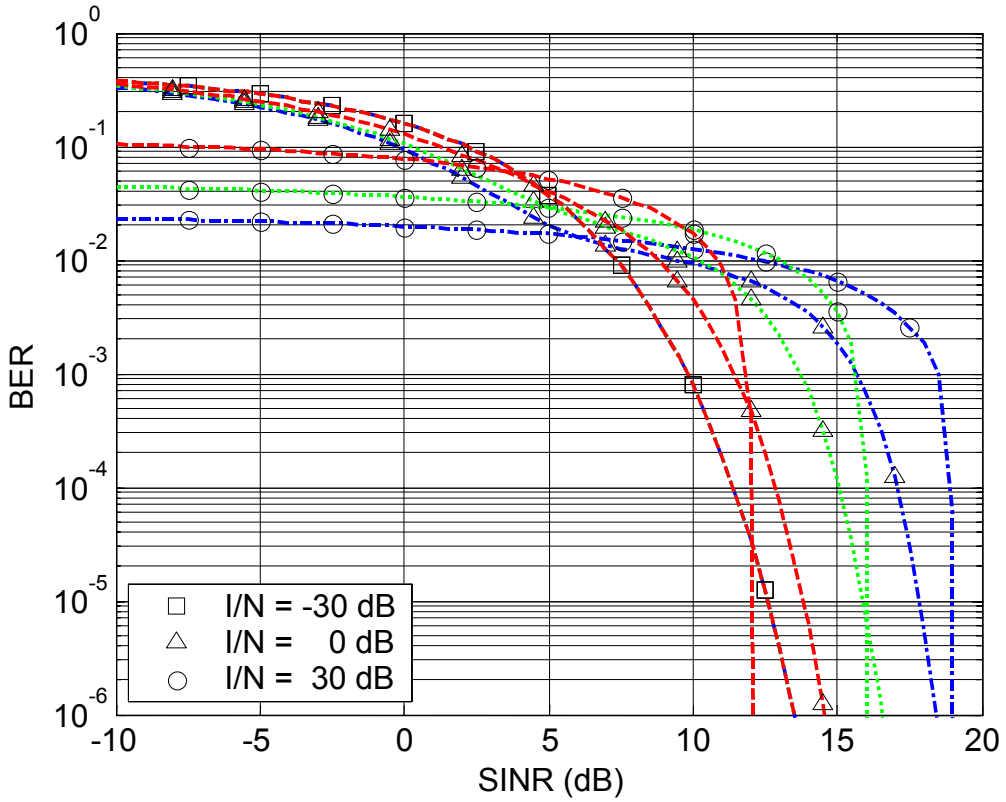

Figure 7-7: *BER performance using UWB Pulse model; Dashed-dotted blue line ($N_u = 0.05$), Dotted green line ($N_u = 0.1$), Dashed red line ($N_u = 0.25$)*

Table 7-1: *SINR Values Extracted from Figure Chapter 7:-1 for Interference Limited Case ($I/N = 30$ dB)*

N_u	$10\log_{10}(N_u / 0.05)$	*SINR @ BER of* 10^{-4}
0.05	13 dB	19 dB
0.1	10 dB	16 dB
0.25	6 dB	12 dB

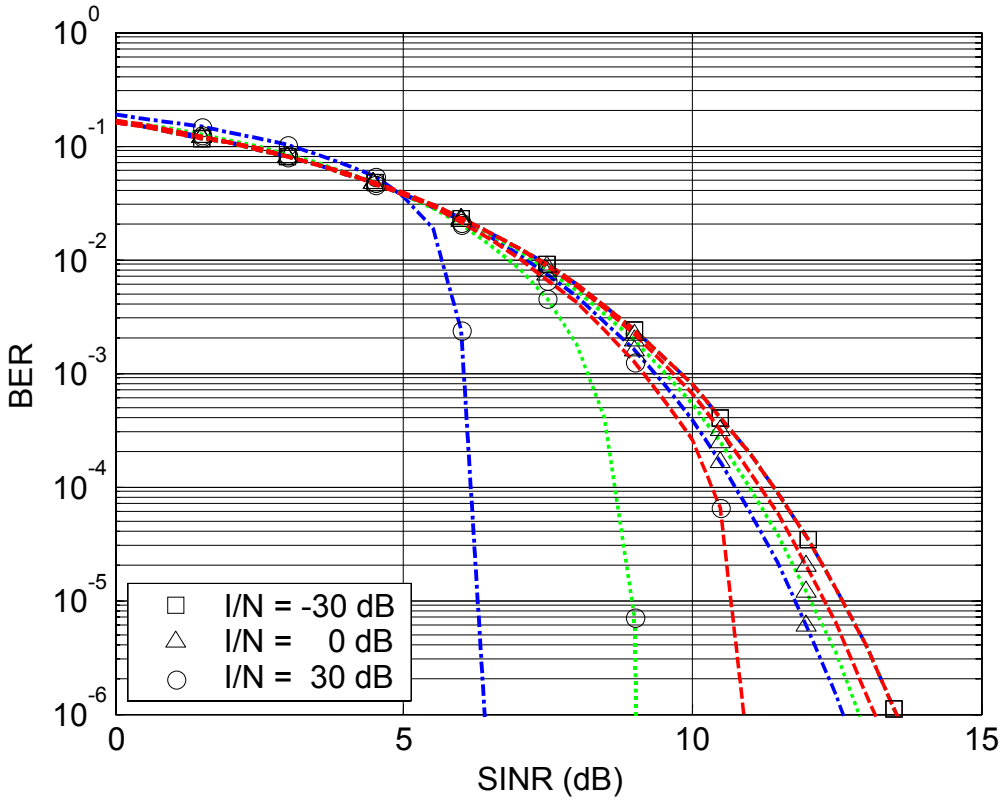

Figure 7-8: BER performance using UWB Pulse model; Dashed-dotted blue line ($N_u = 1$), Dotted green line ($N_u = 5$), Dashed red line ($N_u = 10$)

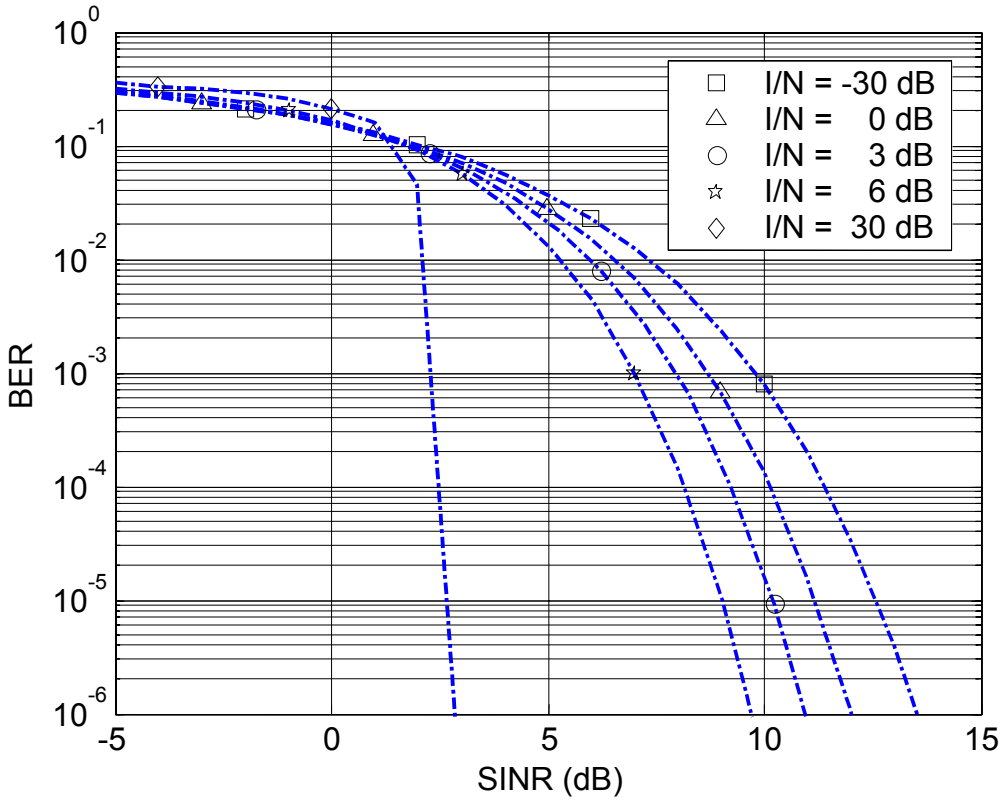

Figure 7-9: *BER using UWB Tone Model; $\Delta\omega_u$ =0 (tone at the center of the "mark" and "space" frequencies)*

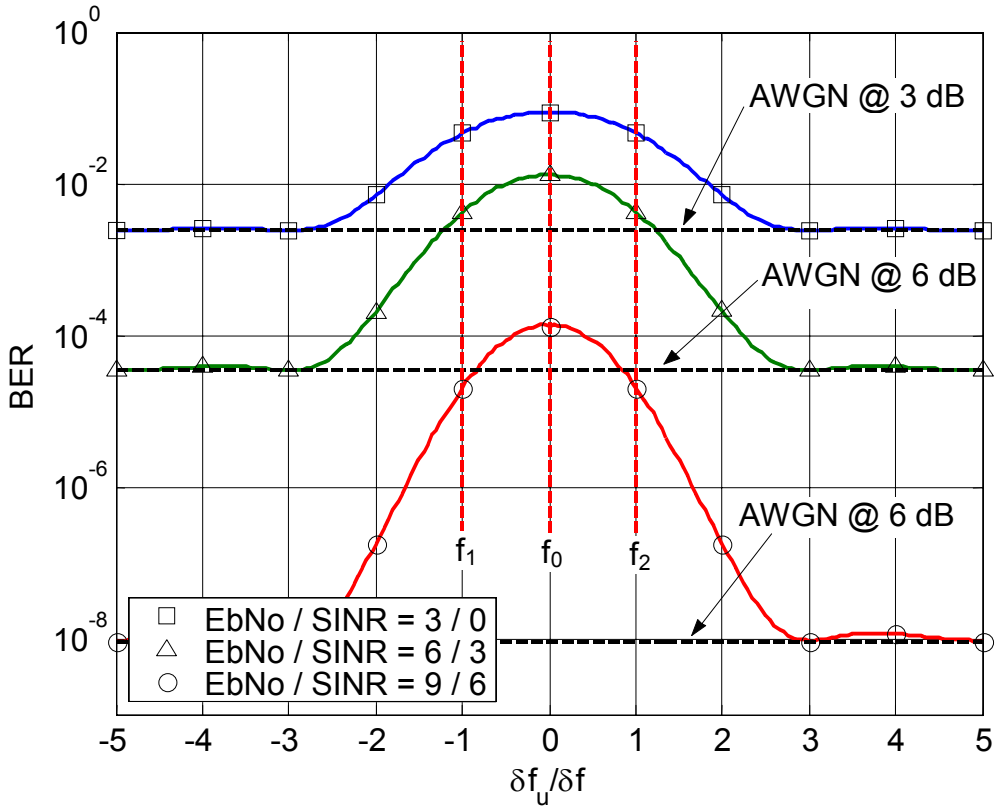

Figure 7-10: *BER using UWB Tone Model; Performance as a function of spectral line location; I/N=6 dB*

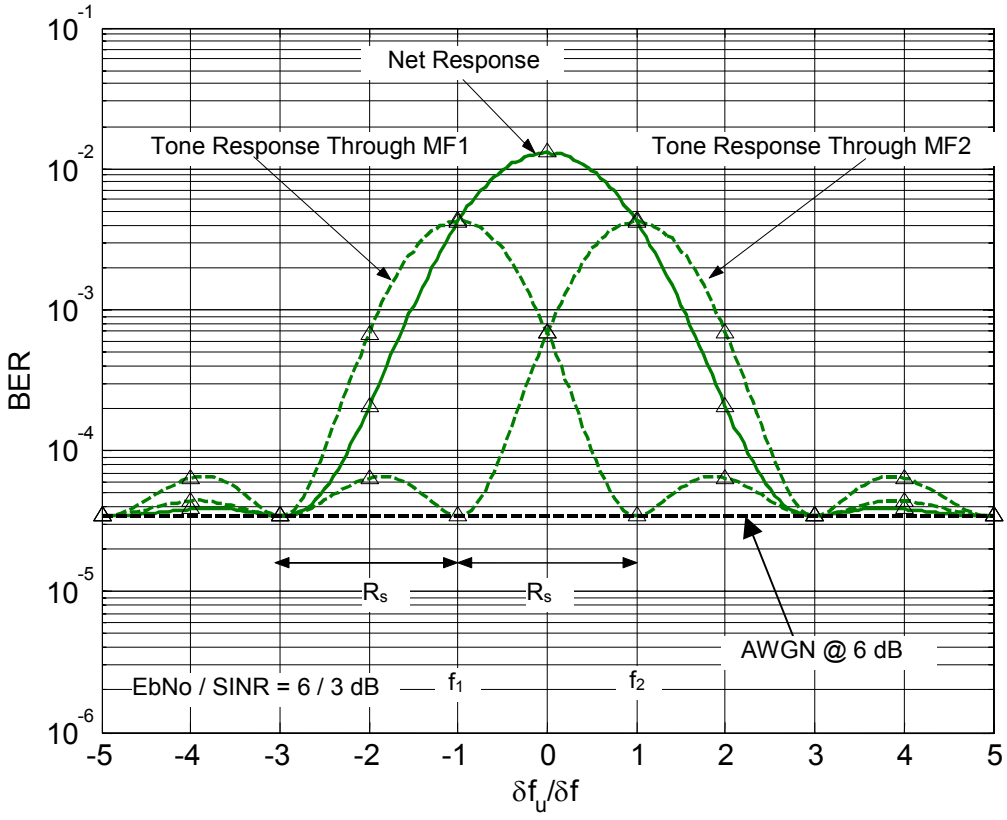

Figure 7-11: *BER using UWB Tone Model; Shows tone response through each branch separately; I/N=6 dB*

7.4. Conclusions

In this chapter, the BER performance of a coherent FSK receiver in the presence of a UWB interferer has been analyzed. The UWB interference has been modeled using a pulse model and a tone model. The latter is used to represent the case where UWB places a spectral line in the bandwidth of the narrowband victim receiver. Using the analytical model, some sample cases were simulated to study the effect of UWB PRF relative to the NB signaling rate, spectral line location and the effect of UWB interference relative to white noise. The observations show that the FSK system in the presence of the UWB interference shows many of the same qualitative trends as the PSK system.

Using the UWB pulse model, it is generally seen that UWB interference is less harmful than white noise of the same strength. For the low PRF (that is, when the UWB PRF is less than FSK symbol rate) case, in the low signal strength regime, a higher PRF is more detrimental. Whereas at high signal strengths, a lower PRF poses a greater problem for the NB radio. In fact, it is shown that in the high signal strength regime, the required NB signal strength for a fixed BER and data rate is inversely proportional to the UWB PRF. That is every halving of the UWB PRF requires an additional 3 dB power for the NB radio.

When the PRF is greater than the NB symbol rate, the interference can be approximated by the white Gaussian noise model when dithering over a large code-span is applied. As the number of UWB pulses per NB symbol increases, the performance becomes less dependent on the actual number of pulses and converges to the noise limited case where the effect of UWB pulses depends only on the average interference power seen by the NB receiver and not the number of the UWB pulses received in a symbol duration.

Using the pulsed UWB model, FSK is 3-6 dB worse than PSK. The difference is closer to 3 when the interference begins to look like white Gaussian noise (as is the case for UWB PRF greater than the NB bandwidth by a factor of 5). When the UWB PRF is lower than the NB bandwidth and interference dominates, the difference is closer to 6 dB.

The analysis using the tone model also indicates that the tone or spectral line is less harmful than white noise of the same strength. As expected, the effect of the line is shown to depend on its location. The UWB system causes most harm when it places a spectral line right between the “mark” and “space” tones. Conversely, it is also seen that when the lines are separated from the nominal center frequency by about 3-5 times the peak frequency deviation, the interference completely vanishes. Further, it is seen that the BER as a function of the tone location follows the magnitude response of the sum of the Fourier transform of the NB pulse shaping centered about the two FSK tones. AWGN performance is observed at the nulls, which occur at multiples of the FSK bandwidth above f_2 and below f_1. At the nulls, FSK will be 3 dB worse than PSK since this is the noise-limited performance.

Chapter 8: UWB INTERFERENCE TO A NON-COHERENT FSK RECEIVER

8.1. FSK with AWGN

As an introduction to the analysis of non-coherent FSK receivers, we will first analyze the simple case of a non-coherent FSK detector with only additive white Gaussian noise (AWGN). This will provide an analytic framework to which we can refer when analyzing the case with only interference (high-SNR) and with interference plus noise.

A simple non-coherent binary FSK detector is shown in Figure 8-1. This detector operates by filtering the incoming signal with a bandpass filter centered at the two desired frequencies and then passing these signals through envelope detectors. The decision stage makes a "1" or "0" decision based on time samples from the envelope detectors taken at time T_s. In the simplest form, the decision stage samples the output of the envelope filters every T_s seconds and compares the level of the two envelopes. If $\gamma_1 > \gamma_2$, the decision is made that signal 1 (s_1) was transmitted, if $\gamma_2 > \gamma_1$, it the decision is made that signal 2 (s_2) was transmitted.

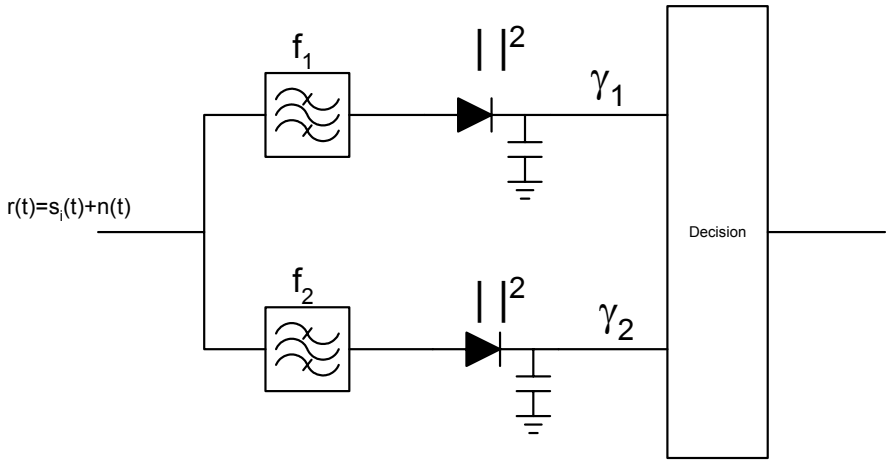

Figure 8-1: *Non-coherent FSK detector.*

The transmitted signals considered here will be equally likely binary FSK signals:

$$s_i(t) = \sqrt{\frac{2E}{T}} \cos(2\pi f_i t + \phi), \quad 0 \le t \le T, \quad i = 1, 2 \tag{8-1}$$

Note that the signals have rectangular envelopes in time, and are modulated by carriers of two distinct frequencies f_1 and f_2. The rectangular time pulses lead to a frequency response for each signal having a *sinc* shape with center frequencies f_1 and f_2, thus:

$$S_i(f) = T_s \text{sinc}(f - f_i)T_s \tag{8-2}$$

We will assume that filters shown are matched to the incoming pulses. The minimum tone spacing for noncoherent FSK detection with matched filtering is them $1/T_s$ Hz, so that the two signaling tones falls on the nulls of each other's frequency responses.

The noise term $n(t)$ at the input of the receiver is white Gaussian noise with two-sided spectral density of $N_0/2$. As mentioned above, we know that f_1 and f_2 are separated in a way such that that the output of filter f_1 is zero when excited with s_2, and vice versa, i.e., f_2-f_1=$1/T_s$. The probability of error is then expressed as the sum of the probability of error when s_1 is sent and the probability of error when s_2 is sent,

$$P_e = \frac{1}{2} P(\gamma_1 > \gamma_2 | s_2) + \frac{1}{2} P(\gamma_2 > \gamma_1 | s_1) \tag{8-3}$$

Because of symmetry, we can write the probability of error:

$$P_e = P(\gamma_1 > \gamma_2 | s_2) \tag{8-4}$$

Without loss of generality, we assume signal 2 is sent. Since only the noise term will make it though filter f_1, the output of that filter is a Gaussian random process. When passed though an envelope detector, it becomes a Rayleigh random process with distribution

$$p(\gamma_1 | s_2) = \frac{\gamma_1}{\sigma_0^2} e^{-\frac{\gamma_1^2}{2\sigma_0^2}} \quad , \quad \gamma_1 \geq 0 \tag{8-5}$$

where σ_0^2 is the noise power at the output of the filter. Since the output of the filter f_2 contains a noise term and a sinusoidal term, the envelope detector produces a Rician distribution, thus

$$p(\gamma_2 | s_2) = \frac{\gamma_2}{\sigma_0^2} \exp\left[-\frac{(\gamma_2^2 + A^2)}{2\sigma_0^2} \right] I_0\left(\frac{\gamma_2 A}{\sigma_0^2} \right) \quad , \quad \gamma_2 \geq 0 \tag{8-6}$$

where $A = \sqrt{2E/T_s}$.

The probability of error is then expressed in terms of the conditional probability densities obtained when s_1 is sent and when s_2 is sent, i.e.,

$$P_e = \int_0^\infty p(\gamma_2|s_2)\int_{\gamma_2}^\infty p(\gamma_1|s_2)d\gamma_1 d\gamma_2$$
$$= \int_0^\infty \frac{\gamma_2}{\sigma_0^2}\exp\left[-\frac{(\gamma_2^2+A^2)}{2\sigma_0^2}\right]I_0\left(\frac{\gamma_2 A}{\sigma_0^2}\right)\int_{\gamma_2}^\infty \frac{\gamma_1}{\sigma_0^2}e^{-\frac{\gamma_1^2}{2\sigma_0^2}}d\gamma_1 d\gamma_2 \quad (8\text{-}7).$$

The inner integral can be integrated by parts, i.e.,

$$\int_{\gamma_2}^\infty \frac{\gamma_1}{\sigma_0^2}e^{-\frac{\gamma_1^2}{2\sigma_0^2}}d\gamma_1 = e^{-\frac{\gamma_2^2}{2\sigma_0^2}} \quad (8\text{-}8)$$

The resulting expression for the probability of error is:

$$P_e = \int_0^\infty \frac{\gamma_2}{\sigma_0^2}\exp\left[-\frac{(2\gamma_2^2+A^2)}{2\sigma_0^2}\right]I_0\left(\frac{\gamma_2 A}{\sigma_0^2}\right)d\gamma_2 = \frac{1}{2}e^{-\frac{A^2}{4\sigma_0^2}} = \frac{1}{2}e^{-\frac{E_b}{2N_0}}, \quad (8\text{-}9)$$

where the noise power and energy per bit are $\sigma_0^2 = 2\left(\frac{N_0}{2}\right)W$, and $E_b = \frac{1}{2}A^2T_s$, respectively.

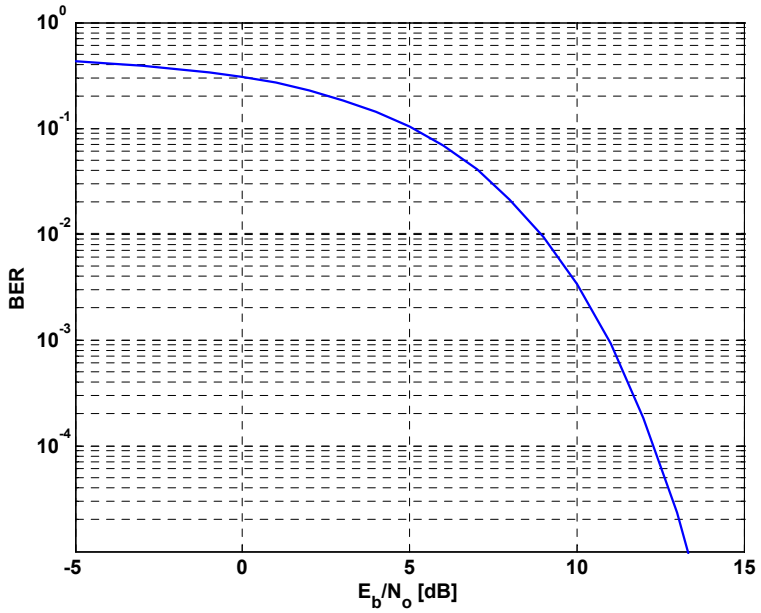

Figure 8-2: *Probability of bit error for non-coherent FSK with AWGN*

8.2. FSK with a Single UWB Pulse and high SNR

We will assume the same binary FSK detector as is shown in Figure 8-1. The input in this case will be a desired tone and a single UWB impulse that is randomly placed within

the bit period T_s, this assumption implies that the UWB system operates with a pulse repetition rate that is approximately equal to the FSK data rate. We will assume that the received signal plus interferer are much greater than any noise introduced in the receive chain. The input signal is then

$$s_1(t) = \sqrt{\frac{2E_b}{T_s}}\cos(\omega_1 t) + \nu(t), \tag{8-10}$$

where, in this case

$$\nu(t) = \sqrt{\frac{P_u}{2B_u R_u}}\delta(t-\varepsilon), \tag{8-11}$$

B_u is the noise equivalent rectangular bandwidth of the UWB signal, R_u is the UWB pulse repetition rate, and ε is the random pulse position of the UWB pulse within one signal bit period, which is uniformly distributed over the interval $[0, T_s]$.

We will assume the FSK discrimination filters are matched to the desired signal pulses, giving the impulse response for both filters as

$$h_i(t) = \frac{2}{T_s}\cos[\omega_i(T_s - t)], \quad 0 \le t \le T, \quad i = 1,2. \tag{8-12}$$

The output of filter one, with the input signal as defined above, can now be expressed as

$$v_1(t) = \sqrt{\frac{2E_b}{T_s}}\cos(\omega_1 t) \otimes \frac{2}{T_s}\cos[\omega_1(T_s - t)] + \sqrt{\frac{P_u}{2B_u R_u}}\delta(t-\varepsilon) \otimes \frac{2}{T_s}\cos[\omega_1(T_s - t)]. \tag{8-13}$$

The output of filter 2 (the second branch) is

$$v_2(t) = \sqrt{\frac{P_u}{2B_u R_u}}\delta(t-\varepsilon) \otimes \frac{2}{T_s}\cos[\omega_2(T_s - t)]. \tag{8-14}$$

where $\otimes$ represents convolution. After performing the convolution in Eq. 8-13, the signal in the upper (first) branch can be written in terms of inphase and quadrature components as

$$\begin{aligned} v_1(t) &= \left[\sqrt{\frac{2E_b}{T_s}}\cos\omega_1 T_s + \sqrt{\frac{P_u}{2B_u R_u}}\frac{2}{T_s}\cos\omega_1(T_s+\varepsilon)\right]\cos\omega_1 t \\ &+ \left[\sqrt{\frac{2E_b}{T_s}}\sin\omega_1 T_s + \sqrt{\frac{P_u}{2B_u R_u}}\frac{2}{T_s}\sin\omega_1(T_s+\varepsilon)\right]\sin\omega_1 t\ , \\ &= A\cos\omega_1 t + B\sin\omega_1 t \end{aligned} \tag{8-15}$$

where

$$\begin{aligned} A &= \left[\sqrt{\frac{2E_b}{T_s}}\cos\omega_1 T_s + \sqrt{\frac{P_u}{2B_u R_u}}\frac{2}{T_s}\cos\omega_1(T_s+\varepsilon)\right] \text{ and} \\ B &= \left[\sqrt{\frac{2E_b}{T_s}}\sin\omega_1 T_s + \sqrt{\frac{P_u}{2B_u R_u}}\frac{2}{T_s}\sin\omega_1(T_s+\varepsilon)\right] \end{aligned} \tag{8-16}$$

In the second branch, we have

$$v_2(t) = \sqrt{\frac{P_u}{2B_u R_u}}\frac{2}{T_s}\cos\omega_1(T_s - t + \varepsilon). \tag{8-17}$$

In order to analyze the behavior of this non-coherent FSK system based on envelope detection, we need to express each signal branch in terms of its envelope and phase. The expression for v_1 can be expressed as baseband envelope and phase:

$$v_1(t) = \sqrt{A^2 + B^2}\cos(\omega_1 t - \theta), \tag{8-18}$$

with $\theta = \tan^{-1}\frac{B}{A}$. The signal after the envelope detector is now written as:

$$\gamma_1 = A^2 + B^2 = \frac{2E_b}{T_s} + \frac{P_u}{B_u R_u}\frac{2}{T_s^2} + \frac{4}{T_s}\sqrt{\frac{E_b P_u}{T_s B_u R_u}}\cos\omega_1\varepsilon\ . \tag{8-19}$$

The signal passed through the lower (second) filter is just that of the UWB pulse; the envelope of this signal is constant and can be written as:

$$\gamma_2 = \frac{P_u}{B_u R_u}\frac{2}{T_s^2}. \tag{8-20}$$

We can now normalize by dividing both envelopes by the constant value of the second branch envelope, i.e.,

$$\hat{\gamma}_1 = \frac{\gamma_1}{\gamma_2} = \frac{E_b T_s}{2}\frac{B_u R_u}{P_u} + 1 + \sqrt{2\frac{E_b T_s}{2}\frac{2B_u R_u}{P_u}}\cos\omega_1\varepsilon, \text{ and } \hat{\gamma}_2 = 1 \tag{8-21}$$

To define the signal to interference ratio, we find the average signal power, and average envelope interference power from the UWB pulses. The average signal power is defined as:

$$P_{sig} = \frac{1}{T_s}\int \frac{2E_b}{T_s}\cos^2\omega_1(t - T_s)dt = \frac{E_b}{T_s} \tag{8-22}$$

If the one-sided UWB pulse bandwidth is B_u, then the energy per pulse is $2B_u|P(f_0)|^2$ and the total power in the UWB signal is

$$P_u = 2B_u|P(f_0)|^2 \cdot R_u, \tag{8-23}$$

so

$$|P(f_0)| = \sqrt{\frac{P_u}{2B_u R_u}}. \tag{8-24}$$

The interference power out of the matched filter due to one pulse is now:

$$P_{\text{int}} = 2|P(f_0)|^2\frac{R_u}{T_s} = P_u\frac{1}{T_s B_u} \tag{8-25}$$

The signal-to-total-interference ratio is then:

$$SIR = E_b\frac{B_u}{P_u}. \tag{8-26}$$

If we want to examine the average power for only one pulse in a train of pulse, we can write the power for that one pulse as

$$P_{\text{int}1} = P_{\text{int}}\frac{R_s}{R_u} \tag{8-27}$$

This gives the SIR for the desired signal to one UWB pulse as

$$SIR_1 = N_u SIR, \tag{8-28}$$

where $N_u = R_u/R_s$. In this case, $N_u = 1$ and $SIR_1 = SIR$. We will use the SIR definition with multiple pulses in Section 8.4, where we discuss multiple interfering pulses.

Using these definitions, the normalized envelopes in each branch can be written in terms of signal-to-interference ratio (total interference, or single pulse interference), i.e.,

$$\begin{aligned}\hat{\gamma}_1 &= SIR + 1 + 2\sqrt{SIR}\cos\omega_1\varepsilon \\ \hat{\gamma}_2 &= 1\end{aligned} \tag{8-29}$$

or, equivalently

$$\begin{aligned}\hat{\gamma}_1 &= 1 + \frac{1}{SIR} + 2\sqrt{\frac{1}{SIR}}\cos\omega_1\varepsilon \\ \hat{\gamma}_2 &= \frac{1}{SIR}\end{aligned} \tag{8-30}$$

Using the envelope definitions in Eq. 8-29 or 8-30, we can rewrite Eq. 8-29 as

$$\hat{\gamma}_1 = k_1 + k_2\cos\phi\,, \tag{8-31}$$

where ϕ is uniformly distributed over [0,2π].

The distribution of the squared envelope received $\hat{\gamma}_1$ given that signal s_1 is sent can easily be shown to be [2]

$$p\left(\hat{\gamma}_1|s_1\right) = \begin{cases} \dfrac{1}{\pi\sqrt{k_2^2 - \left(\hat{\gamma}_1 - k_1\right)^2}} & , \quad k_1 - k_2 < \hat{\gamma}_1 < k_1 + k_2 \\ 0 & , \quad \textit{elsewhere} \end{cases} \tag{8-32}$$

The squared envelope of the second branch is simply constant and equal to 1, i.e., $\hat{\gamma}_2 = 1$. This leads to the mean probability of error, averaged over the random pulse position within one FSK bit period, being expressed as:

$$P_e = \Pr\left\{k_1 + k_2\cos\phi < 1\right\} = \int_0^1 p\left(\hat{\gamma}_1|s_1\right)d\hat{\gamma}_1 = \frac{1}{\pi}\int_{\min(0,k_1-k_2)}^{\max(1,k_1+k_2)} \frac{d\hat{\gamma}_1}{\sqrt{k_2^2 - \left(\hat{\gamma}_1 - k_1\right)^2}} \tag{8-33}$$

or,

$$P_e = \begin{cases} \dfrac{1}{\pi}\left\{\sin^{-1}\left(\dfrac{\max\left(1, k_1 + k_2\right) - k_1}{k_2}\right) - \sin^{-1}\left(\dfrac{\min\left(0, k_1 - k_2\right) - k_1}{k_2}\right)\right\} & , \quad k_1 - k_2 \le 1 \\ 0 & , \quad \textit{elsewhere} \end{cases} \tag{8-34}$$

The constants k_1 and k_2 are defined as

$$k_1 = 1 + SIR$$
$$k_2 = 2\sqrt{SIR} \tag{8-35}$$

The probability of error is then 0 if $SIR \geq 4$, or $SIR_{dB} \geq 6$ dB. The probability of error for other values of *SIR* is shown in Figure 8-3.

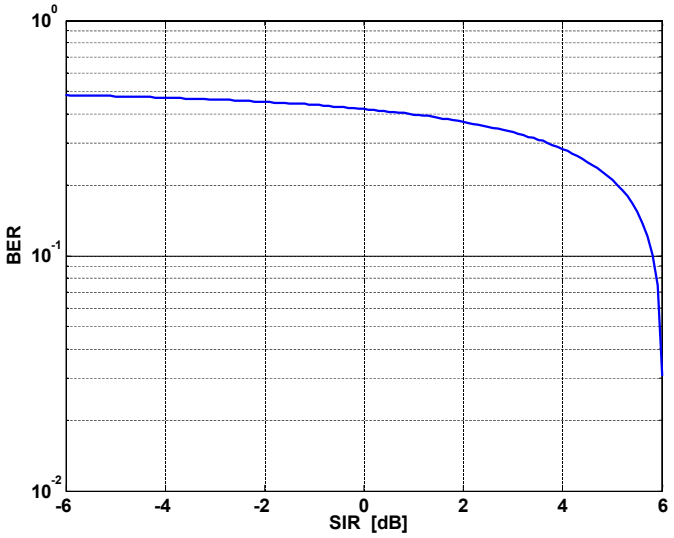

Figure 8-3: BER versus SIR for the case of high E_b/N_o.

The BER curve shown in Figure 8-3 has a very steep dropoff as we approach the 6 dB mark, which means there is still a fairly high BER for SIR just a couple of dB below the 6 dB (zero BER) point, e.g., for SIR = 4 dB, the BER is a very high 0.3. This leads to a capture-type effect around the SIR of 6 dB, that is, when the SIR is below 6 dB, the BER is high, but as soon as the SIR exceeds 6 dB, the BER drops to zero.

8.3. FSK with Single UWB Pulse per Bit Period and AWGN (low SNR)

The following analysis will again assume a receiver structure as shown in Figure 8-1, but will assume a low SNR, which leads to Gaussian noise being added to each receiver branch. There are now two random processes involved in the detection process. The first is the random pulse position within the FSK bit period, and the second is the noise process (actually two independent noise processes, one in each FSK branch). In the following, we will analyze the probability of bit error averaged over the noise processes with the pulse position fixed, and will then numerically average over many realizations of pulse positions using Monte Carlo techniques.

As was done in section 8.2, we can express the signals in both branches in terms of inphase and quadrature components, but we will now add a Gaussian noise term to each receive branch.

The signal in branch 1 after matched filtering, but just before the envelope detector can be expressed as

$$v_1 = (A + n_I)\cos\omega_1 t + (B + n_Q)\sin\omega_1 t\,, \tag{8-36}$$

where A and B are defined in Eq. 8-16, but are shown here again for convenience.

$$A = \left[\sqrt{\frac{2E_b}{T_s}}\cos\omega_1 T_s + \sqrt{\frac{P_u}{2B_u R_u}}\frac{2}{T_s}\cos\omega_1(T_s+\varepsilon)\right] \text{ and}$$
$$B = \left[\sqrt{\frac{2E_b}{T_s}}\sin\omega_1 T_s + \sqrt{\frac{P_u}{2B_u R_u}}\frac{2}{T_s}\sin\omega_1(T_s+\varepsilon)\right] \tag{8-37}$$

The inphase and quadrature noise components are assumed to be zero mean white Gaussian noise processes, each with standard deviation σ_0^2.

In branch 2, the signal at the same point is expressed as

$$v_2 = \left(\sqrt{\frac{P_u}{2B_u R_u}}\frac{2}{T_s}\cos 2\pi f_2[T_s+\varepsilon] + n_I\right)\cos\omega_2 t + \left(\sqrt{\frac{P_u}{2B_u R_u}}\frac{2}{T_s}\sin\omega_2[T+\varepsilon] + n_Q\right)\sin\omega_2 t \tag{8-38}$$

The envelopes are then:

$$\gamma_1 = (A+n_I)^2 + (B+n_Q)^2 \text{ and}$$
$$\gamma_2 = \left(\sqrt{\frac{P_u}{2B_u R_u}}\frac{2}{T_s}\cos\omega_2[T+\varepsilon] + n_I\right)^2 + \left(\sqrt{\frac{P_u}{2B_u R_u}}\frac{2}{T_s}\sin\omega_2[T+\varepsilon] + n_Q\right)^2 \tag{8-39}$$

This leads to the PDFs of the two envelopes being Ricean random variables [1], i.e.,

$$p(\gamma_1|s_1) = \frac{\gamma_1}{\sigma_0^2}\exp\left[-\frac{(A^2+B^2)+\gamma_1^2}{2\sigma_0^2}\right]I_0\left(\frac{\gamma_1\sqrt{A^2+B^2}}{\sigma_0^2}\right), \tag{8-40}$$

$$p(\gamma_2|s_1) = \frac{\gamma_2}{\sigma_0^2}\exp\left[-\frac{C^2+\gamma_2^2}{2\sigma_0^2}\right]I_0\left(\frac{\gamma_2 C}{\sigma_0^2}\right). \tag{8-41}$$

Where we have introduced a single parameter to represent the UWB interference power in the second branch:

$$C^2 = \frac{P_u}{B_u R_u}\frac{2}{T_s^2} \tag{8-42}$$

The probability of error for a given UWB pulse position ε is then

$$\begin{aligned} P_e(\varepsilon) &= \Pr\{\gamma_2 > \gamma_1 | s_1; \varepsilon\} = \int_0^\infty p(\gamma_1|s_1) \int_{\gamma_1}^\infty p(\gamma_2|s_1) d\gamma_2 d\gamma_1 \\ &= \int_0^\infty p(\gamma_2|s_1) \int_0^{\gamma_2} p(\gamma_1|s_1) d\gamma_1 d\gamma_2 \end{aligned} \tag{8-43}$$

This probability of error is the probability that one Rice variate exceeds another, and was first functionally expressed and tabulated by Marcum [3] by introducing what is now called the Marcum Q function. Its definition is:

$$Q(a,b) = \int_b^\infty x \exp\left(-\frac{a^2+x^2}{2}\right) I_0(ax) dx \tag{8-44}$$

Using the fact that the Gaussian random variables introduced in Eq. 8-36 have two sided power spectral density of $N_0/2$, we can write $\sigma_0^2 = N_0/T_s$. The terms in the exponentials of Eqs. 8-40 and 8-41 representing the desired signal and interferer envelopes can now be written as:

$$b(\varepsilon) = \frac{A^2+B^2}{2\sigma_0^2} = \frac{E_b}{N_0}\left(1 + \frac{1}{SIR} + 2\sqrt{\frac{1}{SIR}}\cos\omega_1\varepsilon\right) \tag{8-45}$$

and

$$a(\varepsilon) = \frac{C^2}{2\sigma_0^2} = \frac{E_b}{N_0}\left(\frac{1}{SIR}\right) \tag{8-46}$$

Using these definitions and the definition of the Marcum Q function, the probability of error is

$$P_e(\varepsilon) = Q\left(\sqrt{a(\varepsilon)}, \sqrt{b(\varepsilon)}\right) - \frac{1}{2}\exp\left(-\frac{a(\varepsilon)+b(\varepsilon)}{2}\right) I_0\left(\sqrt{a(\varepsilon)b(\varepsilon)}\right) \tag{8-47}$$

Note that this is the probability of error for one pulse position ε only. The mean probability of error is then found by averaging over all pulse positions ε, where $\omega_1\varepsilon$ is uniformly distributed over the interval $[0,2\pi]$.

Probability of error versus E_b/N_o for various SIRs is shown in Figure 8-4. It can be seen that for high SIR, the case analyzed above degenerates to the standard FSK with AWGN case derived in Section 8.1. As SIR decreases, the required E_b/N_o to maintain the same

BER performance increases. For instance, at a BER of 10^{-2}, the required E_b/N_o, with no interference is approximately 8 dB, but with an SIR of 10 dB, the required E_b/N_o is now approximately 13 dB; this is a degradation of 5 dB in required E_b/N_o.

Probability of error versus SIR for various fixed E_b/N_o values is shown in Figure 8-5. It can be seen that for a given E_b/N_o, the BER asymptotically approaches the value taken from Figure 8-4 at that E_b/N_o level as SIR becomes very large. This represents an error floor for which better performance cannot be achieved no matter how high the SIR.

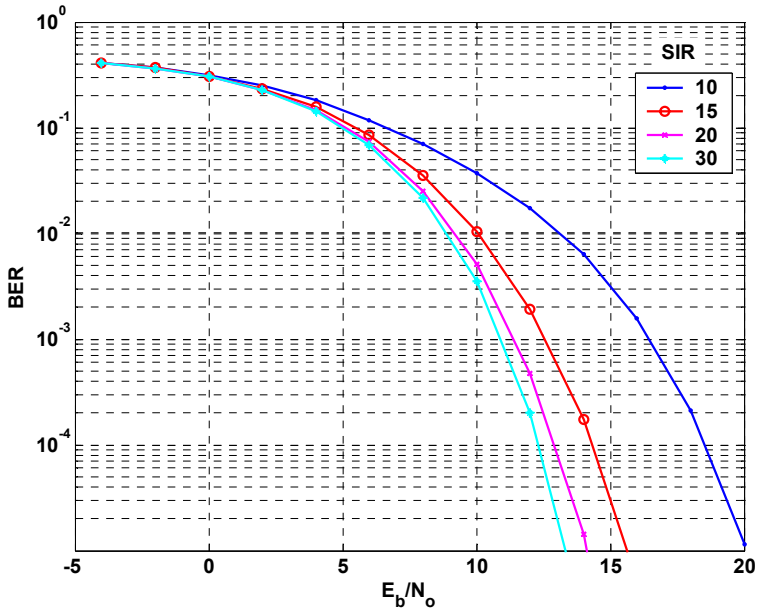

Figure 8-4: *BER versus Eb/No for various SIRs.*

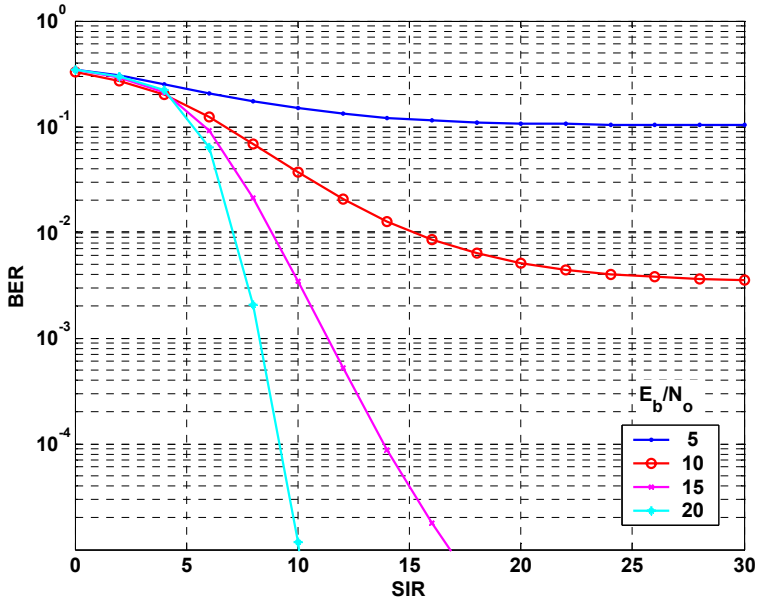

Figure 8-5: *BER versus SIR for various Eb/No values.*

8.4. FSK with Multiple UWB Pulses per Bit Period and AWGN

Proceeding as in Section 8.3, we can write the signal seen after the matched filter in the upper (first) branch of the FSK receiver as a sum of a desired signal, a train of interfering signals, and noise terms. The UWB signal is now a train of impulses that are seen within one bit period T_s. This received signal can be written in the same way as was done in Eq. 8-36, i.e., in terms of inphase and quadrature components.

$$v_1 = (A + n_I)\cos\omega_1 t + (B + n_Q)\sin\omega_1 t \tag{8-48}$$

Now, however, the amplitude terms contain contributions from multiple UWB pulses that are received within on bit period.

$$s_u(t) = \sqrt{\frac{P_u}{2B_u R_u}} \sum_k a_k \delta(t - \varepsilon_k) \tag{8-49}$$

After matched filtering, the UWB time envelope is restricted to a width of T_s seconds, but arrives with a random delay.

$$A = \left[\sqrt{\frac{2E_b}{T_s}} \cos\omega_1 T_s + \frac{2}{T_s} \sqrt{\frac{P_u}{2B_u R_u}} \sum_{k=1}^{N_u} a_k \cos\omega_1 \varepsilon_k \right] \tag{8-50}$$

$$B = \left[\sqrt{\frac{2E_b}{T_s}} \cos\omega_1 T_s + \frac{2}{T_s} \sqrt{\frac{P_u}{2B_u R_u}} \sum_{k=1}^{N_u} a_k \sin\omega_1 \varepsilon_k \right] \tag{8-51}$$

The sums of UWB interference contributions are over N_u pulses, where N_u is the ratio of UWB pulse repetition rate to FSK bit rate, i.e.,

$$N_u = R_u / R_s = T_s / T_u \,, \tag{8-52}$$

or the number of UWB pulses within one FSK bit period.

After some algebraic manipulations, we can arrive at the desired signal plus interference envelope term:

$$A^2 + B^2 = \frac{2E_b}{T_s} + \frac{4}{T_s} \sqrt{\frac{E_b P_u}{2T_s B_u R_u}} \sum_{k=1}^{N_u} a_k \cos\omega_1 \varepsilon_k + \frac{1}{T_s^2} \frac{P_u}{B_u R_u} \sum_{j=1}^{N_u} \sum_{k=1}^{N_u} a_j a_k \cos\omega_1 (\varepsilon_j - \varepsilon_k) \tag{8-53}$$

The envelope term due to only the interference in the second (lower) branch of the detector is, c.f., Eq. 8-42:

$$C^2 = \frac{P_u}{B_u R_u}\frac{2}{T_s^2}\sum_{j=1}^{N_u}\sum_{k=1}^{N_u} a_j a_k \cos\omega_1\left(\varepsilon_j - \varepsilon_k\right) \tag{8-54}$$

Again, as in the previous section, the envelopes in the first and second branches of the detector are Ricean variates, i.e., the distributions of these envelopes for fixed values of ε_k are

$$p\left(\gamma_1 | s_1\right) = \frac{\gamma_1}{\sigma_0^2}\exp\left[-\frac{\left(A^2+B^2\right)+\gamma_1^2}{2\sigma_0^2}\right] I_0\left(\frac{\gamma_1\sqrt{A^2+B^2}}{\sigma_0^2}\right), \tag{8-55}$$

$$p\left(\gamma_2 | s_1\right) = \frac{\gamma_2}{\sigma_0^2}\exp\left[-\frac{C^2+\gamma_2^2}{2\sigma_0^2}\right] I_0\left(\frac{\gamma_2 C}{\sigma_0^2}\right). \tag{8-56}$$

The parameters describing the signal plus interference envelopes in the exponentials can be written in terms of E_b/N_o and SIR in order to parameterize results. We can use the same SIR definition as in Eq. 8-28. These terms are now

$$b\left(\varepsilon_1,...,\varepsilon_{N_o}\right) = \frac{A^2+B^2}{2\sigma_0^2} = \frac{E_b}{N_o}\left(1 + \frac{1}{N_u SIR}\sum_{j=1}^{N_u}\sum_{k=1}^{N_u} a_j a_k \cos\omega_1\left(\varepsilon_j - \varepsilon_k\right) + 2\sqrt{\frac{1}{N_u SIR}}\sum_{k=1}^{N_u} a_k \cos\omega_1\varepsilon_k\right) \tag{8-57}$$

$$a\left(\varepsilon_1,...,\varepsilon_{N_o}\right) = \frac{C^2}{2\sigma_o^2} = \frac{E_b}{N_o}\left(\frac{1}{N_u SIR}\sum_{j=1}^{N_u}\sum_{k=1}^{N_u} a_j a_k \cos\omega_1\left(\varepsilon_j - \varepsilon_k\right)\right) \tag{8-58}$$

The probability of error can now be expressed in terms of these envelopes, which are functions of the random pulse positions of each of the UWB pulses ε_k, where $\omega_1\varepsilon_k$ are distributed uniformly over the interval $[0,2\pi]$. The expression for the probability of error again makes use of the Marcum Q-function and modified Bessel function, i.e.,

$$P_e\left(\varepsilon_1,...,\varepsilon_k\right) = Q\left(\sqrt{a},\sqrt{b}\right) - \frac{1}{2}\exp\left(-\frac{a+b}{2}\right) I_0\left(\sqrt{ab}\right), \tag{8-59}$$

where the dependence on $\varepsilon_1,...,\varepsilon_k$ has been suppressed for simplicity. The average probability of error can again be found by averaging over εs.

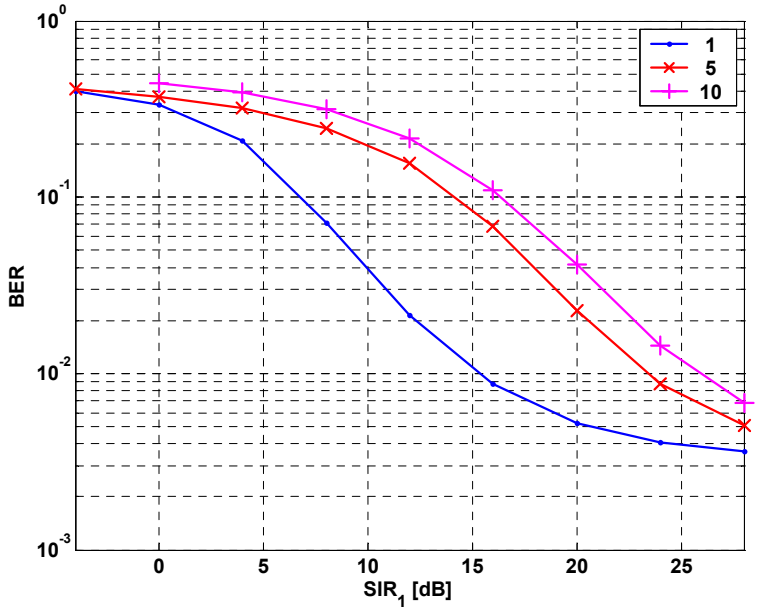

Figure 8-6: *BER versus SIR_1 with varying number of interfering pulses N_u with Eb/No=10 dB.*

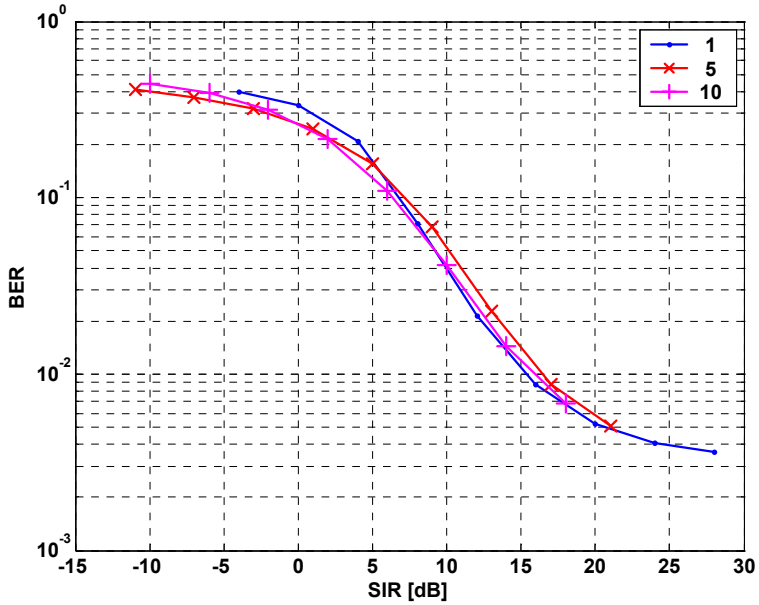

Figure 8-7: *BER versus SIR with varying number of interfering pulses N_u with Eb/No=10 dB*

Figure 8-6 shows the performance of the FSK detector in the presence of multiple UWB pulses per bit period with a fixed E_b/N_o of 10 dB. It can be seen that all curves asymptotically approach each other for very low and very high values of SIR. At the high SIR end, they all asymptotically approach the case with no interference for E_b/N_o of 10 dB, i.e., BER = $3x10^{-3}$. For the low SIR case, they all naturally approach a BER of

0.5. However, if we examine a fixed BER case, we can see that if more pulses are included in one bit period, we need a higher SIR to achieve that BER. This occurs because the abscissa represents SIR on a per pulse basis, and as we add more pulse, we are adding more interference. If we examine the BER at an SIR of 10 dB with a single pulse, N_u=1, we obtain a value of BER = $4\text{x}10^{-2}$. If we then look at the curve for N_u=10 at an SIR of 20 dB (this represents 10 interfering pulses) we find that the BER is approximately the same, i.e., BER = $4\text{x}10^{-2}$, or the same as that for the curve with SIR = 10 dB. This is because the total interference power is actually 10 dB higher, or will have a signal-to-total-interference power ratio of 10 dB instead of 20 dB on a per pulse basis. We are, therefore, able to use the curves from figures 8-4 and 8-5 with a derating for the number of pulses in one bit period, N_u, or the ratio of UWB pulse repetition rate to FSK bit rate. To explicitly show the relationship described above, a plot of BER versus the total interference power for all pulses is shown in Figure 8-7.

All of the curves significantly overlap in the high SIR region, but slightly diverge when SIR is lower. This is due to the fact that the variations in interference contribution to the envelope contribute more strongly when SIR is low, i.e., total interference power is higher. The interference terms are the sums of cosines of uniformly distributed random variables. As SIR decreases, the differences due to these random variations are more evident. We also notice that these variations lead to lower BER for increasing number of pulses. This is because the multiple pulses do not always add coherently (in-phase) and thus can reduce the interference contribution compared to a single pulse.

8.5. FSK with CW Interference and AWGN

We now turn to examination of the case of a non-coherent FSK system with a single tone CW interferer present along with additive white Gaussian noise. The single tone CW interferer is meant to be representative of a spectral line present in the output of a UWB interferer. The CW interferer will be assumed present at a frequency slightly offset from one of the FSK tones, and will have an average power P_{CW}. We will also assume matched filtering in each branch, matched to that branch's desired pulse. Thus, we can write an expression for the signal received after matched filtering in the first FSK branch, but before envelope detection as:

$$v_1(t) = \sqrt{\frac{2E_b}{T_s}}\cos\omega_1 t \otimes \frac{2}{T_s}\cos\omega_1(T_s - t) + \sqrt{2P_u}\cos(\omega_1 + \Delta\omega)t \otimes \frac{2}{T_s}\cos\omega_1(T_s - t) \quad (8\text{-}60)$$

where $\otimes$ means convolution. In the second (lower) branch of the FSK detector, assuming signal 1 was sent, after the matched filter, but before the envelope detector, we have

$$v_2(t) = \sqrt{2P_{CW}}\cos(\omega_1 + \Delta\omega)t \otimes \frac{2}{T_s}\cos\omega_2(T_s - t) \quad (8\text{-}61)$$

Performing the convolution in 8-60, and making the assumption that $\omega_1 >> 1$, we arrive at an expression for the signal in the first FSK branch in terms of inphase and quadrature components with additive white Gaussian noise present,

$$\begin{aligned} v_1(t) &= \left[\sqrt{\frac{2E_b}{T_s}} \cos \omega_1 T_s + \frac{\sqrt{2P_{CW}}}{\Delta\omega T_s} \left\{ \sin(\Delta\omega - \omega_1)T_s + \sin \omega_1 T_s \right\} + n_I \right] \cos \omega_1 t \\ &+ \left[\sqrt{\frac{2E_b}{T_s}} \sin \omega_1 T_s + \frac{\sqrt{2P_{CW}}}{\Delta\omega T_s} \left\{ \cos(\Delta\omega - \omega_1)T_s - \cos \omega_1 T_s \right\} + n_Q \right] \sin \omega_1 t \\ &= (A + n_I)\cos \omega_1 t + (B + n_Q)\sin \omega_1 t \end{aligned} \tag{8-62}$$

The envelope for this branch can then be written in a format similar to the format of the envelopes from the previous sections, i.e.,

$$\gamma_1 = (A + n_I)^2 + (B + n_Q)^2 \tag{8-63}$$

This envelope is a Ricean variate as discussed previously and has probability density of

$$p(\gamma_1 | s_1) = \frac{\gamma_1}{\sigma_0^2} \exp\left[-\frac{(A^2 + B^2) + \gamma_1^2}{2\sigma_0^2} \right] I_0\left(\frac{\gamma_1 \sqrt{A^2 + B^2}}{\sigma_0^2} \right). \tag{8-64}$$

The waveform present after the second branch matched filter can be written as,

$$v_2(t) = \frac{\sqrt{2P_{CW}}}{T_s\left(\frac{2\pi}{T_s} + \Delta\omega \right)} \sin\left[2\pi + \Delta\omega T_s + \omega_2 (t - T_s) \right]. \tag{8-65}$$

We can write the envelope in the second branch as

$$\begin{aligned} \gamma_2 &= \left(\frac{\sqrt{2P_{CW}}}{(2\pi + \Delta\omega T_s)} \left[\sin(\Delta\omega - \omega_2)T_s + \sin \omega_2 T_s \right] + n_I \right)^2 \\ &+ \left(\frac{\sqrt{2P_{CW}}}{(2\pi + \Delta\omega T_s)} \left[\cos(\Delta\omega - \omega_2)T_s - \cos \omega_2 T_s \right] + n_Q \right)^2 \end{aligned} \tag{8-66}$$

The probability density function of this random variable is also Ricean, and is expressed as

$$p(\gamma_2 | s_1) = \frac{\gamma_2}{\sigma_0^2} \exp\left[-\frac{C^2 + \gamma_2^2}{2\sigma_0^2} \right] I_0\left(\frac{\gamma_2 C}{\sigma_0^2} \right), \tag{8-67}$$

where

$$C^2 = \frac{2P_u}{\left(2\pi + \Delta\omega T_s\right)^2} \sin^2\left(\frac{2\pi + \Delta\omega T_s}{2}\right) \tag{8-68}$$

The parameters describing the signal plus interference in the envelopes of these Ricean random variables can be expressed in terms of signal-to-interference ratio and E_b/N_o as was previously done. Now, though the signal-to-interference ratio is

$$SIR = \frac{P_s}{P_{CW}} \tag{8-69}$$

This allows parameterization of the performance curves to be easily performed. We thus express these parameters in the Ricean distributions in terms of a deterministic frequency offset parameter, $\Delta\omega$,

$$b_1 = \frac{A^2 + B^2}{2\sigma_0^2} = \frac{E_b}{N_o}\left(1 + \frac{4}{SIR}\operatorname{sinc}^2\frac{\Delta\omega T_s}{2} + 2\sqrt{\frac{1}{SIR}}\operatorname{sinc}\Delta\omega T_s\right) \tag{8-70}$$

and

$$a_1 = \frac{C^2}{2\sigma_0^2} = \frac{E_b}{N_o}\left(\frac{4}{SIR}\operatorname{sinc}^2\frac{2\pi + \Delta\omega T_s}{2}\right) \tag{8-71}$$

The appearance of the sinc function is a result of the fact that we are using a filter matched to a CW signal with a rectangular time envelope of extent T_s.

As was done in the previous section, we can express the probability of an error when sending signal 1 when a CW interferer and additive white Gaussian noise are present as:

$$P_e\left(SIR, \Delta\omega T_s \middle| s_1\right) = Q\left(\sqrt{a_1}, \sqrt{b_1}\right) - \frac{1}{2}\exp\left(-\frac{a_1 + b_1}{2}\right) I_0\left(\sqrt{a_1 b_1}\right) \tag{8-72}$$

To find the total error, we need to also examine the case where s_2 was sent. In order to analyze this case, however, we need to know something about the spacing between the two FSK signaling frequencies. We will make the standard assumption that $f_1 - f_2 = \frac{1}{T_s}$. Making this assumptions, we can write the waveform present in the second branch given that the FSK signal with carrier f_2 has been sent and we have performed filtering matched on that waveform, i.e.,

$$v_2(t) = \sqrt{\frac{2E_b}{T_s}}\cos\omega_2 t \otimes \frac{2}{T_s}\cos\omega_2(T_s - t) + \sqrt{2P_u}\cos(\omega_1 + \Delta\omega)t \otimes \frac{2}{T_s}\cos\omega_2(T_s - t) \quad (8\text{-}73)$$

The signal in the first branch after matched filtering is now,

$$v_1(t) = \sqrt{2P_u}\cos(\omega_1 + \Delta\omega)t \otimes \frac{2}{T_s}\cos\omega_1(T_s - t). \quad (8\text{-}74)$$

After performing some algebraic manipulation and using the fact that $\omega_1 - \omega_2 = \frac{2\pi}{T_s}$, we arrive at the result that the probability of error is now.

$$P_e(SIR, \Delta\omega T_s | s_2) = Q\left(\sqrt{a_2}, \sqrt{b_2}\right) - \frac{1}{2}\exp\left(-\frac{a_2 + b_2}{2}\right) I_0\left(\sqrt{a_2 b_2}\right) \quad (8\text{-}75)$$

with

$$b_2 = \frac{A^2 + B^2}{2\sigma_0^2} = \frac{E_b}{N_o}\left(1 + \frac{4}{SIR}\text{sinc}^2\frac{2\pi + \Delta\omega T_s}{2} + 2\sqrt{\frac{1}{SIR}}\text{sinc}(2\pi + \Delta\omega T_s)\right) \quad (8\text{-}76)$$

and

$$a_2 = \frac{C^2}{2\sigma_0^2} = \frac{E_b}{N_o}\left(\frac{4}{SIR}\text{sinc}^2\frac{\Delta\omega T_s}{2}\right). \quad (8\text{-}77)$$

The average error is now:

$$P_e(SIR, \Delta\omega T_s) = \frac{1}{2}P_e(SIR, \Delta\omega T_s | s_1) + \frac{1}{2}P_e(SIR, \Delta\omega T_s | s_2). \quad (8\text{-}78)$$

Probability of error is shown in Figure 8-9 for different values of $\Delta\omega T_s$ with SIR varying and E_b/N_o = 20 dB. For $\Delta\omega T_s$ between 0 and +1, the interfering tone is between the two FSK tones. For $\Delta\omega T_s$ negative, the tone is to the left of (lower in frequency) the first FSK tone ω_1. It can be seen that for a fixed SIR, the probability of error decreases as the tone is placed further to the left of this first FSK tone. This is shown graphically in Figure 8-8.

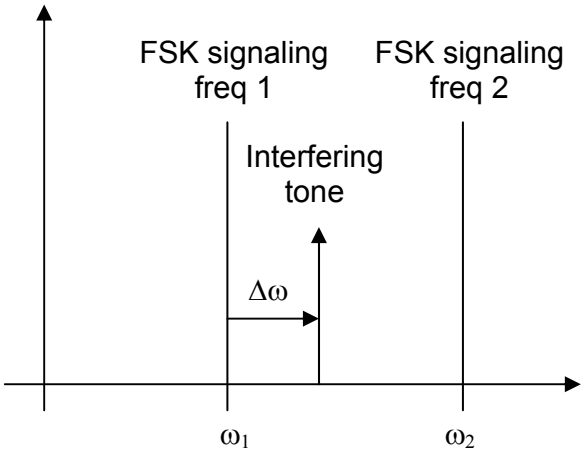

Figure 8-8: *Placement of interfering CW tone with respect to the two FSK signaling frequencies.*

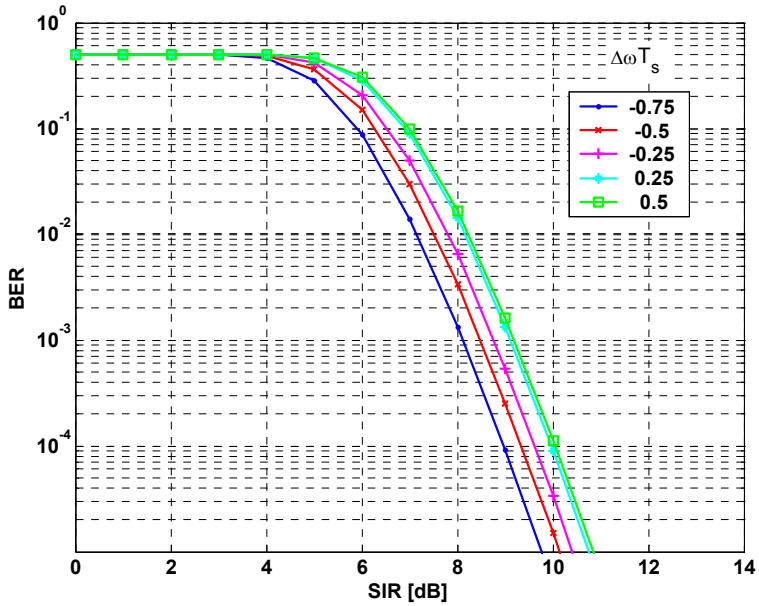

Figure 8-9: *BER versus SIR for various values of interferer position* $\Delta\omega T_s$.

The results of Figure 8-9 show that if the interfering tone is placed between the two FSK tones, the BER versus SIR curves are essentially the same (the case for $\Delta\omega T_s = 0.25$ falls on top of 0.5), whereas the effect of the interferer is reduced as the tone is moved further to the left of the first FSK tone.

Conclusions for Non-coherent FSK

We have examined a non-coherent FSK receiver with matched filtering and envelope detection for the cases of a single and multiple interfering UWB pulses per FSK bit period with both high and low SNR, and have seen that there is a marked degradation in BER performance as SIR is reduced. Specifically, in the high SNR case with a single interfering UWB pulse, we observed a capture-type effect that shows BER quickly

increasing from zero as we move from SIR greater than 6 dB to SIR less than 6 dB. As the interfering pulse increases in power, regardless of pulse position, the duration of the interfering signal will be the length of the FSK bit period, since it is passing through the matched filter. This means at the FSK sampling instant, will always see the full envelope value of the UWB interfering pulse along with the desired signal.

When noise is considered with a single UWB pulse per FSK bit period, we observe that for a fixed BER we need a much higher E_b/N_o to maintain the same performance as interference is added, as is seen in Figure 8-4. This stems from the fact that the interference added to the system, even from a single UWB pulse, does not add equally to both branches of the FSK envelope detectors. The desired branch envelope contains an extra interference term that depends on the position in time of the UWB pulse that can destructively interfere with the desired signal, and thus contributes to increasing error. For the case of multiple pulses per FSK bit period, we obtain approximately the same results as shown for the single pulse case if we examine the BER versus total interference power. This is due to the fact that the envelopes of the multiple pulses have an additive contribution in each branch, but contribute an extra term to the desired branch that, again can destructively interfere with the desired signal. However, if the total interference power for the multiple pulse case is kept the same as it was in the single pulse case, the end error effects remain the same.

The case of a CW interferer represents the case where a spectral line generated by a UWB source falls within the IF bandwidth of the FSK detector. The results shown in Figure 8-9 show that the FSK detector is most affected when the CW tone falls between the two FSK signaling tones, and the effect diminishes as the interfering tone moves further away from the two signaling tones, as would be expected.

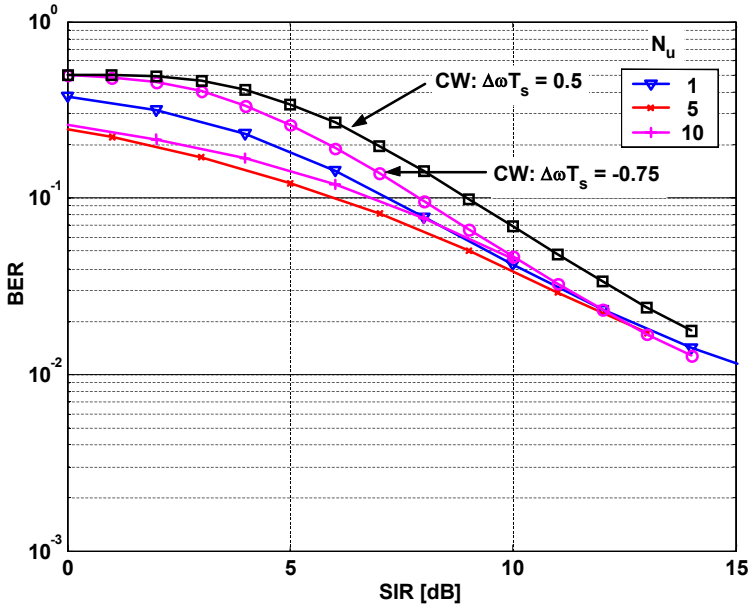

Figure 8-10: *BER versus SIR for various values of interferer position $\Delta\omega T_s$ compared with results for various number of pulses. E_b/N_o = 10 dB.*

Figure 8-10 provides a summary of results in Gaussian noise with $E_b/N_o = 10\ dB$ versus SIRs as defined in 8-26 and 8-69. The figure shows that for a given amount of interference power, i.e., a fixed SIR, the worst case BER is obtained when we have a CW interferer located between the "mark" and "space" frequencies. The best case seems to be the case where multiple pulses are present. This is due to the fact that the multiple pulses do not necessarily add in-phase to produce N_u times the power in a single pulse. Therefore, for a given amount of total interference power, we can actually obtain better BERs when we have multiple pulses present, than when we have a single pulse or a spectral line with the same power. This is due to the fact that the total interference power for multiple pulses was taken as a sum of powers from single pulses, and in the FSK receiver, the pulses add in voltage with random phases before envelope detection, thus leading to a smaller interference envelope than if all the pulses were added in power (coherently).

Chapter 8 References

[1] M. Schwartz, W.R. Bennett, and S. Stein, *Communication Systems and Techniques*. New York, NY. IEEE Press.

[2] A. Papoulis, *Probability, Random Variables, and Stochastic Processes*. New York, NY. McGraw-Hill, Inc., 1991.

[3] J.L. Marcum, "A Statistical Theory of Target Detection by Pulsed Radar," *IRE Trans. Inform. Theory*, vol. IT-6, pp. 59—267, April, 1960.

Chapter 9: UWB INTERFERENCE TO AN FM RECEIVER

9.1. Introduction

The purpose of this Chapter is to develop models for the effect of a UWB signal on an FM receiver. The block diagram of a basic FM receiver is shown in Figure 9-1. The output of the limiter/discriminator is proportional to the instantaneous frequency (relative to the carrier) of the input. The discriminator output is then passed through a filter with a bandwidth equal to that of the desired (modulating) signal. This baseband filter is sometimes termed the "video" filter.

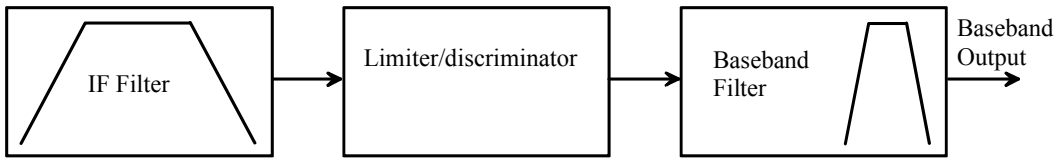

Figure 9-1: *Basic FM receiver model*

Because the FM receiver is nonlinear, FM signal-to-noise analysis tends to be complicated; however, there is a wealth of literature on the topic, the most relevant of which is well summarized in Schwartz, Bennett, and Stein [1], pp. 120-170. The discussion here will rely generally on that material, with references to specific results as appropriate.

At the transmitter, the baseband signal with cutoff frequency f_m modulates the carrier frequency. The unmodulated carrier has a frequency f_0 and the maximum frequency deviation is Δf. The modulation index is $\beta \equiv \Delta f / f_m$. For analysis purposes, a distinction is often made between "wideband FM" ($\beta >> 1$) and "narrowband FM" $\beta \approx 1$). By "Carson's rule" the occupied bandwidth for an FM signal is often approximated as $B_{IF} \cong 2(f_m + \Delta f) = 2(1+\beta) f_m$.

In the presence of additive Gaussian noise, FM exhibits a well-know threshold effect, whereby the baseband signal-to-noise ratio (SNR) drops rapidly as the RF carrier-to-noise ratio (CNR) falls below its threshold value. In the absence of threshold extension techniques using feedback demodulators or phase-locked loops, the threshold tends to be roughly 10 dB. Another property of FM is that above the threshold, the SNR increases rapidly with the modulation index:

$$SNR = 3\beta^2 \frac{B_{IF}/2}{f_m} \cdot CNR \tag{9-1}$$

Both of these effects are evident from Figure 9-2, which shows the SNR vs. the CNR for several different modulation indices. As can be seen, the threshold effect is much more pronounced with wideband FM than with narrowband FM. In fact, for $\beta = 1$, the threshold effect is barely noticeable.

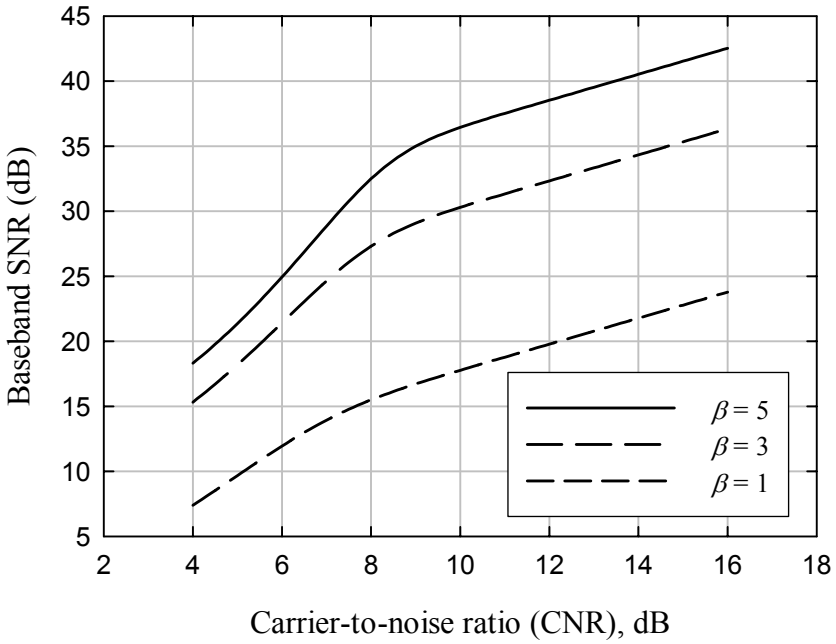

Figure 9-2: *Example baseband SNR vs. CNR for an FM receiver (no modulation).*

The curves in Figure 9-2 were computed using eq. 3-8-25a (p. 152) of [1]:

$$SNR = \frac{3\beta^2 \left(B_{IF}/2f_m\right) CNR}{1 + 4\sqrt{3}\, CNR \left(B_{IF}/2f_m\right)^2 \operatorname{erfc}\sqrt{CNR}} \tag{9-2}$$

which applies to the unmodulated case. With modulation, the SNR is somewhat less than shown for CNR below threshold (see Figure 3-8-7 of [1]).

9.2. Signal and Interference Model

The desired signal at the receiver can be written as

$$s(t) = A\cos\left[2\pi f_0 t + \phi(t)\right] \tag{9-3}$$

with $\phi(t) = k_m \int^t v(\tau) d\tau$ where $v(t)$ is the frequency-modulating signal and k_m is a modulation scaling constant. Since the interest here is the output signal-to-noise ratio, k_m can be taken as 1 without loss of generality.

The undesired signal (interference plus noise) can be represented in narrowband form as

$$n(t) = b(t)\cos[2\pi f_0 t + \theta(t)] \tag{9-4}$$

and the composite received signal is

$$r(t) = s(t) + n(t) = \mathrm{Re}\left\{e^{j2\pi f_0 t}\left[Ae^{j\phi(t)} + b(t)e^{j\theta(t)}\right]\right\} = \mathrm{Re}\left\{c(t)e^{j2\pi f_0 t}e^{j\gamma(t)}\right\} \tag{9-5}$$

where $c(t)e^{j2\pi\gamma(t)} = Ae^{j\phi(t)} + b(t)e^{j\theta(t)}$.

The baseband interference is $\frac{d}{dt}[\gamma(t) - \phi(t)]$, denoted here $\dot{\gamma} - \dot{\phi}$. The time dependence often will not be explicitly shown here where it is obvious from context.

From the simple phasor diagram in Figure 9-3, it is clear that:

$$\gamma - \phi = \tan^{-1}\left[\frac{b(t)\sin(\theta - \phi)}{A + b(t)\cos(\theta - \phi)}\right] \tag{9-6}$$

and

$$c = \sqrt{A^2 + b^2 + 2Ab\cos(\theta - \phi)} \tag{9-7}$$

The (ideal) discriminator output is proportional to $\frac{d\gamma}{dt}$, denoted $\dot{\gamma}$. Differentiating (9-6) gives

$$\dot{\gamma} = \dot{\phi} + \frac{A\dot{b}\sin(\theta - \phi) + (\dot{\theta} - \dot{\phi})b^2 + Ab(\dot{\theta} - \dot{\phi})\cos(\theta - \phi)}{c^2} \tag{9-8}$$

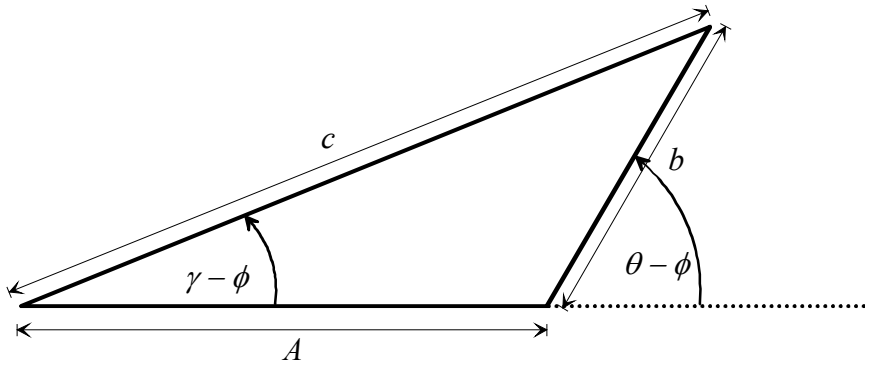

Figure 9-3: *Phasor diagram for FM interference analysis*

9.3. Receiver Response to a Single UWB Pulse

From Chapter 5, the IF filter output in response to a single UWB pulse that arrives at time T_k is

$$g_k(t) = 2|P(f_0)|\,|h_{if}(t - T_k)|\cos[2\pi f_0(t - T_k) + \varphi(t) + \psi(f_0)] \tag{9-9}$$

where $P(f)$ is the Fourier transform of the basic UWB pulse $p(t)$, $\psi(f_0)$ is the phase of $P(f)$ at f_0, $h_{if}(t)$ is the baseband-equivalent impulse response of the IF filter (in general complex), and $\varphi(t)$ is the phase response of the IF filter. For simplicity, the IF filter is assumed symmetric; that is, $H_{if}(f) = H_{if}^*(-f)$, so $h_{if}(t)$ is real and $\varphi(t) = 0$. Letting $t_k = t - T_k$ and $\theta_k = \psi(f_0) - 2\pi f_0 T_k$, the effective UWB interference into the discriminator is

$$g_k(t) = 2|P(f_0)|h_{if}(t_k)\cos(2\pi f_0 t + \theta_k) \tag{9-10}$$

Note that $\dot{\theta}_k = 0$. With no modulation $\phi = 0$ and (9-8) becomes:

$$\dot{\gamma} = \frac{A\dot{b}\sin\theta}{A^2 + b^2 + 2Ab\cos\theta} \tag{9-11}$$

where $\dot{\gamma}$ represents noise at the discriminator output in this case. Clearly, $b(t) = 2|P(f_0)|h_{if}(t_k)$ and $\theta = \theta_k$.

It is useful to define a normalized (unity bandwidth) version of the IF impulse response as: $h_1(t) \equiv h_{if}(t/B_{if})/B_{if}$, so $h_{if}(t) = B_{if}h_1(B_{if}t)$ and $b(t) = 2B_{if}|P(f_0)|h_1(B_{if}t_k)$. This

allows the IF bandwidth to be used explicitly as a parameter in the analysis. To be clear about notation with this normalization, $\dot{h}_1(\xi) \equiv dh_1(\xi)/d\xi$, so $d\left[h_1(B_{if}t_k)\right]/dt = B_{if}\dot{h}_1(B_{if}t_k)$ and $\dot{h}_{if}(t) = B_{if}^2\dot{h}_1(B_{if}t_k)$. Letting

$$\rho \equiv \frac{A}{2B_{if}|P(f_0)|} \tag{9-12}$$

(9-11) becomes

$$\dot{\gamma} = \frac{B_{if}\rho\dot{h}_1(B_{if}t_k)\sin\theta_k}{\rho^2 + h_1^2(B_{if}t_k) + 2\rho h_1(B_{if}t_k)\cos\theta_k} \tag{9-13}$$

Figure 9-4 shows $h_1(t)$ and $\dot{h}_1(t)$ for a 4-pole filter. For the *n*-pole filter in general,

$$h_1(t) = \frac{x^n}{(n-1)!}t^{n-1}e^{-xt} \qquad \dot{h}_1(t) = h_1(t)\left(\frac{n-1}{t} - x\right) \tag{9-14}$$

where $x = \frac{2\pi(n-1)!}{\Gamma(1/2)\Gamma(n-1/2)}$. For $n = 4$, $x = 6.4$.

The maximum value of the filter response is about 1.4. Thus, if $\rho >> 1$ (high SNR), then the discriminator output is approximately

$$\dot{\gamma} \cong B_{if}\frac{\dot{h}_1(B_{if}t_k)\sin\theta_k}{\rho} = \frac{2|P(f_0)|}{A}\dot{h}_{if}(t - T_k)\sin\theta_k \tag{9-15}$$

and its transform is

$$\mathsf{F}\left[\dot{\gamma}(\mathrm{t})\right] \cong \frac{2|P(f_0)|}{A}\sin\theta_k \cdot j2\pi f H_{if}(f)e^{-j2\pi f T_k}. \tag{9-16}$$

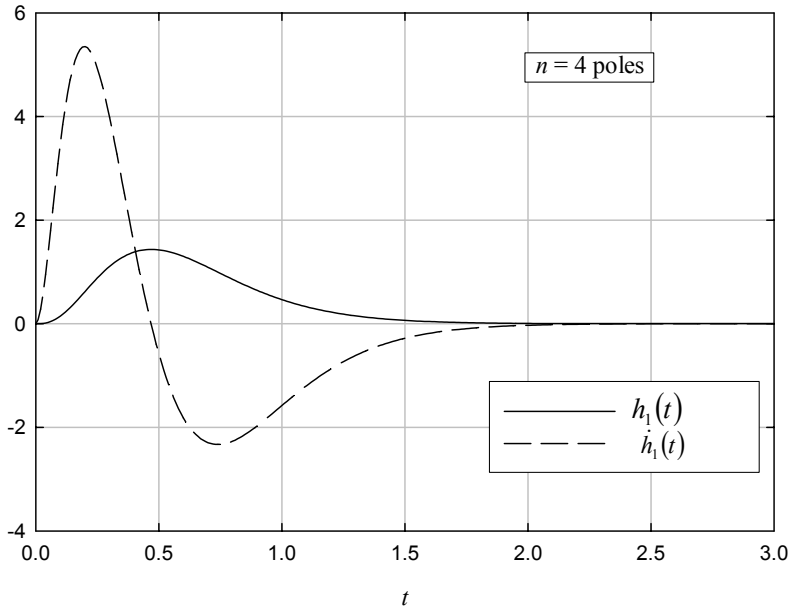

Figure 9-4: *Impulse response and its time derivative for normalized 4-pole filter*

After passing through the baseband filter with transfer function $H_{bb}(f)$ following the discriminator, the output baseband noise due to the UWB pulse is

$$N_{bb}(f) \cong \frac{2|P(f_0)|}{A} \sin\theta_k \cdot j2\pi f H_{if}(f) H_{bb}(f) e^{-j2\pi f T_k} \tag{9-17}$$

Assuming $H_{if}(f)$ is approximately flat over the baseband bandwidth, this becomes

$$N_{bb}(f) \cong \frac{2|P(f_0)|}{A} H_{if}(0) \sin\theta_k \cdot j2\pi f H_{bb}(f) e^{-j2\pi f T_k} \tag{9-18}$$

and

$$n_{bb}(t) \cong \frac{2|P(f_0)|}{A} H_{if}(0) \sin\theta_k \; \dot{h}_{bb}(t - T_k) \tag{9-19}$$

9.4. Baseband Signal-to-Noise Ratio

The energy spectral density of the baseband response to a single UWB pulse is

$$\left|N_{bb}(f)\right|^2 \cong \frac{4\left|P(f_0)\right|^2}{A^2}\left|H_{if}(0)\right|^2 \sin^2\theta_k \cdot 4\pi^2 f^2 \left|H_{bb}(f)\right|^2 \tag{9-20}$$

If the demodulator constant, which has units of volts/Hz, is taken into account, then $\left|N_{bb}(f)\right|^2$ will have a dimension of joules/Hz, as should be the case for a voltage waveform.

Assuming that $\left|H_{if}(0)\right| = 1$ and $H_{bb}(f)$ is rectangular with one-sided bandwidth B_b, this simplifies to

$$\left|N_{bb}(f)\right|^2 \cong \frac{4\left|P(f_0)\right|^2}{A^2}\sin^2\theta_k \cdot 4\pi^2 f^2 \qquad -B_b \le f \le B_b \tag{9-21}$$

The desired signal power is $C = A^2/2$, and the average UWB interference power at the IF output (discriminator input) is

$$I_{IF} = 2B_{IF}\left|P(f_0)\right|^2 R \tag{9-22}$$

where R is the average UWB pulse rate. Hence,

$$\frac{C}{I_{IF}} = \frac{A^2}{4\left|P(f_0)\right|^2 B_{IF} R} \tag{9-23}$$

and

$$\left|N_{bb}(f)\right|^2 = \frac{I_{IF}}{C}\frac{\sin^2\theta_k \cdot 4\pi^2 f^2}{B_{IF} R} \qquad -B_b \le f \le B_b \tag{9-24}$$

The total energy in the baseband response to the single UWB pulse is

$$E_{bb} = \int_{-B_b}^{B_b}\left|N_{bb}(f)\right|^2 df = \frac{I_{IF}}{C}\frac{\sin^2\theta_k \cdot 4\pi^2}{B_{IF} R}\cdot\frac{2B_b^3}{3} \tag{9-25}$$

and the average baseband interference power is $I_{bb} = R \cdot E_{bb}$.

Assuming θ_k is uniformly-distributed on $(0,2\pi)$, $\langle \sin\theta_k \rangle = 1/2$, and the average baseband interference power is

$$I_{bb} = \frac{I_{IF}}{C}\frac{4\pi^2}{B_{IF}} \cdot \frac{B_b^3}{3}. \tag{9-26}$$

To compute the baseband SNR, a sinusoidal modulating signal is assumed:

$$v(t) = 2\pi\Delta f \cos 2\pi f_m t \tag{9-27}$$

where Δf is the maximum frequency deviation and f_m is the modulating frequency. The maximum value of f_m is B_b. The baseband signal power is

$$S_{bb} = 2\pi^2 (\Delta f)^2 \tag{9-28}$$

so the baseband S/I is

$$\frac{S_{bb}}{I_{bb}} = \frac{3}{2}\frac{C}{I_{IF}} \cdot \frac{B_{IF}(\Delta f)^2}{B_b^3} \tag{9-29}$$

With the usual definition of modulation index

$$\beta \equiv \frac{\Delta f}{B_b} \tag{9-30}$$

$$\frac{S_{bb}}{I_{bb}} = \frac{3}{2}\frac{C}{I_{IF}}\beta^2\frac{B_{IF}}{B_b} \tag{9-31}$$

which is identical to the result for Gaussian noise with high CNR (~ 10 dB or better).

9.5. Applicability of the High-CIR Approximation

It is useful to clearly establish the conditions under which this relationship applies for the UWB case, in terms of C/I_{IF}, B_{IF}, and R. Recall that the condition for the approximation was that $\rho >> 1$, where $\rho = \dfrac{A}{2B_{IF}\left|P(f_0)\right|}$. Hence,

$$\rho^2 = \frac{A^2}{4B_{IF}^2\left|P(f_0)\right|^2} = \frac{R}{B_{IF}}\frac{C}{I_{IF}} = N_u\frac{C}{I_{IF}} \tag{9-32}$$

where $N_u = R/B_{IF}$ is the average number of UWB pulses per IF response time. The quantity $\rho^2 = N_u C/I_{IF}$ can be viewed as the "per pulse" CIR at the IF.

Figure 9-5 through Figure 9-10 show the normalized discriminator output $\dot{\gamma}/B_{if}$ and the high-CNR approximation $\dot{h}_1 \sin\theta_k/\rho$ for different combinations of ρ and θ_k. As can be seen, the approximation is very good for $\rho = 2$ (6 dB) but becomes inaccurate when ρ is reduced to 1 (0 dB).

Figure 9-11 through Figure 9-13 show the normalized discriminator output for a wide range of ρ, for three different values of θ_k. As can be seen, for very low values of ρ, the discriminator output is characterized by a sharp positive voltage "spike", followed by a gentle negative voltage waveform. The high-frequency energy in the initial voltage pulse will be rejected by the narrowband baseband filter.

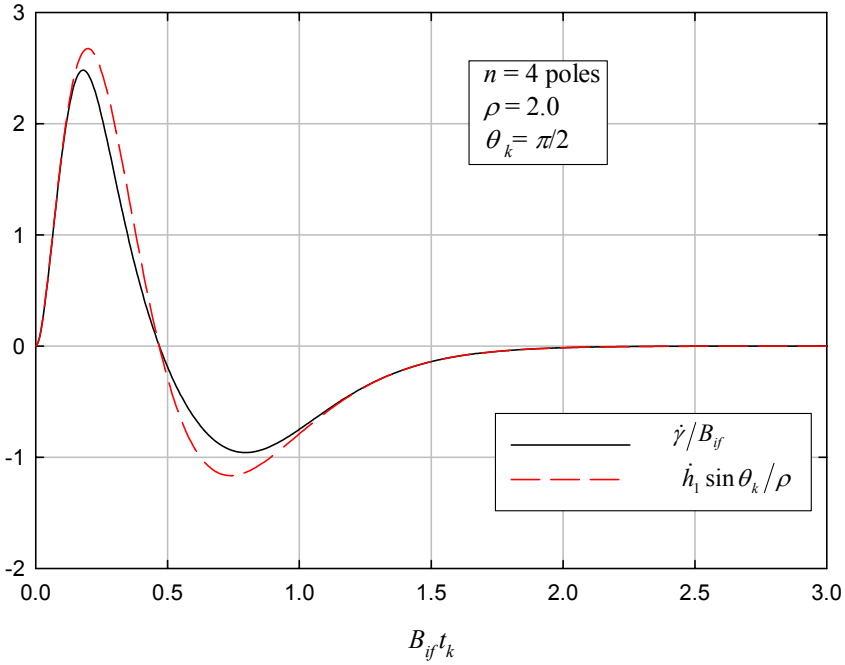

Figure 9-5: *Discriminator output and high-CIR approximation* for $\rho = 2$ *and* $\theta_k = \pi/2$.

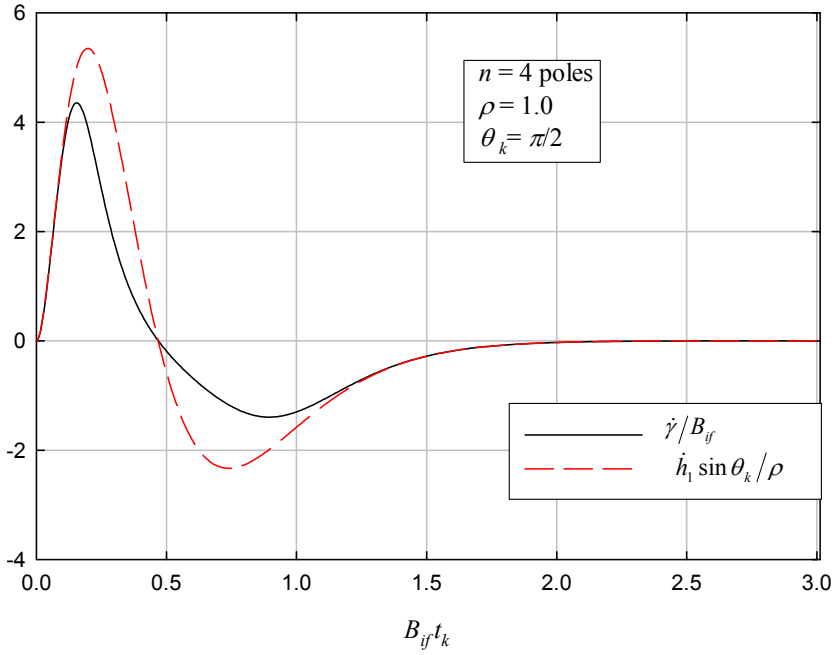

Figure 9-6: *Discriminator output and high-CIR approximation for* $\rho = 1$ *and* $\theta_k = \pi/2$.

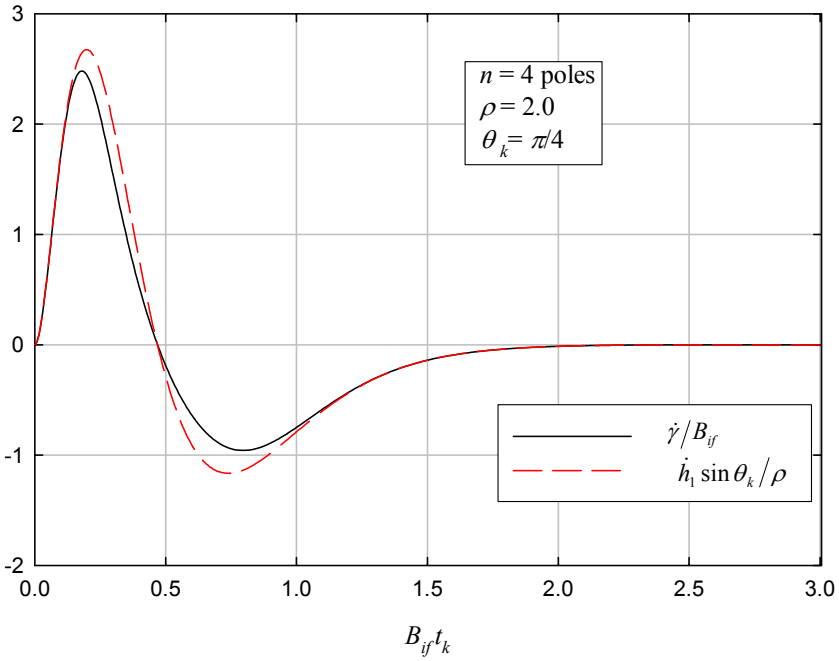

Figure 9-7: *Discriminator output and high-CIR approximation for* $\rho = 2$ *and* $\theta_k = \pi/4$.

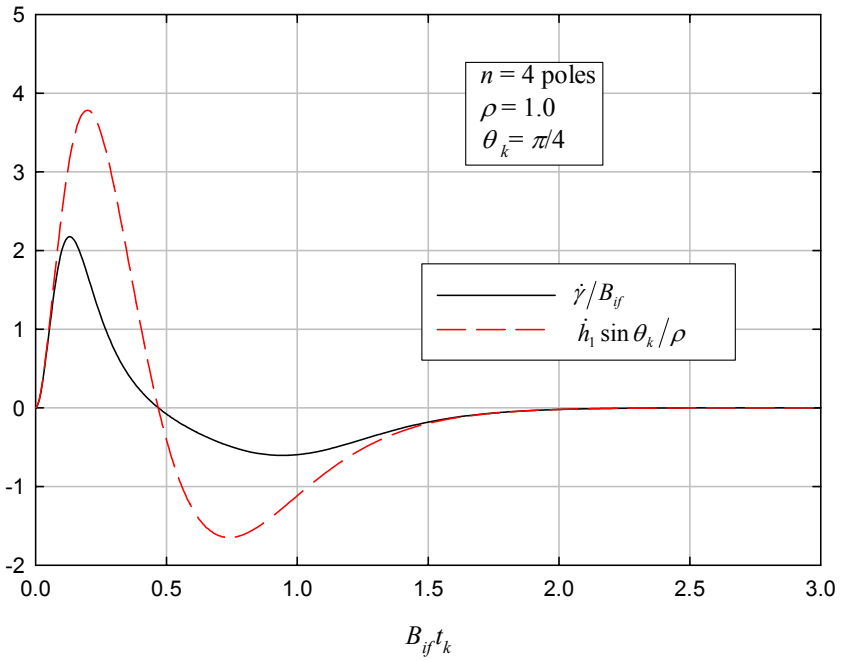

Figure 9-8: *Discriminator output and high-CIR approximation for* $\rho = 1$ *and* $\theta_k = \pi/4$.

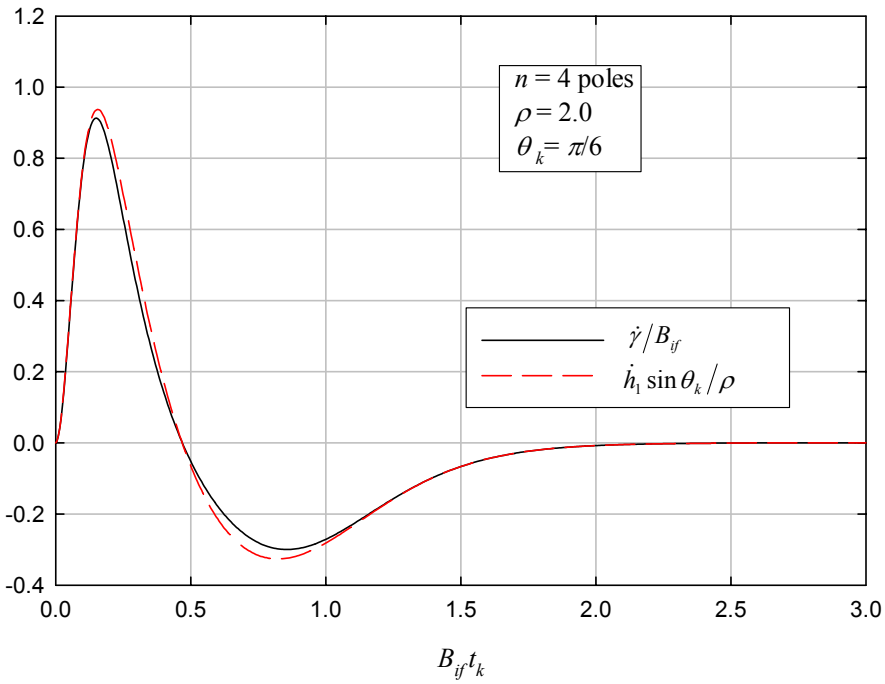

Figure 9-9: *Discriminator output and high-CIR approximation for* $\rho = 2$ *and* $\theta_k = \pi/6$.

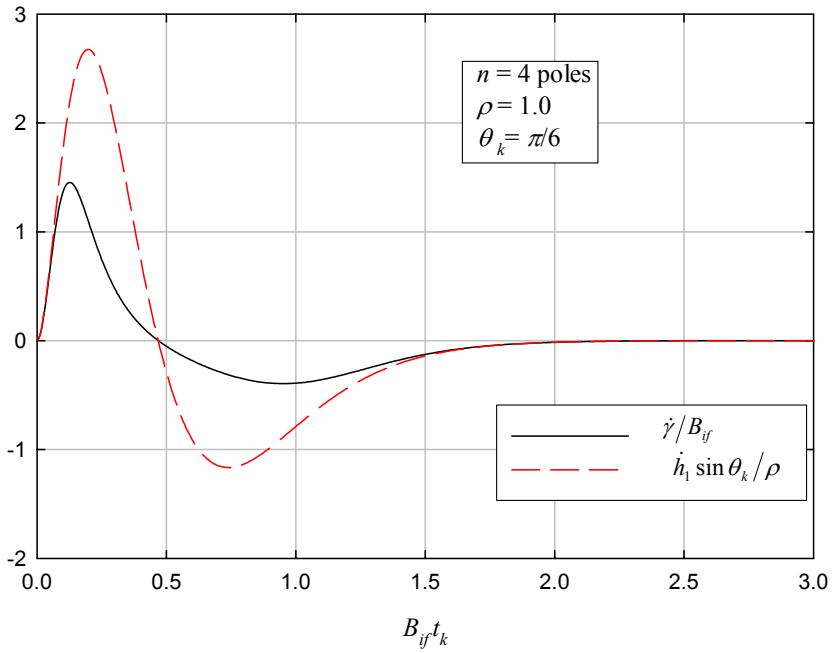

Figure 9-10: *Discriminator output and high-CIR approximation for* $\rho = 1$ *and* $\theta_k = \pi/6$.

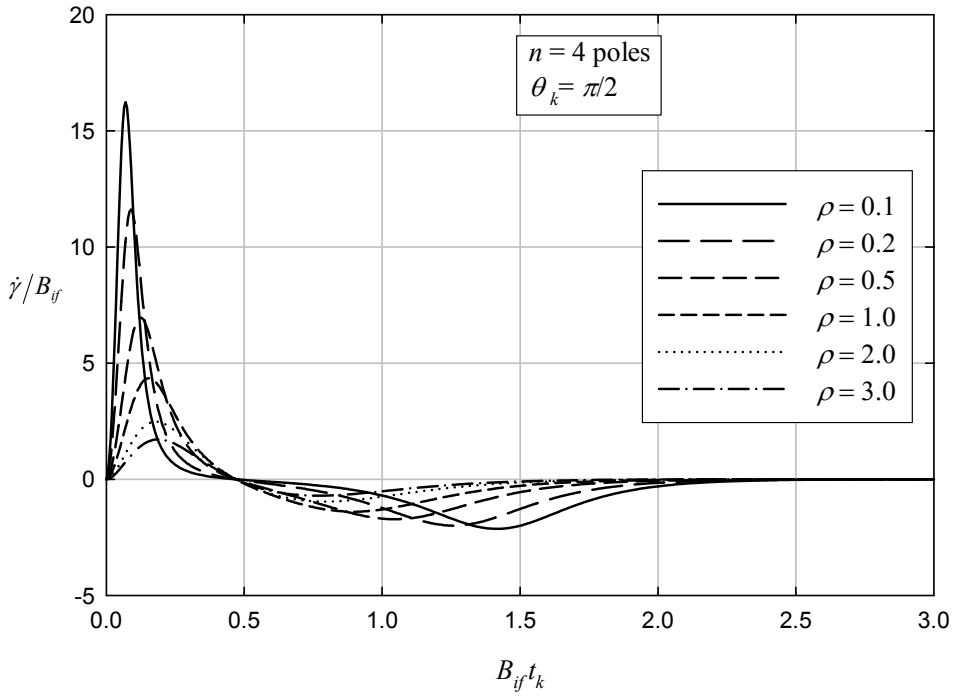

Figure 9-11: *Discriminator output for* $\theta_k = \pi/2$ *and a range of* ρ.

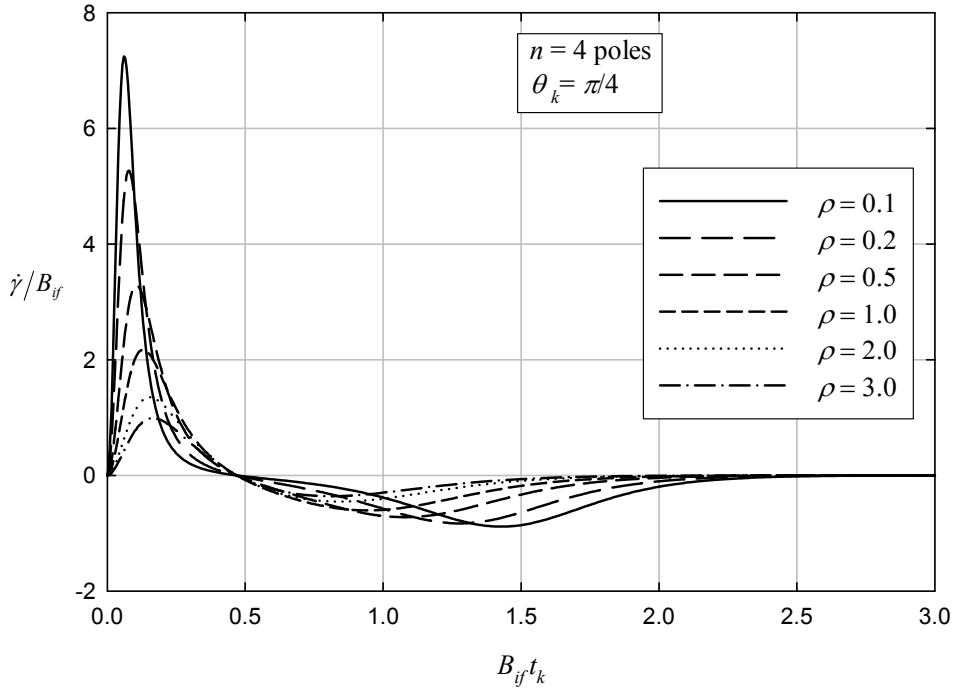

Figure 9-12: *Discriminator output for* $\theta_k = \pi/4$ *and a range of* ρ.

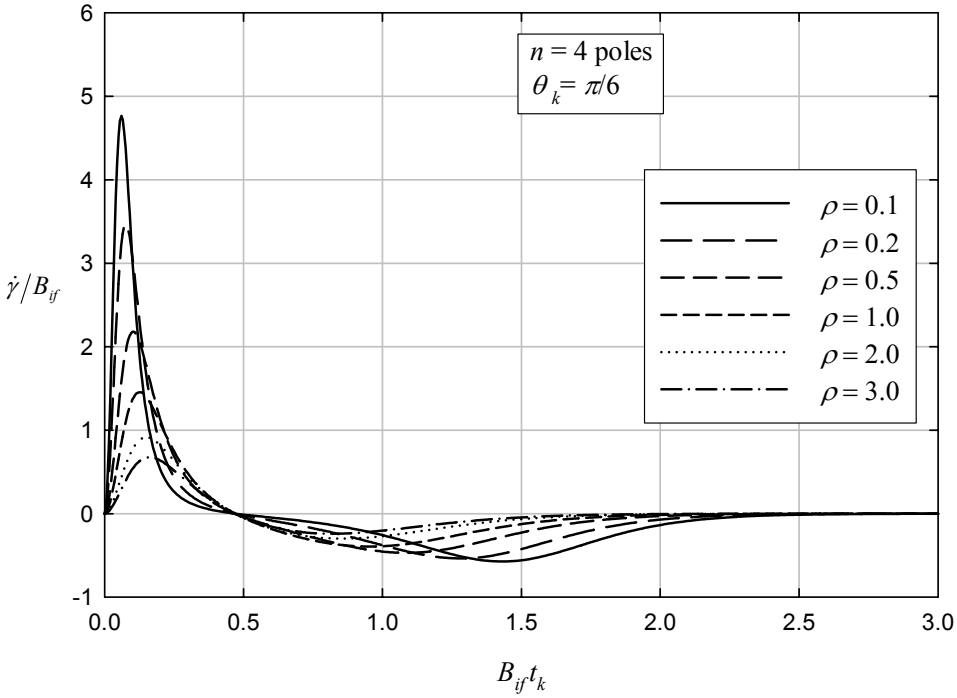

Figure 9-13: *Discriminator output for* $\theta_k = \pi/6$ *and a range of* ρ.

Overall, it appears from these results that when the pulse rate is equal to the IF bandwidth or less, the high-CNR model applies for $10\log\left(N_u C/I_{IF}\right) \geq 6$ dB. Below this 6-dB

threshold, the high-CNR model starts to become inaccurate, and the discriminator output begins to appear impulsive. A quantitative analysis of the baseband noise power below this threshold would require further analysis, which could be quite involved, given the complexity of FM threshold analysis for the Gaussian noise case. Moreover, since the performance of a narrowband FM receiver below threshold is likely to be unacceptable, a precise quantitative understanding of the SNR vs. CNR below the threshold is of limited value.

It is worth noting that UWB pulses that are resolvable in time by the IF (the pulse rate is less than the IF bandwidth) may interact at baseband, because of the narrower bandwidth of the baseband filter. That is, if the pulse rate exceeds the baseband bandwidth, the pulse effects will not be individually distinguishable at baseband.

9.6. Receiver Response to a UWB Pulse Sequence

The UWB signal is a sequence of pulses and can be represented as

$$w(t) = \sum_k a_k \, p(t - T_k) \tag{9-33}$$

where $p(t)$ is the pulse waveform and the $\{a_k\}$ represent the amplitude modulation of the pulses. The output of the IF filter in response to the UWB signal is a bandpass process, and can be expressed in terms of narrowband quadrature components as

$$g(t) = x(t)\cos 2\pi f_0 t - y(t)\sin 2\pi f_0 t \tag{9-34}$$

where

$$\begin{aligned} x(t) &= 2\left|P(f_0)\right| \sum_k a_k h_{if}(t - T_k)\cos\theta_k \\ y(t) &= 2\left|P(f_0)\right| \sum_k a_k h_{if}(t - T_k)\sin\theta_k \end{aligned} \tag{9-35}$$

Comparing to (9-4), $x(t) = b(t)\cos\theta(t)$ and $y(t) = b(t)\sin\theta(t)$. With no modulation, (9-8) becomes

$$\dot{\gamma} = \frac{A\dot{b}\sin\theta + \dot{\theta}b^2 + Ab\dot{\theta}\cos\theta}{c^2} \tag{9-36}$$

but $\dot{y} = \dot{b}\sin\theta + b\dot{\theta}\cos\theta$, so

$$\dot{\gamma} = \frac{A\dot{y} + \dot{\theta} b^2}{c^2}, \tag{9-37}$$

which for high SNR ($A^2 >> b^2$) becomes

$$\dot{\gamma} \cong \frac{\dot{y}}{A} \tag{9-38}$$

and its transform is

$$\mathsf{F}\left[\dot{\gamma}(t)\right] = \frac{j2\pi f Y(f)}{A} \tag{9-39}$$

Since $Y(f) = 2|P(f_0)|\, H_{if}(f) \sum_k a_k e^{-j2\pi T_k} \sin\theta_k$, the output baseband noise is

$$N_{bb}(f) \cong \frac{2|P(f_0)|}{A} H_{if}(0) \cdot j2\pi f H_{bb}(f) \sum_k a_k e^{-j2\pi f T_k} \sin\theta_k \tag{9-40}$$

$$n_{bb}(t) \cong \frac{2|P(f_0)|}{A} H_{if}(0) \sum_k a_k \sin\theta_k \dot{h}_{bb}(t - T_k) \tag{9-41}$$

With this expression, the baseband response to the UWB signal under high SNR conditions can be simulated in the manner described in Chapter 5 as the response of a filter with impulse response $\dot{h}_{bb}(t)$ to a UWB signal with amplitude coefficients $\{a_k \sin\theta_k\}$, with appropriate scaling to account for $|P(f_0)|$, A, and $|H_{if}(0)|$.

9.7. Baseband Noise Power

One performance measure for analog modulation is the baseband SNR. Calculation of the SNR requires that the average baseband noise power be computed, and the most straightforward way to do this is to integrate the baseband noise PSD, which is

$$S_{n_{bb}}(f) = \frac{(2\pi f)^2 S_y(f) |H_{bb}(f)|^2}{A^2} \tag{9-42}$$

where $S_y(f)$ is the PSD of $y(t)$, the quadrature baseband component of the IF filter output due to the UWB interference.

From Chapter 5,

$$S_x(f) = S_y(f) = \left|H_{if}(f)\right|^2 S_w(f + f_0) + \left|H_{if}(-f)\right|^2 S_w(-f + f_0) \tag{9-43}$$

where $S_w(f)$ is the PSD of the UWB signal $w(t)$. Note that if $H_{if}(f)$ is symmetric and $S_w(f)$ is flat across the IF passband (or at least symmetric about f_0 within the passband), then

$$S_x(f) = S_y(f) = 2\left|H_{if}(f)\right|^2 S_w(f + f_0) \tag{9-44}$$

$S_w(f)$ depends on $|P(f)|^2$, the energy spectral density of the pulse, and the position and amplitude modulation/coding applied to the pulse sequence. Accordingly, the UWB signal can be expressed as

$$w(t) = p(t) * d(t) \tag{9-45}$$

where

$$d(t) = \sum_k a_k \delta(t - T_k) \tag{9-46}$$

where $\delta(t)$ is the Dirac delta function. The Fourier transform of $w(t)$ is

$$W(f) = P(f)D(f) = P(f)\sum_k a_k e^{-j2\pi f T_k} \tag{9-47}$$

with $T_k = kT + \varepsilon_k$, where $1/T$ is the average pulse rate, and $c_k(f) \equiv a_k e^{-j2\pi f \varepsilon_k}$ this becomes

$$W(f) = P(f)\sum_k c_k(f) e^{-j2\pi f k T} \tag{9-48}$$

It can be shown that in general, the PSD of $d(t)$ is

$$S_d(f) = \frac{1}{T}\sum_l R_c[l] e^{j2\pi f l T} \tag{9-49}$$

where $R_c[l] = \left\langle c_n(f) c^*_{n+l}(f) \right\rangle$. The PSD of $w(t)$ is

$$S_w(f) = |P(f)|^2 S_d(f) \tag{9-50}$$

and

$$\begin{aligned} S_x(f) = S_y(f) = &|H_{if}(f)|^2 |P(f+f_0)|^2 S_d(f+f_0) \\ &+ |H_{if}(-f)|^2 |P(-f+f_0)|^2 S_d(-f+f_0) \end{aligned} \tag{9-51}$$

In many cases, $P(f)$ will be approximately constant across the IF passband, in which case

$$S_x(f) = S_y(f) = |P(f_0)|^2 \left\{ |H_{if}(f)|^2 S_d(f+f_0) + |H_{if}(-f)|^2 S_d(-f+f_0) \right\} \tag{9-52}$$

If $|H_{if}(f)| = |H_{if}(-f)|$ then

$$S_x(f) = S_y(f) = |P(f_0)|^2 |H_{if}(f)|^2 [S_d(f+f_0) + S_d(-f+f_0)] \tag{9-53}$$

and assuming that $|H_{bb}(f)| = |H_{bb}(-f)|$ the PSD of the baseband noise is

$$S_{n_{bb}}(f) = \frac{4\pi^2}{A^2} |P(f_0)|^2 |H_{if}(f)|^2 |H_{bb}(f)|^2 f^2 [S_d(f+f_0) + S_d(-f+f_0)] \tag{9-54}$$

The average noise power at the output of the baseband filter is

$$\left\langle n_{bb}^2(t) \right\rangle = \int_{-\infty}^{\infty} S_{n_{bb}}(f) df \ . \tag{9-55}$$

$S_d(f)$ depends on the average pulse rate and the statistics of the $\{a_k\}$ and $\{\varepsilon_k\}$. For example, if $a_k = 1$ and $\varepsilon_k = 0 \ \forall k$, then $S_d(f)$ consists of spectral lines separated in frequency by the pulse rate $1/T$ Hz. The power in the k^{th} spectral line in $S_w(f)$ in that case is $|P(k/T)|^2 / T^2$ At the other extreme, if the $\{\varepsilon_k\}$ are randomly distributed uniformly on $[0, T]$ (i.e., random dithering), then there are no spectral lines and $S_d(f)$ is smooth. Specifically, in that case, $S_d(f) = 1/T$. In general, $S_d(f)$ includes both a

continuous component as well as discrete CW tones. Clearly, the characteristics of the baseband noise will depend on the characteristics of $S_d(f)$ within the IF passband.

9.8. Effect of an In-band Tone

When the pulse rate is high relative to the IF bandwidth, there are two extreme cases of primary interest. The first is that of randomly-dithered pulses, which will produce a result similar to that of Gaussian noise. The second case is that in which there is a tone within the receiver passband due to periodicity in the pulse transmission scheme. Clearly, combinations of tones and noise-like signals can also occur (see Chapter 5).

For the noise-like case, results widely available in the literature apply. For the in-band tone case, assume that an interfering tone from the UWB signal of power *P* appears at frequency f_I, and let $\Delta f_I = f_I - f_0$, where as usual f_0 is the RF carrier frequency to which the FM receiver is tuned. From Chapter 5, the PSD of the baseband quadrature component $y(t)$ is:

$$S_y(f) = \frac{P}{2}\left|H_{if}(\Delta f_I)\right|^2\left[\delta(f-\Delta f_I)+\delta(f+\Delta f_I)\right] \tag{9-56}$$

and the average baseband interference power is

$$\begin{aligned} I_{bb} &= \frac{(2\pi)^2}{A^2}\frac{P}{2}\int\left|H_{bb}(f)\right|^2 f^2\left[\delta(f-\Delta f_I)+\delta(f+\Delta f_I)\right]df \\ &= \frac{(2\pi)^2}{A^2}P\left|H_{bb}(\Delta f_I)\right|^2(\Delta f_I)^2 \end{aligned} \tag{9-57}$$

The baseband signal power, for a sinusoidal modulating signal with frequency deviation Δf, is

$$S_{bb} = 2\pi^2(\Delta f)^2 \tag{9-58}$$

so, with the carrier and interference equal to $C = A^2/2$ and $I_{IF} = P$, respectively, the baseband SNR is

$$\frac{S_{bb}}{I_{bb}} = \frac{C}{I_{IF}}\left(\frac{\Delta f}{\left|H_{bb}(\Delta f_I)\right|\Delta f_I}\right)^2 \tag{9-59}$$

which is not a surprising result, since baseband voltage is proportional to frequency deviation, so baseband power is proportional to the square of the frequency deviation. Tones near the carrier frequency f_0 will cause relatively little interference. If the baseband filter rolls off at a rate higher than 6 dB per octave outside of its passband, then interfering tones separated from f_0 by more than the baseband bandwidth will be suppressed by the baseband filter characteristic.

It is interesting to make a simple comparison of this expression and that for the noise case. Assuming a rectangular baseband filter with one-sided bandwidth B_b, and assuming that $|H_{bb}(f)| = 1$ for $|f| \le B_b$, then the worst-case tone interference is $\Delta f_I = B_b$, in which case

$$\frac{S_{bb}}{I_{bb}} = \frac{C}{I_{IF}} \beta^2 , \tag{9-60}$$

which is lower than with noise-like interference. If the tone location is uniformly randomly distribution between 0 and B_b, then the average interference is

$$\overline{I_{bb}} = \frac{(2\pi)^2}{A^2} P \cdot \frac{B_b^2}{3} \tag{9-61}$$

and

$$\frac{S_{bb}}{\overline{I_{bb}}} = \frac{C}{I_{IF}} \cdot 3\beta^2 \tag{9-62}$$

which is less than the SNR for the noise case by a factor of $\frac{B_{IF}}{2B_b}$. If the tone is assumed randomly-distributed between f_0 and $f_0 + B_{IF}/2$, then the probability that it falls within the baseband filter bandwidth is $2B_b / B_{IF}$, and the expected value of the interference is then

$$\overline{I_{bb}} = \frac{(2\pi)^2}{A^2} P \cdot \frac{2B_b^3}{3B_{IF}} \tag{9-63}$$

and the baseband SNR is

$$\frac{S_{bb}}{\overline{I_{bb}}} = \frac{C}{I_{IF}} \cdot 3\beta^2 \cdot \frac{B_{IF}}{2B_b} \tag{9-64}$$

which is identical to the SNR for the noise case.

9.9. Conclusions

As with Gaussian noise, the baseband SNR depends on the total average received UWB interference power that falls within the IF bandwidth of the receiver. This average interference is denoted I_{IF} and the carrier (desired signal) power is denoted C. The exact relationship between the SNR and C/I_{IF} depends on the relationship between the UWB pulse rate R and the receiver IF bandwidth B_{IF}, the ratio of which is denoted $N_u = R/B_{IF}$.

For $R \le B_{IF}$ and $10\log(N_u C/I_{IF}) \ge 6$ dB, the SNR is proportional to C/I_{IF}, and the proportionality constant is the same as it would be with Gaussian noise of the same average power level within the receiver passband.

For $R > B_{IF}$, interference can take the form of a tone, if the UWB pulses are repeated at constant intervals, or can be noise-like, if pulses positions are randomly dithered. With tone interference, the proportionality constant depends on the frequency of the interfering tone relative to the receiver center frequency. If $R >> B_{IF}$ and pulses are randomly dithered, the IF output will be similar in character to Gaussian noise, and the relationship between the SNR and C/I_{IF} will be the same as for Gaussian noise, which is a well-known result.

What has not been provided here is a detailed analysis for the case of C/I_{IF} below the threshold for a pulse rate that is comparable to the IF bandwidth or less; that is, for $10\log(N_u C/I_{IF}) < 6$ dB with N_u on the order of 1 or less. Given the well-known complexities of FM threshold analysis, such an analysis is likely to be complicated, and is probably of limited interest, since the SNR is likely to be unacceptable if C/I_{IF} is below threshold, especially for narrowband (low-index) FM systems that primarily are used to transmit speech.

Chapter 9 References

[1] Mischa Schwartz, William Bennett, and Seymour Stein, *Communication Systems and Techniques,* 1966, McGraw-Hill, reprinted by IEEE Press, 1996.